University of Cape Town

Department of Physics

HADRONIC MATTER: FROM VACUUM TO EXTREME TEMPERATURE IN THE PRESENCE OF MAGNETIC FIELDS.

T H E S I S

SUBMITTED FOR THE DEGREE OF

DOCTOR OF PHYLOSOPHY

BY:

LUIS ALBERTO HERNANDEZ ROSAS

University of Cape Town

SUPERVISOR: EMER. PROF. CESAREO A. DOMINGUEZ (UCT)

CO-SUPERVISORS: PROF. HERIBERT WEIGERT (UCT)

PROF. KARL SCHILCHER (MAINZ)

AUGUST 2016

The copyright of this thesis vests in the author. No quotation from it or information derived from it is to be published without full acknowledgement of the source. The thesis is to be used for private study or non-commercial research purposes only.

Published by the University of Cape Town (UCT) in terms of the non-exclusive license granted to UCT by the author.

University of Cape Town

ABSTRACT.

This work consists of two themes. First, we work with Finite Energy QCD Sum Rules (FESR) approach in the vacuum. We tackle the problem of quark-hadron duality violation (DV), using the vector and axial-vector hadronic spectral function from tau-decay. A pinched integration kernel is introduce in the FESR in order to quench potential duality violations on the real axis in the complex squared energy plane and effectively extend the analysis well beyond the kinematical τ-decay end-point. As the sum rules are well satisfied, we conclude that possible DV must be buried under the experimental uncertainties. Also, using the latest updated ALEPH data on hadron decays, we use FESR to determine the vacuum condensates of dimension $d = 2$ and $d = 4$, to check the validity of the Weinberg sum rules, and to determine the chiral condensates of dimension $d = 6$ and $d = 8$, and values of the chiral perturbation theory $\bar{L}_{10}$ and C_{87}. Finally we computed the gluon condensate from e^+e^- annihilation data in the charm-quark region. This determination is based on FESR, weighted by a suitable integration kernel. We find a reasonably precise determination of the condensate $\langle \frac{\alpha_s}{\pi} G^2 \rangle = 0.037 \ \pm \ 0.015 \ GeV^4$.

The second theme is QCD/Hadronic matter in the presence of magnetic fields. This theme is made of two topics (1) We study the effects of magnetic fields in the chiral symmetry restoration and confinement/deconfinement transition. Within this theme we study FESR for axial-vector current correlator in the presence of a magnetic field, in the weak field limit and at zero temperature. We show the magnetic dependence on the deconfinement phenomenological parameter s_0 and on the gluon condensate $\langle \frac{\alpha_s}{\pi} G^2 \rangle$. We find that s_0 and $\langle \frac{\alpha_s}{\pi} G^2 \rangle$ increase with increasing field strength. Thus, at zero temperature the magnetic field is a catalysing agent of confinement. Also, the QCD phase diagram is studied in the presence of magnetic fields, using the linear sigma model coupled to quarks. It is

shown that the critical temperature for the phase transition decreases with increasing field intensity. It is also found that with increasing field strength the location of the critical end point in the phase diagram moves toward lower values of the critical quark chemical potential and larger values of the critical temperature. Besides we compute the vacuum one-loop quark-gluon vertex correction at zero temperature in the presence of a magnetic field. From the vertex function we extract the effective quark-gluon coupling and show that it grows with increasing magnetic field strength. The effect is due to a subtle competition between the colour charge associated to gluons and the colour charge associated to quarks, the former being larger than the latter. Thus, the gluons induce a kind of screening of the quark colour charge, in spite of the quark-antiquark proximity. Moreover we study the thermo-magnetic behaviour of the strong coupling constant and quark mass entering the Nambu–Jona-Lasinio model. The behaviour of the quark condensate as function of magnetic field strength and temperature is also obtained and confronted with lattice QCD results. We find that for temperatures above the chiral/deconfinement phase transitions, where the condensate decreases monotonically with increasing field, the coupling also decreases monotonically. For temperatures below the transition temperature we find that the coupling initially grows and then decreases with increasing field strength. (2) We look for clear observables which prove conclusively the existence of strong magnetic fields, for this purpose we compute the production of thermal photons in relativistic heavy-ion collisions by gluon fusion in the presence of an intense magnetic field, and during the early stages of the reaction. This photon yield is an excess over calculations that do not consider magnetic field effects. We add this excess to recent hydrodynamic calculations that are close to describing the experimental transverse momentum distribution in RHIC and LHC. We then show that our results provide a very good description of such excess. These results support the idea that the origin of at least some of the photon excess observed in heavy-ion experiments may arise from magnetic field induced processes.

ACKNOWLEDGEMENTS.

Foremost, I want to thank Prof. Cesareo A. Dominguez who supervised this work. You always trusted and supported me during my PhD, also I will never forget the many times at your office when we talked a lot about physics and some other funny topics, I appreciate very much you always share all your knowledge with me and of course I thank you for your friendship, it is priceless.

I want to thank my love María José, you are my force and you were my inspiration to give the best effort in the PhD, everyday you were present in my mind and my heart. I do not have words to explain how valuable was your support. I remember when I decided to study in South Africa and you supported my decision regardless I had to live far away of you, with all my heart I tell you: *Thank you so much, all of this work was done together.*

I want to thank my parents Ana María and José Luis for supporting any of my dreams, this is the end of my academic dream and it was possible only because you made it happen.

Undoubtedly other important person during this time is my brother Abimael who always supported and gave me words of encouragement, I missed you but at the same time all these feelings gave to me enough fortress to work hard. Many other people were important during this time and I thank to all of you for supporting me: Maikirrina, Pame, Jr, Pao, Mely, Elena, Juan, Leonardo, Munive, Cambri, Bere, Assa, Ale, ...

Of course I want to thank Prof. Heribert Weigert who has always had his door open for me and I want to thank to all of my partners in each research work in which I participated, your knowledge and your help are priceless, to work with all of you was so great: Marcelo, Karl, Hubert, Cristian, Renato, María Elena, Alfredo and Cristobal. An special mention to Alejandro Ayala who always had time to talk about physics, your knowledge and intuition were fundamental in much of this work.

An special mention to my dear friends Mawande, Preshin and Mirette, thanks a lot guys, you were like my family during the time that I have lived in Cape Town, I will always remember you with great affection.
Finally, I thank to Andy Buffler for the support and I thank the Faculty of Science of University of Cape Town and the National Research Foundation for funding assistance.

PUBLICATIONS

This thesis is based on the work done in the following publications:

- C. A. Dominguez, L. A. Hernandez, K. Schilcher and H. Spiesberger, *Chiral sum rules and vacuum condensates from tau-lepton decay data*, Journal of High Energy Physics **03** (2015) 053, `arXiv:1410.3779`.

- C. A. Dominguez, L. A. Hernandez and K. Schilcher, *Determination of the gluon condensate from data in the charm-quark region*, Journal of High Energy Physics **07** (2015) 110, `arXiv:1410.4500`.

- A. Ayala, C. A. Dominguez, L. A. Hernandez, M. Loewe, J. C. Rojas and C. Villavicencio, *Quark deconfinement and gluon condensate in a weak magnetic field from QCD sum rules*, Physical Review D**92** (2015) no.1, 016006, `arXiv:1504.01308`.

- A. Ayala, C. A. Dominguez, L. A. Hernandez, M. Loewe and R. Zamora, *Magnetized effective QCD phase diagram*, Physical Review D**92** (2015) no.9, 096011, `arXiv:1509.03345`.

- A. Ayala, C. A. Dominguez, L. A. Hernandez, M. Loewe and R. Zamora, *Inverse magnetic catalysis from the properties of the QCD coupling in a magnetic field*, Physics Letters B**759** (2016) 99-103, `arXiv:1510.09134`.

- A. Ayala, C. A. Dominguez, L. A. Hernandez, M. Loewe, A. Raya, J. C. Rojas and C. Villavicencio, *Thermo-magnetic properties of the strong coupling in the local Nambu-Jona-Lasinio model*, Physical Review D**94** (2016) no.5, 054019, `arXiv:1603.00833`.

- A. Ayala, J. D. Castaño-Yepes, C. A. Dominguez and L. A. Hernandez, *Thermal photon production from gluon fusion induced by magnetic fields in relativistic heavy-ion collisions*, arXiv:1604.02713.

- C. A. Dominguez, L. A. Hernandez, K. Schilcher and H. Spiesberger, *Quark-hadron duality: pinched kernel approach*, Modern Physics Letters A**31** (2016) no.27, 1630026, arXiv:1607.01701.

- C. A. Dominguez, L. A. Hernandez, K. Schilcher and H. Spiesberger, *Test of quark-hadron duality in tau-decays*, Modern Physics Letters A**31** (2016) no.31, 1630036, arXiv:1607.02048.

CONTENTS

CHAPTER 1

INTRODUCTION

Quantum Chromodynamics (QCD) is a non-Abelian gauge field theory which was constructed to explain the strong interaction [1], one of the four fundamental forces, it describes the interaction among quarks and gluons, they are the degrees of freedom of this theory and the fundamental constituents of nuclear matter. Unfortunately QCD is a theory which can not be solved analytically, then our option to describe strongly interactive systems is through numerical methods or effective theories.

Also we know quarks and gluons at current stage of the universe are confined particles, at least when hadronic matter is not at extreme conditions, understanding hadronic matter as all kind of colourless matter which is made of quark and gluons, like mesons and baryons. Due to the asymptotic freedom in QCD [2], hadronic matter exposes to extreme conditions, high temperatures and/or large densities, can be described in terms of free quarks and gluons, in other words we get access to the energies where perturbative calculations are allowed in QCD. Systems in extreme conditions are present in the universe or they can be created in experiments as well, examples are dense stars, relativistic heavy-ion collisions and the universe itself at its early stages.

As a consequence of finding different energetic regimes where the strongly interactive matter shows different nature, hadrons or free quarks and gluons, we immediately begin to think about some kind of phase transition. Actually the change from one kind of phase matter to other one happens and it is being explored from the theoretical point of view. Two options exist up to now if we want to analyse this phenomenon, chiral symmetry restoration and confinement/deconfinement transition.

To explore QCD phase transition we must harness suitable numerical methods or effective theories. Lattice QCD (LQCD) is the best numerical option to compute observables in QCD related to the phase transition, as long as the density of the system is zero or near to zero. On the other hand, effective theories are models which try to reproduce as many QCD symmetries as possible, with the goal to mimic QCD, some of the most successful models are Linear Sigma model, Nambu-Jona-Lasinio model and MIT bag model. Other very useful technique is QCD Sum Rules (QCDSR), it allows us to relate properties of hadronic matter with perturbative QCD (pQCD) information and vice-versa, therefore QCDSR looks like a nice starting point to study phenomenology related with QCD and hadrons.

At this point we have mentioned physical systems which could exhibit QCD phase transition but at the same time we have omitted the existence of the other three fundamental interactions, and it is not good, because we must remember that many kind of hadrons and quarks carry electric charge, hence a natural question is: Are electromagnetic fields important in the systems made of hadronic matter at extreme conditions? The answer should be yes they are important, actually the behaviour of strongly interactive matter in the presence of magnetic fields has become a subject of increasing interest over the past few years. The reason of this increasing interest is due to almost all the hadronic systems at extreme conditions could be in presence of very intense magnetic fields, such that strength field is comparable or bigger to other energy scales in those systems.

Nowadays all the effort of the community interested on systems like those described above is addressed to prove the existence of magnetic fields, by finding observables that exhibit the existence of them, and to analyse consequences of finite magnetic fields in the phenomenology of strongly interactive systems at extreme conditions.

Over the course of this work, we will report results related with observables which can shed light on the existence of magnetic fields in relativistic heavy-ion collisions and on the other hand we will present results found in effective theories and in pQCD which show how and why magnetic fields modify QCD phase transition. However if we want to explore what happens with hadronic matter at finite temperature and/or densities, we must begin from the vacuum properties of hadronic/QCD matter. In this work, we will use QCDSR to reach this last issue.

The thesis is organized as follows: In chapter 2 we recall the features of Finite Energy QCD Sum Rules (FESR) and discuss the quark-hadron Duality Violation (DV) problem presents in it, we show how the implementation of a proper kernel in the FESR can quench the DV without any model. In chapter 3 we use FESR together with ALEPH data on

hadronic decays of the tau-lepton in order to compute the condensates $d = 2$ and $d = 4$, also we use these data to verify the validity of the Weinberg Sum Rules, and to determine the chiral condensates of dimension $d = 6$ and $d = 8$, we compute the counter terms in chiral perturbation theory $\bar{L}_{10}$ and C_{87}. We show in this chapter another result from FESR, it is the determination of the gluon condensate using e^+e^- annihilation data in the charm-quark region. All previous quantities are important to have information of QCD in the vacuum and it shows the efficiency of FESR. In chapter 4 we introduce a preamble of how take into account the magnetic effects in QCD/hadronic matter, for this purpose we include the magnetic effects into scalar and fermion charged propagators, also we write the weak field approximation and Lowest Landau Level approximation for these propagators. Once we know how to introduce magnetic effects in the propagations of charged particles, in chapter 5 we study the magnetic modifications into the axial-vector current correlator and by using FESR, we get the magnetic behaviour of s_0, the phenomenological parameter of deconfinement in this framework, and the gluon condensate. Once we have used magnetic fields, we begin to study strongly interactive systems at extreme conditions, focusing on the QCD phase transition when magnetic fields are finite, we analyse deeply the (Inverse) Magnetic Catalysis phenomenon, we make use of different approach to understand the phenomenon itself, its consequences and its origin. We mention at the beginning of this chapter, QCD can not be solved analytically, therefore in chapter 6 we choose use an effective theory, it is linear sigma model coupled to quarks, with this model we study the magnetized effective QCD phase diagram in the temperature versus quark chemical potential plane. QCD phase diagram receives modifications due to finite magnetic fields, this modification are displayed: (1) the pseudo-critical temperature behaviour as function of magnetic field strength, and (2) the magnetic effects into Critical End Point (CEP) features. We put on the table a possible description in the behaviour of the QCD coupling when magnetic fields vary, this idea sheds light on the physics behind (Inverse) Magnetic Catalysis. Besides we try to strengthen this idea, showing in the Nambu–Jona-Lasinio model the relation between the light quark condensate and the strong coupling constant of this model. In chapter 7 we put a great effort showing a feasible observable which shows irrefutably the existence of strong magnetic fields in relativistic heavy-ion collisions, it is the photon production from gluon fusion. Finally in chapter 8 we enclose all the ideas exposed, we write the conclusions and we give ideas for future work.

CHAPTER 2

FINITE ENERGY QCD SUM RULES.

At the end of 1970's the work that laid foundations of QCDSR was published [3]; M. A. Shifman, A. I. Vainshtein and V. I. Zakharov proposed this new tool model independent which interpolate quark currents at large virtuality. One fundamental element in this new idea was the Wilson's Operator Product Expansion (OPE) [4], this expansion of correlation function of these currents was based under the following ideas, (1) As a consequence of asymptotic freedom, the theoretical results obtained from QCD can be compared with the experimental situation known hard processes, this processes where at short distances the quark-gluon coupling α_s becomes small and a perturbative treatment can be used. (2) On the other hand, any comprehensive theory of strong interaction must include large distance dynamics as well, in particular we should have in mind the quark interaction within hadrons is strong, since it binds quarks into inseparable objects (At present there is not accurate quantitative framework within QCD for dealing with the strong interaction regime).

OPE is a series made of vacuum expectation values of the Wilson lines, where the coefficients of each term in the series is computed in QCD perturbation theory, they are known as Wilson coefficients. The idea behind this expansion, allowed due to the high virtuality, it is without solving the confinement problem but assuming that confinement exists, effects of confinement can be described through the use of a few parameters, the so called vacuum condensates which within the OPE carry with the non-perturbative information, this allows to obtain many hadronics properties through an appropriate use of sum rules. Once we have the information from OPE, using QCDSR we are able to match, via disper-

sion relations, with a sum over hadronic states. Thereby, by the link formed with QCDSR, we have the possibility of computing hadronic observables or inversely QCD observables can be computed.

There are different ways to relate QCD with hadronic sector, it means different kinds of sum rules, for more details see reviews in [5]. Nevertheless in this thesis we are going to talk about only of *Finite Energy QCD Sum Rules* (FESR), this ideas was developed by R. Shankar in 1977 [6]. FESR lies on two pillars, as we mention above one is OPE and the second one is the Cauchy's theorem in the square-energy complex plane. Below we are going to show essential steps to have a clear image of both FESR pillars.

Operator Product Expansion.

Let us consider a QCD two-point function or in other words a current correlator, through Fourier transform it is written in momentum space as follows

$$\Pi(q^2) = i \int d^4x e^{iqx} \langle 0 \mid T(J(x)J(0)) \mid 0 \rangle, \tag{2.1}$$

where $J(x)$ is a local current which is built from quarks and gluons, it is a colourless current and it can be an scalar, pseudo-scalar, vector, pseudo-vector current or some other kind of current. In the two-point function, the initial and final states contain no hadrons and are therefore identified with the vacuum state of QCD. Also eq. (2.1) should contain perturbative information and non-perturbative information that reflects the confinement behaviour of quarks and gluons. As we mention before, there is not analytical solution to answer the problem of confinement in QCD, then to include this effect in the correlator, we must introduce it effectively, by parametrizing quark and gluon propagator corrections in terms of vacuum condensates, Figure 2.1 shows schematically the series structure of these vacuum condensates. The idea is the following, because we have quarks and gluons, we need to treat them separately, then for quarks, the propagator is

$$S(p) = \frac{i}{\not{p} - m} \rightarrow \frac{i}{\not{p} - m + \Sigma(p^2)}, \tag{2.2}$$

where $\Sigma(p^2)$ is the propagator correction, it contains the information of confinement. This correction should be maximized at $p \simeq 0$, for light quarks. This corresponds to *on-mass* shell quarks where the effects of confinement should be maximal. This effect is then parametrized in terms of the quark condensate $\langle 0 \mid \bar{q}(0)q(0) \mid 0 \rangle$ (second term in the series that appears at the *r.h.s.* in Figure 2.1). Analogously, in the case of the gluon propagator

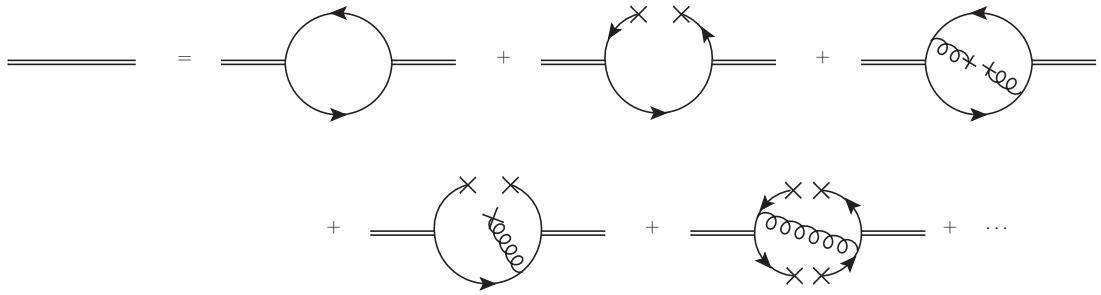

Figure 2.1: Schematic representation of operator product expansion for $\Pi(q^2)$. Double line refers to current $J(x)$, solid line with arrow means quark field and curly line is the gluon field.

$$D(k) = \frac{i}{k^2} \rightarrow \frac{i}{k^2 + \Lambda(k^2)}, \tag{2.3}$$

being $\Lambda(k^2)$ the propagator correction and it is maximized at $k \simeq 0$. This effect is then parametrized in terms of the gluon condensate $\langle 0 \mid \frac{\alpha_s}{\pi} \overrightarrow{G}^{\mu\nu} \cdot \overrightarrow{G}_{\mu\nu} \mid 0 \rangle$ (third term in the series that appears at the *r.h.s.* in Figure 2.1). These two condensates are part of a series of condensates, all others condensate are higher contributions in OPE, then the current correlator at short distances is

$$\Pi(q^2) \mid_{QCD} = C_0 \widehat{I} + \sum_{N=1} \frac{C_{2N}(q^2, \mu^2)}{Q^{2N}} \langle 0 \mid \widehat{O}_{2N}(\mu^2) \mid 0 \rangle, \tag{2.4}$$

where μ^2 is the regularization scale and $C_{2N}(q^2, \mu^2)$ are the Wilson coefficients, they depend on the Lorentz indexes and quantum numbers of $J(x)$. $\widehat{O}_{2N}(\mu^2)$ are the local gauge invariant condensates built from the quark and gluon fields, these operators appear within the series ordered by increasing dimensionality. Since there are no gauge invariant operators of dimension $d = 2$ involving quarks and gluons fields, it is usually assumed that the OPE starts at dimension $d = 4$. The unit operator $\widehat{I}$ in eq. (2.4) has dimension $d = 0$ and $C_0\widehat{I}$ stands for the purely perturbative contribution. The Wilson coefficients as well as the vacuum condensates depend on the renormalization scale. Also the numerical values of the vacuum condensates cannot be calculated analytically from first principles as this would be tantamount to solving QCD exactly. However, some condensates can be calculated using QCD low energy theorem or through QCDSR together with experimental data. Other alternative is LQCD where the condensate values can be calculated numerically with good accuracy.

Cauchy's theorem.

The positive real axis in the complex energy-squared, s-plane, contains all the information of hadronic sector, it means, bound states and resonances live in this real axis, they appear as poles and singularities in the second Riemann sheet, respectively. All these singularities lead to a discontinuity across the positive real axis. On the other hand, QCD is valid elsewhere in the complex s-plane. Thus choosing an integration contour as shown in Figure 2.2, and given that there are no other singularities in the complex s-plane, Cauchy's theorem leads to the FESR

$$\oint ds\ P(s)\ \Pi(s) = \int_{s_{th}}^{s_0} ds\ P(s)\ \Pi(s+i\epsilon) + \int_{s_0}^{s_{th}} ds\ P(s)\ \Pi(s-i\epsilon) + \oint_{C(|s_0|)} ds\ P(s)\ \Pi(s)$$
$$= \int_{s_{th}}^{s_0} ds\ P(s)\ 2i\ \mathrm{Im}\Pi(s) + \oint_{C(|s_0|)} ds\ P(s)\ \Pi(s) = 0, \tag{2.5}$$

where the kernel $p(s)$ is an arbitrary analytic function, s_{th} is the hadronic threshold, and the finite radius of the circle $|s_0|$, is large enough for QCD and the OPE to be used on the circle. Taking the limit $\epsilon \to 0$ we already get the imaginary part of the hadronic correlator, it is proportional to the hadronic spectral function.

$$\int_{s_{th}}^{s_0} ds\ \frac{1}{\pi}\ p(s)\ \mathrm{Im}\Pi(s)\ |_{HAD} = -\frac{1}{2\pi i} \oint_{C(|s_0|)} ds\ p(s)\ \Pi(s)\ |_{QCD}, \tag{2.6}$$

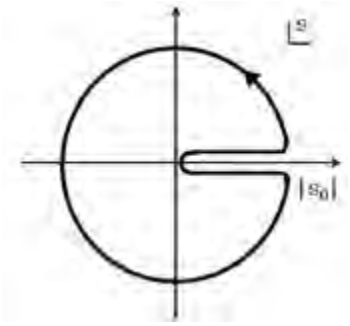

Figure 2.2: Integration contour in the complex s-plane. The discontinuity across the real axis brings in the hadronic spectral function, while integration around the circle involves the QCD correlator. The radius of the circle is $|s_0|$ the onset of QCD.

Eq. (2.6) is the mathematical statement of what is usually referred to as quark-hadron duality. Since pQCD is not valid in the time-like region ($s \geq 0$), in principle there is a possibility of problems on the circle near the real axis (global duality violation, DV), promptly we will discuss on detail this issue. In eq. (2.6) the right hand side involves the

QCD correlator which is expressed in terms of the OPE as in eq. (2.4). The left hand side involves the hadronic spectral function, which may contain a ground state pole, followed by resonances which merge smoothly into the hadron continuum above some threshold s_0. This continuum is expected to be well represented by pQCD if s_0 is large enough.

Quark-hadron duality violation.

Let me begin this section quoting the following phrase wrote by Poggio, Quinn and Weinberg [7]: *certain inclusive hadronic cross sections at high energies, being appropriately averaged over an energy range, had to (approximately) coincide with the cross sections one could calculate in the quark-gluon perturbation theory.* We can see in 1970's, the physicists put a lot of effort to solve the QCD/Hadron puzzle or DV. They tried to bridge the gap between the kind of particles observed and the fundamental particles theoretically computed (We must remember quarks and gluons are never detected experimentally. What is actually produced and detected in experimental devices are hadrons). QCDSR then played a very important role to bridge the gap and until these days it still being very useful. We are going to do the mental exercise to settle the "ingredients" that could make possible to solve analytically the QCD/Hadron puzzle from QCDSR side.

As above I said, QCDSR has one fundamental piece, it is the correlator of currents, these currents are written in terms of quark and gluon fields or in terms of hadronic fields, both correlator must have the same quantum numbers. To achieve both correlator are the same object, except that they are only written in different basis, we need to satisfy the following: (a) From the hadronic side, since these particles can be detected, we need an exact measurement of the spectral function $\rho(s \equiv q^2)$ (the imaginary part of $\Pi(s)$ is proportional to $\rho(s)$). (b) From the QCD side, since full short- and large-distance contributions must be taken into account, we can not truncate the OPE series, then we must know all Wilson coefficients, it means we must know the complete perturbative series on QCD and the exact value of α_s, and we must know all vacuum condensates. All the previous quantities must be independent of the renormalization scale as well. Moreover, QCD/Hadron puzzle must be independent of s.

Each of those requirements, to achieve the hadronic and the QCD correlators give us the same and complete information, can not be satisfied (Otherwise QCD would be solved). As consequence, we find then some limitation that QCDSR has. However, it does not imply QCDSR is a poor technique, by contrast when QCDSR and the correlators are optimized, either by large and involved calculations or by clever ideas which reduce the

impact of the omitted information, QCDSR becomes a nice framework to compute hadron and QCD observables.

Then, by using FESR, we are going to discuss the predictive scope of FESR to compute observables, by including suitable integrand kernels which quench DV. The integrand kernels that help to reduce DV are known as *pinching* kernels [8], they are including into FESR in order to squeeze the integrand at the crossing of the positive real axis, and therefore it improves the reliability of the theoretical analysis through the OPE and it can reduce the experimental uncertainties in the integral over the spectral function near the kinematic limit. The structure of these kind of kernels is $(1 - s/s_0)^N$, remembering s_0 is the onset of QCD and $N \epsilon \mathbb{Z}$.

We know that these kernels can not improve the problems which come from the truncation of OPE and pQCD, however we can show that small changes provide a very good saturation of FESR and hence an appreciable improved accuracy of observable quantities. On the other hand many DV models are in the "market" [9–11], they try to increase the accuracy of observable values by implementing methods in a not clear way, they try to quench the systematic errors from the information lost due to the truncation of OPE and pQCD. Morover, these models do not solve the QCD/Hadron puzzle and they are unable to improve with enough accuracy the majority of observables values computed with FESR. Then we think our approach needs to be checked in each and every application.

In order to compare results of both approaches, one table comes next, with the determination of the effective low-energy constants in chiral perturbation theory $\bar{L}_{10}$ and C_{87}, from spectral function data on hadronic decays of the τ-lepton [12–14] and quantities more sensitive to DV, the chiral condensates $\langle \mathcal{O}_{6,8} \rangle$

	$-\bar{L}_{10}$	C_{87} [GeV^{-2}]	$-\langle O_6 \rangle$ [GeV^6]	$\langle O_8 \rangle$ [GeV^8]
Boito *et al.* [11]	$6.52 \pm 0.11 \times 10^{-3}$	$8.47 \pm 0.29 \times 10^{-3}$	$6.6 \pm 1.1 \times 10^{-3}$	$5.0 \pm 5.0 \times 10^{-3}$
Pich *et al.* [15]	$6.48 \pm 0.05 \times 10^{-3}$	$8.40 \pm 0.18 \times 10^{-3}$	$3.6^{+0.7}_{-0.6} \times 10^{-3}$	$-1.0 \pm 0.4 \times 10^{-2}$
this work [16]	$6.5 \pm 0.1 \times 10^{-3}$	$8.0 \pm 0.2 \times 10^{-3}$	$5.0 \pm 0.7 \times 10^{-3}$	$-9 \pm 5 \times 10^{-3}$

Table 2.1: Determination of chiral parameters with FESR, with inclusion of DV model (Boito and Pich), and without DV model (this work).

From Table 2.1, we can observe the good agreement between both approaches. Another sensitive test of DV is provided by the two Weinberg sum rules (WSR). Using corrected

ALEPH data [14] on the vector and axial-vector spectral functions from hadronic decays of the τ-lepton, the two WSR are not saturated, except possibly very near the kinematical end point [16]- [20]. However, as already shown in [16] and [17] both WSR become well saturated after using a very simple linear pinched kernel, without any need for an explicit DV model.

As some models of duality violations for the application considered in this section lead to results fully compatible with those from simple pinched FESR, there arises the question as to what extent these models are really necessary, given the rather large number of parameters they require. In this section we expect to shed some light on this issue, i.e. we show that FESR are already saturated when only pinched kernels are used.

It is unfortunate that the τ-lepton is not heavier, as otherwise one could have tested for DV with reasonable precision at high enough energies. However, as discussed in [21] a suitable pinched integration kernel allows to perform a FESR analysis beyond the region of existing τ-decay data, i.e. up to $s \simeq 10\,\mathrm{GeV}^2$, in both the vector and the axial-vector channels. This procedure is based on the expectation that in this region the non-existing data would be reasonably well accounted for by pQCD. This last statement can be verified in the vector channel by using actual data from e^+e^- annihilation into hadrons. If the end-point of the τ-decay data on the positive real axis, in the complex squared-energy s-plane, is denoted by $s = s_1$, and $s_0 > s_1$ is the radius of the Cauchy integration circle, the pinched kernel in the FESR, $P(s)$, is a function $P(s) = P(s, s_0, s_1)$. In order to verify the method one needs to compare an integral of the data, weighted with $P(s, s_0, s_1)$, with some quantity known from experiment. In the axial-vector case this is the pion decay constant, f_π, and in the vector case it is simply zero (no pole in this channel). In [21] the spectral function for $s > s_1$ was assumed constant and $P(s)$ was subject to the constraint

$$\int_{s_1}^{s_0} P(s)\, ds = 0. \tag{2.7}$$

For $s > s_1$ the spectral function should most likely be given by pQCD, rather than by a constant. Since the pQCD spectral function is well known, it is possible to improve this analysis by changing the constraint, eq. (2.7), into

$$\int_{s_1}^{s_0} P(s)\, \mathrm{Im}\,\Pi_{PQCD}(s)\, ds = 0\ , \tag{2.8}$$

where

$$\mathrm{Im}\,\Pi_{PQCD}(s) = \frac{1}{4\pi}\left[1 + \frac{\alpha_s(s)}{\pi} + ...\right]\ . \tag{2.9}$$

We consider FESR involving a pinched kernel satisfying eqs. (2.8) and (2.9), together with ALEPH data on hadronic τ-decays, supplemented with e^+e^- data in the vector channel, in order to establish if pinched FESR are fulfilled without taking into account potential DV. We find this to be the case, as supported by the excellent agreement between the FESR and their expected experimental results (f_π and zero) in the wide region $s \simeq M_\tau^2 - 10\,\text{GeV}^2$. In spite of this we also consider an explicit DV model [22], obtained from fits to data in the energy range below the τ-mass, and confront results from both methods with vector and axial-vector data from τ-decay. In the axial-vector channel results for f_π from the DV model and from our pinched kernel are both in good agreement in the region of the data above $s \simeq 1.5\,\text{GeV}^2$. In the vector channel there is also good agreement between the two methods. It should be highlighted that the explicit DV model [22] involves eight free parameters, while the pinched kernel method has none, other than the value of the end-point squared energy of the τ-decay data, s_1.

Let us develop the FESR we are using. We begin by defining the vector and the axial-vector current correlator relevant to τ-decay,

$$\Pi^{VV}_{\mu\nu}(q) = i\int d^4x\, e^{iqx}\,\Big\langle 0|T(V_\mu(x)V^\dagger_\nu(0))|0\Big\rangle = (-g^{\mu\nu}q^2 + q^\mu q^\nu)\Pi_V(q^2)\,, \tag{2.10}$$

$$\begin{aligned}\Pi^{AA}_{\mu\nu}(q) &= i\int d^4x\, e^{iqx}\,\Big\langle 0|T(A_\mu(x)A^\dagger_\nu(0))|0\Big\rangle \\ &= (-g^{\mu\nu}q^2 + q^\mu q^\nu)\Pi^{(1)}_A(q^2) + q^\mu q^\nu \Pi^{(0)}_A(q^2)\,,\end{aligned} \tag{2.11}$$

where $V^\mu(x) = \bar{d}(x)\gamma^\mu u(x)$ and $A^\mu(x) = \bar{d}(x)\gamma^\mu\gamma_5 u(x)$ (with $u(x)$ and $d(x)$, the up- and down-quark fields, respectively). The pQCD spectral functions in the chiral limit are normalized as

$$\text{Im}\,\Pi_V|_{PQCD}(s) \equiv \text{Im}\,\Pi_A|_{PQCD}(s) = \frac{1}{4\pi}\left[1 + \mathcal{O}(\alpha_s)\right]\,. \tag{2.12}$$

The OPE in QCD can be written as

$$4\pi^2\Pi_{OPE}(Q^2) = \sum_{N=0}^{\infty}\frac{1}{Q^{2N}}\,C_{2N}(Q^2,\mu^2)\,\langle\mathcal{O}_{2N}(\mu^2)\rangle\,, \tag{2.13}$$

where $Q^2 \equiv -q^2$, and q^2 is large and space-like. Next, using Cauchy's theorem in the complex squared energy s-plane (see Figure 2.2) the FESR become

$$(-1)^N\,C_{2N+2}\,\langle\mathcal{O}_{2N+2}\rangle = 4\pi^2\int_0^{s_0} ds\,s^N\,\frac{1}{\pi}\,\text{Im}\,\Pi^{DATA}(s) - s_0^{N+1}M_{2N+2}(s_0) + DV, \tag{2.14}$$

where the dimensionless pQCD moments $M_{2N+2}(s_0)$ are given by

$$M_{2N+2}(s_0) = \frac{4\,\pi^2}{s_0^{(N+1)}} \int_0^{s_0} ds s^N \frac{1}{\pi} \mathrm{Im}\,\Pi_{PQCD}(s), \tag{2.15}$$

and we have indicated that duality violations are present in eq. (2.14), which we will discuss later. Following we will first discuss whether the sum rules are satisfied without including DV.

The FESR, eq. (2.14), omitting DV, in the axial-vector channel can be written as

$$\begin{aligned} 2f_\pi^2 = &- \int_0^{s_1} ds\; P(s) \frac{1}{\pi} \mathrm{Im}\,\Pi_A^{DATA}(s) - \int_{s_1}^{s_0} ds\; P(s) \frac{1}{\pi} \mathrm{Im}\,\Pi_A^{DATA}(s) \\ &- \frac{1}{2\pi i} \oint_{|s|=s_0} ds\, P(s)\, \Pi_A^{OPE}(s) \end{aligned} \tag{2.16}$$

where the hadronic (data) integral has been split into two parts, one from threshold to somewhere near the kinematical endpoint of the τ-decay data, $s_1 \simeq 2.7\,\mathrm{GeV}^2$, and the other part from s_1 to an upper limit $s_0 \lesssim 10\,\mathrm{GeV}^2$. This expression holds for every meromorphic kernel $P(s)$, but we shall only consider here polynomial kernels. Since there are no τ-decay data in the region $s_1 < s < s_0$, we assume them to be accounted for by pQCD, at least in an integrated sense, i.e.

$$\frac{1}{\pi} \mathrm{Im}\,\Pi_A^{DATA}(s) \approx \frac{1}{\pi} \mathrm{Im}\,\Pi_A^{PQCD}(s)\;, \qquad (s_1 \le s \le s_0)\,. \tag{2.17}$$

Then the sum rule, eq. (2.16), becomes

$$\begin{aligned} 2f_\pi^2 = &- \int_0^{s_1} ds\; P(s) \frac{1}{\pi} \mathrm{Im}\,\Pi_A^{DATA}(s) - \int_{s_1}^{s_0} ds\; P(s) \frac{1}{\pi} \mathrm{Im}\,\Pi_A^{PQCD}(s) \\ &- \frac{1}{2\pi i} \oint_{|s|=s_0} ds\, P(s)\, \Pi_A^{OPE}(s)\,. \end{aligned} \tag{2.18}$$

For the vector channel the FESR is identical to eq. (2.18), except for the left hand side which now becomes zero (no pole in this channel). How well this sum rule is satisfied will depend crucially on the kernel $P(s)$. Given the absence of experimental data beyond $s = m_\tau^2$, we design the integration kernel $P(s)$ so as to minimize the (unknown) hadronic contribution to the second integral in eq. (2.16). For a polynomial kernel, $P(s)$, the highest power should not be too high, as each additional power of s results in FESR involving higher dimensional (unknown) condensates. We have found that the optimal degree is in fact the simplest, i.e. a linear function

$$P(s) = 1 + \gamma s. \tag{2.19}$$

Assuming eq. (2.17), the parameter $\gamma \equiv \gamma(s_0, s_1)$ is determined from the condition

$$\int_{s_1}^{s_0} P(s)\ \mathrm{Im}\,\Pi^{PQCD}(s)\, ds = 0\,, \tag{2.20}$$

which can be written as

$$\begin{aligned} 0 &= \int_{s_1}^{s_0} ds\, P(s) \frac{1}{\pi}\, \mathrm{Im}\,\Pi_A^{PQCD}(s) \\ &= \frac{1}{2\pi i} \oint_{|s|=s_0} ds\, P(s)\, \Pi_A^{PQCD}(s) - \frac{1}{2\pi i} \oint_{|s|=s_1} ds\, P(s)\, \Pi_A^{PQCD}(s) \\ &= \left[s_1\, M_0(s_1) + \gamma(s_0,s_1)\, s_1^2\, M_1(s_1)\right] - \left[s_0\, M_0(s_0) + \gamma(s_0,s_1)\, s_0^2\, M_1(s_0)\right]\,, \end{aligned} \tag{2.21}$$

where the moments $M_N(s_0)$ were defined in eq. (2.15). This leads to

$$\gamma(s_0,s_1) = -\frac{\left[s_0\, M_0(s_0)\ -\ s_1\, M_0(s_1)\right]}{\left[s_0^2\, M_1(s_0)\ -\ s_1^2\, M_1(s_1)\right]}\ . \tag{2.22}$$

To lowest order in pQCD $\mathrm{Im}\,\Pi^{PQCD}(s)$ is a constant, and

$$\gamma = -\frac{2}{s_0 + s_1}\,, \qquad\qquad P(s) = 1 - \frac{2s}{s_0 + s_1}\,, \tag{2.23}$$

which is the kernel used in [21]. Notice that if $s_0 = s_1$, then $\gamma(s_0, s_0) = -\frac{1}{s_1}$, and

$$P(s) = 1 - \frac{s}{s_1}\,, \tag{2.24}$$

which is the pinched kernel used in earlier analyses [17]. Next, to order α_s, with $\alpha_s(s) = (-2\,\pi/\beta_1)\,/\ln\left(s/\Lambda^2_{QCD}\right)$, and $\Lambda_{QCD} \simeq 360\,\mathrm{MeV}$, the parameter $\gamma(s_0, s_1)$ can be written as

$$\gamma(s_0,s_1) = -\,\frac{2\,\beta_1(s_0 - s_1) - 4\,\Lambda^2_{QCD}\left[\mathrm{li}\left(\frac{s_0}{\Lambda^2_{QCD}}\right) - \mathrm{li}\left(\frac{s_1}{\Lambda^2_{QCD}}\right)\right]}{\beta_1\,(s_0^2 - s_1^2) - 4\,\Lambda^4_{QCD}\left[\mathrm{li}\left(\frac{s_0^2}{\Lambda^4_{QCD}}\right) - \mathrm{li}\left(\frac{s_1^2}{\Lambda^4_{QCD}}\right)\right]}\,, \tag{2.25}$$

where $\mathrm{li}(x)$ is the logarithmic integral, $\mathrm{li}(x) = \int_0^x dt/\ln t$. Using instead the strong coupling to five-loop order leads to a long expression for $\gamma(s_0, s_1)$, which is numerically in excellent agreement with eq. (2.25). Using eq. (2.20) in eq. (2.18) the FESR can be written as

$$2\,f_\pi^2 = -\int_0^{s_1} ds\,P(s)\,\frac{1}{\pi}\,\mathrm{Im}\,\Pi_A^{DATA}(s) - \frac{1}{2\pi i}\oint_{|s|=s_0} ds\,P(s)\,\Pi_A^{PQCD}(s) + \frac{1}{4\pi^2}\left[C_2\,\langle O_2\rangle - \gamma(s_0,s_1)\,C_4\,\langle O_4\rangle\right]\,. \tag{2.26}$$

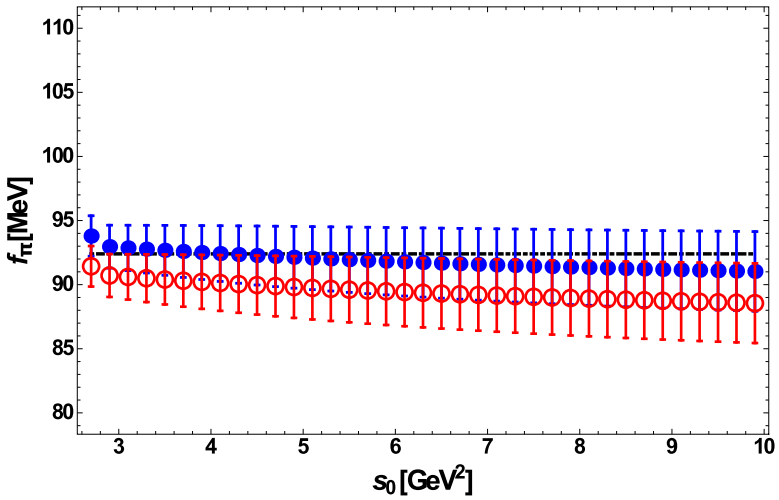

Figure 2.3: Results for f_π as a function of s_0 from the FESR, eq. (2.26), for the pinched kernel eq. (2.19), with $s_1 = 2.7\,\mathrm{GeV}^2$. The corrected ALEPH data [14] has been used in the hadronic integral. Blue dots are for $\alpha_s = 0.354$, and open red circles for $\alpha_s = 0.328$, corresponding to the maximum and minimum values of $\alpha_s = 0.341 \pm 0.013$ from [20]. The gluon condensate gives a negligible contribution.

Numerically, the condensates give a negligible contribution to this sum rule as $C_2\langle\mathcal{O}_2\rangle = 0$, and $C_4\langle\mathcal{O}_4\rangle = 0.017 \pm 0.012\,\mathrm{GeV}^4$ [16]. The uncertainty in the strong coupling lies well within the error bars due to the data. The result for f_π as a function of s_0, with $\alpha_s(m_\tau^2) = 0.341 \pm 0.013$ [20] is shown in Figure 2.3. There is good agreement between the right-hand-side of this FESR and the experimental value of f_π. The central values show a systematic downward slope which, at first sight, might be an indication of DV with increasing s_0. However, this specific decreasing behaviour is essentially due to the specific functional form of the pinched kernel, eq. (2.19).

The sum rule in eq. (2.26) was constructed in such a way that the contribution from pQCD in the energy range between s_1 and s_0 disappears completely. If hypothetical data in the extended energy range were not described by pQCD, for example if there are DV in this s-range, one would obtain a result for the right-hand side of eq. (2.26) which disagrees with the expectation $2f_\pi^2$. The nice agreement observed in Figure 2.3 is thus an indication that DV are either irrelevant in this channel, or they are also suppressed to a negligible level by pinching with the kernel eq. (2.19).

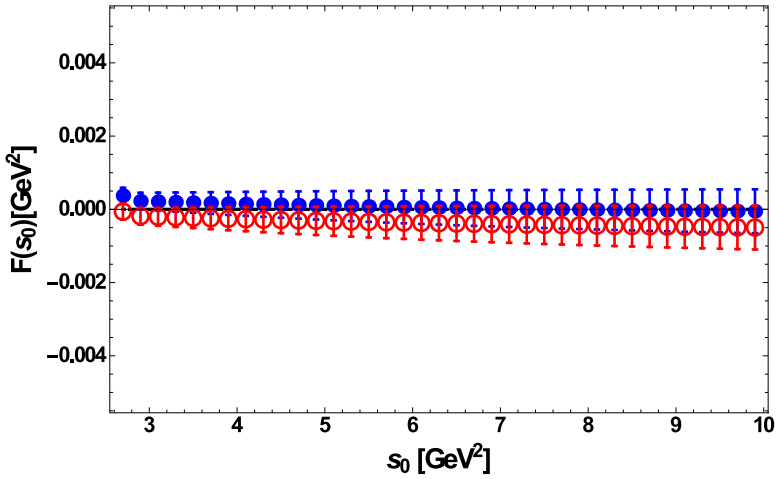

Figure 2.4: Results in the vector channel, i.e. $F(s_0)$ as a function of s_0 from the FESR, eq. (2.27), for the pinched kernel eq. (2.19), with $s_1 = 2.7\,\text{GeV}^2$. The corrected ALEPH data [14] has been used in the hadronic integral. Blue dots are for $\alpha_s = 0.354$, and open red circles for $\alpha_s = 0.328$, corresponding to the maximum and minimum values of $\alpha_s = 0.341 \pm 0.013$ from [20]. The gluon condensate gives a negligible contribution.

Turning to the vector channel, and in analogy with eq. (2.26), we define

$$F(s_0) = -\int_0^{s_1} ds\, P(s)\, \frac{1}{\pi}\, \text{Im}\Pi_V^{DATA}(s) - \frac{1}{2\pi i} \oint_{|s|=s_0} ds\, P(s)\, \Pi(s)_V^{PQCD}(s)$$
$$+ \frac{1}{4\pi^2} \left[C_2\langle\mathcal{O}_2\rangle - \gamma(s_0, s_1)\, C_4\langle\mathcal{O}_4\rangle\right] . \tag{2.27}$$

Since there is no pole in this channel, we expect to obtain $F(s_0) = 0$ if the data are described by the OPE. Results from this FESR using the kernel, eq. (2.19), are shown in Figure 2.4, indicating a very good saturation of the sum rule within errors. Since in this channel there are independent data from e^+e^- annihilation into hadrons [23, 24] we can use these data beyond the end-point of the τ-data in the FESR to obtain

$$F(s_0) = -\int_0^{s_1} ds\, P(s)\, \frac{1}{\pi}\, \text{Im}\,\Pi_V^{DATA}(s) - \frac{1}{8\,\pi^2} \int_{s_1}^{s_0} ds\, P(s)\, R(s)$$
$$- \frac{1}{2\pi i} \oint_{C(|s_0|)} ds\, P(s)\, \Pi_V^{PQCD}(s)\,, \tag{2.28}$$

where the condensates have been omitted, and $\text{Im}\ \Pi_V|^{DATA}(s)$ is the experimental spectral function from τ-decay, and $R(s)$ is the experimental R-ratio from e^+e^- annihilation,

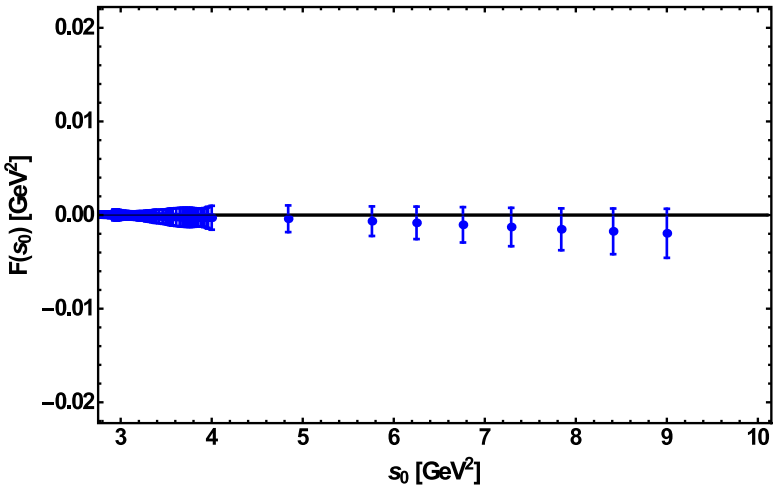

Figure 2.5: Results in the vector channel, i.e. $F(s_0)$ as a function of s_0 from the FESR eq. (4.28), with the pinched kernel, eq. (2.24). The corrected ALEPH data [14] has been used in the hadronic integral followed by e^+e^- data [24] beyond the τ-decay end point. The strong coupling is $\alpha_s(M_\tau^2) = 0.341 \pm 0.013$ [20], but with this scale there is no visible difference between results for the maximum and minimum values of α_s. Error bars are fully dominated by the data, and the gluon condensate gives a negligible contribution.

$R(s) = 8\,\pi\,\mathrm{Im}\,\Pi_V(s)$. Results from eq. (2.28), using contour improved perturbation theory are shown in Figure 2.5. The good agreement between the expected value of zero and the right-hand side of eq. (2.28) renders further support to the procedure followed before in this analysis, i.e. using the pinched kernel eq. (2.19) to minimize the contribution above the kinematical end-point of the measured τ-data. This approach allows us to extend the analysis well beyond that end-point, involving data accounted for by pQCD.

It is important to observe the difference between results for $F(s)$ in Figure 2.4, where pQCD but no e^+e^- data was used in the extension, and $F(s)$ in Figure 2.5 where these data were used instead of pQCD. The central values shown in Figure 2.5 exhibit a small systematic deviation from $F(s_0) = 0$, which increases slightly with increasing energy. This deviation is already quite noticeable from the graph of $R(s)$, in this energy region, on page 535 of [23]. Indeed, the data lie systematically above pQCD in the region $2.0\,\mathrm{GeV} \lesssim \sqrt{s} \lesssim 3.0\,\mathrm{GeV}$. This issue could be quite important in connection with the leading hadronic contribution to the $g-2$ of the muon [25] or for the evaluation of the hadronic contribution to $\alpha_{\mathrm{em}}(M_Z^2)$. In any case, the slight negative slope shown by the results in Figure 2.5 could be understood as consequence of the pinched kernel, eq. (2.24), it is far less efficient at energies well beyond $s \equiv s_1 \simeq 2.7\,\mathrm{GeV}^2$, where it vanishes.

We consider FESR with explicit DV using the model of [22], and in the region of the τ-decay data, to wit. The starting point is Cauchy's theorem in the complex s-plane

$$\int_0^{s_0} ds\, P(s)\, \frac{1}{\pi} \mathrm{Im}\, \Pi(s) = -\frac{1}{2\pi i} \oint_{C(|s_0|)} ds\, P(s)\, \Pi(s)\,, \tag{2.29}$$

where $P(s)$ is an arbitrary polynomial, and $\Pi(s)$ is either the vector, $\Pi(s)_V$ or the axial-vector correlator, $\Pi(s)_A$. The integrand on the right-hand side above is now written as

$$\Pi(s) = \Pi^{OPE}(s) + \Delta(s)\,, \tag{2.30}$$

where $\Delta(s)$ is the difference between the correlator and its OPE expansion, $\Delta(s) = \Pi(s) - \Pi^{OPE}(s)$. The DV contribution $\mathcal{D}(s_0)$ is now defined as

$$\mathcal{D}(s_0) = -\frac{1}{2\pi i} \oint_{C(|s_0|)} ds\, P(s)\, \Delta(s)\,, \tag{2.31}$$

and Cauchy's theorem, eq. (2.29), becomes

$$\int_0^{s_0} ds\, P(s)\, \frac{1}{\pi} \mathrm{Im}\, \Pi(s) = -\frac{1}{2\pi i} \oint_{C(|s_0|)} ds\, P(s)\, \Pi^{OPE}(s) + \mathcal{D}(s_0)\,. \tag{2.32}$$

Finally, the DV can also be written in terms of the line integral

$$\mathcal{D}(s_0) = -\int_{s_0}^{\infty} ds\, P(s)\, \frac{1}{\pi}\, \mathrm{Im}\, \Delta(s)\,, \tag{2.33}$$

where $\mathrm{Im}\, \Delta(s)$ is model dependent. Notice that in principle $\Delta(s)$ is not chiral symmetric, true also in practice [22].

In the explicit DV model of [22] $\mathrm{Im}\, \Delta(s)$ in eq. (2.33) is given as

$$\frac{1}{\pi}\, \mathrm{Im}\, \Delta_{V,A}(s) = e^{-(\delta_{V,A} + \gamma_{V,A}\, s)}\, \sin\left(\alpha_{V,A} + \beta_{V,A}\, s\right)\,. \tag{2.34}$$

The eight free parameters $\delta_{V,A}$, $\gamma_{V,A}$, $\alpha_{V,A}$, and $\beta_{V,A}$ were determined in [22] from the corrected ALEPH τ-decay data [14]. Here we use the results obtained from fits in the region $1.475\,\mathrm{GeV}^2 \leq s \leq M_\tau^2$, i.e. $\delta_V = 3.45 \pm 0.32$, $\gamma_V = 0.61 \pm 0.20\,\mathrm{GeV}^{-2}$, $\alpha_V = -0.63 \pm 0.67$, $\beta_V = 3.42 \pm 0.38\,\mathrm{GeV}^{-2}$, $\delta_A = 2.23 \pm 0.33$, $\gamma_A = 1.25 \pm 0.21\,\mathrm{GeV}^{-2}$, $\alpha_A = 3.45 \pm 0.81$, and $\beta_A = -3.02 \pm 0.42\,\mathrm{GeV}^{-2}$. We note that there are some other fits in [22] for different minimum values (s_{min}) of s, however we would be making a mistake if we consider fits that do not include the complete region of our analysis, because the fits can not provide information in regions where they are not computed, otherwise these models would be based on first principles, thus they should solve DV completely.

This model was used in [22] without a specific pinched kernel, as well as with the kernel

$$P(s) = 1 - \left(\frac{s}{s_0}\right)^2\,. \tag{2.35}$$

With this kernel containing a second power of s, the condensate of dimension $d = 6$ contributes. We take its value from Ref. [22] and use (in our notation) $C_6\langle\mathcal{O}_6\rangle = -0.300$ GeV^6 in the vector channel and $C_6\langle\mathcal{O}_6\rangle = 0.233$ GeV^6 in the axial-vector channel.
It should be pointed out that a kernel linear in s, e.g. eq. (2.24), was not considered in [22] for reasons given in [26]. This explicit model of DV will be used to determine f_π and $F(s_0)$, in the axial-vector and in the vector channel, respectively, and in the region of the ALEPH data. Results will be contrasted with those from our FESR without an explicit DV model, but with the pinched kernel eq. (2.24). In the axial-vector channel the FESR is now

$$8\,\pi^2\,f_\pi^2 = -4\,\pi^2\int_0^{s_0} ds\,\left(1-\frac{s}{s_0}\right)\frac{1}{\pi}\,\mathrm{Im}\,\Pi_A|^{DATA}(s) + s_0\,[M_2(s_0)-M_4(s_0)] + \left[C_2\langle\mathcal{O}_2\rangle + \frac{C_4\langle\mathcal{O}_4\rangle}{s_0}\right]. \tag{2.36}$$

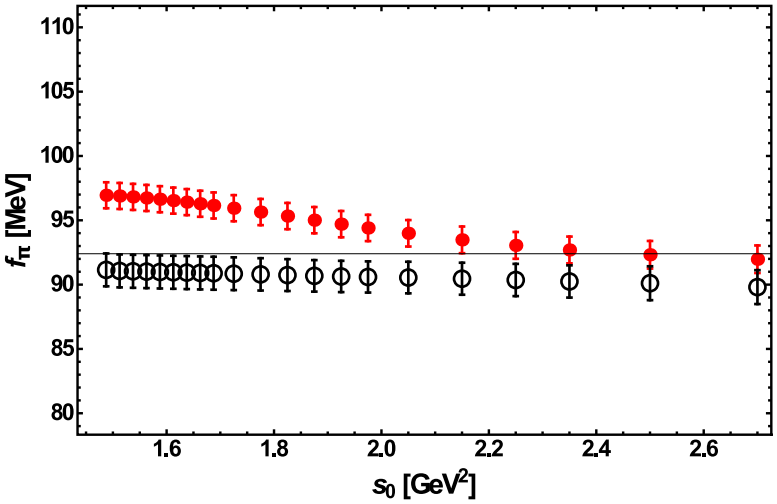

Figure 2.6: Results in the axial-vector channel for f_π as a function of s_0 from the FESR eq. (2.36) with the pinched kernel, eq. (2.24), and no DV model (red dots), and with the DV model of [22] with their pinching kernel, eq. (2.35)), (open black circles). The corrected ALEPH [14] data has been used in the hadronic integral. The strong coupling is $\alpha_s(M_\tau^2) = 0.341$ for the red dots, and $\alpha_s(M_\tau^2) = 0.338$ for the open black circles, the latter chosen to agree with the value used in [22] for the calculation with DV.

Results for f_π in the τ-decay data region are shown in Figure 2.6. Red dots are from our FESR, eq. (2.36), with the pinched kernel eq. (2.24) and no DV model. Open black circles are from the DV model of [22], eq. (2.34), with the pinched kernel eq. (2.35). The FESR in the vector channel is obtained from eq. (2.36) by replacing the left hand side

by $F(s_0)$, and $\Pi_A(s)$ by $\Pi_V(s)$. The results are shown in Figure 2.7, where the symbols have the same meaning as in Figure 2.6. There is good agreement between all results for $s \gtrsim 2.0\,\mathrm{GeV}^2$.

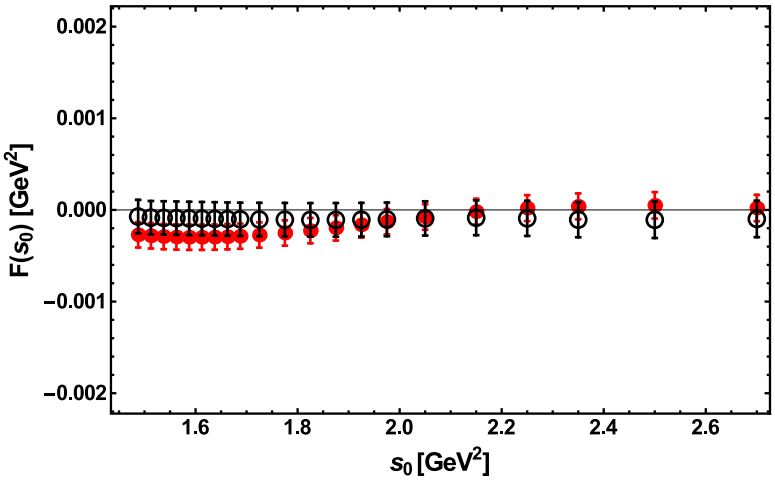

Figure 2.7: Results in the vector channel, i.e. $F(s_0) = 0$ as a function of s_0 from the FESR eq. (2.27), with the pinched kernel, eq. (2.24) and no DV model (red dots), and with the DV model of [22] with their pinching kernel, eq. (2.35), (open black circles). The corrected ALEPH [14] data has been used in the hadronic integral. The strong coupling is $\alpha_s(M_\tau^2) = 0.341$ for the red dots, and $\alpha_s(M_\tau^2) = 0.338$ for the open black circles, the latter chosen to agree with the value used in [22] for the calculation with DV. Notice the vertical scale being different from Figure 2.4 to allow for differentiation.

As we can see, DV is still an open problem, far to be solved, therefore we think our following work should be targeted to a quantitative analysis in as much as possible observables. But it is worth to mention flatly that based on the results we have shown here, at least in these observables there is not space to argue that DV models are imperative to improve FESR with pinching kernels results, or in other words that DV models omission is equivalent to ignore DV itself as in [11], and [22] argue.

CHAPTER 3

APPLICATIONS OF QCD SUM RULES.

We have already developed in chapter 2 the basis of FESR, the importance of pinching kernels and their implications in the DV problem. Then in this chapter we apply both of them and show how FESR+pinching kernels work very well, for this purpose we compute the following quantities: (1) The chiral perturbation theory parameters $\bar{L}_{10}$, C_{87}, the chiral vacuum condensates $\langle\mathcal{O}_6\rangle$, $\langle\mathcal{O}_8\rangle$ and the vacuum condensate $\langle C_2O_2\rangle$, $\langle C_4O_4\rangle$. All of these quantities are from QCD, thus as input information in FESR we use the hadronic spectral function. Actually we use experimental data on hadronic decays of the τ-lepton, to compute all the quantities previously mentioned. A key advantage of hadronic τ-decay data is that it determines both the vector and the axial-vector spectral functions. (2) The gluon condensate $\langle\frac{\alpha}{\pi}G^2\rangle$ another QCD quantity is determined from e^+e^- annihilation data in the charm-quark region. Then this chapter is split in two parts as follow.

FESR at τ-lepton decay regime.

Most of $\bar{L}_{10}$, C_{87}, $\langle\mathcal{O}_6\rangle$, $\langle\mathcal{O}_8\rangle$, $\langle C_2O_2\rangle$ and $\langle C_4O_4\rangle$ determinations made use of the hadronic spectral functions in the vector and axial-vector channel as measured by the ALEPH Collaboration [12]. This data base was known to be problematic due to the incompleteness of the data correlations [26], thus casting some doubt on the uncertainties in results obtained using these data. A new ALEPH data set has recently become available [14], with the data organized in different bins, and with a corrected error correlation matrix. Now we employ these data to revisit the vacuum condensate determinations, the saturation of

chiral sum rules, and the determination of $\bar{L}_{10}$, C_{87}, the chiral condensates of dimension $d = 6$ and $d = 8$. The procedure is based on FESR, weighted with suitable integration kernels to account for potential DV. Our results mostly confirm central values obtained previously using the original ALEPH data base, with uncertainties being slightly higher in some cases, and lower in others.

We consider the (charged) vector and axial-vector current correlators

$$\begin{aligned}\Pi^{VV}_{\mu\nu}(q^2) &= i\int d^4x\; e^{iqx}\langle 0|T(V_\mu(x)V^\dagger_\nu(0))|0\rangle \\ &= (-g_{\mu\nu}\; q^2 + q_\mu q_\nu)\;\Pi_V(q^2)\;,\end{aligned} \tag{3.1}$$

$$\begin{aligned}\Pi^{AA}_{\mu\nu}(q^2) &= i\int d^4x\; e^{iqx}\langle 0|T(A_\mu(x)A^\dagger_\nu(0))|0\rangle \\ &= \;(-g_{\mu\nu}q^2 + q_\mu q_\nu)\;\Pi_A(q^2) - q_\mu q_\nu\;\Pi_0(q^2)\;,\end{aligned} \tag{3.2}$$

where $V_\mu(x) =: \bar{u}(x)\gamma_\mu d(x)\;:$, $A_\mu(x) =: \bar{u}(x)\gamma_\mu\gamma_5 d(x)\;:$, with $u(x)$ and $d(x)$ the quark fields, and $\Pi_{V,A}(q^2)$ normalized in pQCD (in the chiral limit) according to eq. (2.9), where $s \equiv q^2 > 0$ is the squared energy. Lorentz decomposition is used to separate the correlation function into its $J = 1$ and $J = 0$ parts. To the accuracy needed in the following, the vector current can be assumed to be conserved. The correlators are well-known up to five-loop order [27]. Solving the renormalization group equation for the strong coupling, one can express $\alpha_s(s)$ in terms of the coupling at a given scale s_0, with the result at four-loop order being [28]

$$\begin{aligned}a_s(s) = a_s(s_0) &+ a_s^2(s_0)\left(\frac{1}{2}\,\beta_1\,\eta\right) + a_s^3(s_0)\left(\frac{1}{2}\,\beta_2\,\eta + \frac{1}{4}\,\beta_1^2\,\eta^2\right) \\ &+ a_s^4(s_0)\left[\frac{1}{2}\,\beta_3\,\eta + \frac{5}{8}\,\beta_1\,\beta_2\,\eta^2 + \frac{1}{8}\,\beta_1^3\,\eta^3\right] \\ &+ a_s^5(s_0)\left[-b_3\,\eta + \frac{3}{8}\,\beta_2^2\,\eta^2 + \frac{3}{4}\,\beta_1\,\beta_3\;\eta^2 + \frac{13}{24}\,\beta_1^2\,\beta_2\,\eta^3 + \frac{1}{16}\,\beta_1^4\,\eta^4\right]\end{aligned} \tag{3.3}$$

with

$$\eta = \ln\left(\frac{s}{s_0}\right)\;. \tag{3.4}$$

The coefficients of the β -function are given by

$$\beta_1 = -\frac{1}{2}\left(11 - \frac{2}{3}n_F\right) , \quad \beta_2 = -\frac{1}{8}\left(102 - \frac{38}{3}n_F\right) ,$$
$$\beta_3 = -\frac{1}{32}\left(\frac{2857}{2} - \frac{5033}{18}n_F + n_F^2\right) , \tag{3.5}$$

and

$$b_3 = \frac{1}{4^4}\left[\frac{149753}{6} + 3564\zeta_3 - \left(\frac{1078361}{162} + \frac{6508}{27}\zeta_3\right) n_F \right.$$
$$\left. + \left(\frac{50065}{162} + \frac{6472}{81}\zeta_3\right) n_F^2 + \frac{1093}{729}n_F^3\right] , \tag{3.6}$$

with $\zeta_3 = 1.202$.

As we mention in chapter 2, non-perturbative contributions are parametrized in terms of the vacuum condensates entering the OPE

$$4\pi^2\Pi(Q^2)|_{V,A} = \sum_{N=1}^{\infty} \frac{1}{Q^{2N}}\, C_{2N}(Q^2,\mu^2)\, \langle O_{2N}(\mu^2)\rangle|_{V,A} , \tag{3.7}$$

where $Q^2 = -q^2$, and μ is a renormalization scale. In principle, the lowest dimension is $d = 4$ as there are no gauge invariant operators of dimension $d = 2$ in QCD. However, the absence of such a condensate will be confirmed by the results of this analysis. At dimension $d = 4$, and in the chiral limit, the only contribution is from the (chiral-symmetric) gluon condensate

$$C_4\langle O_4\rangle|_{V,A} = \frac{\pi^2}{3}\,\langle \frac{\alpha_s}{\pi}\, G_{\mu\nu}\, G^{\mu\nu}\rangle , \tag{3.8}$$

where α_s is the running strong coupling, and in the sequel $\langle 0|O_{2N}|0\rangle \equiv \langle O_{2N}\rangle$ is to be understood. This condensate is renormalization group invariant to all orders in pQCD (in the chiral limit).

Invoking Cauchy's theorem in the complex squared energy s-plane, and assuming (global) quark-hadron duality leads to the FESR

$$-\frac{1}{2\pi i}\oint_{|s|=s_0} ds\; f(s)\; \Pi(s)|_{V,A}^{QCD} = \int_0^{s_0} ds\; f(s)\; \rho_{V,A}(s) , \tag{3.9}$$

where $f(s)$ is an integration kernel and $\rho_{V,A}(s)$ are the hadronic spectral functions,

$$\rho_{V,A}(s) = \frac{1}{\pi}\,\mathrm{Im}\,\Pi(s)|_{V,A}^{HAD} = \frac{1}{2\pi^2}\,[v(s),a(s)]_{\mathrm{ALEPH}} \tag{3.10}$$

provided by the ALEPH data. Since pQCD is not applicable on the positive real s-axis, as we discussed in chapter 2, pinching kernels are used to reduce the impact of $\Pi(s)|^{QCD}_{V,A}$ in the contribution of the integration contour near the positive real axis in eq. (3.9). In particular, in [29] shown for the old ALEPH data that there is clear evidence that duality is satisfied towards the end of the decay spectrum. In practice, the absence of DV can be inferred from sum rules where their values are known from other sources or, less compelling, from the stability of the integral against variations of the upper limit of integration s_0. We will demonstrate below that duality can be observed with the new ALEPH data for many sum rules.

The contour integral in eq. (3.9) is usually computed using fixed order perturbation theory (FOPT) or contour improved perturbation theory (CIPT). In the former case the strong coupling is frozen at a scale s_0 and the renormalization group (RG) is implemented after integration. In CIPT, $\alpha_s(s)$ is running and the RG is used before integrating, thus requiring solving numerically the RG equation for $\alpha_s(s)$ at each point on the integration contour. In the specific case of the determination of the vacuum condensates we found CIPT to be superior to FOPT in that results turn out to be more stable as a function of s_0. To implement CIPT it is convenient to introduce the Adler function

$$D(s) \equiv -s\frac{d}{ds}\Pi(s) \ , \tag{3.11}$$

with $\Pi(s) \equiv \Pi_{V,A}(s)$. Invoking Cauchy's theorem and after integration by parts the following relation is obtained

$$\oint_{|s|=s_0} ds \ \left(\frac{s}{s_0}\right)^N \ \Pi(s) = \frac{1}{N+1}\ \frac{1}{s_0^N}\ \oint_{|s|=s_0} \frac{ds}{s}\ \left(s^{N+1} - s_0^{N+1}\right)\ D(s) \ . \tag{3.12}$$

After RG improvement, the perturbative expansion of the Adler function becomes

$$D(s) = \frac{1}{4\,\pi^2} \sum_{m=0} K_m \left[\frac{\alpha_s(-s)}{\pi}\right]^m \ , \tag{3.13}$$

where [27] $K_0 = K_1 = 1$, $K_2 = 1.6398$, $K_3 = 6.3710$, for three flavours, and $K_4 = 49.076$ [30]. The vacuum condensates are then determined from the pinched FESR

$$C_{2N+2}\langle O_{2N+2}\rangle = (-1)^{N+1}\ 4\pi^2\ s_0^N\ \int_0^{s_0} ds \left[1 - \left(\frac{s}{s_0}\right)^N\right] \frac{1}{\pi}\text{Im}\ \Pi(s)^{HAD}$$

$$+ (-1)^N s_0^{N+1}[M_0(s_0) - M_N(s_0)] \ , \tag{3.14}$$

where the moments $M_N(s_0)$ are given by

$$M_N(s_0) = \frac{1}{2\pi}\frac{1}{(N+1)}\sum_{m=0} K_m \left[I_{N+1,m}(s_0) - I_{0,m}(s_0)\right] , \tag{3.15}$$

with

$$I_{N,m} \equiv i \oint_{|s|=s_0} ds \left(\frac{s}{s_0}\right)^N \left[\frac{\alpha_s(-s)}{\pi}\right]^m . \tag{3.16}$$

The latest ALEPH data compilation [14] includes the vector and axial-vector channels separately, as well as their sum. Their data are given in tables for the normalised invariant mass-squared distributions. We determine the spectral functions as described, for example, in [12] and approximate the sum rule integrals by sums over bins, taking into account the corrected correlation matrix. We should note that we will omit the last two points with the highest s values in the figures for our results to be discussed below; they have very large experimental uncertainties and do not affect our results. We use the following values for the input parameters

$$\begin{aligned} m_\pi &= 139.57018(35)\ \text{MeV}\,, \\ f_\pi &= 92.21(14)\ \text{MeV}\,, \\ M_\tau &= 1776.82(16)\ \text{MeV}\,, \\ V_{ud} &= 0.97425(22)\,, \end{aligned} \tag{3.17}$$

$$S_{EW} = 1.0198\,, \quad B_e = 0.17818\,. \tag{3.18}$$

The first four values are taken from the particle data group [23]. S_{EW} is needed to include the renormalization-group improved electroweak corrections [31]. As the leptonic branching ratio B_e was not updated in the recent paper [14], we again use the one given in the earlier ALEPH report [12]. From the latest analysis [20], we have $\alpha_s(M_\tau^2) = 0.341 \pm 0.013$ in CIPT and $\alpha_s(M_\tau^2) = 0.319 \pm 0.014$ in FOPT. For consistency we use the CIPT result in the following.

Proceeding with the determination of a potential $d = 2$ condensate (presumably chiral-symmetric) we have used the data base for $V + A$ in the FESR and divided the answer by a factor two. In Figure 3.1 we show the result in the stability region. The red dots correspond to the minimum value of α_s and the blue dots to its maximum value. As expected, this $d = 2$ term is consistent with zero. Notice that in this case there is no pinching integration kernel as $N = 0$ in eq. (3.14).

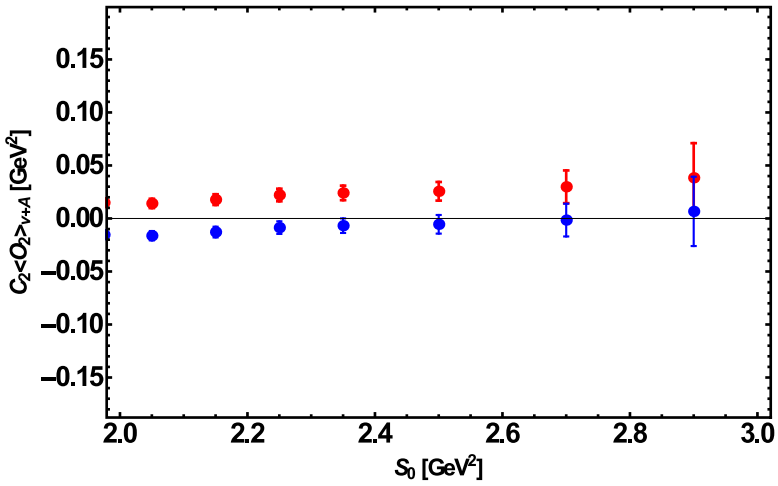

Figure 3.1: The dimension $d = 2$ condensate in CIPT from the FESR, eq. (3.14), with $N = 0$. The ALEPH data for the $V + A$ spectral function was used, and the resulting condensate divided by 2. The two sets of points correspond to $\alpha_s = 0.354$ (blue dots) and $\alpha_s = 0.328$ (red dots).

Next, we make use of this result and consider the pinched FESR, eq. (3.14), with $N = 1$. The condensate of $d = 4$ is shown in Figure 3.2, for V, A and $\frac{1}{2}(V + A)$. We observe that for $s_0 \gtrsim 2.2$ GeV^2 and within errors

$$C_4\langle O_4\rangle_V = C_4\langle O_4\rangle_A = C_4\langle O_4\rangle_{\frac{1}{2}(V+A)} \tag{3.19}$$

over a wide range of s_0. This equality is an essential result of QCD. In addition the $d = 4$ condensate is generally expected to be positive because it is dominated by the gluon condensate, eq. (3.8), which in turn is directly related to the vacuum energy density [3],

$$\varepsilon = \frac{\pi}{8\alpha_s^2}\beta(\alpha_s)\langle\frac{\alpha_s}{\pi}\,G_{\mu\nu}\,G^{\mu\nu}\rangle\,. \tag{3.20}$$

Therefore, the sign and magnitude of the gluon condensate $\langle\frac{\alpha_s}{\pi}\,G_{\mu\nu}\,G^{\mu\nu}\rangle$ are of fundamental importance for the understanding of the strong interactions. A negative value of ε is expected from models such as the bag model. In our analysis we obtain for $\alpha_s(M_\tau^2) = 0.341$

$$C_4\langle O_4\rangle = (0.017 \pm 0.012)\ \text{GeV}^4\,, \tag{3.21}$$

where this value is obtained by reading results from the $V+A$ spectral function at $s_0 = 2.35$ GeV^2, i.e. at the point where $C_4\langle O_4\rangle$ from the V and A channels become equal. This value is consistent within errors with the points at higher values of s_0 and agrees with a previous determination [29] using the original ALEPH data base [12]. However, the uncertainty is

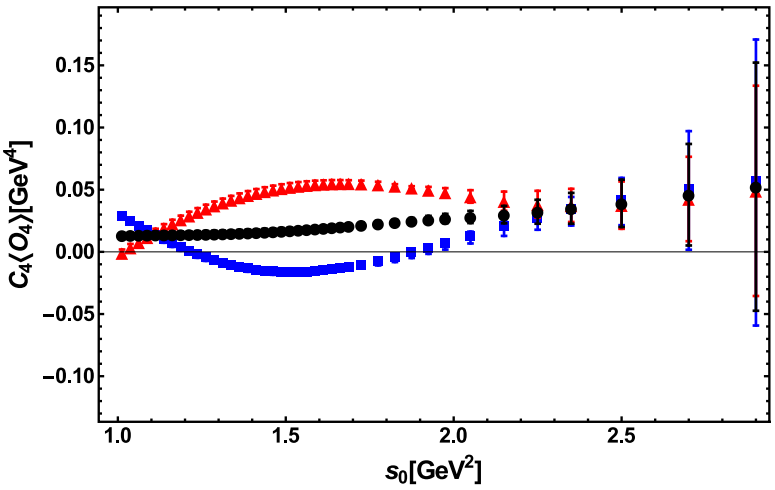

Figure 3.2: The dimension $d = 4$ condensate in CIPT from the FESR, eq. (3.14), with $N = 1$ and $\alpha_s(M_\tau^2) = 0.341$. The ALEPH data for the V (upper red triangles), A (lower blue squares) and $\frac{1}{2}(V + A)$ (middle black dots) spectral function were used.

now larger due to the new ALEPH error correlation matrix. We observe that the precise value for α_s chosen in the evaluation of the condensate has a relatively large impact on the result: the uncertainty of ± 0.013 for $\alpha_s(M_\tau^2)$ given in [20] gives rise to an additional uncertainty of ± 0.018 for $C_4\langle O_4\rangle$. We repeated the analysis using FOPT. The results are very similar, though. For example, for the central FOPT value $\alpha_s(M_\tau^2) = 0.319$ we obtain $C_4\langle O_4\rangle = (0.022 \pm 0.006)$ GeV^4. Combining results, we can say that all evidence points to a positive value of $C_4\langle O_4\rangle \lesssim 0.035$ GeV^4 which is equal for the vector and the axial-vector correlators. In contrast, in the updated analysis of the ALEPH data [14] unequal and negative results for the V and A channels have been obtained.

The next condensates, i.e. with dimension $d = 6$, in the vector and the axial-vector channels do not show a stability region. This type of FESR is not suited to extract higher dimensional condensates because the power weight in the FESR increasingly emphasizes the high energy region, where experimental errors are large and where the condensates are the result of a fine balanced cancellation between the hadronic integral and the pQCD moments, with a marginally meaningful result at $d = 4$, but not beyond. Later we shall determine the chiral condensates of dimension $d = 6$ and $d = 8$, which do not suffer from this handicap as the perturbative contribution cancels exactly (in the chiral limit).

The two Weinberg sum rules (WSR) [32] were first derived in the framework of chiral $SU(2) \times SU(2)$ symmetry and current algebra, retaining their validity in QCD in the chiral limit, and read

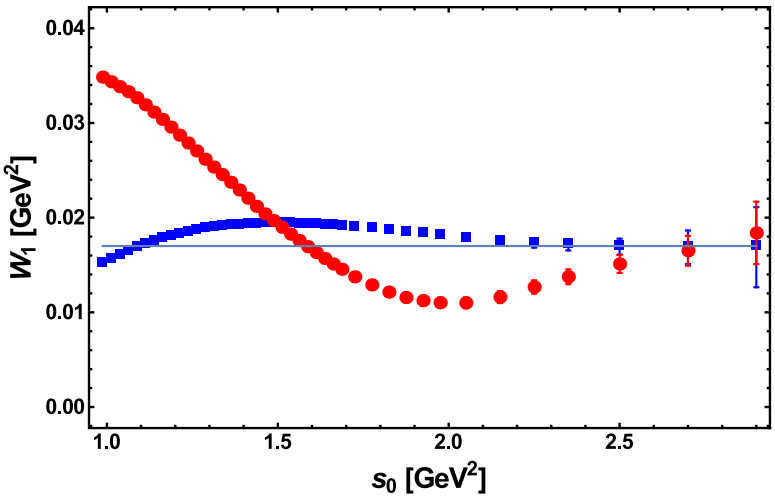

Figure 3.3: Red dots are the left-hand-side of the standard Weinberg sum rule, Eq. (3.22), and blue squares the left hand side of the pinched sum rule, eq. (3.24). The dotted line is the right-hand-side, $2f_\pi^2$.

$$W_1 \equiv \int_0^\infty ds\,\frac{1}{\pi}\,[\mathrm{Im}\Pi_V(s) - \mathrm{Im}\Pi_A(s)] = 2\,f_\pi^2\,, \tag{3.22}$$

$$W_2 \equiv \int_0^\infty ds\,s\,\frac{1}{\pi}\,[\mathrm{Im}\Pi_V(s) - \mathrm{Im}\Pi_A(s)] = 0\,, \tag{3.23}$$

where $f_\pi = 92.21 \pm 0.14\,\mathrm{MeV}$ [23]. The integration region can be split into two parts, one in the range $0 - s_0$ and the other in $s_0 - \infty$. Since the spectral function difference vanishes in pQCD for s_0 sufficiently large, these sum rules effectively become FESR. However, as pointed out long ago [17], the original τ-decay ALEPH data [12] did not saturate these integrals up to the kinematic end point $s_0 \simeq M_\tau^2$. This could also be said for the updated ALEPH data [14] if the existence of a plateau of the central values is taken as a criterion for saturation (see red dots in Figure 3.3 for W_1 and blue dots in Figure 3.4 for W_2). The size of the experimental uncertainties, however, does not allow us to conclude that saturation has not been reached. A much better behaviour is achieved after introducing a simple pinched kernel and combining the two sum rules into one

$$W_{1P}(s_0) \equiv \int_0^{s_0} ds\left(1 - \frac{s}{s_0}\right)\frac{1}{\pi}\,[\mathrm{Im}\Pi_V(s) - \mathrm{Im}\Pi_A(s)] \;= 2\,f_\pi^2\,. \tag{3.24}$$

The result is shown in Figure 3.3 (blue squares), indicating a very good saturation of the pinched sum rule. This supports the use of simple integration kernels, although DV could

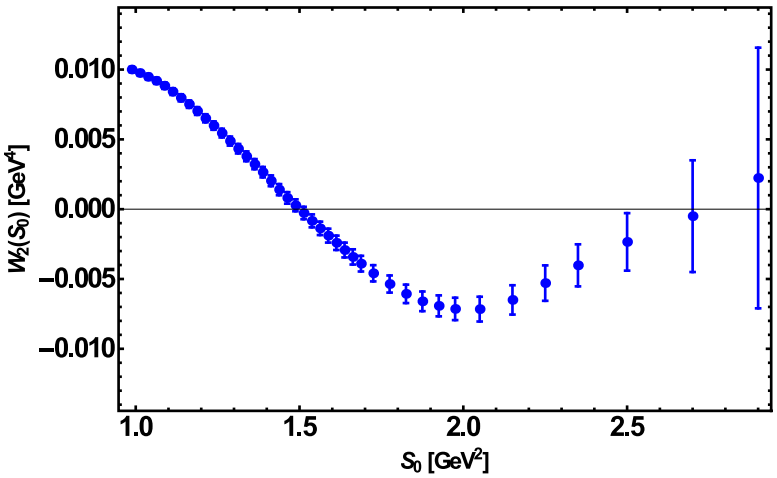

Figure 3.4: The second Weinberg sum rule W_2 as a function the upper limit of integration.

be channel or application dependent.

The two Weinberg sum rules are particularly interesting since they would not be satisfied if there were substantial DV present, i.e. non-perturbative contributions beyond perturbative QCD and OPE contributions. The issue of DV is indeed most prominent in the context of the $V - A$ correlator, since the perturbative component cancels out leaving a purely non-perturbative result. The two simple, i.e. un-pinched Weinberg sum rules agree with the OPE expectations only near the end of the decay spectrum $s_0 \simeq 2.7$ GeV^2. Because of experimental limitations, the errors are relatively large and no definite conclusions on the relevance of duality violations can be drawn in this case. The last two experimental points should be ignored in the discussion because they cannot be accommodated either by pQCD and the OPE or in models for DV . The pinched sum rule, however, is saturated beginning at $s_0 \geq 2.2$ GeV^2 and shows remarkable agreement with the prediction of $2f_\pi^2$. No compelling evidence is seen for the existence of DV in this kinematic domain. We assert that for simple un-pinched Weinberg sum rules, possible DV are not required for $s_0 \gtrsim 2.7$ GeV^2 while for the pinched sum rule possible DV can be ignored beginning at much lower momentum transfers, i.e. already for $s_0 \gtrsim 2.2$ GeV^2. In view of our result it seems very reasonable to take over this conclusion to the separate V and A sum rules. The lack of evidence for DV in the separate V and A correlators at large s_0 was also demonstrated in [21], albeit with the old ALEPH data. These conclusions are in contrast with those following from specific models of DV [11], [15].

Next, we consider the chiral correlator $\Pi(Q^2)|_{V-A}$, and absorb the Wilson coefficients entering eq. (3.7) into the operators, renaming them $\mathcal{O}_N$ to conform with a usual convention

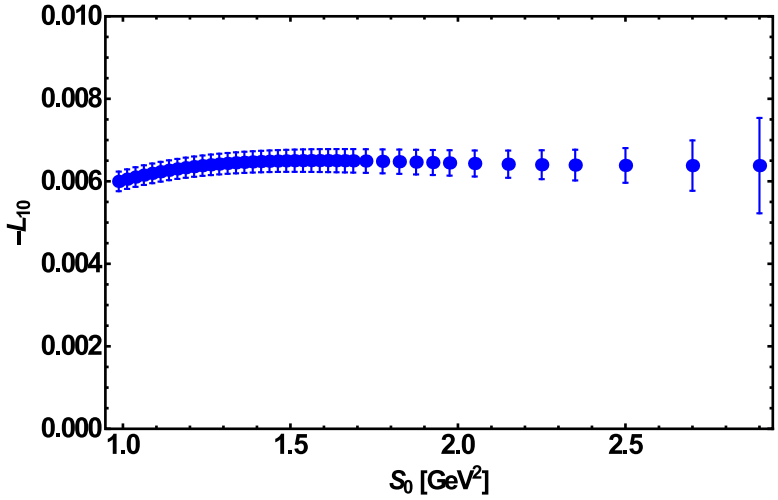

Figure 3.5: The CHPT constant $-\bar{L}_{10}$ obtained from the pinched chiral sum rule for $\bar{\Pi}(0)$ eq. (3.26).

in the literature,

$$\Pi(Q^2)|_{V-A} = \sum_{N=1}^{\infty} \frac{1}{Q^{2N+4}} \langle \mathcal{O}_{2N+4} \rangle \,, \tag{3.25}$$

with the first two chiral condensates being $\langle \mathcal{O}_6 \rangle$ and $\langle \mathcal{O}_8 \rangle$. Dropping the label $V-A$, the finite remainder of this chiral correlator at zero momentum, $\bar{\Pi}(0)$, is given by

$$\bar{\Pi}(0) = \int_0^{s_0} \frac{ds}{s} \frac{1}{\pi} [\mathrm{Im}\Pi_V(s) - \mathrm{Im}\Pi_A(s)] \,, \tag{3.26}$$

where $\mathrm{Im}\Pi_A(s)$ does not include the pion pole.

The chiral correlator at zero momentum, $\bar{\Pi}(0)$, is determined by the Das-Mathur-Okubo (DMO) sum rule [33],

$$\bar{\Pi}(0) = 2\left(\frac{1}{3} f_\pi^2 \langle r_\pi^2 \rangle - \frac{1}{2} F_A\right) = 0.0520 \pm 0.0010 \,, \tag{3.27}$$

where $\langle r_\pi^2 \rangle = 0.439 \pm 0.008$ fm^2 is the electromagnetic radius of the pion [34], and $F_A = 0.0119 \pm 0.0001$ is the radiative pion decay constant [23]. Since the numerical value on the right-hand side of eq. (3.27) is known with high precision, the DMO sum rule is another case where DV would easily become visible. Our results in Figure 3.5 show a wide stability region starting already at $s_0 \simeq 2$ GeV^2 for the pinched DMO sum rule (using eqs. (3.22) and (3.23))

$$\bar{\Pi}(0) = 4\frac{f_\pi^2}{s_0} + \int_0^{s_0} \frac{ds}{s} \left(1 - \frac{s}{s_0}\right)^2 \frac{1}{\pi} [\mathrm{Im}\Pi_V(s) - \mathrm{Im}\Pi_A(s)] \,. \tag{3.28}$$

$\bar{\Pi}(0)$ is proportional to the counter term of the order $\mathcal{O}(p^4)$ Lagrangian of chiral perturbation theory, $\bar{L}_{10}$ [35],

$$\bar{\Pi}(0) = -8\,\bar{L}_{10}\,. \tag{3.29}$$

We find

$$\bar{L}_{10} = -(6.5 \pm 0.1) \times 10^{-3}\,. \tag{3.30}$$

This result is in very good agreement with more recent results using more involved methods to deal with DV (see Table 2.1). It also agrees with lattice QCD determinations within their larger uncertainties [36].

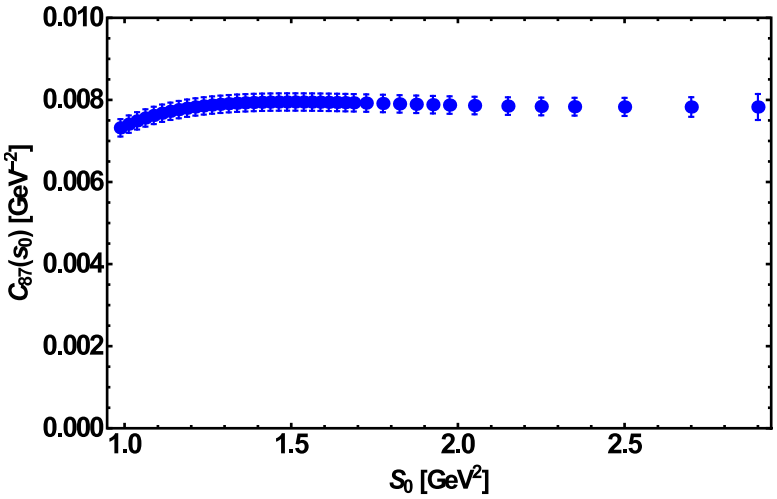

Figure 3.6: The $\mathcal{O}(p^6)$ counter term C_{87} of CHPT according to the pinched chiral sum rule eq. (3.31).

The relation between $\bar{\Pi}(0)$ and the precisely known quantities f_π^2, $\langle r_\pi^2 \rangle$ and F_A, is another case where the presence of DV can be tested. We observe that our result shown in Figure 3.5 is very stable with respect to variations of s_0 in the range above 2 GeV^2 and the result from CHPT is reproduced with amazingly good accuracy.

The FESR for the first derivative of the chiral correlator of eq. (3.28), $\bar{\Pi}'(0)$, is related to $\mathcal{O}(p^6)$ counter term. The pinched sum rule reads

$$C_{87} = \bar{\Pi}'(0) + \frac{2f_\pi^2}{m_\pi^4} = \int_0^{s_0} \frac{ds}{s^2}\left(1 - \frac{s^3}{s_0^3}\right)(\rho_V(s) - \rho_A(s)). \tag{3.31}$$

In Figure 3.6 we shows our result from the *r.h.s.* of eq. (3.31) and we can observe a plateau region starting at $s_0 \simeq 1.8$ GeV^2, from this stable region, we get

$$C_{87} = 8.0 \pm 0.2 \times 10^{-3}\ \text{GeV}^{-2}. \tag{3.32}$$

This result is in agreement within the errors with some results using more involved methods to deal with DV (see Table 2.1).

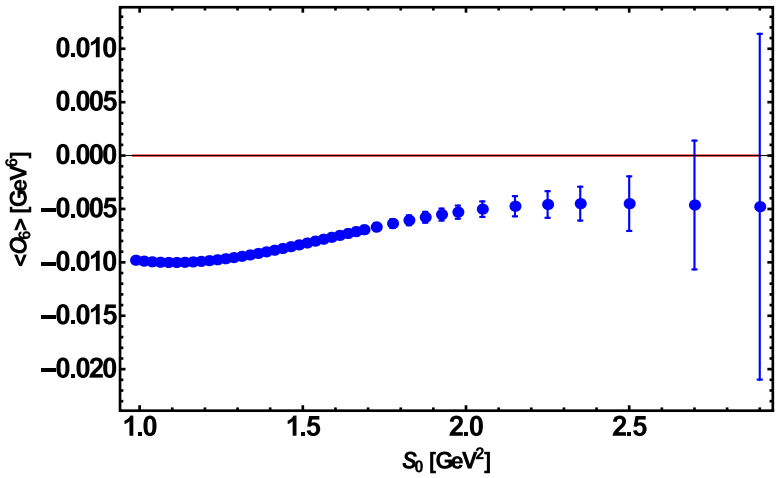

Figure 3.7: The chiral condensate of dimension $d = 6$ from the pinched chiral sum rule eq. (3.33).

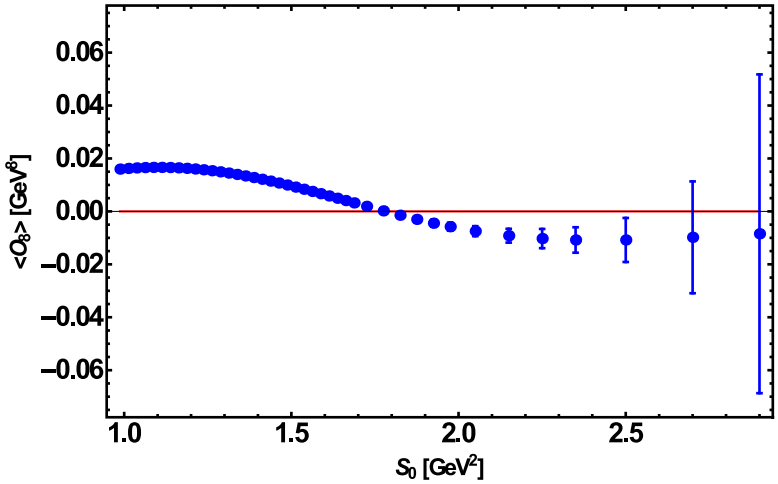

Figure 3.8: The chiral condensate of dimension $d = 8$ from the pinched chiral sum rule eq. (3.36).

Turning to the chiral condensates, for dimension $d = 6$ we use the following pinched FESR [17]

$$\langle \mathcal{O}_6 \rangle = -2\, f_\pi^2\, s_0^2 \,+\, s_0^2 \int_0^{s_0} ds \left(1 - \frac{s}{s_0}\right)^2 \frac{1}{\pi} [\text{Im}\Pi_V(s) - \text{Im}\Pi_A(s)]\ . \tag{3.33}$$

The result is shown in Figure 3.7. Stability is observed for $s_0 \gtrsim 2$ GeV^2. Assuming that DV are not relevant in this kinematic range, we read off the value

$$\langle \mathcal{O}_6 \rangle = -(5.0 \pm 0.7) \times 10^{-3} \text{ GeV}^6. \tag{3.34}$$

This value agrees with results using more involved methods to deal with DV (see Table 2.1). In addition, this value agrees within errors with the four-quark condensate in the vacuum-saturation approximation [37]

$$\langle \mathcal{O}_6 \rangle|_{VS} = -\frac{64\,\pi}{9}\,\alpha_s \langle \bar{q}q \rangle^2 \left[1 + \frac{247}{48\,\pi}\,\alpha_s(s_0)\right] \simeq -4.6 \times 10^{-3}\,\text{GeV}^6. \tag{3.35}$$

Finally, we determine the $d = 8$ chiral condensate from the pinched sum rule [17]

$$\langle \mathcal{O}_8 \rangle = 16 f_\pi^2\, s_0^3 - 3\, s_0^4\, \bar{\Pi}(0) + s_0^3 \int_0^{s_0} \frac{ds}{s} \left(1 - \frac{s}{s_0}\right)^3 (s + 3\, s_0)\, \frac{1}{\pi} [\text{Im}\Pi_V(s) - \text{Im}\Pi_A(s)]\,. \tag{3.36}$$

The result is shown in Figure 3.8, which leads to

$$\langle \mathcal{O}_8 \rangle = -(9.0 \pm 5.0) \times 10^{-3} \text{ GeV}^8\,, \tag{3.37}$$

This value agrees with results using more involved methods to deal with DV (see Table 2.1).

$\langle \frac{\alpha}{\pi} G^2 \rangle$ in the charm-quark region.

As we said in the previous section, in the chiral limit the first non-vanishing power term in the OPE with dimension $d = 4$ has been traditionally identified with the gluon condensate [3], [38], $C_4 \langle \mathcal{O}_4 \rangle = \frac{\pi}{3} \langle \alpha_s G^a_{\mu\nu} G^{a\mu\nu} \rangle$. Having the lowest dimension it dominates the OPE and thus QCDSR analyses of chirality conserving amplitudes, such as e.g. the Adler function. This condensate is also directly related to the vacuum energy density, ε, through eq. (3.20), where $\beta(\alpha_s)$ is the Gell-Mann-Low beta-function normalized as $\beta_1 = -\frac{1}{2}\left(11 - \frac{2}{3} n_F\right)$. The sign and the magnitude of the gluon condensate are of fundamental importance in the understanding of the strong interactions. In addition, the numerical value of the gluon condensate should be chiral symmetric, i.e. determinations from a vector channel correlator should give the same value as those from an axial-vector channel correlator. In spite of more than 35 years of efforts to determine this condensate there is still no clear consensus on its numerical value. There are at least three approaches to determine the gluon condensate. A direct, numerical approach consists in computing the average plaquette in LQCD. Unfortunately, an important and large perturbative component needs

to be subtracted in this approach, and numerical results cover a huge range [39], [40], [41]. The other two approaches to determine the power corrections in the OPE are based on QCDSR.

As we have seen, most of the early determinations of the vacuum condensates in the OPE from FESR, eq. (2.4), were performed with simple kernels $p(s) = s^N$ and using the vector or axial-vector correlators together with data, e.g. from e^+e^- annihilation in the light-quark sector, or τ-lepton hadronic decays [42], [43], as well as data on e^+e^- annihilation in the charm-quark region [44]- [47]. In the framework of fixed order perturbation theory [48] the FESR, eq. (3.20), become

$$(-)^N C_{2N+2}\langle O_{2N+2}\rangle = \int_0^{s_0} ds\, s^N\, \frac{1}{\pi}\, Im\,\Pi(s)|_{HAD} \, - \frac{s_0^{N+1}}{(N+1)}\, I_N(s_0)|_{PQCD}\,, \qquad (3.38)$$

where $N \geq 1$, and $I_N(s_0)|_{PQCD}$ is the integrated pQCD contribution. In this approach, and to next-to-leading order (NLO) in pQCD, radiative corrections to the condensates do not induce mixing of condensates of different dimension [49], a welcome feature. All of these early results relied on available pQCD information at the time, mostly only up to next-to-next-to leading order (NNLO), and on values of α_s considerably lower than at present, i.e. some 40% lower. Due to this, the pQCD contribution to the FESR was a manageable correction leading to relatively high accuracy in the values of the condensates. This situation changed dramatically with the availability of radiative corrections at the five-loop level, and a considerably higher value of the strong quark-gluon coupling. As a result, current determinations based on eq. (3.38) [16], [29], [50]- [51] are affected by such large uncertainties that the dimension $d = 4$ gluon condensate is known with close to 100% error, and no meaningful results are obtained for condensates of higher dimension. For instance, the ALEPH Collaboration [28] has used τ-decay data [14] together with an indiscriminate global fit of all parameters, i.e. strong coupling and power corrections, to obtain an unphysical negative value for the gluon condensate. The source of the problem in this approach is the almost cancellation between two large and comparable quantities on the right hand side of eq. (3.38). In other words, large pQCD logarithmic terms tend to swamp the power corrections in sum rules. Specifically, the condensates determined from FESR are the result of a difference between two integrals, one involving the data and the other pQCD on the circle of radius $s = |s_0|$. Both contributions are large and comparable, thus leading to a large uncertainty. An exception is the case of chiral condensates which can be determined with reasonable accuracy due to the absence of pQCD [11], [16], [18], [29]. The third approach to obtain the dimension $d = 4$ power correction in the OPE is based on QCDSR for the vector current correlator in the charm-quark region, where there is data

from e^+e^- annihilation into hadrons. Early determinations [44]- [47] have been superseded due to the large increase of the strong coupling α_s over the years, and by the availability of NNLO perturbative information.

In this section we discuss a novel determination of this condensate in the charm-quark region using the vector current correlator and involving a pinched integration kernel in the FESR exhibiting a singularity at the origin in the complex s-plane. This allows for *(a)* a substantial enhancement of the hadronic contribution due to the well known first two ψ-poles, followed by a large quenching of the resonance region above them, where the data has large uncertainties, and *(b)* an extraction of the gluon condensate entering in the Cauchy residue of the singularity at the origin through the low energy QCD expansion. This leads to an expression for the gluon condensate involving contributions from three terms, the experimental data, the high energy pQCD contribution and the low energy pQCD expansion in inverse powers of the heavy-quark mass. It turns out that the last two terms have opposite signs, thus rendering the total pQCD contribution to be one order of magnitude smaller than the data. This last feature circumvents the problem with traditional FESR where the condensates are the result of a fine balance between two large contributions, the hadronic and the pQCD integrals. Hence, this leads to a substantially more accurate result.

Let us consider the vector current correlator eq. (3.1), where $V_\mu(x) = \bar{c}(x)\gamma_\mu c(x)$ ($c(x)$ is the charm-quark field). From Cauchy's residue theorem in the complex s-plane one obtains

$$\int_{s_{th}=M^2_{J/\psi}}^{s_0} p(s)\,\frac{1}{\pi} Im\,\Pi(s)\,ds = -\frac{1}{2\pi i}\oint_{C(|s_0|)} p(s)\,\Pi(s)\,ds + \mathrm{Res}[\Pi(s)\,p(s), s=0]\;, \quad (3.39)$$

where $p(s)$ is now a meromorphic function, the integral on the right hand side involves QCD, provided s_0 is large enough, and the left hand side involves the hadronic spectral function

$$\mathrm{Im}\;\Pi(s) = \frac{1}{12\pi}\,R_c(s)\;, \quad (3.40)$$

with $R_c(s)$ the standard R-ratio for charm production in e^+e^- annihilation. Notice the lower limit of integration on the right hand side of eq. (3.39). This threshold lies above the (suppressed) pure gluonic intermediate states entering at NNLO, thus not included in the observable R_c. It was found in [52] that the total background is different from R_{uds} by 0.01%, and thus the non-R_{uds} contributions are entirely negligible.

The pQCD piece of $\Pi(s)$, entering the integral around the circle in eq. (3.39), can be formally written as

$$\Pi(s)|_{PQCD} = e_c^2 \sum_{n=0} \left(\frac{\alpha_s(\mu^2)}{\pi}\right)^n \Pi^{(n)}(s) \,, \tag{3.41}$$

where $e_c = 2/3$ is the charm-quark electric charge, and

$$\Pi^{(n)}(s) = \sum_{i=0} \left(\frac{\bar{m}_c^2}{s}\right)^i \Pi_i^{(n)} \,, \tag{3.42}$$

with $\overline{m}_c \equiv \overline{m}_c(\mu)$ the running charm-quark mass in the $\overline{MS}$-scheme. Up to order $\mathcal{O}[\alpha_s^2(\bar{m}_c^2/s)^6]$ the function $\Pi(s)_{PQCD}$ has been calculated in [53], exact results for $\Pi_0^{(3)}$ and $\Pi_1^{(3)}$ have been found in [54], and $\Pi_2^{(3)}$ is known up to a constant [55]. At five-loop order, $\mathcal{O}(\alpha_s^4)$, the full logarithmic terms for $\Pi_0^{(4)}$ were determined in [30], and for $\Pi_1^{(4)}$ in [56]. Since there is incomplete knowledge at this order we shall use the available information as a measure of the truncation error in pQCD. There is also a non-perturbative QCD contribution to $\Pi(s)$, with the leading term being the gluon condensate. This contribution, though, is negligible on account of s_0 being large. However, the gluon condensate also enters in the sum rules through the Cauchy residue in eq. (3.39), provided $p(s)$ is singular at the origin, a feature that constitutes the essence of this determination. The low energy expansion of the vector correlator around $s = 0$ in pQCD can be written as

$$\Pi_{PQCD}(s) = \frac{3\, e_c^2}{16\, \pi^2} \sum_{n\geq 0} \overline{C}_n \, z^n \,, \tag{3.43}$$

where $z = s/(4\overline{m}_c^2)$. The coefficients $\overline{C}_n$ are then expanded in powers of $\alpha_s(\mu)$

$$\begin{aligned}\bar{C}_n = \bar{C}_n^{(0)} + \frac{\alpha_s(\mu)}{\pi}\left(\bar{C}_n^{(10)} + \bar{C}_n^{(11)} l_m\right) + \left(\frac{\alpha_s(\mu)}{\pi}\right)^2 \left(\bar{C}_n^{(20)} + \bar{C}_n^{(21)} l_m + \bar{C}_n^{(22)} l_m^2\right) \\ + \left(\frac{\alpha_s(\mu)}{\pi}\right)^3 \left(\bar{C}_n^{(30)} + \bar{C}_n^{(31)} l_m + \bar{C}_n^{(32)} l_m^2 + \bar{C}_n^{(33)} l_m^3\right) + \ldots\end{aligned} \tag{3.44}$$

where $l_m \equiv \ln(\bar{m}_c^2(\mu)/\mu^2)$. Up to three loop level the coefficients of $\bar{C}_n$ are known up to $n = 30$ [57]- [60]. At four-loop level $\bar{C}_0$ and $\bar{C}_1$ were determined in [57]- [58], [61], $\bar{C}_2$ is from [59]- [60], and $\bar{C}_3$ from [62]. We shall choose $p(s)$ so that no coefficients $\bar{C}_4$ and above contribute to the Cauchy residue at $s = 0$. The different expansions in eqs. (3.42) and (3.43) are to be understood as a result of the scale hierarchy $\Lambda_{QCD} << m_c << s_0$. The non-perturbative contributions to the OPE involve inverse powers of q^2, and the leading term, of dimension $d = 4$, is the gluon condensate [66]

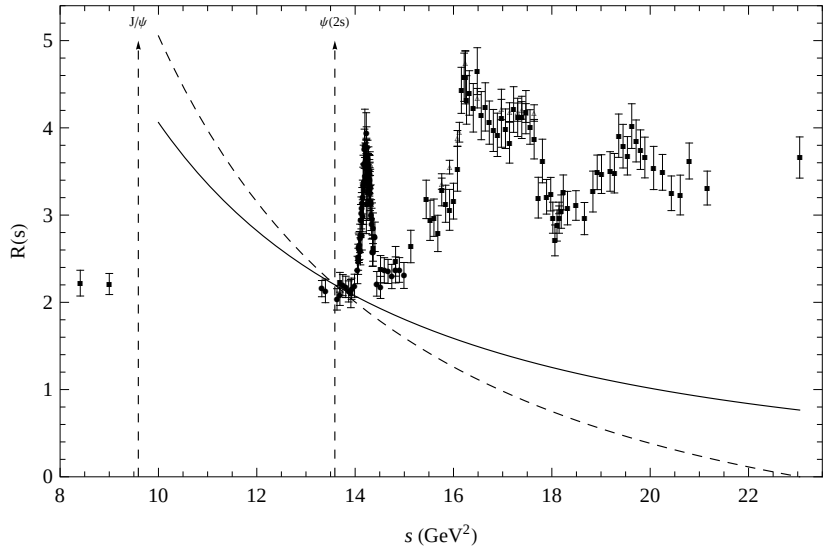

Figure 3.9: Experimental data for the total $R(s)$ ratio [63]- [65] together with the optimal integration kernel, eq. (3.50), with $N = 2$ (dash curve), and $p(s) = 1/s^2$ (solid curve) normalized to coincide with the former at the position of the $\psi(2S)$ peak.

$$\lim_{-q^2\to 0} \Pi(q^2)|_{NPQCD}(q^2) = -\frac{1}{q^4}\,\frac{\langle \frac{\alpha_s}{\pi} G^2\rangle}{12\pi}\,(1+\mathcal{O}(\alpha_s))\,. \tag{3.45}$$

As is well known, in the heavy-quark sector there is no underlying chiral symmetry, and the heavy-quark condensate reduces to the gluon condensate, e.g. to leading order in m_Q^{-1}

$$\langle \bar{Q}Q\rangle = -\frac{1}{12 m_Q}\langle \frac{\alpha_s}{\pi} G^2\rangle\,. \tag{3.46}$$

In the sequel we ignore potential renormalon ambiguities, as we are not aware of renormalon analyses in heavy-quark expansions, with masses expressed in the $\overline{MS}$-regularization scheme. Furthermore, in the present analysis we determine the dimension $d = 4$ power correction in the OPE of the heavy-quark vector correlator. This term has traditionally been identified with the gluon condensate, and could also be viewed simply as a phenomenological parameter of the QCDSR approach. In other words, we are not determining the gluon condensate from first principles, as done e.g. in LQCD, which involves issues which may not arise in phenomenological extractions such as the one presented here.

Finally, the leading non-perturbative contribution to the FESR, eq. (3.39), from singular kernels of the form $p(s) = 1/s^{N+1}$, with $N \geq 0$, has been calculated in [66]. However, we shall make use of the result in [52], which is already expressed in the $\overline{MS}$-scheme, and to NLO reads

$$\text{Res}\left[\frac{\Pi(s)|_{NPQCD}}{s^{N+1}}, s=0\right] = \frac{e_c^2}{(4\bar{m}_c^2)^{N+2}} \langle \frac{\alpha_s}{\pi} G^2 \rangle \, a_N \, \left(1 + \frac{\alpha_s}{\pi} \bar{b}_N\right), \tag{3.47}$$

where the quark mass and the coupling depend on μ, and

$$a_N = -\frac{2N+2}{15} \frac{\Gamma(4+N)\Gamma(7/2)}{\Gamma(7/2+N)\Gamma(4)}, \tag{3.48}$$

$$\bar{b}_N = b_N - (2N+4)\left(\frac{4}{3} - l_m\right), \tag{3.49}$$

with $b_0 = 1469/162$, $b_1 = 135779/12960$, $b_2 = 1969/168$, and other values given in [52], [66]. The NNLO term is unknown so that we will include it as a source of uncertainty later. The fundamental QCD parameters are the charm-quark mass $m_c(\mu^2)$, the running strong coupling $\alpha_s(\mu^2)$, and the gluon condensate $\langle \frac{\alpha_s}{\pi} G^2 \rangle$. For the strong coupling we use the current value from lattice LQCD [41] $\alpha_s(M_Z^2) = 0.1183 \pm 0.0007$, and the charm-quark mass also from LQCD [67] $\bar{m}_c(3 \text{ GeV}) = 986.4 \pm 4.1$ GeV, which agrees with the most recent QCDSR determination [68] $\bar{m}_c(3 \text{ GeV}) = 987 \pm 9$ MeV. Solving the renormalization group equation for the strong coupling and for the quark mass one can obtain their values at any scale s in terms of their values at any given reference scale, e.g. $s = s_0$ [28]. Regarding the renormalization scale μ, we follow the choice [68]- [69] $\mu^2 = (3 \text{ GeV})^2$ in the low energy QCD expansion, and $\mu^2 = s_0$ in the high energy QCD expansion on the circle of radius $s = |s_0|$.

Turning to the experimental data, we follow closely the analysis of [52], [70]. For the first two narrow resonances we use the latest data from the Particle Data Group [23], $M_{J/\psi} = 3.096916(11)$ GeV, $\Gamma_{J/\psi \to e^+e^-} = 5.55(14)$ keV, $M_{\psi(2s)} = 3.68609(4)$ GeV, $\Gamma_{\psi(2s)\to e^+e^-} = 2.35(4)$ keV. These two narrow resonances are followed by the open charm region where it is necessary to subtract from the total R-ratio the contribution from the light quark sector, i.e. R_{uds}. We perform this subtraction as in [71]. In the region 3.97 GeV $\leq \sqrt{s} \leq$ 4.26 GeV we only use CLEO data [63] as they are the most precise. In connection with the two data sets from BES [64]- [65], we assume that the systematic uncertainties are not fully independent and add them linearly, rather than in quadrature. However, we treat these data as independent from the CLEO data set [63], and thus add errors in quadrature. There is no data in the region $s = 25 - 49$ GeV^2, and beyond there is CLEO data up to $s \simeq 90$ GeV^2. The latter data is fully compatible with pQCD.

We discuss next the integration kernels $p(s)$ in eq. (3.39), which we choose as

$$p(s) = \left(\frac{s_0}{s}\right)^N - 1 \, , \tag{3.50}$$

with $N \geq 2$. This choice is motivated by (i) the suppression of potential quark-hadron duality violations, as $p(s_0) = 0$, and (ii) the simultaneous enhancement of the two ground state narrow resonances and the quenching of the resonance region contribution. This second feature can be appreciated from Figure 3.9. In principle, the constant term in the kernel, eq. (3.50), should not contribute to the sum rule, eq. (3.39), due to the absence of a $d = 2$ power correction. If quark-hadron duality were to be exact, then this would be an exact result. We find that while numerically the line integral is not exactly equal to the integral around the circle, the contribution of this constant term in $p(s)$ to eq. (3.39), i.e. the difference between the two integrals is small. However, we shall take this into account later in the final result. Regarding the value of N, as discussed in [52], [70], inverse moments $p(s) = 1/s^N$ should not involve too large values of N. In fact, the convergence of pQCD deteriorates with increasing N, and the uncertainties in α_s and the renormalization scale μ have a greater impact on the total error of the result. We found that eq. (3.50) with $N = 2$ is the optimal kernel as explained next. In Figure 3.9 we show the experimental data for the ratio $R(s)$ together with the kernel eq. (3.50) with $N = 2$ and for $s_0 \simeq 23\ \text{GeV}^2$, and the simple kernel $p(s) = 1/s^2$ normalized such that both kernels coincide at the peak of the second narrow resonance $\psi(2S)$, i.e. $s \simeq 13.6\ \text{GeV}^2$. One can easily appreciate that in comparison with the latter, the former kernel leads to a welcome higher enhancement of the weight of the J/ψ and the $\psi(2S)$, as well as to a stronger suppression of the broad resonance region, particularly near the onset of the continuum. Also, the kernel, eq. (3.50), with $N = 2$ (i) leads to the most stable result for the gluon condensate as a function of s_0, and (ii) gives a result with the smallest uncertainty. In fact, varying s_0 from an initial value $s_0 = 23.04\,\text{GeV}^2$, corresponding to the last BES data point [64]- [65], and $s_0 = 30.0\,\text{GeV}^2$ changes the value of the gluon condensate within the range determined by the uncertainties in α_s and $\bar{m}_c$. The contour integral evaluated using fixed order perturbation theory ($\mu^2 = s_0$) gives essentially the same result as using contour improved perturbation theory.

In Table 3.1 we show the results, together with a breakdown of the relevant uncertainties due to the various parameters. The numerical value is $\langle \frac{\alpha_s}{\pi} G^2 \rangle = 0.048 \pm 0.003\,\text{GeV}^4$ from the kernel eq. (3.50), and $\langle \frac{\alpha_s}{\pi} G^2 \rangle = 0.041 \pm 0.003\,\text{GeV}^4$ for $p(s) = 1/s^2$. Combining these results leads to $\langle \frac{\alpha_s}{\pi} G^2 \rangle = 0.044 \pm 0.007\,\text{GeV}^4$. Of some concern is the large size of the NLO radiative correction to the residue, eq. (3.47), and the fact that the NNLO is unknown. Radiative corrections to condensates at NNLO are currently known only for the quark condensate entering the Adler function [72], and it is of the same sign as the NLO term. Adopting the conservative procedure of assuming the NNLO to be of the same size

	[GeV^4]					
Method	$\langle\frac{\alpha_s}{\pi}G^2\rangle$	Δ_{s_0}	Δ_{α_s}	Δ_{m_c}	$\Delta_{\rm DATA}$	Δ_T
(a)	0.044	0.0028	0.0003	0.0048	0.0043	0.007
(b)	0.026	0.0016	0.0001	0.0027	0.0024	0.004

Table 3.1: Results for the gluon condensate for the kernel, eq.(3.50), for $N = 2$ and its sources of uncertainty from the values of s_0, α_s, m_c, the experimental data, and the total uncertainty. Method (a) refers to using the currently known NLO radiative correction to the residue, eq. (3.47). Method (b) assumes that the NNLO correction is as large, and of the same sign as the NLO one (see text).

and sign as the NLO gives $\langle\frac{\alpha_s}{\pi}G^2\rangle = 0.026 \pm 0.002\,\text{GeV}^4$. Including this uncertainty into the gluon condensate gives our preferred value

$$\langle\frac{\alpha_s}{\pi}G^2\rangle = 0.037 \pm 0.015\,\text{GeV}^4\,. \tag{3.51}$$

This result for the gluon condensate agrees within errors with a recent LQCD value [41] $\langle\frac{\alpha_s}{\pi}G^2\rangle = 0.028 \pm 0.003\,\text{GeV}^4$. Another LQCD determination [40] reports a still smaller value consistent with zero $\langle\frac{\alpha_s}{\pi}G^2\rangle = 0.002 \pm 0.002\,\text{GeV}^4$. On the other hand, our result is larger than our most recent value from the corrected ALEPH data base [16] (see chapter 2) which, however, has a very large uncertainty, i.e. $\langle\frac{\alpha_s}{\pi}G^2\rangle = 0.005 \pm 0.004\,\text{GeV}^4$.
A comparison with our result, eq. (3.51), is not straightforward mainly because (i) our method differs substantially from others as it requires not only high energy QCD information but also the low energy QCD expansion. Both contributions to the gluon condensate are comparable but of different sign, thus becoming an order of magnitude smaller than the data contribution, a more than welcome feature. And (ii) current pQCD information at high energy is far more detailed than 20-30 years ago, and the value of α_s is currently much higher. A more recent QCDSR value in the light-quark region, from an unconventional method, gives [73]

$$\langle\frac{\alpha_s}{\pi}G^2\rangle = 0.062 \pm 0.019\,\text{GeV}^4\,, \tag{3.52}$$

in agreement within errors with our value, eq. (3.51). The result above would support the view that the gluon condensate is channel/sector independent [3], [38].
Throughout this chapter we have showed how FESR works very well when we include suitable kernels, getting very good agreement with LQCD, then it is good idea consider FESR and LQCD a natural complement each other. On the other hand, we can see that the new and better experimental results provide us the possibility of computing one more time values like vacuum condensates, chiral condensates and parameters of chiral perturbation

theory, the results showed agreement with the previous ones, being this agreement one evidence of FESR's consistency. Finally, here we computed the gluon condensate value using two different methods, in two different energy regions and we got different values, hence we have the opportunity to explore gluon condensate's value in other energy regime.

CHAPTER 4

CHARGED PARTICLES IN PRESENCE OF MAGNETIC FIELDS.

Immediately after reading the title of this chapter, the reader could think that we have done an abrupt change of topic, like a first order phase transition, actually it is not as abrupt as seen. Now we take a step forward to understand QCD/Hadronic matter not only in vacuum but at finite temperature/density and/or in presence of external fields, like magnetic fields, as we raised at the beginning of this thesis. Then we want to do this transition smooth, therefore as first step we consider good idea to include only magnetic fields, then we begin working from the basic elements that we need.

In the perturbative regime every field theory has as one indispensable object the propagator, it tells us the probability amplitude for a particle to travel from one temporal-space point to another one. When the particle is electrically charged and external magnetic fields are permeating the space at any time, we need to include this information in the propagator, in other words we must find the two point function that solves the equation of motion, this solution actually is the Green function.

In this chapter, we are going to present the Schwinger's proper time formalism [74] to get the propagator of scalar and fermionic charged fields when the magnetic field is constant in time and homogeneous in space.

Schwinger's proper time formalism.

For a pedagogical purpose, we are going to show explicitly how to get the propagator only for a charged scalar field in the presence of a constant and homogeneous magnetic field, analogously the fermionic case can be computed. But as first step we are going to start showing the general procedure to get the propagator in the Schwinger's proper time formalism.

Let us consider the Green's function $G(x, x')$ for a generic operator $H(x, p)$ that we will call the *Hamiltonian*. The equation that defines the Green's function for this Hamiltonian is

$$H(x,p)G(x,x') = \delta^4(x - x'). \tag{4.1}$$

Recall that

$$\begin{aligned} \langle x \mid x' \rangle &= \delta^4(x - x'), \\ [x^\mu, p^\nu] &= -ig^{\mu\nu}, \\ p_\mu &= i\partial_\mu. \end{aligned} \tag{4.2}$$

We introduce the *proper time* evolution operator $U(x, x'; s)$, where s is the *proper time* variable, this operator satisfies the differential equation

$$i\frac{\partial}{\partial s}U(x,x';s) = H(x,p)U(x,x';s) \tag{4.3}$$

and satisfies the boundary conditions

$$\begin{aligned} \lim_{s\to 0} U(x,x';s) &= \delta^4(x - x'), \\ \lim_{s\to -\infty} U(x,x';s) &= 0. \end{aligned} \tag{4.4}$$

The solution is therefore

$$U(x,x';s) = \langle x \mid e^{-iHs} \mid x' \rangle \equiv \langle x \mid U(s) \mid x' \rangle. \tag{4.5}$$

Note that this means that the Green's function is given by

$$G(x,x') = -i\int_{-\infty}^{0} ds\; U(x,x';s). \tag{4.6}$$

Now we rewrite eq. (4.3) for $U(x,x';s)$

$$\begin{aligned} i\partial_s\langle x \mid U(s) \mid x'\rangle &= \langle x \mid H(x,p)\ U(s) \mid x'\rangle \\ &= \langle x \mid U(s)\ U(s)^\dagger\ H(x,p)\ U(s) \mid x'\rangle \end{aligned} \tag{4.7}$$

and we use that

$$U(s)^\dagger\ H(x,p)\ U(s) = H(x(s),p(s)), \tag{4.8}$$

it is like going from Schrödinger to Heisenberg picture, and then

$$i\partial_s\langle x \mid U(s) \mid x'\rangle = i\partial_s\langle x(s) \mid x'(0)\rangle = \langle x(s) \mid H(x(s),p(s)) \mid x'(0)\rangle. \tag{4.9}$$

The goal is now to express $H(x(s),p(s))$ as a function of the operators $x(s)$, $x'(0)$ in the adequate order, such that $x(s)$ is to the left and $x'(0)$ is to the right, then

$$\langle x(s) \mid H(x(s),p(s)) \mid x'(0)\rangle = f(x,x';s)\langle x(s) \mid x'(0)\rangle, \tag{4.10}$$

in this way the differential equation for $\langle x(s) \mid x'(0)\rangle$ would become

$$i\partial_s\langle x(s) \mid x'(0)\rangle = f(x,x';s)\langle x(s) \mid x'(0)\rangle \tag{4.11}$$

whose solution is

$$\langle x(s) \mid x'(0)\rangle = C(x,x')e^{-i\int_0^s ds'\ f(x,x';s)}. \tag{4.12}$$

Let us apply the above process to the computation of the propagator of a charged scalar field in a magnetic field

$$\begin{aligned} H(x,p)G(x,x') &= [(p_\mu - eA_\mu(x))^2 - m^2]G(x,x') = \delta^4(x-x') \\ &\equiv [\Pi^\mu\Pi_\mu - m^2]G(x,x') = \delta^4(x-x'), \end{aligned} \tag{4.13}$$

with $\Pi^\mu \equiv p^\mu - eA^\mu(x)$ the conjugate momentum in the minimal coupling approach. To compute

$$\langle x(s) \mid H(x(s),p(s)) \mid x'(0)\rangle, \tag{4.14}$$

we require to solve the equation of motion for x_μ and Π_μ, it is

$$\begin{aligned}\frac{dx_\mu(s)}{ds} &= i[H, x_\mu],\\ \frac{d\Pi_\mu(s)}{ds} &= i[H, \Pi_\mu],\end{aligned} \tag{4.15}$$

where the commutators are

$$\begin{aligned}[H, x_\mu] &= [\Pi^\nu \Pi_\nu, x_\mu] = \Pi^\nu[\Pi_\nu, x_\mu] + [\Pi^\nu, x_\mu]\Pi_\nu\\ &= \Pi^\nu[p_\nu - eA_\nu, x_\mu] + [p^\nu - eA^\nu, x_\mu]\Pi_\nu = \Pi^\nu[p_\nu, x_\mu] + [p^\nu, x_\mu]\Pi_\nu\\ &= i\Pi_\mu + i\Pi_\mu = 2i\Pi_\mu.\end{aligned} \tag{4.16}$$

$$\begin{aligned}[H, \Pi_\mu] &= [\Pi^\nu \Pi_\nu, \Pi_\mu] = \Pi^\nu[\Pi_\nu, \Pi_\mu] + [\Pi^\nu, \Pi_\mu]\Pi_\nu\\ &= -ie\Pi^\nu F_{\nu\mu} - ieF^\nu_\mu \Pi^\nu = ie\Pi^\nu F_{\mu\nu} + ieF_{\mu\nu}\Pi^\nu.\end{aligned} \tag{4.17}$$

From eq. (4.17), we can write the following

$$\Pi^\nu F_{\mu\nu} = F_{\mu\nu}\Pi^\nu + [\Pi^\nu, F_{\mu\nu}], \tag{4.18}$$

remembering that $[\Pi^\nu, F_{\mu\nu}]$ applied on scalar field $\phi(x)$ is equal to $i\partial^\nu F_{\mu\nu}$, then

$$\Pi^\nu F_{\mu\nu} = F_{\mu\nu}\Pi^\nu + i\partial^\nu F_{\mu\nu} \tag{4.19}$$

and thus

$$[H, \Pi_\mu] = ie(2F_{\mu\nu}\Pi^\nu + i\partial^\nu F_{\mu\nu}). \tag{4.20}$$

We consider already the case of a constant magnetic field directed along the $\hat{z}$ axis, then $\partial^\nu F_{\mu\nu} = 0$. Therefore the equations of motion eq. (4.15) are

$$\begin{aligned}\frac{dx_\mu(s)}{ds} &= -2\Pi_\mu,\\ \frac{d\Pi_\mu(s)}{ds} &= -2eF_{\mu\nu}\Pi^\nu.\end{aligned} \tag{4.21}$$

We must notice that since space separates naturally in a parallel and a transverse directions with regards to the magnetic field direction, it is useful to introduce a suitable notation for vectors a^μ, b^μ

$$a^{\mu}_{\parallel} = (a_0, 0, 0, a_3),$$
$$a^{\mu}_{\perp} = (0, a_1, a_2, 0), \tag{4.22}$$

such that

$$(a \cdot b)_{\parallel} = a_0 b_0 - a_3 b_3,$$
$$(a \cdot b)_{\perp} = a_1 b_1 + a_2 b_2,$$
$$a \cdot b = (a \cdot b)_{\parallel} - (a \cdot b)_{\perp}. \tag{4.23}$$

Due to the natural separation, it must be reflected into the equations of motion, in the following way

$$\frac{dx_{\parallel}(s)}{ds} = -2\Pi_{\parallel} = -2p_{\parallel},$$
$$\frac{d\Pi_{\parallel}(s)}{ds} = \frac{dp_{\parallel}}{ds} = 0, \tag{4.24}$$

$$\frac{dx_{\perp}(s)}{ds} = -2\Pi_{\perp},$$
$$\frac{d\Pi_{\perp}(s)}{ds} = -2eF_{ij}\Pi^{j}, \tag{4.25}$$

with $i, j = 1, 2$.
Let us first look at the equations in the transverse direction, where

$$x_{\perp}(s) = \begin{pmatrix} x_1(s) \\ x_2(s) \end{pmatrix}; \qquad \Pi_{\perp}(s) = \begin{pmatrix} \Pi_1(s) \\ \Pi_2(s) \end{pmatrix} \tag{4.26}$$

and

$$F = \begin{pmatrix} 0 & -1 \\ 1 & 0 \end{pmatrix}. \tag{4.27}$$

Taking into account eqs. (4.26) and (4.27), notice that the solution to second expression in eq. (4.25) is

$$\Pi_{\perp} = e^{-2eBFs}\Pi(0), \tag{4.28}$$

and substituting into first expression of eq. (4.25)

$$\begin{aligned}\frac{dx_\perp x(s)}{ds} &= -2e^{-2eBFs}\Pi_\perp(0)\\ &= -2[I\cos(2eBs) - F\sin(2eBs)]\Pi_\perp(0),\end{aligned} \tag{4.29}$$

the solution is

$$x_\perp(s) - x_\perp(0) = -2\frac{\sin(eBs)}{eB}e^{-eBFs}\Pi(0). \tag{4.30}$$

We now use the solution for $x_\perp(s) - x_\perp(0)$ to find $\Pi_\perp(0)$, the result is:

$$\Pi_\perp(0) = -\frac{eB}{2\sin(eBs)}e^{eBFs}(x_\perp(s) - x_\perp(0)), \tag{4.31}$$

in this notation, the transverse part of the hamiltonian is written as

$$\begin{aligned}H_\perp &= \Pi_\perp^\top(s)\Pi_\perp(s)\\ &= \Pi_\perp^\top(0)e^{-2eBF^\top s}e^{-2eBFs}\Pi_\perp(0)\\ &= \frac{(eB)^2}{4\sin^2(eBs)}(x_\perp^\top(s)x_\perp(s) - x_\perp^\top(0)x_\perp(s) - x_\perp^\top(s)x_\perp(0) + x_\perp^\top(0)x_\perp(0)),\end{aligned} \tag{4.32}$$

from last line in eq. (4.32) we have to order the second term, that is, we need to place $x_\perp(s)$ to the left and $x_\perp(0)$ to the right, for this purpose, note that

$$x_\perp^\top(0)x_\perp(s) - x_\perp^\top(s)x_\perp(0) = \sum_{i=1}^{2}[x_i(0), x_i(s)], \tag{4.33}$$

where the commutator in eq. (4.33) is

$$\sum_{i=1}^{2}[x_i(0), x_i(s)] = -4i\frac{\sin(eBs)}{eB}\cos(eBs), \tag{4.34}$$

then eq. (4.32) can be written as

$$H_\perp = \frac{(eB)^2}{4\sin^2(eBs)}(x_\perp^\top(s)x_\perp(s) - 2x_\perp^\top(s)x_\perp(0) + x_\perp^\top(0)x_\perp(0)) + i(eB)\cot(eBs). \tag{4.35}$$

Let us now look at the parallel part of the equations of motion, where the parallel part of the hamiltonian is

$$
\begin{aligned}
H_{\parallel} &= p_{\parallel}^{\top}(s)p_{\parallel}(s) \\
&= \frac{1}{4s^2}[x_{\parallel}^{\top}(s) - x_{\parallel}^{\top}(0)][x_{\parallel}(s) - x_{\parallel}(0)] \\
&= \frac{1}{4s^2}[x_{\parallel}^{\top}(s)x_{\parallel}(s) - x_{\parallel}^{\top}(0)x_{\parallel}(s) - x_{\parallel}^{\top}(s)x_{\parallel}(0) - x_{\parallel}^{\top}(0)x_{\parallel}(0)],
\end{aligned} \tag{4.36}
$$

as in the perpendicular case happened, now we need to order the second term in the third line of eq. (4.36), we repeat the procedure and we obtain

$$
H_{\parallel} = \frac{1}{4s^2}[x_{\parallel}^{\top}(s)x_{\parallel}(s) - 2x_{\parallel}^{\top}(s)x_{\parallel}(0) - x_{\parallel}^{\top}(0)x_{\parallel}(0)] - \frac{i}{s}. \tag{4.37}
$$

We can evaluate

$$
\langle x(s) \mid H \mid x'(0)\rangle = \langle x(s) \mid H_{\parallel} - H_{\perp} - m^2 \mid x'(0)\rangle, \tag{4.38}
$$

since all the operator in eqs. (4.35) and (4.37) are in the correct order we can write eq. (4.38) as follows

$$
\begin{aligned}
\langle x(s) \mid H \mid x'(0)\rangle = \Big\{ &- \frac{(eB)^2}{4\sin^2(eBs)}(x_{\perp}^2 - 2x_{\perp}x'_{\perp} + x'^2_{\perp}) - ieB\cot(eBs) \\
&\frac{1}{4s^2}(x_{\parallel}^2 - 2x_{\parallel}x'_{\parallel} + x'^2_{\parallel} - 4is) - m^2\Big\}\langle x(s) \mid x'(0)\rangle \\
&\equiv f(x, x'; s)\langle x(s) \mid x'(0)\rangle,
\end{aligned} \tag{4.39}
$$

integrating and exponentiating $f(x, x'; s)$, we obtain the matrix element of the time evolution operator

$$
\langle x(s) \mid H \mid x'(0)\rangle = \frac{C(x, x')}{s\sin(eBs)} e^{-i\frac{eB}{4}(x-x')_{\perp}^2\cot(eBs) + \frac{i}{4s}(x-x')_{\parallel}^2 + im^2 s}. \tag{4.40}
$$

In eq. (4.40) appears the term $C(x, x')$, it is related to the *phase factor*, let us compute it. For this purpose note that

$$
\langle x(s) \mid \Pi_{\mu}(s) \mid x'(0)\rangle = \left(- i\frac{\partial}{\partial x^{\mu}} - eA_{\mu}(x)\right)\langle x(s) \mid x'(0)\rangle \tag{4.41}
$$

and

$$
\langle x(s) \mid \Pi_{\mu}(0) \mid x'(0)\rangle = \left(- i\frac{\partial}{\partial x'^{\mu}} - eA_{\mu}(x')\right)\langle x(s) \mid x'(0)\rangle. \tag{4.42}
$$

One more time, we split the conjugate momentum in transverse and parallel components, we begin looking only at the transverse components Π_j $(j = 1, 2)$, we work with the left-hand side of eqs. (4.41) and (4.42)

$$\Pi_\perp(s) = e^{-2eBFs}\Pi_\perp(0) = -\frac{eB}{2}[I\cot(eBs) - F](x_\perp(s) - x_\perp(0)), \tag{4.43}$$

where in eq. (4.43) we have used eq. (4.31), therefore

$$\langle x(s) \mid \Pi_j(s) \mid x'(0)\rangle = -\frac{eB}{2}(\cot(eBs) + \varepsilon_{jk3}(x_k - x'_k))\langle x(s) \mid x'(0)\rangle, \tag{4.44}$$

on the other hand

$$\Pi_\perp(0) = -\frac{eB}{2}[I\cot(eBs) + F](x_\perp(s) - x_\perp(0)), \tag{4.45}$$

then

$$\langle x(s) \mid \Pi_j(0) \mid x'(0)\rangle = -\frac{eB}{2}(\cot(eBs) - \varepsilon_{jk3}(x_k - x'_k))\langle x(s) \mid x'(0)\rangle. \tag{4.46}$$

Now look at the right-hand side of eqs. (4.41) and (4.42) and apply either $-i\frac{\partial}{\partial x^\mu}$ or $-i\frac{\partial}{\partial x'^\mu}$

$$\begin{aligned}
&-i\frac{\partial}{\partial x^\mu}\left\{C(x,x')e^{i\frac{eB}{4}(x-x')^2_\perp\cot(eBs)}\right\} \\
&= e^{i\frac{eB}{4}(x-x')^2_\perp\cot(eBs)}\left[-i\frac{\partial}{\partial x^j}C(x,x') - \frac{eB}{2}\cot(eBs)(x-x')_j\right],
\end{aligned} \tag{4.47}$$

$$\begin{aligned}
&-i\frac{\partial}{\partial x'^\mu}\left\{C(x,x')e^{i\frac{eB}{4}(x-x')^2_\perp\cot(eBs)}\right\} \\
&= e^{i\frac{eB}{4}(x-x')^2_\perp\cot(eBs)}\left[-i\frac{\partial}{\partial x'^j}C(x,x') + \frac{eB}{2}\cot(eBs)(x-x')_j\right].
\end{aligned} \tag{4.48}$$

The term proportional to $\cot(eBs)$ cancels on both sides, therefore dividing by the exponential in eqs. (4.47) and (4.48) there is no dependence on s. We can put together the longitudinal part and we get the set of equations

$$\begin{aligned}
\left(i\frac{\partial}{\partial x^\mu} + eA_\mu(x) + \frac{e}{2}F_{\mu\nu}(x-x')^\nu\right)C(x,x') = 0, \\
\left(i\frac{\partial}{\partial x'^\mu} + eA_\mu(x') + \frac{e}{2}F_{\mu\nu}(x-x')^\nu\right)C(x,x') = 0.
\end{aligned} \tag{4.49}$$

The solution is

$$C(x,x') = i\phi(x,x') = ie^{ie\int_{x'}^{x} dy^{\mu}\ \left(A_{\mu}(y)+\frac{1}{2}F_{\mu\nu}(y-x')^{\nu}\right)}, \tag{4.50}$$

being $\phi(x,x')$ the *Schwinger phase* or *phase factor*. We have computed all the pieces of the propagator, i.e. we know the explicit expression of $U(x,x';s)$, then according eq. (4.5) the propagator of the charged scalar field in presence of homogeneous and constant magnetic field in coordinate space is

$$\begin{aligned} G(x,x') &= i\phi(x,x')\int_0^{\infty}\frac{ds}{s\ \sin(eBs)}e^{i\left\{\frac{eB}{4}(x-x')_{\perp}^{2}\cot(eBs)-\frac{1}{4s}(x-x')_{\parallel}^{2}-m^{2}s\right\}} \\ &\equiv i\phi(x,x')\widetilde{G}(x-x'). \end{aligned} \tag{4.51}$$

$\widetilde{G}(x-x')$ is the translational invariant part and it can be rewritten applying a Fourier transform

$$\widetilde{G}(x-x') = \int\frac{d^4k}{(2\pi)^4}e^{-ik\cdot(x-x')}\widetilde{G}(k), \tag{4.52}$$

using the inverse Fourier transform in eq. (4.52) and after some algebra

$$\widetilde{G}(k) = \int_0^{\infty}\frac{ds}{\cos(eBs)}e^{is\left(k_{\parallel}^{2}-k_{\perp}^{2}\frac{\tan(eBs)}{eBs}-m^{2}+i\varepsilon\right)}. \tag{4.53}$$

Finally the propagator in the Schwinger's proper time formalism is

$$\begin{aligned} G(x,x') = ie^{ie\int_{x'}^{x} dy^{\mu}\ \left(A_{\mu}(y)+\frac{1}{2}F_{\mu\nu}(y-x')^{\nu}\right)}\int\frac{d^4k}{(2\pi)^4}e^{-ik\cdot(x-x')} \\ \int_0^{\infty}\frac{ds}{\cos(eBs)}e^{is\left(k_{\parallel}^{2}-k_{\perp}^{2}\frac{\tan(eBs)}{eBs}-m^{2}+i\varepsilon\right)}. \end{aligned} \tag{4.54}$$

In the same way we found Eq. (4.54), the fermionic field case can be computed, for this case the final expression is

$$\begin{aligned} S(x,x') = -ie^{ie\int_{x'}^{x} dy^{\mu}\ \left(A_{\mu}(y)+\frac{1}{2}F_{\mu\nu}(y-x')^{\nu}\right)}\int\frac{d^4p}{(2\pi)^4}e^{-ip\cdot(x-x')} \\ \int_0^{\infty}\frac{ds}{\cos(eBs)}e^{is\left(p_{\parallel}^{2}-p_{\perp}^{2}\frac{\tan(eBs)}{eBs}-m^{2}+i\varepsilon\right)}\left[e^{-ieBs\sigma_3}\left(m+\gamma\cdot p_{\parallel}-\frac{\gamma\cdot p_{\perp}}{\cos(eBs)}\right)\right], \end{aligned} \tag{4.55}$$

with $\sigma_3 = i\gamma_1\gamma_2$. One last comment about the final expressions for the propagators eqs. (4.54) and (4.55) is related with the phase factor, recall that we are working with a

constant magnetic field along the $\hat{z}$ axis, it is produced by a vector potential $A_\mu(x)$ and this can be written in the symmetric gauge as follows

$$A_\mu(x) = \frac{B}{2}(0, -x_2, x_1, 0), \tag{4.56}$$

then the integral that appears in $\phi(x, x')$ does not depend on the trajectory since de integrand has vanishing curl. For simplicity we chose a straight line trajectory to connect x' with x

$$y^\mu = x'^\mu + t(x - x')^\mu \qquad t \,\epsilon\, [0, 1], \tag{4.57}$$

thus from eq. (4.50)

$$\begin{aligned} dy^\mu &\left[A_\mu(y) + \frac{1}{2}F_{\mu\nu}(y - x')^\nu\right] \\ &= [(x - x')^\mu dt]\left[A_\mu(y) + \frac{1}{2}F_{\mu\nu}(y - x')^\nu\right] \\ &= \left[(x - x')^\mu A_\mu(y) + \frac{1}{2}F_{\mu\nu}(x - x')^\nu(x - x')^\mu\ t\right]dt, \end{aligned} \tag{4.58}$$

since $F_{\mu\nu}$ is antisymmetric, the second term in eq. (4.58) does not contribute, thus

$$\phi(x, x') = e^{ie\int_0^1 dt\ A_\mu(y(t))(x-x')^\mu}. \tag{4.59}$$

From eq. (4.59), we can make the phase vanish by choosing an appropriate gauge transform

$$A_\mu(y) \ \rightarrow\ A'_\mu(y) = A_\mu + \frac{\partial}{\partial y^\mu}\Lambda(y), \tag{4.60}$$

if $\Lambda(y) = \frac{B}{2}(x'_2 y_1 - x'_1 y_2)$, note that then

$$\frac{\partial}{\partial y^\mu}\Lambda(y) = \frac{B}{2}(0, x'_2, -x'_1, 0), \tag{4.61}$$

computing the integral in eq. (4.59) after the gauge transform, we can see the integral vanishes, therefore the phase factor is equal to 1 and then when dealing with a single charged line the phase factor can be *gauged* away, in the case when we have two charged propagators that coincide at a given space-time point, once again we can take a suitable gauge transform and to get the phase factor is equal to 1, however when we consider the product of three propagators and they enclose an area, the product of the phase factor is finite, it becomes the exponential of the magnetic flux transverse to the area defined by the position of the in coordinate space of the vertices.

Landau Levels.

In some case the translational invariant part of the propagator written in the Schwinger's proper time formalism is not the most convenient way, then one alternative way to write the propagator is through an infinite sum over the Landau levels, we are going to show how from Schwinger's proper time formalism, we can get the propagator in term of Landau levels, we still work with the case of charged scalar field.
Let us now proceed to work out eq. (4.53) to find $\widetilde{G}(k)$ in terms of Landau levels. First we do the change of variable $eBs \to s$

$$\widetilde{G}(k) = \frac{1}{eB}\int_0^\infty \frac{ds}{\cos(s)} e^{i\frac{s}{eB}\left[k_\parallel^2 - k_\perp^2 \frac{\tan s}{s} - m^2 + i\varepsilon\right]}. \tag{4.62}$$

The integrand in eq. (4.62) is analytical in the lower complex s-plane and the zeros of $\cos(s)$ are all located on the real s-axis. Furthermore, the $i\varepsilon$ in the exponent ensures that for $\mid s \mid \to \infty$, the integrand dies out sufficiently rapidly. Therefore we can close the contour of integration on a path whose first leg is a horizontal line just below the real s-axis, continued along the quarter-circle at infinity in the right-lower quadrant and finally along the negative imaginary s-axis. This is depicted in Figure 4.1. Using Cauchy's theorem, the integral in eq. (4.62) can be written as

$$\widetilde{G}(k) = -\frac{1}{eB}\int_{-i\infty}^0 \frac{ds}{\cos(s)} e^{i\frac{s}{eB}\left[k_\parallel^2 - k_\perp^2 \frac{\tan s}{s} - m^2 + i\varepsilon\right]}. \tag{4.63}$$

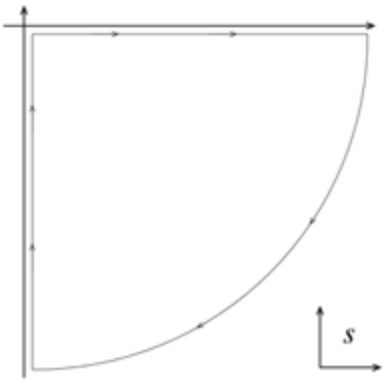

Figure 4.1: Integration contour in the complex s-plane to compute the integral representing the charged scalar propagator.

Since the integration in eq. (4.63) is along the imaginary axis, we make the change of variable $s = -i\tau$ with τ real and thus eq.(4.63) becomes

$$\widetilde{G}(k) = -\frac{i}{eB}\int_0^\infty \frac{d\tau}{\cos(-i\tau)} e^{\frac{\tau}{eB}\left[k_\parallel^2 - k_\perp^2 \frac{\tan(-i\tau)}{-i\tau} - m^2 + i\varepsilon\right]}. \tag{4.64}$$

Notice that since $\tau \geq 0$, this last integral converges for $Re(k_\parallel^2 + i\varepsilon) < 0$, that is $k_0 - k_3 < 0$ which means that we are considering momenta in the euclidean space. Next, we use that

$$\cos(-i\tau) = \frac{e^\tau + e^{-\tau}}{2}, \qquad i\tan -i\tau = \frac{e^\tau - e^{-\tau}}{e^\tau + e^{-\tau}}. \tag{4.65}$$

Introducing the variable $u = e^{-2\tau}$, we can write the eq. (4.64) as

$$\widetilde{G}(k) = -\frac{2i}{eB}\int_0^\infty d\tau\ e^{\frac{\tau}{eB}(k_\parallel^2 - m^2 + i\varepsilon)}\ e^{-\frac{k_\perp^2}{eB}}\ u^{1/2}\ \frac{e^{\frac{2k_\perp^2 u}{eB(1+u)}}}{1+u}. \tag{4.66}$$

Eq. (4.66) is now suited to introduce the generating function for the Laguerre polynomials $L_l(x)$, given by

$$\frac{e^{-xz/(1-z)}}{1-z} = \sum_{l=0}^\infty L_l(x) z^l, \tag{4.67}$$

from which, interchanging the order of the summation and the integration, we can write

$$\widetilde{G}(k) = -\frac{2i}{eB}\sum_{l=0}^\infty (-1)^l L_l\left(\frac{2k_\perp^2}{eB}\right) e^{-\frac{k_\perp^2}{eB}} \int_0^\infty d\tau\ u^{l+1/2}\ e^{\frac{\tau}{eB}(k_\parallel^2 - m^2 + i\varepsilon)}. \tag{4.68}$$

The integral over τ can now be explicitly evaluated with the result

$$\int_0^\infty d\tau\ e^{\frac{\tau}{eB}(k_\parallel^2 - (2l+1)eB - m^2 + i\varepsilon)} = -\frac{eB}{k_\parallel^2 - (2l+1)eB - m^2}, \tag{4.69}$$

for which the expression for the propagator finally becomes

$$\widetilde{G}(k) = 2\sum_{l=0}^\infty \frac{(-1)^l L_l\left(\frac{2k_\perp^2}{eB}\right) e^{-\frac{k_\perp^2}{eB}}}{k_\parallel^2 - (2l+1)eB - m^2}. \tag{4.70}$$

The fermionic field case is computed completely analogous, the final expression is

$$\widetilde{S}(p) = \sum_{l=0}^\infty \frac{-d_n(\alpha)D + d_n'(\alpha)\bar{D}}{m^2 - p_\parallel^2 + 2leB} + \frac{\gamma\cdot p_\perp}{p_\perp^2}, \tag{4.71}$$

where $d_n \equiv (-1)^l e^{-\alpha}(L_l(2\alpha) - L_{l-1}(2\alpha))$, $d_n' \equiv \partial d_n/\partial\alpha$, with $\alpha = p_\perp^2/eB$, and

$$\begin{aligned} D &= (m + \gamma\cdot p_\parallel) + \gamma\cdot p_\perp \frac{m^2 - p_\parallel^2}{p_\perp^2}, \\ \bar{D} &= \gamma_1\gamma_2(m + \gamma\cdot p_\parallel). \end{aligned} \tag{4.72}$$

Weak field approximation

When the magnetic field is small compared to the momenta, we can express the propagator as an infinity series in powers of eB. For this purpose, we follow [75] and reorganize the series in eq. (4.70) in powers of eB to make evident the lowest contributing power of eB which is the most important one in this limit. We begin factorizing $k_\parallel^2 - m^2$ from the denominator in eq (4.70)

$$\widetilde{G}(k) = 2\frac{e^{-\frac{k_\perp^2}{eB}}}{k_\parallel^2 - m^2} \times \sum_{l=0}^{\infty} \frac{(-1)^l L_l\left(\frac{2k_\perp^2}{eB}\right)}{1-(2l+1)eB/(k_\parallel^2 - m^2)}. \tag{4.73}$$

Notice that we can formally write

$$\frac{1}{1-(2l+1)eB/(k_\parallel^2 - m^2)} = \sum_{j=0}^{\infty}\left(\frac{eB[2l+1]}{k_\parallel^2 - m^2}\right)^j, \tag{4.74}$$

from which the propagator can be written as

$$\widetilde{G}(k) = \frac{1}{k_\parallel^2 - m^2}\sum_{j=0}^{\infty}\left(\frac{eB}{k_\parallel^2 - m^2}\right)^j \times \left\{2e^{-\frac{k_\perp^2}{eB}}\sum_{l=0}^{\infty}(-1)^l L_l\left(\frac{2k_\perp^2}{eB}\right)(2l+1)^j\right\}. \tag{4.75}$$

The sum in the term between curly brackets in eq. (4.75), namely

$$S_j \equiv \left\{2e^{-\frac{k_\perp^2}{eB}}\sum_{l=0}^{\infty}(-1)^l L_l\left(\frac{2k_\perp^2}{eB}\right)(2l+1)^j\right\}, \tag{4.76}$$

represents a special case of the identity

$$f(x) \equiv \frac{e^{-i(k_\perp^2/eB)\tan(c)}}{\cos(x)} = 2e^{-\frac{k_\perp^2}{eB}}\sum_{l=0}^{\infty}(-1)^l L_l\left(\frac{2k_\perp^2}{eB}\right)e^{i(2l+1)x}. \tag{4.77}$$

Therefore, we see that for a given j, S_j is given by

$$S_j = i^j\left(\frac{d^j f}{dx^j}\right)_{x=0}. \tag{4.78}$$

It is now a simple exercise to write down the propagator as a series in powers of eB. Keeping only the lowest order terms, we get

$$\widetilde{G}(k)^{eB\to 0} \to \frac{1}{k_\parallel^2 - k_\perp^2 - m^2}\left\{1 - \frac{(eB)^2}{(k_\parallel^2 - k_\perp^2 - m^2)^2} - \frac{2(eB)^2 k_\perp^2}{(k_\parallel^2 - k_\perp^2 - m^2)^3} + \cdots\right\}. \tag{4.79}$$

The weak field approximation for the propagator in the fermionic field case is

$$\widetilde{S}(p)^{eB\to 0} \to \frac{\not{p}+m}{p_{\parallel}^2-p_{\perp}^2-m^2}+\frac{i\gamma_1\gamma_2(\gamma\cdot p_{\parallel}+m)}{(p_{\parallel}^2-p_{\perp}^2-m^2)^2}eB+\cdots. \tag{4.80}$$

Lowest Landau Level approximation.

For the purpose of considering the limit where eB is the biggest energetic scale in the system, we are going to examine the fermionic field case, the reason is simple, in this thesis it will be used and the scalar field will not. We recall that eq. (4.71) expresses the fermionic propagator in terms of Landau levels and if eB is the biggest scale in the propagator, then the first level $l=0$ is the most important term and the dynamics of the system is dominated by the lowest Landau level (LLL) [76], then the LLL pole is

$$\widetilde{S}(p)^{LLL}=2ie^{-p_{\perp}^2/|eB|}\frac{\gamma\cdot p_{\parallel}+m}{p_{\parallel}^2-m^2}\left(\frac{1-i\gamma_1\gamma_2}{2}\right) \tag{4.81}$$

Eq. (4.81) demonstrates a dimensional reduction character of the LLL dynamics in the infrared region, where $p_{\perp}\ll|\ eB\ |$. It is clear that such a dimensional reduction reflects the fact that the motion of charged particles is restricted in directions perpendicular to the magnetic field.

CHAPTER 5

S_0 AND $\langle \frac{\alpha_S}{\pi} G^2 \rangle$, SIGNALS OF MAGNETIC CATALYSIS.

Once we have shown, in the previous chapter, how to incorporate magnetic effects into the propagation of charged fields (scalars and fermionic), the next step is to study physics phenomena in presence of these external magnetic fields. As we mentioned in the introduction of this thesis, the second part of this work develops some ideas trying to get a deep understanding of QCD phase transition when magnetic fields are finite, then from now on, our goal is only related to this topic. We begin exploring the consequences of "turning on" magnetic fields, at zero temperature, into parameters which can give us information, subsequently, about the deconfinement transition.

The properties of strongly interacting matter in the presence of external magnetic fields has become a very active research field. Some of the driving motivations behind this interest is the possibility to study such properties in: peripheral collisions of heavy nuclei at high energy, compact stars and the early universe. In addition, recent LQCD results show that the critical temperature for deconfinement/chiral symmetry restoration decreases with increasing field strength [77,78]. This behaviour is dubbed *inverse magnetic catalysis*, and it reveals an unexpected, non-trivial phenomenon: in a thermal environment, near the transition temperature, the presence of a magnetic field acting on strongly interacting matter hinders the formation of a quark-anti-quark condensate. LQCD calculations [79] show that the quark condensate does increase with increasing magnetic field at low temperatures. This behaviour corresponds to *magnetic catalysis*. However, as the temperature increases

approaching the crossover region $T \simeq 150$ MeV, the quark condensate reaches a maximum value smaller than at $T = 0$ (for the same field strength). Subsequently, the condensate decreases as a function of the field strength. Finally, for temperatures above the cross-over values the condensate decreases monotonically as a function of the magnetic field.

Given the dual nature of the QCD phase transition, a pertinent question is to what extent inverse magnetic catalysis is due to the mechanisms of either chiral symmetry restoration and/or of deconfinement. One way to address this question is to find a relation between deconfinement and chiral symmetry restoration parameters as a function of the magnetic field. Since the transition happens for temperatures in the realm of non-perturbative phenomena, the relation searched for needs to carry non-perturbative information. An extensively used tool in the context of effective models at finite temperature, and zero [80] and finite [81] magnetic field is the *Polyakov loop* [82]. When coupled to quark degrees of freedom [83], this loop sheds light on how chiral symmetry and deconfinement behave during the QCD transition as a function of the field intensity. Another non-perturbative tool that does not rely on effective models is that of FESR. This approach has been successfully applied both at zero (see chapter 2 and chapter 3) and at finite temperature [84] to understand hadronic properties. A key parameter that emerges from this analysis signalling quark-gluon deconfinement is the squared energy threshold, s_0, above which the hadronic spectral function is well approximated by pQCD, looking at Figure 5.1 it is possible to appreciate that from FESR, s_0 decreases when the temperature increases, therefore pQCD begins to be valid for smaller values of s and the region with resonances is reduced. We can interpret this behaviour as resonance melting due to thermal effects, hence hadronic spectrum becomes pQCD spectrum when the temperature is high enough as consequence of deconfinement. An interesting relation between s_0 and the quark condensate $\langle \bar{q}q \rangle$, whereby the former is proportional to the latter has been found, in the absence of a magnetic field and at finite temperature, in [85], and at finite temperature and density in [86].

We use FESR in the axial-vector channel, and in the presence of an external magnetic field, to explore the relation between (i) the deconfinement and chiral symmetry restoration parameters, s_0 and $\langle \bar{q}q \rangle$, and (ii) obtain the behaviour of the gluon condensate as a function of the magnetic field intensity at zero temperature. For this purpose we explicitly compute the pQCD corrections to the current correlator and solve the first two FESR to find the dependence of s_0 and the gluon condensate on the magnetic field strength. We show that for magnetic field strengths eB smaller than s_0, the former follows the magnetic field dependence of the quark condensate, which we parametrize from LQCD results [79]. We also show that the magnetic field dependence of the gluon condensate receives non-trivial

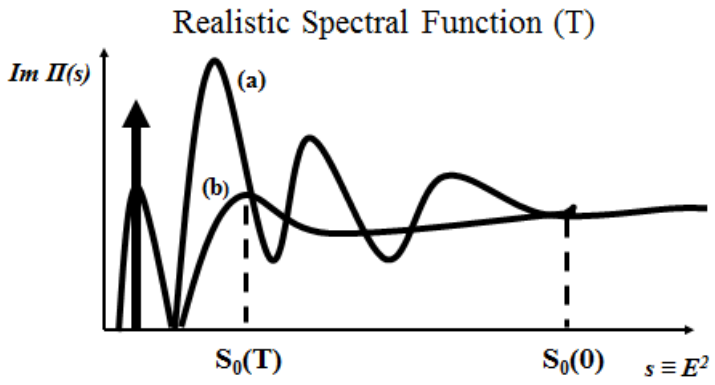

Figure 5.1: From [87]. Schematic thermal behaviour of phenomenological parameter for deconfinement, from spectral function at zero *(a)* and at finite temperature *(b)*.

corrections from the pQCD sector and that overall it is a monotonically increasing function of the field strength.

The charged axial-vector current correlator in the absence of a magnetic field and at $T = 0$ can be written as eq. (2.11). The functions $\Pi_{A,0}(q^2)$ are free of kinematical singularities, an important property needed in writing dispersion relations and sum rules. Concentrating on e.g. $\Pi_0(q^2)$ and invoking the OPE of current correlators at short distances beyond perturbation theory, one has eq. (2.4), the unit operator in eq. (2.4) has dimension $d = 0$ and $C_0\hat{I}$ stands for the purely perturbative contribution normalized according to

$$C_0\,\hat{I} = \frac{1}{4\pi}\ln\left(\frac{-s}{\mu^2}\right)\left[1 + \mathcal{O}(\alpha_s(s))\right]\ , \tag{5.1}$$

since there are no dimension $d = 2$ operators built from the QCD fields, it is generally assumed that the OPE starts at dimension $d = 4$. The dimension $d = 4$ in the chiral limit is proportional to the renormalization group invariant gluon condensate

$$C_4\langle\hat{\mathcal{O}}_4\rangle = \frac{\pi}{3}\langle\alpha_s\,G^2\rangle. \tag{5.2}$$

QCD sum rule method is to consider an integration contour in the complex square energy plane, as in Figure 2.2, and invoke Cauchy's theorem assuming that QCD can be used on the circle of radius $|s_0|$, provided $|s_0|$ is large enough (quark-hadron duality). On the real axis there is a discontinuity associated with the hadronic states entering the spectral function. Since there are no further singularities this leads to the FESR

$$-\frac{1}{2\pi i}\oint_{C(|s_0|)} ds\ s^{N-1}\ \Pi_0^{\rm QCD}(s) = \frac{1}{\pi}\int_0^{s_0} ds\ s^{N-1}{\rm Im}\ \Pi_0^{\rm HAD}(s), \tag{5.3}$$

with $N \geq 1$, and $\Pi_0^{\rm QCD}(s)$ given by the OPE. It will be shown later that in the presence of a magnetic field, and in the weak field limit $eB < s_0$, the Wilson coefficients acquire themselves a B-field dependence. We shall compute the corrections to the FESR due to a weak magnetic field, which can be expressed as a series in powers of eB. Since the magnetic field carries dimension of energy squared, on dimensional grounds one finds the replacements

$$\begin{aligned} C_0 \ln\left(\frac{-s}{\mu^2}\right) &\to C_0 \ln\left(\frac{-s}{\mu^2}\right) + \sum_{n=1} C_0^{(n)} \frac{(eB)^n}{s^n} \\ C_{2N} &\to \sum_{m=0} C_{2N}^{(m)} \frac{(eB)^m}{s^m} \end{aligned} \tag{5.4}$$

where $C_{2N}^{(m)}$ are dimensionless quantities that can be computed in pQCD at a given order in eB. Substituting eqs. (5.4) and (2.4) into eq. (5.3), one obtains

$$\begin{aligned} -\sum_{m=0}^{N-1}(-1)^{N-m} C_{2(N-m)}^{(m)} (eB)^m \langle O_{2(N-m)}\rangle = \frac{1}{\pi}\int_0^{s_0} ds\, s^{N-1} {\rm Im}\,\Pi_0^{\rm HAD}(s) \\ - \frac{C_0}{N} s_0^N + C_0^{(N)} (eB)^N. \end{aligned} \tag{5.5}$$

Note that in general the presence of the magnetic field mixes operators of different dimension in the FESR. For instance, the first two sum rules ($N = 1, 2$) become

$$0 = \frac{1}{\pi}\int_0^{s_0} ds\ {\rm Im}\Pi_0^{\rm HAD}(s) - C_0 s_0 + C_0^{(1)}(eB)\ , \tag{5.6}$$

$$-C_4^{(0)}\langle O_4\rangle + C_2^{(1)}(eB)\langle O_2\rangle = \frac{1}{\pi}\int_0^{s_0} ds\ s\ {\rm Im}\,\Pi_0^{\rm HAD}(s) - \frac{C_0}{2} s_0^2 + C_0^{(2)}(eB)^2. \tag{5.7}$$

In order to set up explicitly the relevant FESR we start by computing the hadronic contribution. The axial-vector current in the presence of a magnetic field can be interpolated by the charged pion current

$$A_\mu = -f_\pi D_\mu \pi^+ = -f_\pi(\partial_\mu - ie\mathcal{A}_\mu)\pi^+, \tag{5.8}$$

where $f_\pi = 130.28(14)$ MeV [23] is the pion decay constant, π^+ the pion field, and $\mathcal{A}_\mu = (B/2)(0, -y, x, 0)$ the vector potential in the symmetric gauge, which gives rise

to a constant magnetic field along the $\hat{z}$ direction. Therefore, the axial-vector correlator in the hadronic sector can be written as

$$\begin{aligned}\Pi^{\rm HAD}_{\mu\nu}(x,y) \equiv& < 0|T(A_\mu(x)\ ,\ A^\dagger_\nu(y))|0 > \\ &= if_\pi^2\langle 0|T\left[D_\mu\pi^+(x)D^*_\nu\pi^-(y)\right]|0\rangle \\ &= if_\pi^2 D_\mu(x)D^*_\nu(y)G_\pi(x,y) \\ &= ie^{ie\Phi(x,y)}f_\pi^2\frac{\partial}{\partial x^\mu}\frac{\partial}{\partial y^\mu}\widetilde{G}_\pi(x-y) \\ &\equiv e^{ie\Phi(x,y)}\widetilde{\Pi}^{\rm HAD}_{\mu\nu}(x-y),\end{aligned} \tag{5.9}$$

where we have used the fact that the charged pion propagator $G_\pi(x,y)$ in the presence of a magnetic field can be written as a product of a transnationally invariant piece $\widetilde{G}_\pi(x-y)$ and a *phase* factor $e^{ie\Phi(x,y)}$. The phase factor is equal to 1 as we showed in chapter 4. Hence, we keep only the translational invariant part of the hadronic correlator whose Fourier transform is

$$\Pi^{\rm HAD}_0(q^2) = if_\pi^2\widetilde{G}_\pi(q^2), \tag{5.10}$$

where $\widetilde{G}_\pi(q^2)$ stands for the Fourier transform of $\widetilde{G}_\pi(x-y)$. Using Schwinger's proper time method this quantity can be written as

$$\widetilde{G}_\pi(q^2) = \int_0^\infty \frac{d\tau}{\cos(eB\tau)}e^{i\tau[q_\parallel^2 - q_\perp^2\,\tan(eB\tau)/eB\tau + i\epsilon]}, \tag{5.11}$$

where $m_\pi = 0$ as we consider the chiral limit. Hereafter we shall use the notation

$$\begin{aligned} g_{\mu\nu} &= g^\parallel_{\mu\nu} - g^\perp_{\mu\nu} \\ g^\parallel_{\mu\nu} &= {\rm diag}(1,0,0,-1) \\ g^\perp_{\mu\nu} &= {\rm diag}(0,1,1,0). \end{aligned} \tag{5.12}$$

Consequently

$$\begin{aligned} a\cdot b = (a\cdot b)_\parallel - (a\cdot b)_\perp, \qquad g^\parallel_{\mu\nu}g^{\mu\nu} = 2, \qquad g^\perp_{\mu\nu}g^{\mu\nu} = -2, \\ (a\cdot b)_\parallel = g^\parallel_{\mu\nu}a^\mu b^\nu = a_0b_0 - a_3b_3, \\ (a\cdot b)_\perp = g^\perp_{\mu\nu}a^\mu b^\nu = a_1b_1 + a_2b_2. \end{aligned} \tag{5.13}$$

Following the steps explained in chapter 4, eq. (5.11) can be written in terms of a sum over Landau levels, being

$$\widetilde{G}_\pi(q^2) = 2i \sum_{l=0}^{\infty} \frac{(-1)^l L_l(2q_\perp^2/eB) e^{-q_\perp^2/eB}}{q_\parallel^2 - (2l+1)eB}. \tag{5.14}$$

Hereafter we study the behaviour of the correlator setting $\bar{q}^2 = 0$, the rest frame. In this limit, eq. (5.14) becomes

$$\widetilde{G}_\pi(q^2) = 2i \sum_{l=0}^{\infty} \frac{(-1)^l}{q_0^2 - (2l+1)eB}. \tag{5.15}$$

Therefore the hadronic contribution to the correlator becomes explicitly

$$\Pi_0^{\rm HAD}(q_0^2 = s) = -2f_\pi^2 \sum_{l=0}^{\infty} \frac{(-1)^l}{s - (2l+1)eB}. \tag{5.16}$$

Eq. (5.16) can be split into two sums, one for the even and the other for the odd values of l, namely

$$\Pi_0^{\rm HAD}(s) = -2f_\pi^2 \left\{ \sum_{l=0,even} \frac{1}{s-(2l+1)eB} - \sum_{l=odd} \frac{1}{s-(2l+1)eB} \right\}. \tag{5.17}$$

Pulling out a factor $-1/4eB$ from both sums and adding and substracting the element with $l = -1$ we obtain from eq. (5.17)

$$\Pi_0^{\rm HAD}(s) = 2f_\pi^2 \left\{ \frac{1}{4eB} \sum_{l'=0}^{\infty} \frac{1}{l' - \frac{s/eB-1}{4}} - \frac{1}{4eB} \sum_{l'=0}^{\infty} \frac{1}{l' - \frac{s/eB+1}{4}} - \frac{1}{s+eB} \right\}, \tag{5.18}$$

where we defined $l' = \frac{l}{2}$ for the sum with even l and $l' = \frac{l+1}{2}$ for the sum with odd l. The sums in eq. (5.18) are divergent. In order to extract the finite piece we regularize them as

$$\begin{aligned} \Pi_0^{\rm HAD}(s) &= 2f_\pi^2 \lim_{\epsilon \to 1} \left\{ \frac{1}{4eB} \sum_{l'=0}^{\infty} \frac{1}{(l' - \frac{s/eB-1}{4})^\epsilon} - \frac{1}{4eB} \sum_{l'=0}^{\infty} \frac{1}{(l' - \frac{s/eB+1}{4})^\epsilon} - \frac{1}{s+eB} \right\} \\ &= 2f_\pi^2 \lim_{\epsilon \to 1} \left\{ \frac{1}{4eB} \zeta(\epsilon, (s/eB-1)/4) - \frac{1}{4eB} \zeta(\epsilon, (s/eB+1)/4) - \frac{1}{s+eB} \right\}, \end{aligned} \tag{5.19}$$

where $\zeta(a, z)$ is the Hurwitz zeta function. Expanding around $\epsilon = 1$ we find

$$\begin{aligned}\Pi_0^{\rm HAD}(s) =& 2f_\pi^2\Bigg\{\frac{1}{4eB}\left[\frac{1}{\epsilon-1}-\psi\left(\frac{-(s/eB-1)}{4}\right)\right]\\ &-\frac{1}{4eB}\left[\frac{1}{\epsilon-1}-\psi\left(\frac{-(s/eB+1)}{4}\right)\right]-\frac{1}{s+eB}\Bigg\}\\ =& -2f_\pi^2\Bigg\{\frac{1}{4eB}\psi\left(\frac{-(s/eB-1)}{4}\right)\\ &+\frac{1}{4eB}\psi\left(\frac{-(s/eB+1)}{4}\right)+\frac{1}{s+eB}\Bigg\},\end{aligned} \tag{5.20}$$

where $\psi(x)$ is the di-gamma function. We note that the divergent pieces cancel when $\epsilon \to 1$. Recall that $\psi(x)$ is singular for $x = 0, -1, -2, \ldots$. In the region $0 \leq eB < s_0$, neither of the di-gamma functions in eq. (5.20) becomes singular. The first singularity for $\psi(-(s/eB-1)/4)$ happens at $s = eB$ and for $\psi(-(s/eB+1)/4)$ at $s = 3eB$. Therefore, by restricting the analysis to the region $eB \leq s_0 < 3eB$ we can compute the discontinuity, or imaginary part of eq. (5.20), with the result

$$\mathrm{Im}\Pi_0^{\rm HAD}(s) = f_\pi^2\pi\delta(s-eB), \tag{5.21}$$

where since s is strictly larger or equal to 0, one has

$$\lim_{\epsilon\to 0}\frac{\epsilon}{(s-eB)+\epsilon^2} = \frac{\pi}{2}\delta(s-eB). \tag{5.22}$$

Finally, in the limit $eB \to 0$ the imaginary part of the correlator becomes

$$\mathrm{Im}\Pi_0^{\rm HAD}(s) = f_\pi^2\pi\delta(s), \tag{5.23}$$

which coincides with the known value in the absence of a magnetic field.

Recall that s_0 represents the onset for the pQCD description for the axial-vector spectral density and that this quantity is a decreasing function of temperature [88]. For cold nuclear matter, as in the case of a neutron star, the condition $eB < s_0 < 3eB$ may be difficult to meet, specially for a weak field where not only the situation $eB < s_0$, but even $neB < s_0$, $(n \geq 1)$ can happen. However, for a heavy-ion collision, around the deconfinement/chiral symmetry restoration transition, when s_0 has dropped off to small values, the weak field condition can also be made compatible with $eB < s_0 < 3eB$. Hereafter we keep in mind this last observation as the working scenario, aiming to eventually incorporate thermal effects to describe the behaviour of a magnetized medium near the phase transition.

Using eq. (5.21), the hadronic line integral in the FESR is given explicitly by

$$\frac{1}{\pi}\int_0^{s_0} ds\, s^{N-1} \mathrm{Im}\Pi_0^{\mathrm{HAD}}(s) = f_\pi^2\, (eB)^{N-1}\,. \tag{5.24}$$

Substituting eq. (5.24) into the QCD sum rules eqs. (5.6)-(5.7) gives

$$\begin{aligned} 0 &= f_\pi^2 - C_0 s_0 + C_0^{(1)}(eB) \\ -C_4\langle O_4\rangle &= f_\pi^2(eB) - \frac{C_0}{2}s_0^2 + C_0^{(2)}(eB)^2. \end{aligned} \tag{5.25}$$

In order to solve these equations, we now proceed to compute explicitly the coefficients $C_0^{(1)}$ and $C_0^{(2)}$.

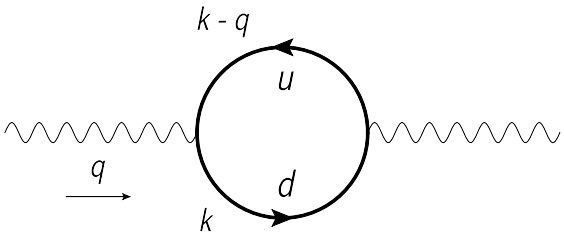

Figure 5.2: pQCD contribution to the axial-vector current correlator in the presence of a magnetic field. The thick internal lines represent the full quark propagators in the magnetic field background.

To perform the perturbative calculation of the coefficients $C_0^{(1)}$ and $C_0^{(2)}$ in the weak field limit we make use of the weak field expansion of the quark propagator in the presence of a constant magnetic field (see chapter 4), and in the chiral limit, up to order $\mathcal{O}(B^2)$

$$iS_B(k) = i\frac{\not{k}}{k^2} - (e_q B)\frac{\gamma_1\gamma_2(\gamma\cdot k)_\parallel}{k^4} - 2i(e_qB)^2\frac{\left[k_\perp^2(\gamma\cdot k)_\parallel - k_\parallel^2(\gamma\cdot k)_\perp\right]}{k^8}, \tag{5.26}$$

where e_q is the absolute value of the quark's charge.

The pQCD contribution to the axial-vector current correlator in the presence of a magnetic field is depicted in Figure 5.2, where we also define the kinematics. The thick internal lines represent the full quark propagators in the magnetic field background. To first order in e_qB only one of the two quark propagators carries the magnetic effects. This is depicted in Figure 5.3 where the wavy line starting from a cross represents the external magnetic field. The two diagrams in Figure 5.3 that determine the coefficient $C_0^{(1)}$, vanish identically when contracted with the momenta carried by the axial-vector currents. This is due to a

straightforward application of Furry's theorem in QCD context, and to the fact that the vector and axial-vector correlators are chiral symmetric. However, we show explicitly in Appendix A that each of the contributions in the diagrams, Figure 5.3, vanishes.

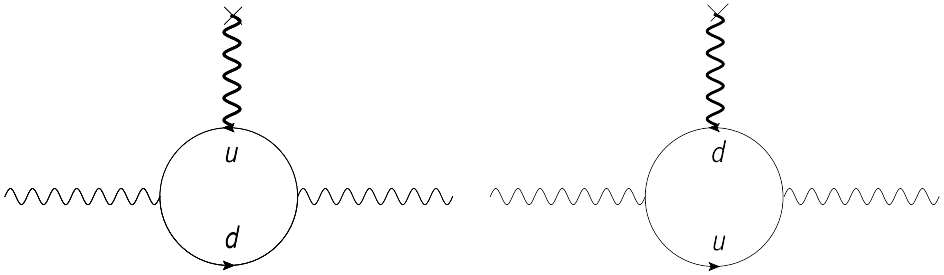

Figure 5.3: pQCD contribution to the axial-vector current correlator in the presence of a magnetic field to first order in $e_q B$. The thick wavy lines ending in a cross represent the external magnetic field.

The first non-trivial magnetic contribution to the pQCD axial-vector current correlator is of order $(e_q B)^2$. The relevant diagrams are shown in Figure 5.4. First, we compute the diagram where one magnetic field line is attached to each one of the two quark propagators. For these, we use eq. (5.26) to first order in $e_q B$. We call this contribution $\Pi^{(11)}_{\mu\nu}(q^2)$, and its explicit expression is

$$\Pi^{(11)}_{\mu\nu}(q^2) = -iN_c(q_u q_d B^2) \int \frac{d^4k}{(2\pi)^4} \frac{\mathrm{Tr}\left[\gamma_\mu\gamma_1\gamma_2\left[\gamma\cdot(k-q)_\parallel\right]\gamma_\nu\gamma_1\gamma_2(\gamma\cdot k)_\parallel\right]}{(k-q)^4k^4}. \tag{5.27}$$

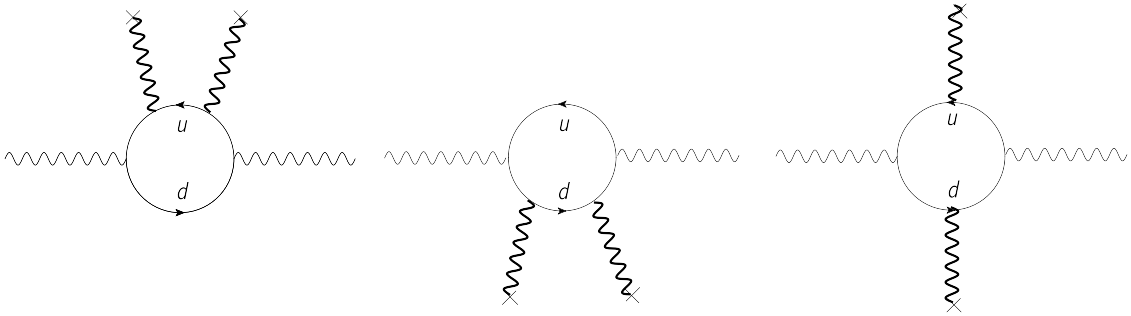

Figure 5.4: pQCD contribution to the axial-vector current correlator in the presence of a magnetic field to second order in $e_q B$. The thick wavy lines ending in a cross represent the external magnetic field.

Since according to eq. (5.3), we are interested in the magnetic corrections to the coefficient of the longitudinal structure, $\Pi_0(q^2)$ we project $\Pi^{(11)}_{\mu\nu}(q^2)$ with $q^\mu q^\nu$ and define

$$\Pi^{(11)}_0(q^2) = q^\mu q^\nu \Pi^{(11)}_{\mu\nu}(q^2). \tag{5.28}$$

Using

$$\gamma_1\gamma_2 \left[\gamma \cdot (k-q)_\parallel\right] = \left[\gamma \cdot (k-q)_\parallel\right] \gamma_1\gamma_2, \tag{5.29}$$

together with

$$\gamma_1\gamma_2 \not{q} \gamma_1\gamma_2 = 2(\gamma \cdot q)_\perp - \not{q}, \tag{5.30}$$

gives

$$\Pi_0^{(11)} = \; iN_c(q_u q_d B^2) \int \frac{d^4k}{(2\pi)^4} \frac{\mathrm{Tr}\left[\not{q}\left[\gamma \cdot (k-q)\right]_\parallel (-2(\gamma \cdot q)_\perp + \not{q})(\gamma \cdot k)_\parallel\right]}{(k-q)^4 k^4}. \tag{5.31}$$

The evaluation of the trace yields

$$\begin{aligned} \mathrm{Tr}\left[\not{q}\left[\gamma \cdot (k-q)\right]_\parallel (-2(\gamma \cdot q)_\perp + \not{q})(\gamma \cdot k)_\parallel\right] = & -4(q_\parallel^2 + q_\perp^2)\left[(k-q)\cdot k\right]_\parallel \\ & + \; 8(q\cdot k)_\parallel \left[(k-q)\cdot q\right]_\parallel . \end{aligned} \tag{5.32}$$

We now use the Feynman parametrization

$$\frac{1}{(k-q)^4 k^4} = 3! \int_0^1 dx \frac{x(x-1)}{\left[(k-xq)^2 - x(x-1)q^2\right]^4}, \tag{5.33}$$

and the change of variable

$$k \to l = k - xq, \tag{5.34}$$

to obtain

$$\begin{aligned} \Pi_0^{(11)}(q^2) = 4iN_c(q_u q_d B^2) 3! \int_0^1 x(x-1) \int \frac{d^4l}{(2\pi)^4} \frac{1}{\left[l^2 - \Delta\right]^4} \\ \times \left[q^2 q_\parallel^2 x(x-1) - (q_\parallel^2 + q_\perp^2) l_\parallel^2 + 2(q\cdot l)_\parallel^2\right], \end{aligned} \tag{5.35}$$

where we have discarded terms with odd powers of l and defined $\Delta = x(x-1)q^2$. The integrals over l are computed by means of

$$\begin{aligned} \int \frac{d^dl}{(2\pi)^d} \frac{1}{\left[l^2-\Delta\right]^n} &= i\frac{(-1)^n}{(4\pi)^{d/2}} \frac{\Gamma(n-d/2)}{\Gamma(n)} \left(\frac{1}{\Delta}\right)^{n-d/2} \\ \int \frac{d^dl}{(2\pi)^d} \frac{l^\mu l^\nu}{\left[l^2-\Delta\right]^n} &= i\frac{(-1)^{n-1}}{(4\pi)^{d/2}} \frac{g^{\mu\nu}}{2} \frac{\Gamma(n-d/2-1)}{\Gamma(n)} \left(\frac{1}{\Delta}\right)^{n-d/2-1}, \end{aligned} \tag{5.36}$$

with $n = 4$ and $d = 4$. Using eq. (5.36) in eq. (5.35), and after integrating over x, we find

$$\Pi_0^{(11)} = -\frac{N_c}{4\pi^2}(q_u q_d B^2)\frac{\left[q_\parallel^2 + q_\perp^2\right]}{q^2}. \tag{5.37}$$

In the limit $\bar{q}^2 \to 0$, eq. (5.37) becomes

$$\Pi_0^{(11)} \overset{\bar{q}^2\to 0}{\longrightarrow} -\frac{N_c}{4\pi^2}(q_u q_d B^2). \tag{5.38}$$

In a similar fashion we compute the diagrams in Figure 5.4 to second order in eB in the u-quark and in the d-quark propagator. Calling the longitudinal projections $\Pi_0^{(20)}(q^2)$ and $\Pi_0^{(02)}$, respectively, the result is

$$\begin{aligned}
\Pi_0^{(20)}(q^2) &= -\frac{N_c}{24\pi^2}(q_u B)^2\left[\frac{(q_\parallel^2 + q_\perp^2)}{q^2} + 2\frac{q_\parallel^2 q_\perp^2}{q^4}\right] \overset{\bar{q}^2\to 0}{\longrightarrow} -\frac{N_c}{24\pi^2}(q_u B)^2 \\
\Pi_0^{(02)}(q^2) &= -\frac{N_c}{24\pi^2}(q_d B)^2\left[\frac{(q_\parallel^2 + q_\perp^2)}{q^2} + 2\frac{q_\parallel^2 q_\perp^2}{q^4}\right] \overset{\bar{q}^2\to 0}{\longrightarrow} -\frac{N_c}{24\pi^2}(q_d B)^2.
\end{aligned} \tag{5.39}$$

Adding all three contributions, and using the absolute values $q_u = 2/3\ e$, $q_d = 1/3\ e$, and $N_c = 3$, we obtain the coefficient of the longitudinal structure of the axial-vector current correlator to second order in the magnetic field

$$\Pi_0^{B^2} = -\left(\frac{17}{18}\right)\frac{(eB)^2}{4\pi^2}. \tag{5.40}$$

Using this result together with the first equation in eq. (5.4), we obtain the Wilson coefficient of the pQCD contribution to second order in the magnetic field

$$C_0^{(2)} = -\left(\frac{17}{18}\right)\frac{1}{4\pi^2}. \tag{5.41}$$

The last ingredient needed to find s_0 and $C_4\langle O_4\rangle$ is the magnetic field dependence of f_π. Invoking the Gell-Mann-Oakes-Renner (GMOR) relation f_π is related to the light quark condensate $\langle\bar{q}q\rangle$

$$f_\pi^2 = -\frac{2}{\mathcal{B}}\langle\bar{q}q\rangle\ , \tag{5.42}$$

where $\mathcal{B}$ is a CHPT parameter, and m_π^2 is related to the quark masses as

$$m_\pi^2 = \mathcal{B}(m_u + m_d)\ , \tag{5.43}$$

so that the GMOR relation reads

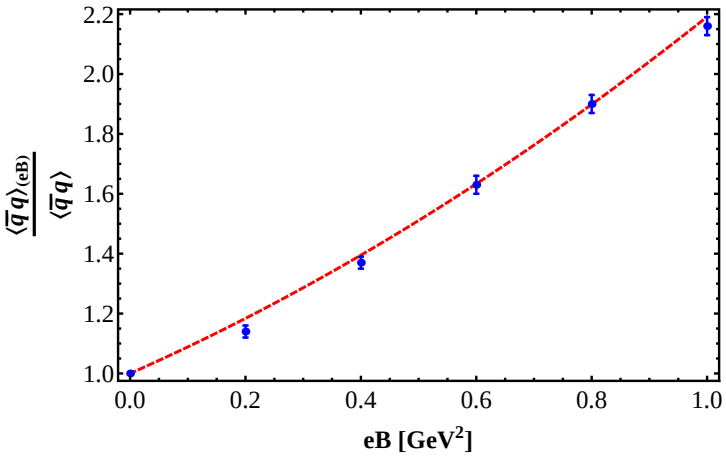

Figure 5.5: Light-quark condensate normalized to its vacuum value as a function of the magnetic field strength eB in units of GeV^2. The data points are from [79] and the dashed line corresponds to the fit $\langle \bar{q}q \rangle_{(eB)} / \langle \bar{q}q \rangle = 1 + a(eB) + b(eB)^2$, with $a = 0.85$ GeV^{-2}, $b = 0.34$ GeV^{-4}.

$$m_\pi^2 \, f_\pi^2 = -2 \, (m_u + m_d) \langle \bar{q}q \rangle. \tag{5.44}$$

The GMOR relation is a result of the chiral algebra of QCD, and in its derivation it is only the pion propagator that is involved. There is no quark propagator as the quark fields combine to form the quark condensate. In the chiral limit eq. (5.43) states that the pion mass squared vanishes as the quark masses, and eq. (5.42) becomes

$$\frac{f^2_{\pi(eB)}}{f^2_\pi} = \frac{\langle \bar{q}q \rangle_{(eB)}}{\langle \bar{q}q \rangle} \, , \tag{5.45}$$

which we exploit to determine the pion decay constant in the presence of a magnetic field in terms of the quark condensate. The general validity of the GMOR relation in the presence of a magnetic field was shown in [89]. However, we only use this relation in the restricted sense of relating f_π to $\langle \bar{q}q \rangle$. The light-quark condensate in the presence of the magnetic field has been computed in [79]. We make use of this result, and parametrize the magnetic field dependence of the light-quark condensate with a quadratic fit

$$\langle \bar{q}q \rangle_{(eB)} / \langle \bar{q}q \rangle = 1 + a(eB) + b(eB)^2, \tag{5.46}$$

where $a = 0.85$ GeV^{-2}, $b = 0.34$ GeV^{-4} and (eB) is given in GeV^2. The data from [79] together with the fit are shown in Figure 5.5. Using this information we finally write the explicit solutions for s_0 and $C_4\langle O_4 \rangle$ from eq. (5.25)

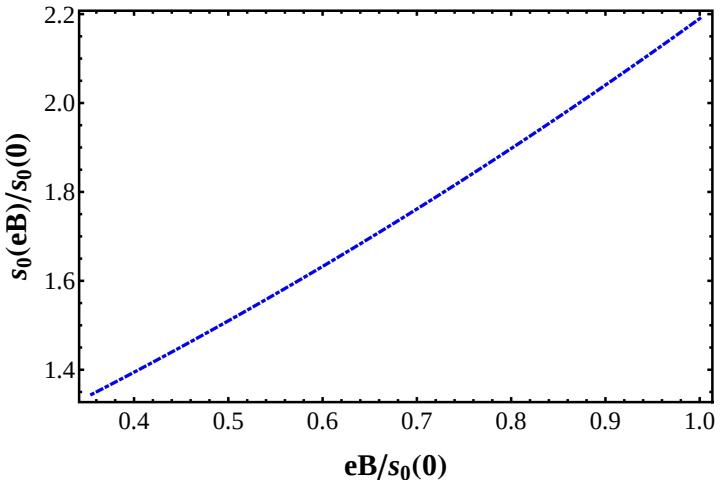

Figure 5.6: Squared energy pQCD threshold, s_0, normalized to its $eB = 0$ value, as a function of the field strength eB. Note that the plotted range is consistent with the requirement $eB < s_0 < 3eB$..

$$s_0 = -8\pi\mathcal{B}\langle\bar{q}q\rangle_{(eB)}$$
$$C_4\langle O_4\rangle = -2(eB)\mathcal{B}\langle\bar{q}q\rangle_{(eB)} + 8\pi(\mathcal{B}\langle\bar{q}q\rangle_{(eB)})^2 + \left(\frac{17}{18}\right)\frac{(eB)^2}{4\pi^2}. \tag{5.47}$$

The solutions for s_0 and for $C_4\langle O_4\rangle$ as functions of eB are plotted in Figure 5.6 and Figure 5.7, respectively. Note that s_0 is proportional to the absolute value of the light-quark condensate, and that together with $C_4\langle O_4\rangle$ it increases with increasing magnetic field. FESR and the low energy GMOR relation, in presence of weak magnetic fields, have provided a non-trivial behaviour of s_0 and $\langle\frac{\alpha_s}{\pi}G^2\rangle$, actually without any model Figure 5.6 and Figure 5.7 confirm the so called magnetic catalysis, through the relation between the chiral parameter $\langle\bar{q}q\rangle$ and the phenomenological deconfinement parameter s_0. As final comment, we can see that LQCD shown a monotonically decreasing behaviour of the light quark condensate, we found here, analytically and from model-independent technique, the same kind of behaviour as well for a region $\frac{s_0}{3} < eB < s_0$. It is important clarify that this regime of magnetic field, as we said above, is thinking to explore in the future the case at finite temperature, and because we want to describe QCD phase transition in physical systems like heavy-ion collisions and near to the critical, the situation when magnetic field strength is smaller than s_0 is the best one, insomuch as theoretical prediction of magnetic field intensity at times when QCD phase transition happens is one order of magnitude smaller than m_π^2 [90].

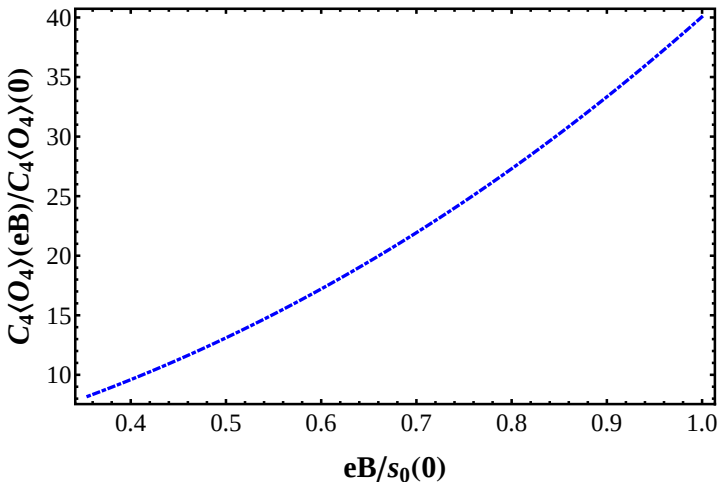

Figure 5.7: The gluon condensate, $C_4\langle O_4\rangle$, normalized to its $eB = 0$ value, as a function of eB. Note that the plotted range is consistent with the requirement $eB < s_0 < 3eB$.

CHAPTER 6

UNDERSTANDING INVERSE MAGNETIC CATALYSIS

The Inverse Magnetic Catalysis phenomenon, found by LQCD [77, 78]- [79], has been the center of attention in a large number of model-dependent analyses [91]- [102] (do not forget QCD is a unsolvable analytic theory). In general terms, it seems that inverse magnetic catalysis is not obtained in mean field approaches describing the thermal environment [81], [103]- [107], nor when calculations beyond mean field do not include magnetic effects on the coupling constants [108].

The novel feature implemented in effective models, able to account self-consistently for inverse magnetic catalysis, is the decrease of the coupling constants with increasing field strength obtained from the model itself [109]- [110] without resorting to *ad hoc* parametrizations. This has been achieved within the Abelian Higgs model and the linear sigma model coupled to quarks (LSMq). This behaviour is made possible by accounting for the screening properties of the plasma, which have been recently formulated consistently for theories with spontaneous symmetry breaking [108]. This results in a formalism beyond the mean field approximation [109]. Screening is also important to obtain a decrease of the QCD coupling constant with the magnetic field in the Hard Thermal Loop approximation [111]. Recently LSMq has been used to explore the QCD phase diagram at zero magnetic field and it was found that there are values for the model couplings that allow locating a critical end point (CEP) in the region where lattice inspired calculations find it [112]. Since the LSMq does not exhibit confinement, this behaviour is attributed to the proper

treatment of plasma screening, instead of to the existence of a given confinement length scale [113]. A pertinent question is whether the above description in the presence of a magnetic field can be used to study how such CEP changes with the field intensity and whether the inverse magnetic catalysis persists at finite chemical potential. Recent LQCD calculations [114] show that for very strong magnetic fields, inverse magnetic catalysis prevails and the phase transition becomes first order at asymptotically large values of the magnetic field for vanishing quark chemical potential μ. A similar behaviour is obtained in the Nambu–Jona-Lasinio model if one includes a magnetic field dependence of the critical temperature in agreement with LQCD [115].

At once we use the LSMq to explore the consequences of a proper handling of the plasma screening properties in the description of the magnetized effective QCD phase diagram. We show that when including self-consistently magnetic field effects in the calculation of both the effective potential as well as on the thermo-magnetic dependence of the coupling constants, the CEP's location moves toward smaller values of the critical quark chemical potential, and larger values of the critical temperature. In addition, above a certain value of the field strength the CEP moves to towards the T-axis. *We argue that this behaviour can be understood on general grounds, as the magnetic field produces a dimension reduction, whereby virtual charged particles from the vacuum are effectively constrained to occupy Landau levels, thus restricting their motion to a plane. This makes these particles to lay closer to each other on average, thus reducing the interaction strength for strongly coupled theories. This situation takes place regardless of how weak the external field is.*

We begin recalling the basic features of the linear sigma model coupled to quarks. The Lagrangian of the sigma model, including quark degrees of freedom, is given by

$$\begin{aligned}\mathcal{L} =& \frac{1}{2}(\partial_\mu\sigma)^2 + \frac{1}{2}(D_\mu\vec{\pi})^2 + \frac{a^2}{2}(\sigma^2+\vec{\pi}^2) - \frac{\lambda}{4}(\sigma^2+\vec{\pi}^2)^2 \\ &+ i\bar{\psi}\gamma^\mu D_\mu\psi - g\bar{\psi}(\sigma + i\gamma_5\vec{\tau}\cdot\vec{\pi})\psi,\end{aligned} \tag{6.1}$$

where ψ is an SU(2) isospin doublet, $\vec{\pi} = (\pi_1, \pi_2, \pi_3)$ is an isospin triplet and σ is an isospin singlet, with

$$D_\mu = \partial_\mu + iqA_\mu, \tag{6.2}$$

is the covariant derivative. A^μ is the vector potential corresponding to an external magnetic field directed along the $\hat{z}$ axis. In the symmetric gauge it is given by

$$A^\mu = \frac{B}{2}(0, -y, x, 0), \tag{6.3}$$

where q is the particle's electric charge. A^μ satisfies the gauge condition $\partial_\mu A^\mu = 0$. The gauge field couples only to the charged pion combinations, namely

$$\pi_\pm = \frac{1}{\sqrt{2}}\left(\pi_1 \mp i\pi_2\right). \tag{6.4}$$

The neutral pion is taken as the third component of the pion isovector, $\pi^0 = \pi_3$. The gauge field is taken as classical and thus we do not consider loops involving the propagator of the gauge field in internal lines. The squared mass parameter a^2 and the self-coupling λ and g are taken to be positive.

To allow for spontaneous symmetry breaking, we let the σ field to develop a vacuum expectation value v

$$\sigma \to \sigma + v, \tag{6.5}$$

this vacuum expectation value can later be identified as the order parameter of the theory. After this shift, the Lagrangian can be rewritten as

$$\begin{aligned}\mathcal{L} = &-\frac{1}{2}[\sigma(\partial_\mu + iqA_\mu)^2\sigma] - \frac{1}{2}\left(3\lambda v^2 - a^2\right)\sigma^2 \\ &-\frac{1}{2}[\vec{\pi}(\partial_\mu + iqA_\mu)^2\vec{\pi}] - \frac{1}{2}\left(\lambda v^2 - a^2\right)\vec{\pi}^2 + \frac{a^2}{2}v^2 \\ &-\frac{\lambda}{4}v^4 + i\bar{\psi}\gamma^\mu D_\mu\psi - gv\bar{\psi}\psi + \mathcal{L}_I^b + \mathcal{L}_I^f,\end{aligned} \tag{6.6}$$

where $\mathcal{L}_I^b$ and $\mathcal{L}_I^f$ are given by

$$\begin{aligned}\mathcal{L}_I^b = &-\frac{\lambda}{4}\Big[(\sigma^2 + (\pi^0)^2)^2 \\ &\quad + 4\pi^+\pi^-(\sigma^2 + (\pi^0)^2 + \pi^+\pi^-)\Big], \\ \mathcal{L}_I^f = &-g\bar{\psi}(\sigma + i\gamma_5\vec{\tau}\cdot\vec{\pi})\psi.\end{aligned} \tag{6.7}$$

The terms given in eq. (6.7) describe the interactions among the fields σ, $\vec{\pi}$ and ψ, after symmetry breaking. From eq. (6.6) one can see that the σ, the three pions and the quarks have masses given, respectively, by

$$\begin{aligned}m_\sigma^2 &= 3\lambda v^2 - a^2, \\ m_\pi^2 &= \lambda v^2 - a^2, \\ m_f &= gv.\end{aligned} \tag{6.8}$$

From the information above, we can see the LSMq's lagrangian exhibits an spontaneous symmetry breaking along the σ-field direction, where the classical- or tree-level potential is given by

$$V^{\text{tree}} = -\frac{a^2}{2}v^2 + \frac{\lambda}{4}v^4. \tag{6.9}$$

The minimum is obtained for

$$v_0 = \frac{a}{\sqrt{\lambda}}. \tag{6.10}$$

Notice that dynamic masses in eq. (6.8) evaluated at v_0 show $\vec{\pi}$ are the Nambu-Goldstone bosons [116] in this model. Due to we have a symmetry spontaneously broken, then we need to consider matter effects (thermal modifications) which restore the symmetry, thus we compute the effective potential to account such matter effects, the first term in the effective potential is the tree-level potential, eq. (6.9) (thermal independent), the second term considers the quantum corrections at 1-loop order, however because we want to include thermal effects, we need to use quantum field theory at finite temperature, and because we always consider the system is in thermal equilibrium, we choose the imaginary time formalism [117].

Using Schwinger's proper-time method, the expression for the 1-loop effective potential (mean field approximation) for one boson field with squared mass m_b^2 and absolute value of its charge q_b at finite temperature T in the presence of a constant magnetic field can be written as

$$\begin{aligned} V_b^{(1)} =& \frac{T}{2}\sum_n \int dm_b^2 \int \frac{d^3k}{(2\pi)^3}\int_0^\infty \frac{ds}{\cosh(q_bBs)} \\ &\times e^{-s(\omega_n^2+k_3^2+k_\perp^2\frac{\tanh(q_bBs)}{q_bBs}+m_b^2)}, \end{aligned} \tag{6.11}$$

where $\omega_n = 2n\pi T$ are boson Matsubara modes. As we already know, magnetic fields split the momentum components in parallel and transverse respect the magnetic field direction, then the d^3k integral in eq. (6.11) can be written as $dk_3\ d^2k_\perp$, computing the transverse components, the proper time variable s and mass integrals, and rewriting the integrand in terms of Landau Levels, then the sum over n (the sum over all Matsubara modes) is done and the result is

$$V_b^{(1)} = \frac{eB}{4\pi}\sum_{l=0}^{\infty}\int \frac{dk_3}{2\pi}[\omega_l + 2T\log(1-e^{-\omega_l/T})], \tag{6.12}$$

with $\omega_l = \sqrt{k_3^2 + m_b^2 + (2l+1)eB}$, the integrand in eq. (6.12) has two terms, the first one in the *r.h.s.* is the vacuum quantum correction at 1-loop and the second one is the thermal correction at the same order.

Similarly, the expression for the one-loop effective potential for one fermion field with mass m_f and absolute value of its charge q_f at finite temperature T and chemical potential μ, in the presence of a constant magnetic field can be written as

$$V_f^{(1)} = -\sum_{r=\pm 1} T \sum_n \int dm_f^2 \int \frac{d^3k}{(2\pi)^3} \int_0^\infty \frac{ds}{\cosh(q_f B s)} \times e^{-s[(\tilde{\omega}_n - i\mu)^2 + k_3^2 + k_\perp^2 \frac{\tanh(q_f B s)}{q_f B s} + m_f^2 + r q_f B]}, \tag{6.13}$$

where $\tilde{\omega}_n = (2n+1)\pi T$ are fermion Matsubara modes. The sum over the index r corresponds to the two possible spin orientations along the magnetic field direction. By performing the integration over $d^2k_\perp$, ds and dm_f^2, rewriting the integrand in term of Landau Levels, the sum of Matsubara frequencies is computed and the answer is

$$V_f^{(1)} = -\frac{eB}{2\pi} \sum_{l=0}^{\infty} \sum_{r=\pm 1} \int \frac{dk_3}{2\pi} [\omega_{l,r} + T \log(1 - e^{-(\omega_{l,r} - \mu)/T}) + T \log(1 - e^{-(\omega_{l,r} + \mu)/T})], \tag{6.14}$$

with $\omega_{l,r} = \sqrt{k_3^2 + m_f^2 + (2l + 1 + r)q_f B}$, eq. (6.14) shows the vacuum quantum correction and the thermal correction, both at 1-loop order, but in this fermionic case the thermal correction has information of finite density through the quark-chemical potential.

In eqs. (6.12) and (6.14) is necessary to compute the sum over all Landau levels, though those sums diverge when we do not take any approximation, hence we will use the weak field approximation, *i.e.* $eB < T^2$, in order to obtain the leading magnetic field contribution in this approximation, we use Euler-MacLaurin expansion; a short explanation of it and how we use this approximation is shown in Appendix B. Computing the new integrals we get

$$
\begin{aligned}
V_b^{(1)} &= \frac{m_b^4}{64\pi^2}\left[1-\log\left(\frac{2a^2}{(4\pi T)^2}\right)-2\gamma_E\right]-\frac{\pi^2T^4}{90}+\frac{m_b^2T^2}{24}-\frac{m_b^3T}{12\pi}\\
&+\frac{(eB)^2}{192\pi^2}\left[\frac{2\pi T}{m_b}+\log\left(\frac{2a^2}{(4\pi T)^2}\right)+2\gamma_E-1-\zeta(3)\left(\frac{m_b}{2\pi T}\right)^2+\frac{3}{4}\zeta(5)\left(\frac{m_b}{2\pi T}\right)^2\right],\\
V_f^{(1)} &= -\Bigg\{\frac{m_f^4}{16\pi^2}\left[\log\left(\frac{(4\pi T)^2}{2a^2}\right)+\psi^{(0)}\left(\frac{1}{2}+\frac{i\mu}{2\pi T}\right)+\psi^{(0)}\left(\frac{1}{2}-\frac{i\mu}{2\pi T}\right)\right]\\
&+8m_f^2T^2\left[\mathrm{Li}_2(-e^{\mu/T})+\mathrm{Li}_2(-e^{-\mu/T})\right]-32T^4\left[\mathrm{Li}_4(-e^{\mu/T})+\mathrm{Li}_4(-e^{-\mu/T})\right]\\
&+\frac{(eB)^2}{24\pi^2}\Bigg[\log\left(\frac{(\pi T)^2}{2a^2}\right)-2\gamma_E+1-\psi^{(0)}\left(\frac{1}{2}+\frac{i\mu}{2\pi T}\right)-\psi^{(0)}\left(\frac{1}{2}-\frac{i\mu}{2\pi T}\right)\\
&+\frac{2\pi}{[(\pi+i\mu/T)^2+(m_f/T)^2]^{1/2}}+\frac{2\pi}{[(\pi-i\mu/T)^2+(m_f/T)^2]^{1/2}}-\frac{4\pi}{[\pi^2+(m_f/T)^2]^{1/2}}\Bigg]\Bigg\},
\end{aligned}
\tag{6.15}
$$

where $\psi^0(x)$ is the digamma function, Li_n is the polylogarithm function of order n, and γ_E is the Euler's gamma. Both expressions that appear in eq. (6.15), after choosing the renormalization scale $\widetilde{\mu} = e^{-1/2}a$, are the contributions to the effective potential at 1-loop order. Besides bosonic expression shows problematic terms, such as odd powers of m_b, insomuch as these terms could be imaginary, according eq. (6.8), for some values of v. However when we introduce the leading temperature plasma screening effects for the boson masses squared, encoded in the boson self-energy, they remove or at least reduce drastically the values of v which generate imaginary terms into the effective potential. The contribution that corresponds to screening effects is the so called *ring diagrams* and it contributes as follows

$$
\begin{aligned}
V_b^{(ring)} &= \frac{T}{2}\int\frac{d^3k}{(2\pi)^3}\log[1+\Pi\, D(\omega_{n=0},k,qB)]\\
&= \frac{T}{12\pi}\left[m_b^3-\frac{(qB)^2}{8m_b}+\frac{T(2qB)^{3/2}}{8\pi}\zeta\left(-\frac{1}{2},\,\frac{1}{2}+\frac{m_b^2+\Pi}{2qB}\right)\right],
\end{aligned}
\tag{6.16}
$$

with Π the leading contribution for the boson self-energy in a high temperature expansion, and at finite μ and it is given

$$
\Pi = \lambda\frac{T^2}{2}-N_fN_cg^2\frac{T^2}{\pi^2}[\mathrm{Li}_2(-e^{\mu/T})+\mathrm{Li}_2(-e^{-\mu/T})]. \tag{6.17}
$$

Substituting eq. (6.17) into eq. (6.16), and putting all the contributions of effective potential together, the final expression is

$$
\begin{aligned}
V^{(\mathrm{eff})} = & -\frac{a^2}{2}v^2 + \frac{\lambda}{4}v^4 + \sum_{i=\sigma,\pi^0}\left\{\frac{m_i^4}{64\pi^2}\left[\ln\left(\frac{(4\pi T)^2}{2a^2}\right) - 2\gamma_E + 1\right] - \frac{\pi^2 T^4}{90} + \frac{m_i^2 T^2}{24}\right. \\
& \left. - \frac{T}{12\pi}(m_i^2 + \Pi)^{3/2}\right\} + \sum_{i=\pi_+,\pi_-}\left\{\frac{m_i^4}{64\pi^2}\left[\ln\left(\frac{(4\pi T)^2}{2a^2}\right) - 2\gamma_E + 1\right] - \frac{\pi^2 T^4}{90}\right. \\
& + \frac{m_i^2 T^2}{24} + \frac{T(2qB)^{3/2}}{8\pi}\zeta\left(-\frac{1}{2}, \frac{1}{2} + \frac{m_i^2 + \Pi}{2qB}\right) - \frac{(qB)^2}{192\pi^2}\left[\ln\left(\frac{(4\pi T)^2}{2a^2}\right) - 2\gamma_E\right. \\
& \left.\left. + 1 + \zeta(3)\left(\frac{m_i}{2\pi T}\right)^2 - \frac{3}{4}\zeta(5)\left(\frac{m_i}{2\pi T}\right)^4\right]\right\} - N_c\sum_{f=u,d}\left\{\frac{m_f^4}{16\pi^2}\left[\ln\left(\frac{(4\pi T)^2}{2a^2}\right)\right.\right. \\
& \left.\left. + \psi^0\left(\frac{1}{2} + \frac{i\mu}{2\pi T}\right) + \psi^0\left(\frac{1}{2} - \frac{i\mu}{2\pi T}\right)\right] + 8m_f^2 T^2[Li_2(-e^{\mu/T}) + Li_2(-e^{-\mu/T})]\right. \\
& - 32T^4[Li_4(-e^{\mu/T}) + Li_4(-e^{-\mu/T})] + \frac{(q_f B)^2}{24\pi^2}\left[\ln\left(\frac{(\pi T)^2}{2a^2}\right) - 2\gamma_E + 1\right. \\
& - \psi^0\left(\frac{1}{2} + \frac{i\mu}{2\pi T}\right) - \psi^0\left(\frac{1}{2} - \frac{i\mu}{2\pi T}\right) + \frac{2\pi}{((\pi + i\mu/T)^2 + m_f^2/T^2)^{1/2}} \\
& \left.\left. + \frac{2\pi}{((\pi - i\mu/T)^2 + m_f^2/T^2)^{1/2}} - \frac{4\pi}{(\pi^2 + m_f^2/T^2)^{1/2}}\right]\right\}. \qquad (6.18)
\end{aligned}
$$

Though we take the quark masses as equal, the notation emphasizes that the effective potential is evaluated after accounting for the different quark charges. The effective potential has contributions of neutral boson fields as well, that contributions are equal to the charged bosons but in the limit $qB \to 0$. For the Hurwitz zeta function $\zeta(-1/2, z)$ in eq. (6.18) to be real, one needs

$$
-a^2 + \Pi > qB, \qquad (6.19)
$$

a condition that arises from requiring that the second argument of the Hurwitz zeta function satisfies $z > 0$, even for the lowest value of m_b^2 which is obtained for $v = 0$. Furthermore, for the large T expansion to be valid, one also requires

$$
qB/T^2 < 1. \qquad (6.20)
$$

The conditions expressed in eqs. (6.19) and (6.20) provide the limits of applicability of the high temperature expansion of the effective potential in eq. (6.18).

We now compute the one-loop correction to the coupling λ, including thermal and magnetic effects. Figure 6.1 shows the Feynman diagrams that contribute to this correction. Columns (a), (b), (c), (d), (e) and (f) contribute, respectively, to the correction to the σ^4, $(\pi^0)^4$, $(\pi^+)^2(\pi^-)^2$, $\sigma^2\pi^+\pi^-$, $(\pi^0)^2\pi^+\pi^-$ and $\sigma^2(\pi^0)^2$ terms of the interaction Lagrangian

in eq. (6.6), respectively. Since each of these corrections lead to the same result, we concentrate on the diagrams in column (a). Each of the three diagrams involves two propagators of the same boson. For the first two diagrams the intermediate bosons are neutral and for the third one the intermediate bosons are charged.

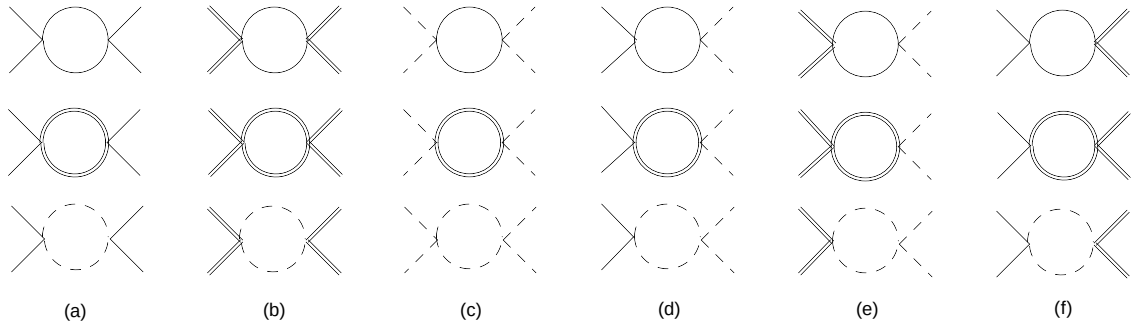

Figure 6.1: One-loop Feynman diagrams that contribute to the thermal and magnetic correction to the coupling λ. The dashed line denotes the charged pion, the continuous line is the sigma and the double line represents the neutral pion.

The explicit computation has been performed in [110]. This involves the use of the weak field expansion of the charged boson Schwinger's proper-time propagator for the intermediate charged particles and its corresponding $qB \to 0$ limit for the intermediate neutral bosons. Since the analysis of [110] was carried out in the very high temperature case, the four-boson vertex correction was evaluated in the *infrared limit*, namely $P_i = (0, \mathbf{p} \to 0)$, where P_i are the momenta of each of the four external legs. However, for the present analysis, where T is close to T_c a more appropriate treatment is to evaluate the vertex function at the typical energy of the external particles. This corresponds to the *static limit*, namely $P_i = (\Pi, \mathbf{p} = 0)$, where Π is given by eq. (6.17) and represents the purely thermal (and density) component of the boson mass. In the Appendix C, we explicitly reproduce such calculation, evaluating the vertex function in the static limit. Notice that λ_{eff} depends on v through the dependence on the boson masses. We further consider the approximation where λ_{eff} is evaluated at $v = 0$ since we are pursuing the effect on the critical temperature, which is the temperature where the curvature of the effective potential at $v = 0$ vanishes.

Next we turn to the calculation of the thermo-magnetic correction of the coupling g. Figure 6.2 shows the Feynman diagrams that contribute to this correction. We are interested in computing an effective value for this coupling, g_{eff}, as well as for $v = 0$, in the same manner done for λ_{eff}. Columns (a), (b) and (c) contribute to the correction to the quark-σ, quark-π^0 and quark-$\pi^\pm$ terms of the interaction Lagrangian of eq. (6.6), respectively.

Since each of these corrections leads to the same result, we concentrate on the diagrams in column (a). Notice that for $v = 0$ in eq. (6.8), the masses of the σ and the π^0 become degenerate. Hence, the middle and bottom diagrams in column (a) of Figure 6.2 cancel out, since they contribute with opposite signs. This also happens with the two bottom diagrams in columns (b) and (c).

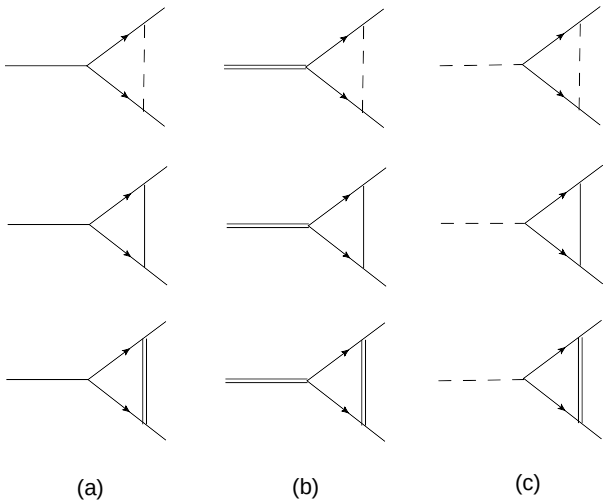

Figure 6.2: One-loop Feynman diagrams that contribute to the thermal and magnetic correction to the coupling g. The dashed line denotes the charged pion, the continuous line is the sigma, the double line represents the neutral pion and the continuous line with arrows represents the quarks.

The explicit computation is carried out in the weak field limit of the charged boson and fermion Schwinger proper-time propagators. The calculation is done in Appendix D, in this case the contribution $\mathcal{O}(qB)$ does not vanish. This is because the spin average is not needed, as we are not considering a decay process, but rather a vertex function. We have also evaluated g_{eff} in the static limit $P_i = (m_f^{\text{therm}}, \mathbf{p} = 0)$ where P_i are the momenta of the quark and antiquark and m_f^{therm} is the fermion thermal (and density)-dependent mass, which we compute in the Appendix E and whose square is given explicitly by

$$(m_f^{\text{therm}})^2 = g^2 T^2 \left(\frac{1}{3} - \frac{Li_2(-e^{\mu/T})}{\pi^2} - \frac{Li_2(-e^{-\mu/T})}{\pi^2} \right). \tag{6.21}$$

To fix the bare values of the couplings λ, g and a appropriate for the description of the phase transition, we notice that the boson masses are modified when considering the thermal effects, since they acquire a thermal component. For $\mu = 0$ they become

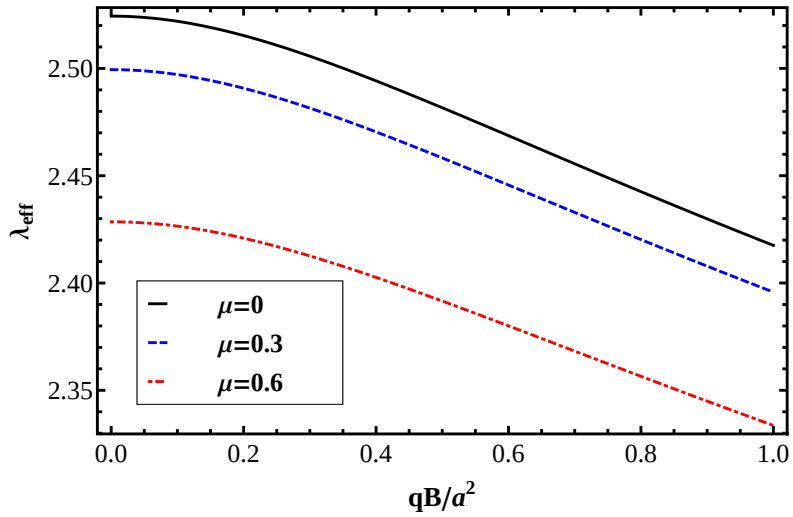

Figure 6.3: Effective boson coupling λ_{eff} evaluated a the temperature $T = 180$ MeV with $\lambda = 0.4$, $g = 0.63$ as a function of the magnetic field strength for different values of μ.

$$m_\sigma^2(T) = 3\lambda v^2 - a^2 + \frac{\lambda T^2}{2} + \frac{N_f N_c g^2 T^2}{6}$$
$$m_\pi^2(T) = \lambda v^2 - a^2 + \frac{\lambda T^2}{2} + \frac{N_f N_c g^2 T^2}{6}. \tag{6.22}$$

At the phase transition, the curvature of the effective potential vanishes for $v = 0$. Since the boson masses are proportional to this curvature, these also vanish at $v = 0$. In this case, and from any of eq. (6.22), we then obtain a relation between T_c^0 and the model parameters at the critical temperature with $\mu = 0$

$$\frac{a}{T_c^0} = \sqrt{\frac{\lambda}{2} + \frac{N_f N_c g^2}{6}}. \tag{6.23}$$

Furthermore, we can fix the value of a by noting from eq. (6.8) that the vacuum boson masses satisfy

$$a = \sqrt{\frac{m_\sigma^2 - 3m_\pi^2}{2}}. \tag{6.24}$$

Since the effective potential is written as an expansion in powers of a/T we need that this ratio satisfies $a/T < 1$. From eqs. (6.23) and (6.24) the coupling constants are proportional to m_σ which, from the above conditions, restricts the analysis to considering not too large values of m_σ as well as not too small values of T_c^0. Since our purpose is not to pursue a precise determination of the couplings but instead to call attention to the fact that the

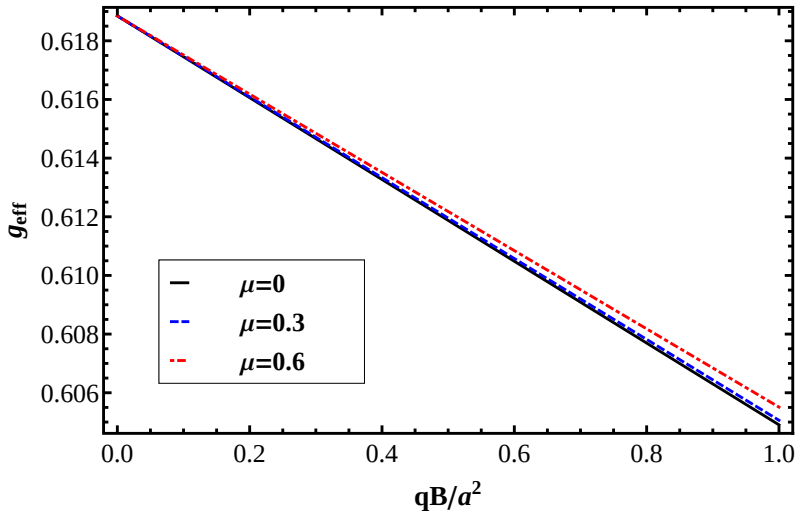

Figure 6.4: Effective boson-fermion coupling $g_{\rm eff}$ evaluated a the temperature $T = 180$ MeV with $\lambda = 0.4$, $g = 0.63$ as a function of the magnetic field strength for different values of μ.

proper treatment of screening effects allows the linear sigma model to provide solutions for the CEP even at finite values of μ, we consider small values for m_σ. Given that σ is anyhow a broad resonance, in order to satisfy the above requirements let us take for definitiveness $m_\sigma = 300$ MeV namely, close to the two-pion threshold. For T_c^0 with two light quark flavours we take $T_c^0 = 172$ MeV [118]. Thus, $a/T_c^0 = 0.77$.

Eq. (6.23) provides a relation between λ and g. A possible solution consistent with the above requirements is given by $\lambda = 0.4$, $g = 0.63$. Figure 6.3 shows the behaviour of the effective boson coupling $\lambda_{\rm eff}$ evaluated using $T = 180$ MeV, as a function of magnetic field strength for different values of μ. The considered temperature is slightly larger that T_c^0. Note that $\lambda_{\rm eff}$ is a monotonically decreasing function of qB and that the decrease is larger for larger values of μ. Figure 6.4 shows the behaviour of $g_{\rm eff}$ as a function of qB evaluated also using $T = 180$ MeV with $\lambda = 0.4$, $g = 0.63$ for three different values of μ. Note that $g_{\rm eff}$ is also a monotonically decreasing function of qB. However, the decrease is less pronounced for larger values of μ. Note that the μ-dependence of the effective coupling comes from its dependence on $m_f^{\rm them}$.

We now study the effect of the thermo-magnetic corrections to the couplings on the critical temperature. For a given value of the magnetic field, and for a second order phase transition, the critical temperature is determined after setting to zero the second derivative of the effective potential at $v = 0$ in eq. (6.18). When the phase transition becomes first order, the critical temperature is computed by determining the temperature where a

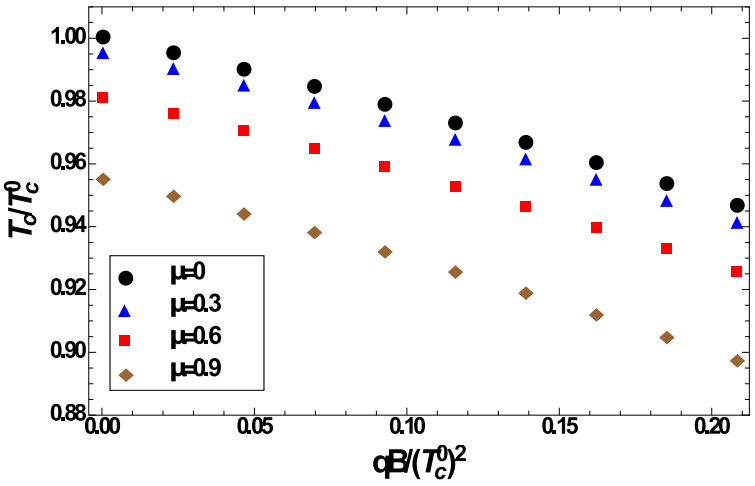

Figure 6.5: Critical temperature as a function of the magnetic field strength evaluated using effective couplings including thermo-magnetic corrections with the bare values of the couplings $\lambda = 0.4$, $g = 0.63$ for different values of μ. Note that in all cases the critical temperature is a monotonically decreasing function of the magnetic field strength.

secondary minimum for $v \neq 0$ is degenerate with a minimum at $v = 0$. Figure 6.5 shows the critical temperature as a function of field strength, for different values of μ, and for the bare values $\lambda = 0.4$, $g = 0.63$. Note that in all cases the critical temperature is a decreasing function of the field strength.

On the contrary when the calculation is performed without including the thermo-magnetic modification to the couplings, the critical temperature turns out to be an increasing function of the field strength. This is shown in Figure 6.6 where we plot the critical temperature as a function of qB for different values of μ with the bare values of the couplings $\lambda = 0.4$, $g = 0.63$.

To test the relative importance of the magnetic field-dependence on the couplings, we compute the critical temperature when one of the couplings depends on the magnetic field while we keep the other one constant. Figure 6.7 shows the behaviour of the critical temperature keeping $\lambda = 0.4$ fixed and with the full magnetic field and temperature-dependence of the quark-meson coupling computed with $g = 0.63$, for different values of μ. Figure 6.8 shows the behaviour of the critical temperature keeping $g = 0.63$ fixed and with the full magnetic field and temperature-dependence of the meson self-coupling computed with $\lambda = 0.63$, for different values of μ. We can see that the magnetic field-dependent corrections to the couplings produce a similar relative effect on the behaviour of the critical temperature. These findings show that the thermo-magnetic corrections to

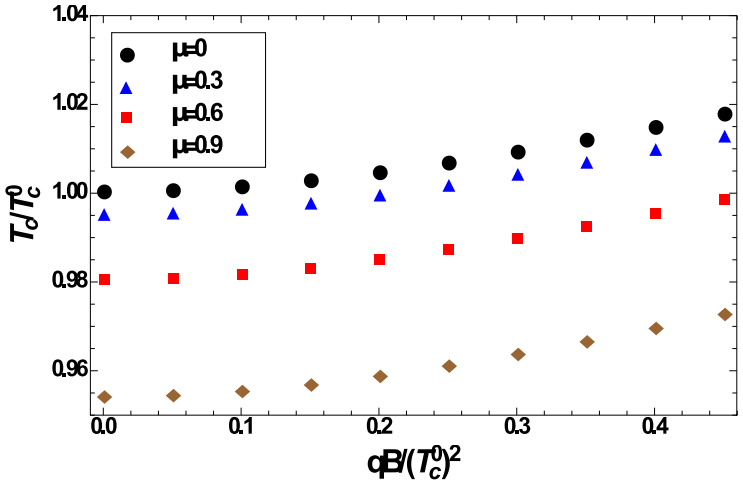

Figure 6.6: Critical temperature as a function of the magnetic field strength evaluated without effective couplings and instead with the bare values of the couplings $\lambda = 0.4$, $g = 0.63$ for different values of μ. Note that in all cases the critical temperature is a monotonically increasing function of the magnetic field strength.

both couplings are crucial to obtain inverse magnetic catalysis.

We now turn to describe the phase diagram in the temperature-quark chemical potential plane. Figure 6.9 shows the phase diagram obtained for the bare couplings $\lambda = 0.4$, $g = 0.63$ for different values of the magnetic field strength. The thermo-magnetic corrections enter the analysis both in the effective potential of eq. (6.18), and in the effective couplings. Notice that as the field intensity increases, the CEP moves toward lower values of the critical quark chemical potential, and to larger values of the critical temperature and in this case, it reaches the T-axis. However, since our analysis is carried out in the weak field limit $qB/T^2 < 1$, we can only say that there is a tendency for the CEP to eventually reach the T-axis for large values of the field strength.

To see the effect of a change of parameters we now explore the case where the ratio a/T_c^0, appearing in eq. (6.23), changes. We take $a/T_c^0 = 0.66$ which is obtained maintaining $m_\sigma = 300$ MeV and increasing the value of T_c^0 to $T_c^0 = 200$ MeV. With this ratio, a possible solution to eq. (6.23) for the bare values of the couplings is given by $\lambda = 0.36$, $g = 0.51$. Figure 6.10 shows the phase diagram thus obtained. Notice that the CEP for $qB = 0$ happens for values of $T_c^{\rm CEP}$ and $\mu_c^{\rm CEP}$ slightly smaller and larger, respectively, than for the corresponding values in Figure 6.9. When the magnetic field intensity increases the CEP also moves toward lower values of the critical quark chemical potential and larger values of the critical temperature but this time, for the largest value of qB considered,

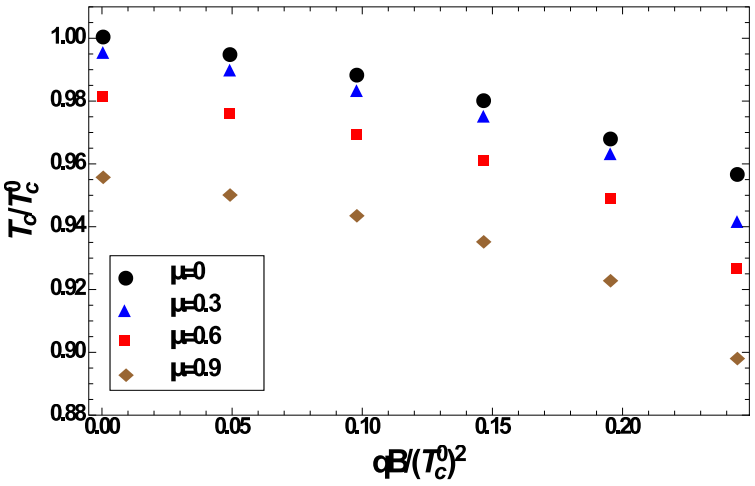

Figure 6.7: Critical temperature as a function of the magnetic field strength evaluated keeping $\lambda = 0.4$ fixed and with the full magnetic field and temperature-dependence of the quark-meson coupling computed with $g = 0.63$, for different values of μ.

the CEP does not reach the T-axis. Nevertheless we observe a tendency for the CEP to eventually reach the T-axis for larger values of qB that can not be studied within the present small field approach.

We have shown that working in the LSMq in the presence of magnetic fields, it is possible to obtain values for the couplings that allow to locate a CEP that for $qB = 0$, lays in the region found by mathematical extensions of lattice analyses. The analysis is done from the effective potential computed in the presence of a weak magnetic field and accounting for the plasma screening effects. Since the LSMq does not have confinement, we attribute the CEP's location to the adequate description of the plasma screening properties. Screening is included into the calculation in two manners: First, in the effective potential through the boson's self-energy and second in the thermo-magnetic corrections of the couplings. We have shown that this last correction is crucial to obtain inverse magnetic catalysis. To define the allowed range for the bare coupling constants we observe that the thermal boson masses vanish at the phase transition for $\mu = 0$. This condition determines a relation between the model parameters which can be put in quantitative terms from knowledge of T_c^0 and a. The first can be obtained from lattice results and the second from the vacuum boson masses. Since the model is computed in the high temperature limit, we are limited to consider ratios of the parameter a/T_c^0 a bit off their usual values. Nevertheless, the model shows in quantative terms that the CEP moves toward lower values of the critical quark chemical potential and larger values of the critical temperature as the field intensity

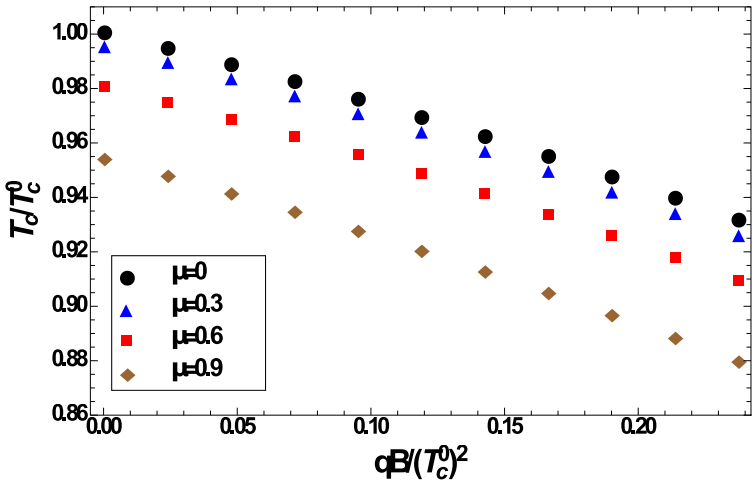

Figure 6.8: Critical temperature as a function of the magnetic field strength evaluated keeping $g = 0.63$ fixed and with the full magnetic field and temperature-dependence of the meson self-coupling computed with $\lambda = 0.63$, for different values of μ.

increases and that there is a tendency for the CEP to eventually reach the T-axis for a larger value of the field strength.

The overall features of the phase diagram can be understood in general terms when we recall that the magnetic field produces a dimension reduction whereby the virtual charged particles that make up the vacuum are effectively constrained to occupy Landau levels which, in semiclassical terms, implies that their motion is restricted to planes. This produces that these particles lay on average closer to each other. Since as a function of the field intensity we have shown that the strength of the interaction is reduced, and that this happens no matter how weak the external field may be, we infer that a similar effect is taking place in QCD where due to asymptotic freedom, the strength of the interaction gets reduced as the virtual particles get closer to each other. This weakening of the interaction with proximity between the virtual particles that make up the vacuum should manifest itself as well in the weakening of the quark condensate with the field strength, as is also observed in lattice QCD around the critical temperature. We believe this description will play an important role in the interpretation of the lattice QCD results for the behaviour of the critical temperature and the quark condensate with the field intensity as well as in determining the location of the CEP in QCD with and without magnetic fields.

As we have already seen, inclusion of effective coupling constants into effective models play a primordial role in the understanding of the inverse magnetic catalysis. We have pointed out above that the proper treatment of screening effects are very important to

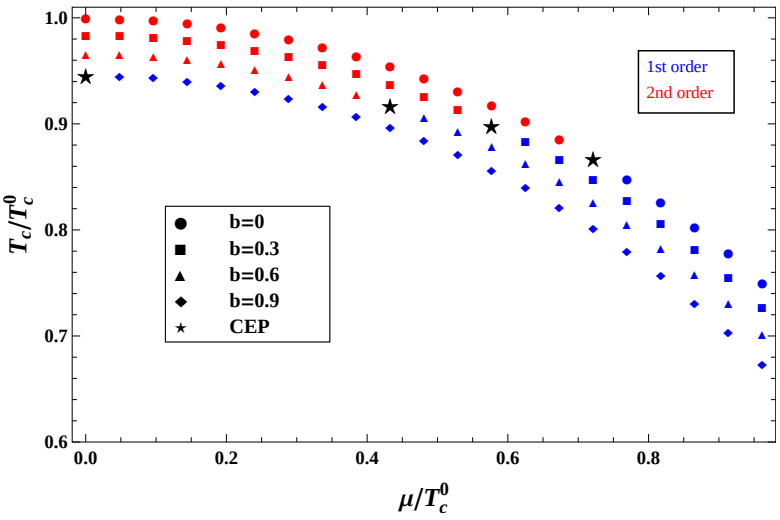

Figure 6.9: Phase diagram in the temperature quark chemical potential plane computed with thermomagnetic corrections to the couplings using the bare values $\lambda = 0.4$, $g = 0.63$ corresponding to $a/T_c^0 = 0.77$ for different values of the magnetic field strength. The phase transitions to the left (right) of the CEP in each case are of second (first) order.

describe the LQCD results, however if we are still working with effective models at some point we are not able to be conclusive in our results, therefore we think is possible to put a little bit bigger effort and trying to explore QCD itself, we can be closer to describe the real nature of the inverse magnetic catalysis at least at some kinematical regime.

Let us do a brief remainder about the status of the magnetic catalysis and the inverse magnetic catalysis. In recent LQCD determinations, properties of strongly interacting matter in the presence of magnetic fields exhibit intriguing characteristics. In a thermal environment, at and above the transition temperature for deconfinement/chiral symmetry restoration, the magnetic field hinders the formation of the quark condensate and makes the critical temperature decrease with increasing field strength. This behaviour is corresponds to the inverse magnetic catalysis. In contrast, the vacuum ($T = 0$) condensate grows with the magnetic field strength. As the temperature increases near, but below the transition temperature, the condensate begins to grow for weak fields reaching a maximum value, smaller than for $T = 0$ and the same field strength. Subsequently, the condensate decreases with increasing field strength. This growth of the quark condensate with magnetic field strength corresponds to magnetic catalysis. Overall, this behaviour indicates, from our point of view, that the strength of the QCD interaction at $T = 0$ is enhanced by the magnetic field, thus strengthening the binding of quark-antiquark pairs that make up the condensate. However, as the temperature increases, such binding becomes weaker.

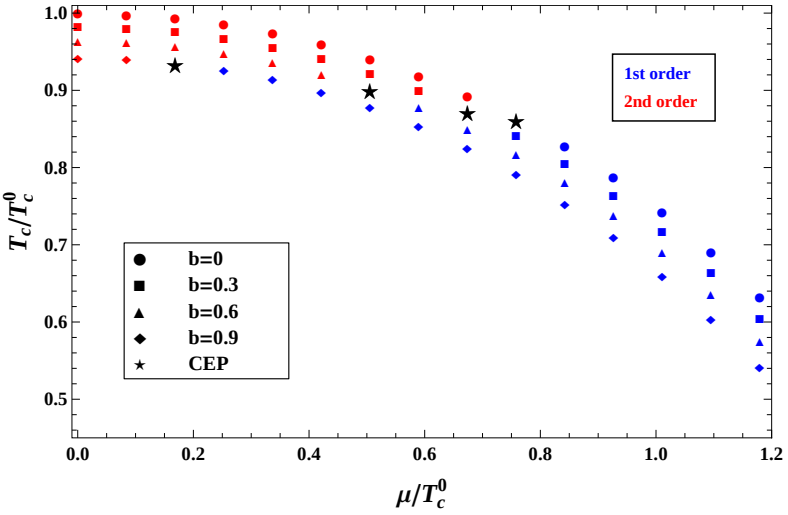

Figure 6.10: Phase diagram in the temperature quark chemical potential plane computed with thermomagnetic corrections to the couplings using the bare values $\lambda = 0.36$, $g = 0.51$ corresponding to $a/T_c^0 = 0.66$ for different values of the magnetic field strength. The phase transitions to the left (right) of the CEP in each case are of second (first) order.

When the temperature reaches the transition region the magnetic field dominates the interaction, quenching monotonically the binding for all field strengths. The search for an explanation of such properties has attracted the attention of a great deal of research over the last years as we mention some times during this thesis. A possible way to look at this effect has been casted in terms of the competition between the valence and the sea contributions to the quark condensate. It has been argued that at $T = 0$ both contributions are growing as a function of eB. However, around the critical temperature T_c the valence contribution is still increasing whereas the sea contribution decreases, as a function of eB. This seemingly results in a decrease of T_c as a function of eB.

On general grounds a magnetic field interacting with electrically charged particles acts as an *ordering agent.* In other words, the motion of virtual or real charges takes place around the magnetic field lines. This ordered motion has an important geometrical consequence: charged particles are closer to each other on average. When the intensity of the magnetic field increases, so does the proximity between charges. As is well known, due to asymptotic freedom, the closer strongly interacting particles are, the weaker the interaction is. However strongly interacting matter, either at zero or at finite temperature, is not only made out of quarks and antiquarks but also of electrically neutral gluons. If the geometrical effect produced by the magnetic field were related to inverse magnetic catalysis, then at low temperatures the colour interactions produced by gluons should dominate, while

quarks would take over at high temperatures.

An important clue on the properties of strongly interacting matter in the presence of a magnetic field has been provided in [119] for the case of high temperature. There it was shown that under such conditions the quark-gluon effective coupling decreases with the field intensity and that the colour charge contribution from the gluons cancels exactly. Furthermore, the magnetic field-dependent vertex correction satisfies a Ward-like identity involving the magnetic field dependent quark self-energy. This means that at high temperature colour dynamics is dominated by quarks. This behaviour can be understood in terms of the geometrical picture whereby the proximity between electric charges induced by the magnetic field dominates the colour interaction. An outstanding question is whether this picture holds also at $T = 0$, namely, whether under such circumstances the strength of the colour interaction becomes, instead, gluon dominated.

Taking into account the result from [119], we now compute the magnetic field contribution to the quark-gluon vertex in vacuum and show that, indeed, the strong interaction becomes dominated by the contribution of the electrically neutral gluons. This generates an effective coupling that grows with increasing field strength, in contrast with the high-temperature result. Recall that inverse magnetic catalysis can also be quantified in terms of the properties of the quark condensate as a function of the magnetic field. Since the condensate is a measure of the strength of the bound between either vacuum ($T = 0$) or thermal ($T \neq 0$) quark-antiquark pairs and α_s is a measure of the strength of the interaction between these quark-antiquark pairs, both quantities represent the strength of the quark-antiquark binding. We show a mechanism that can help understand inverse magnetic catalysis consists on pursuing the relation between the properties of α_s as a function of the magnetic field and the condensate. In this context we recall that several calculations that address the behaviour of the quark condensate in the presence of a magnetic field, coincide in that the condensate is an increasing function of the field strength [120]. Both, the coupling constant and the condensate, should behave similarly as a function of the field strength. We find that in the two extreme cases, namely, at high and zero T, they do. Here we do not address the details of how this change happens, which certainly require non-perturbative information for their description. However, by establishing that this change in the properties of α_s happens at these two extremes, we put forward a novel scenario to study inverse magnetic catalysis in terms of the thermo-magnetic properties of the strong coupling constant.

We begin by considering the case of a magnetic field pointing along the $\hat{z}$ direction. In a magnetic background, the fermion propagator in coordinate space can no longer be

written as a simple Fourier transform of a momentum propagator but instead it is written as eq. (4.55), it has the *Schwinger phase factor* times the translational invariant part of the propagator, the latter is given by

$$iS(p) = \int_0^\infty \frac{ds}{\cos(qBs)} e^{is(p_\parallel^2 - p_\perp^2 \frac{\tan(qBs)}{qBs} - m^2)} \left\{ [\cos(qBs) + \gamma_1\gamma_2 \sin(qBs)] (m + \not{p}_\parallel) - \frac{\not{p}_\perp}{\cos(qBs)} \right\}, \tag{6.25}$$

where m and q are the quark mass and absolute value of the quark charge, in units of the electron charge, respectively. Hereafter we use the following definitions for the parallel and perpendicular components of the scalar product of any two vectors a^μ and b^μ

$$\begin{aligned} (a \cdot b)_\parallel &= a_0 b_0 - a_3 b_3 \\ (a \cdot b)_\perp &= a_1 b_1 + a_2 b_2. \end{aligned} \tag{6.26}$$

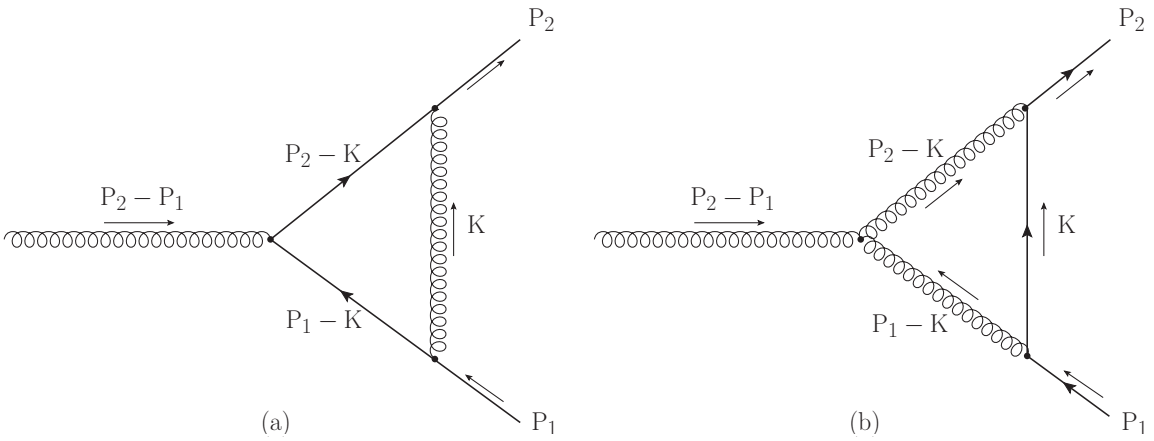

Figure 6.11: Feynman diagrams contributing to the magnetic dependence of the quark-gluon vertex. Diagram (a) corresponds to a QED-like contribution whereas diagram (b) corresponds to a pure QCD contribution.

Figure 6.11 shows the Feynman diagrams contributing to the quark-gluon vertex. Diagram (a) corresponds to a QED-like contribution whereas diagram (b) corresponds to the pure QCD contribution. The computation of these diagrams requires the fermion propagator given by eq. (4.55), which involves the Schwinger phase factor $\Phi(x, x')$. We have already shown in chapter 4 that when only one or two fermion propagators are involved in this

kind of triangle loop, the phase factor can be *gauged away* and we can just work with the translational invariant part of the fermion propagators.

Since the effect we are after shows up already for small magnetic field strengths, we consider the case of a weak field for which the fermion propagator can be written as

$$iS(p) = i\frac{\not{p}}{p^2} - (qB)\gamma_1\gamma_2\frac{\not{p}_\parallel}{p^4}, \tag{6.27}$$

notice eq. (6.27) is in fact eq. (4.80) in the chiral limit, namely $m = 0$. The chiral limit of the weak field expansion of the fermion propagator is a well defined object. In fact, this expansion can be viewed as a power series in eB of the full propagator, independently of any relation between the field and the fermion mass. In the present context a field is weak if compared with the gluon momentum squared, which must be large in a perturbation calculation.

Working in the Feynman gauge, the contributions to the magnetic field dependent part of the quark-gluon vertex from diagrams (a) and (b) of Figure 6.11, in the weak field limit are

$$\begin{aligned}\delta\Gamma^{\mu\alpha}_{(a)} &= ig^3(qB)\left(C_F - \frac{C_A}{2}\right)t^\alpha \int \frac{d^4k}{(2\pi)^4}\frac{1}{k^2} \\ &\times \left\{\gamma^\nu \frac{(\not{p}_2 - \not{k})}{(p_2-k)^2}\gamma^\mu \frac{\gamma_1\gamma_2(\not{p}_1 - \not{k})_\parallel}{(p_1-k)^4}\gamma_\nu + \gamma^\nu \frac{\gamma_1\gamma_2(\not{p}_2 - \not{k})_\parallel}{(p_2-k)^4}\gamma^\mu \frac{(\not{p}_1 - \not{k})}{(p_1-k)^2}\gamma_\nu\right\},\end{aligned} \tag{6.28}$$

$$\begin{aligned}\delta\Gamma^{\mu\alpha}_{(b)} =& -2ig^3(qB)\frac{C_A}{2}t^\alpha \int \frac{d^4k}{(2\pi)^4}\frac{1}{k^4}\Big[g^{\mu\nu}(2p_2 - p_1 - k)^\rho + g^{\nu\rho}(2k - p_2 - p_1)^\mu \\ &+ g^{\rho\mu}(2p_1 - k - p_2)^\nu\Big]\gamma_\rho \frac{\gamma_1\gamma_2\not{k}_\parallel}{(p_2-k)^2(p_1-k)^2}\gamma_\nu,\end{aligned} \tag{6.29}$$

where C_F, C_A are the colour factors corresponding to the fundamental and adjoint representations of the $SU(N)$ Casimir operators, $C_F = (N^2-1)/2N$, and $C_A = N$ and t^α is a Gell-Mann matrix. The explicit factor of 2 in eq. (6.29) takes care of the two possible charge fluxes in diagram (b) of Figure 6.11.

We consider $\Gamma^{\mu\alpha}_{(a)}$ and $\Gamma^{\mu\alpha}_{(b)}$ as functions of the relative and average quark-pair four-momenta, $Q = p_1 - p_2$ and $P = (p_1 + p_2)/2$, respectively. According to the kinematics depicted in Figure 6.11, Q corresponds to the four-momentum carried by the gluon. For simplicity we consider the symmetric three-momentum configuration where $p_1 = (E, \vec{p})$, $-p_2 = (E, -\vec{p})$, thus $Q = (2E, \vec{0})$ and $P = (0, \vec{p})$. In this case, Q^2 is proportional to the energy and P^2 to the momentum squared carried by the gluon. To make a closer connection to

the case discussed in [119], we work in the *static* limit, namely $P \to 0$. Furthermore, in order to make sure that the perturbative calculation makes sense, we take Q^2 large. In this sense, the expansion parameter for the validity of the calculation becomes qB/Q^2. In this limit, after a lengthy but straightforward exercise, eqs. (6.28) and (6.29) become

$$\delta\Gamma^{\mu\alpha}_{(a)} = -ig^3\left(C_F - \frac{C_A}{2}\right)t^\alpha \frac{[1+\ln(4)]}{3\pi^2}\frac{q\vec{\Sigma}\cdot\vec{B}}{Q^2}\left(\not{u}u^\mu + \not{b}b^\mu\right)\,, \tag{6.30}$$

$$\delta\Gamma^{\mu\alpha}_{(b)} = -ig^3 C_A t^\alpha \frac{[-1+\ln(4)]}{15\pi^2}\frac{q\vec{\Sigma}\cdot\vec{B}}{Q^2}\left(\not{u}u^\mu + \not{b}b^\mu\right), \tag{6.31}$$

where $\vec{\Sigma}\cdot\vec{B} = \Sigma_3 B = i\gamma_1\gamma_2 B$ is the dot product between the spin operator and the magnetic field vector and we have defined $u^\mu = (1,0,0,0)$ and $b^\mu = (0,0,0,1)$. Notice that the first order magnetic field-dependent correction is proportional to the coupling between the quark spin and the magnetic field, affecting only the longitudinal components ($\mu = 0, 3$). The same longitudinal matrix structure has been found for the vertex correction in the presence of a magnetic field in the context of an effective QCD model and in QED [121]. The explicit computation of eqs. (6.28)-(6.31) is in Appendix F.
From the longitudinal components of the full vertex (to this order), namely

$$\Gamma^\alpha_\parallel = i\gamma^\mu_\parallel t^\alpha + \delta\Gamma^{\mu\alpha}_{(a)} + \delta\Gamma^{\mu\alpha}_{(b)}, \tag{6.32}$$

one can extract the effective vacuum quark-gluon coupling in the presence of a magnetic field

$$\begin{aligned} g^{\text{vac}}_{\text{eff}} &= g - \left[g^3\frac{1}{3\pi^2}\frac{q\vec{\Sigma}\cdot\vec{B}}{Q^2}\right]\left\{\left(C_F - \frac{C_A}{2}\right)[1+\ln(4)] + \frac{C_A}{5}[-1+\ln(4)]\right\} \\ &= g - \left[g^3\frac{1}{3\pi^2}\frac{q\vec{\Sigma}\cdot\vec{B}}{Q^2}\right]\left\{[1+\ln(4)]\,C_F - \frac{[7+3\ln(4)]}{10}C_A\right\}. \end{aligned} \tag{6.33}$$

For $N = 3$ (even $N = 2$), the contribution from the colour charge associated to gluons (C_A) dominates over the contribution from the colour charge associated to quarks (C_F). The net effect is that in vacuum, the effective coupling between quarks and gluons grows with the magnetic field strength. In contrast, we recall that the effective thermo-magnetic coupling computed at high temperature becomes [119]

$$g^{\text{therm}}_{\text{eff}} = g\left[1 - \frac{m_f^2}{T^2} + \left(\frac{8}{3T^2}\right)g^2 C_F M^2(T, m_f, qB)\right], \tag{6.34}$$

where m_f is the quark thermal mass and the function $M^2(T, m, qB)$ is given by

$$M^2(T, m, qB) = \frac{q\vec{\Sigma}\cdot\vec{B}}{16\pi^2}\left[\ln(2) - \frac{\pi}{2}\frac{T}{m}\right], \tag{6.35}$$

which for high temperature is negative definite. Notice that contrary to the $T = 0$ case, the magnetic field-dependent correction at high temperature is proportional only to the contribution from the colour charge associated to quarks, *i.e.* C_F. This is because the contribution from the colour charge associated to gluons, C_A, cancels identically.

Equations (6.33) and (6.34) show that in the presence of a magnetic field, at $T = 0$, the contribution from the colour charges associated to gluons dominates marginally over the contribution from the colour charge associated to quarks. Since the former has the opposite sign of the latter, the overall effective coupling grows with the magnetic field strength. At high temperature however, the contribution from the colour charge associated to gluons cancels and the colour dynamics is quark-dominated. Since the surviving magnetic field-dependent contribution has an overall negative sign, the effective coupling decreases with the magnetic field strength. We point out that calculations carried out in the opposite limit, namely the very strong field case, find that the coupling constant at $T = 0$ decreases as a function of the field strength [122]. Altogether this means that the behaviour found in this work should be valid up to a certain (albeit large) value of the magnetic field.

Notice that the perturbative calculation at $T = 0$ requires that Q^2 is large and that the weak field approximation is valid provided $qB \ll Q^2$. At finite temperature, the large temperature assumption provides the large energy scale for the perturbative calculation (Hard Thermal Loop approximation) as well as for the weak field approximation to be valid.

Also, notice that the kinematical conditions we have implemented include studying the configuration where the quark and antiquark travel back to back. This means that their relative orbital angular momentum L vanishes. Since the gluon spin is $S = 1$, the quarks must carry a total spin $S = 1$ with a preferred projection aligned with the magnetic field direction. If we consider a different kinematical configuration whereby the quark-antiquark pair emerged with another relative angle different from 180 degrees, then conservation of angular momentum and parity implies that the relative angular momentum L has to be either 0 or 2. In both cases, the total quark-antiquark spin needs to be $S = 1$.

Also, we point out that this calculation provides not only the behaviour of the effective coupling constant but also of the effective quark-gluon vertex as a function of the magnetic field (in the weak field limit). This vertex can in turn be used to compute a given process that may be influenced by the presence of the magnetic field. Consider for instance $\bar{q}q \to \bar{q}q$ process. Also the effective vertex found here, the amplitude for this process can

be constructed attaching the gluon line to the incoming $\bar{q}q$ whereas the outgoing $\bar{q}q$ is already provided by the vertex. The process can be described in any given Lorentz frame. We thus see that choosing the symmetric configuration is tantamount to working in the center of mass of the colliding pair. Since the matrix element is Lorentz invariant, the choice of frame is a matter of convenience. The use of the static limit is an approximation that is valid provided there is a large scale (larger than the quark momenta or the masses) present in the calculation. This large scale is the gluon virtuality Q^2. When this quantity is large so it is the energy of the collision in the above-described process. This means that the calculation lends itself to be applied to describing hard $\bar{q}q$ annihilation (or scattering). This kind of processes are relevant in collisions of hadronic systems, namely A+p or p+p and even A+A with a large momentum transfer involved, where the energy is larger than the temperature, if any. In summary, we can say that the choice of configuration and of kinematics is general enough under these circumstances.

Finally, notice that the study is performed by looking at two extreme scenarios, the result showed here at $T = 0$ and the result at $T \neq 0$ in [119], where perturbation theory at leading order is under control, therefore avoiding the ambiguities of non-perturbative elements where modelling is oftentimes involved (see for example in [123]). In these limits a first order calculation in the magnetic field intensity suffices for two reasons: First, since there is a large energy scale provided either by the temperature (squared) or by the quark's momentum (squared), the field can be taken as small with respect to either of these energy scales. Second, the LQCD calculation for the condensate in the (high) zero temperature limit is a monotonically (decreasing) increasing function of the field strength. In order to study if α_s behaves similarly with the magnetic field strength, what matters is knowledge of the sign of the first derivative of α_s at $qB = 0$. This can be computed merely from the linear term in qB which is the term computed in this work.

Although interesting effects take place in the opposite limit, namely the strong field case (see for example in [114]), for the purpose of this work, as argued, it suffices to work in the weak field limit. In the same context, applying a standard renormalization group analysis to explore the change of the coupling with scale will not affect the sign of its rate of change with the magnetic field. Moreover, it is precisely said that both approximations can not describe with enough efficiency real physical situation, instead from the pragmatic point of view, both approximation are equal important because with them, we can refine our knowledge on this issue and at the same time that we will be able to reduce the gap between both extremes and therefore to be closer of describing the real physical systems.

The result in [119] and our results show that the geometrical effect produced by the

magnetic field at high temperature, whereby quarks and anti-quarks get closer on average, is accompanied by the decrease of their effective interaction due to asymptotic freedom. This takes place because in that scenario the strong interactions are due entirely to the colour charge associated to quarks. The strength of the interaction thus decreases with increasing magnetic field strength. In contrast, at $T = 0$ such geometrical effect does not take place. This is because the colour charge associated to gluons produces a kind of screening of the colour charge associated to quarks. In turn, and in spite of the quark-anti-quark proximity, this leads to an increase in the effective strong coupling with increasing magnetic field strength. Such larger coupling results in a tighter quark-anti-quark bond, leading to a larger quark condensate as obtained in LQCD at $T = 0$. In contrast, a smaller coupling translates into a looser quark-anti-quark bond and thus into a decreasing condensate at large T, as also found by LQCD. Similar considerations phrased in terms of the competition between valence and sea-quark contributions around T_c have been argued in [124].

One consequence of analysing the QCD phase diagram in presence of magnetic fields, using the linear sigma model coupled to quarks, was the clear effect of effective coupling constants. Only when the coupling constants know about finite thermal and magnetic effects then *inverse magnetic catalysis* happens, even when finite density is considered. All of this behaviour was in the context of effective models, however the immediately question at that time was related to looking for the same kind of analysis in the context of pQCD, the computations were done at finite temperature in [119] and at zero temperature was reported in this thesis some lines above and in [125], the results showed an equivalent behaviours between the light-quark condensate and the effective strong coupling, at zero temperature and at temperatures above of pseudo-critical temperature, in other words, we found that at zero temperature both light-quark condensate and effective strong coupling have monotonic increasing behaviour, while at temperatures above of pseudo-critical temperature they have monotonic decreasing behaviour. However, these behaviours are valid in the perturbative region, we are not able to conclude the same in the region where non-perturbative effects are dominant, then if we want to know more about the relation between the light-quark condensate and the effective strong coupling not only in the perturbative region, we should come back to use some effective model, and that is what we did, promptly we talk about this.

Different approaches have been explored in order to either find or include IMC in QCD [91, 92, 98, 103, 107, 114, 126, 127], some of these provide an explanation [93–95, 100, 128], and almost all suggest the need to include extra ingredients in terms of magnetic-induced

modifications of QCD properties. In particular, the modification of the QCD coupling due to magnetic screening at low temperature and antiscreening at high temperature has been shown to be a plausible mechanism to explain IMC [97, 99, 101, 102, 109, 110, 119, 125, 129, 130]. This also seems to be the reason why effective models without such modifications do not describe neither the behaviour of the critical temperature nor the properties of the quark-antiquark condensate at high temperature [81, 104–106, 131–134].

Deducing the detailed screening/antiscreening properties of the strong coupling as a function of the field strength is not a simple task since these properties belong for the largest portion of the parameter space to the non-perturbative domain. Nevertheless, it should be possible to extract general features of this coupling by resorting to combining information from effective models and LQCD.

The Nambu–Jona-Lasinio (NJL) is one of such models. It has been extensively used to explore the chiral transition [135, 136]. In particular, the NJL model can be used to formulate a simplified version of the QCD gap equation by means of the Schwinger-Dyson technique where the dynamically generated mass M is constant (momentum independent) and the interaction is given by a four-fermion contact term whose strength is controlled by a coupling G. A pertinent question is whether it is possible to extract information on the behaviour of the coupling G as a function of the magnetic field strength and temperature by combining the NJL model with LQCD data for the quark-antiquark condensate in the presence of a magnetic field, and whether this information can be used to get clues on the microscopical origins of IMC.

In this time we take this approach. We use the NJL model to extract the behaviour of G and M as a function of the magnetic field for different temperatures using LQCD data for the quark-antiquark condensate [79], as a function of the field strength, as input into the gap equation. Notice that if there is a link between the fading-out of the condensate as a function of eB above the transition temperature for the chiral/deconfinement transition and the thermo-magnetic dependent coupling, then the latter should also decrease with the field intensity. This behaviour would signal that a decreasing coupling contributes to a less intense bound between quark-antiquark pairs above the critical temperature, as the field intensity grows. In this work we show that this is the case.

For this purpose, we set up the framework writing the expression for the gap equation and the quark propagator obtained from the NJL model in the constant (momentum independent) mass approximation. These equations, together with the expression for the quark-antiquark condensate given in terms of the quark propagator provide the set of equations that allow finding the behaviour of M and G as a function of the field strength

for different temperatures. Besides, we include the effects of the magnetic field by means of Schwinger's proper time method. Since the NJL model is not renormalizable, in order to find the behaviour of M and G as a function of the magnetic field, we first isolate the pure vacuum contribution from the thermo-magnetic one. Thus, the equation to the quark condensate is written by inlcuding only *thermo-magnetic* contribution, then we solve the equation to quark condensate to find the thermo/magentic M, using as input the LQCD behaviour of the average u and d quark-antiquark condensate as a function of the field strength. After find M, we also compute G through the gap equation. Since the light quarks have different charges, we actually find the values for M and G by averaging over the light-quark flavours. As test to check the validity of our results we also compute the thermo-magnetic pressure and show that above T_c the isotropic pressure starts off being positive for small field strength values. Below T_c this pressure starts from zero and then becomes negative as the field strength increases, in agreement with LQCD calculations. We argue that this result goes in line with the idea that above (below) T_c quarks are brought together (pushed apart) and this triggers the coupling becomes weaker (stronger) due to the asymptotic freedom.

Let us begin defining the NJL model by means of the Lagrangian density

$$\mathcal{L} = \bar{\psi}(i\partial\!\!\!/ - m)\psi + G\left(\left(\bar{\psi}\psi\right)^2 + \left(\bar{\psi}i\gamma^5\boldsymbol{\tau}\psi\right)^2\right), \tag{6.36}$$

where $\boldsymbol{\tau}$ are the Pauli matrices in isospin space, and ψ is a quark field.

On general grounds, in the mean field approximation, and after a bosonization process, the Lagrangian can be rewritten as a vacuum term plus a free fermion Lagrangian with a dressed mass, namely

$$\mathcal{L}_{MF} = -\frac{\sigma^2}{4G} + \bar{\psi}(i\partial\!\!\!/ - M)\psi\ , \tag{6.37}$$

where $\sigma = 4G\langle\bar{\psi}\psi\rangle$ and $M = m + \sigma$. Here we do not consider pion condensation effects, so the only contribution comes from the sigma meson in the bosonization procedure. The value of the mean field is determined through the *gap equation*, obtained by minimizing the effective potential with respect to the mean field [135, 136]

$$M - m = 4G\int \frac{d^4p}{(2\pi)^4}\mathrm{Tr}[iS(p)], \tag{6.38}$$

with the trace referring to colour and Lorentz indices. We notice that the quark condensate $\langle\bar{\psi}\psi\rangle$ is given by

$$\langle\bar{\psi}\psi\rangle = -\int \frac{d^4p}{(2\pi)^4}\mathrm{Tr}[iS(p)]. \tag{6.39}$$

In absence of magnetic fields, the propagator is given by

$$S(p) = \frac{\not{p} + M}{p^2 - M^2 + i\epsilon}. \tag{6.40}$$

Eqs. (6.38) and (6.39) represent the two independent equations providing information on the thermo-magnetic behaviour of the coupling G and the dynamically generated mass M, after using LQCD results for the quark condensates [79].

To account for the magnetic field, we emphasize that the above described bosonization does not affect the form of the gap equation (6.38) nor the condensate (6.39), and the effect of the magnetic field is reflected in the dressing of the quark propagator in a magnetic field, for which we resort to Schwinger's proper time representation for the two-point function

$$\begin{aligned} iS(p) = \int_0^\infty \frac{ds}{\cos(q_f Bs)} e^{is(p_\parallel^2 - p_\perp^2 \frac{\tan(q_f Bs)}{q_f Bs} - M^2 + i\epsilon)} \\ \left[(\cos(q_f Bs) + \gamma_1\gamma_2 \sin(q_f Bs))\,(M + \not{p}_\parallel) - \frac{\not{p}_\perp}{\cos(q_f Bs)}\right], \end{aligned} \tag{6.41}$$

where q_f is the absolute value of the quark charge (i.e. $q_u = 2|e|/3$ and $q_d = |e|/3$), and we have chosen the homogeneous magnetic field to point in the $\hat{z}$ direction, namely $\boldsymbol{B} = B\hat{z}$. This configuration can be obtained from an external vector potential which we choose in the so called *symmetric gauge* and it is shown in eq. (6.3). We have also use the prescriptions for four-momenta vectors in eqs. (4.22) and (4.23). Notice that since the magnetic field breaks Lorentz invariance, the propagator involves a non-local, albeit path independent phase. However, by taking the trace over a closed one-loop diagram, as is required for the calculation of the condensate, this phase does not contribute (see chapter 4) and thus we ignore it in the sequel.

Using eq. (6.41) to take the trace in eq. (6.39), we obtain

$$\langle\bar{\psi}_f\psi_f\rangle = -4N_c M \frac{1}{2}\sum_f \int \frac{d^4p}{(2\pi)^4}\int_0^\infty ds\; e^{is(p_\parallel^2 - p_\perp^2 \frac{\tan(q_f Bs)}{q_f Bs} - M^2 + i\epsilon)}. \tag{6.42}$$

where the factor one half in eq. (6.42) refers to the average over quark-flavours.

The integration over the transverse momentum components can be carried out, leading to

$$\int \frac{d^2p_\perp}{(2\pi)^2}\; e^{-i\frac{\tan(q_f Bs)}{q_f B}p_\perp^2} = \frac{q_f B}{4\pi i}\frac{1}{\tan(q_f Bs)}. \tag{6.43}$$

In order to introduce a finite temperature, within the Matsubara formalism, we transform the integrals to Euclidean space by means of

$$\int \frac{d^2p_{\parallel}}{(2\pi)^2} \to iT \sum_{n=-\infty}^{+\infty} \int \frac{dp_3}{(2\pi)}, \tag{6.44}$$

where the integral over the zeroth component of the fermion momentum has been discretized. We also perform the change of variable $s = -i\tau$. Therefore, the expression for the quark condensate becomes

$$\langle \bar{\psi}_f \psi_f \rangle = -N_c M \frac{1}{2} \sum_f \frac{q_f B}{\pi} T \sum_{n=-\infty}^{+\infty} \int_{-\infty}^{+\infty} \frac{dp_3}{(2\pi)} \int_{\tau_0}^{+\infty} \frac{d\tau}{\tanh(q_f B\tau)} e^{-\tau(\tilde{\omega_n^2}+\omega^2)}, \tag{6.45}$$

where we have introduced the fermion Matsubara frequencies $\tilde{\omega}_n = (2n+1)\pi T$ and $\omega^2 = p_3^2 + M^2$. Since the NJL model is non-renormalizable, we must regularize one of the two integrals that appears in eq. (6.45). One method consists to regularize the integral respect p_3, namely 3D cut-off regularization type, the other method is regularizing the integral respect the proper time, it is called proper time regularization method, both cases consist to introduce a cut-off, the parameter τ_0 represents such regulator. In this occasion, we choose to use the second method, the mean reason is due to with this method is possible to isolate the vacuum term from the thermo-magnetic one, at the same time that we guarantee the regularization does not involve any magnetic or thermal effect, since we know the vacuum structure has ultraviolet divergence and it is just what we have already regularized. This procedure is shown next.

In eq. (6.45), we find two integrals and one sum to be done, and they commute, thus we have the freedom for choosing the order to compute them. We start to compute the integral respect p_3 and we obtain

$$\langle \bar{\psi}_f \psi_f \rangle = -N_c M \frac{1}{2} \sum_f \frac{q_f B}{\pi^{3/2}} T \sum_{n=-\infty}^{+\infty} \int_{\tau_0}^{+\infty} \frac{d\tau}{\sqrt{\tau}\tanh(q_f B\tau)} e^{-\tau(\tilde{\omega_n^2}+M^2)}. \tag{6.46}$$

We now express the sum in eq. (6.46) in terms of Jacobi's $\vartheta_3(z,x)$ function, defined as

$$\vartheta_3(z,x) = \sum_{n=-\infty}^{+\infty} e^{(i\pi x n^2 + 2i\pi z n)}, \tag{6.47}$$

whereby

$$\sum_{n=-\infty}^{+\infty} e^{-\tau(2n+1)^2\pi^2T^2} = e^{-2\pi^2\tau T^2}\vartheta_3(2\pi i\tau T^2, 4\pi i\tau T^2). \tag{6.48}$$

For our purposes it is useful to invoke the inversion formula

$$\vartheta_3(z,x) = \sqrt{\frac{i}{x}}\; e^{z^2\pi/ix}\; \vartheta_3\left(\frac{z}{x}, -\frac{1}{x}\right), \tag{6.49}$$

By using eqs. (6.48) and (6.49) into eq. (6.46), we have

$$\langle\bar{\psi}_f\psi_f\rangle = -N_c M \frac{1}{2}\sum_f \frac{q_f B}{4\pi^2}\int_{\tau_0}^{\infty}\frac{d\tau}{\tau\tanh(q_f B\tau)}e^{-\tau M^2}\vartheta_3(\frac{1}{2},\frac{i}{4\tau\pi T^2}). \tag{6.50}$$

The Jacobi's $\vartheta_3(z,x)$ function can be written in term of a series, as follows

$$\vartheta_3(\frac{1}{2},\frac{i}{4\tau\pi T^2}) = 1 + 2\sum_{k=1}^{\infty}(-1)^k e^{-k^2/4\tau T^2}, \tag{6.51}$$

we notice that the $T = 0$ term correspond to $n = 0$ in the above expression. Therefore the vacuum contribution is obtained from the $n = 0$ term in the limit where $q_f B \to 0$. Adding and subtracting 1 in the integrand we get

$$\begin{aligned}\langle\bar{\psi}_f\psi_f\rangle = &-\frac{N_c M}{4\pi^2}\Bigg\{\int_{\tau_0}^{\infty}\frac{d\tau}{\tau^2}e^{-\tau M^2} + \frac{1}{2}\sum_f q_f B\int_{\tau_0}^{\infty}\frac{d\tau}{\tau^2}e^{-\tau M^2}\left[\frac{q_f B\tau}{\tanh(q_f B\tau)} - 1\right]\\ &+\sum_f q_f B\sum_{k=1}^{\infty}(-1)^k\int_{\tau_0}^{\infty}d\tau\frac{e^{-\tau M^2}}{\tau\tanh(q_f B\tau)}e^{-k^2/4\tau T^2}\Bigg\},\end{aligned} \tag{6.52}$$

where we can identify the vacuum condensate as given by the expression

$$\langle\bar{\psi}_f\psi_f\rangle_0 = -\frac{N_c M_0}{4\pi^2}\int_{\tau_0}^{\infty}\frac{d\tau}{\tau^2}e^{-\tau M_0^2}, \tag{6.53}$$

whereas the thermo-magnetic contribution is given by

$$\begin{aligned}\langle\bar{\psi}_f\psi_f\rangle_{B,T} = &-\frac{N_c M}{4\pi^2}\sum_f q_f B\Bigg\{\frac{1}{2}\int_0^{\infty}\frac{d\tau}{\tau^2}e^{-\tau M^2}\left[\frac{q_f B\tau}{\tanh(q_f B\tau)} - 1\right]\\ &+\sum_{k=1}^{\infty}(-1)^k\int_0^{\infty}d\tau\frac{e^{-\tau M^2}}{\tau\tanh(q_f B\tau)}e^{-k^2/4\tau T^2}\Bigg\}.\end{aligned} \tag{6.54}$$

The quantity $M \equiv M(B,T)$ in eq. (6.54) is such that when $B, T \to 0$, $M \to M_0$. It turn out that the integrals in eq. (6.54) are finite as the lower limit of integration goes to zero. This means that the thermo-magnetic effects are independent of the regulator and we have consequently set this lower limit to zero in eq. (6.54). Also the term that only depends on magnetic field strength can be computed analytically, with the result

$$\int_0^\infty \frac{d\tau}{\tau^2} e^{-\tau M^2}\left[\frac{q_f B\tau}{\tanh(q_f B\tau)} - 1\right] = 2\Bigg[\log\Gamma\left(1+\frac{M^2}{2q_f B}\right) + \frac{M^2}{2q_f B}\left(1-\log\left(\frac{M^2}{2q_f B}\right)\right) - \frac{1}{2}\log\left(\frac{M^2}{2q_f B}\right)\Bigg]. \quad (6.55)$$

$\tau_0\ [GeV^{-2}]$	$-\langle\bar{\psi}_f\psi_f\rangle_0^{1/3}\ [GeV]$	$M_0\ [GeV]$	$G_0\ [GeV^{-2}]$	$m\ [GeV]$	$T_c^{NJL}\ [GeV]$
1.27	0.220	0.224	5.08	7.58×10^{-3}	0.267
0.74	0.260	0.192	2.66	4.65×10^{-3}	0.228

Table 6.1: Two sets of values for the vacuum regulator τ_0, condensate $\langle\bar{\psi}_f\psi_f\rangle_0$ and dynamically generated mass M_0 stemming from requiring that the pion mass and of the pion decay constant in the NJL model attain their physical values. Shown also are the corresponding vacuum values for the coupling constant G_0, current quark mass m and the critical temperature for $eB = 0$.

Eq. (6.53) can be use to fix the vacuum values $\langle\bar{\psi}_f\psi_f\rangle_0$ and M_0 from a choice of τ_0.Two sets of the pion mass and of the pion decay constant are shown in Table 6.1. Shown also are the corresponding vacuum values for the coupling constant G_0 and the current quark mass m.

It is important to notice that the critical temperature given by the model depends on the choice of M_0 and does not coincide with the corresponding value reported by lattice. Therefore, it is necessary to scale the values of the model temperatures to make them correspond to the physical values. The simplest choice is a linear scaling such that

$$T^{NJL} = \left(\frac{T_c^{NJL}}{T_c}\right)T, \quad (6.56)$$

where T represents the physical value of the temperature, T_c and T_c^{NJL} are the physical and model critical temperatures, respectively.

We use as condition to find the critical temperature the vanishing of the derivative of the thermal piece of the quark condensate with respect to the temperature, namely

$$\frac{d}{dT}\langle\bar{\psi}_f\psi_f\rangle_{0,T} = 0, \quad (6.57)$$

where

$$\langle\bar{\psi}_f\psi_f\rangle_{0,T} = \frac{2N_c M}{\pi^2}\int_0^\infty dp \frac{p^2}{\sqrt{p^2+M^2}}\frac{1}{e^{\sqrt{p^2+M^2}/T}+1}. \quad (6.58)$$

A straightforward calculation in the approximation where T_c^{NJL} and M are of the same order gives

$$T_c^{NJL} \simeq 2.38M. \tag{6.59}$$

To have a better estimate of T_c^{NJL}, one needs to evaluate the above equation at an appropriate value of M. We observe that at the critical temperature, the dynamically generated mass drops from its vacuum value to about half of it, namely to $M_0/2$. Using this as the working criterion and the reported LQCD value for the critical temperature $T_c = 0.158$ GeV, we obtain the corresponding values for the model critical temperature, which we also show in Table 6.1.

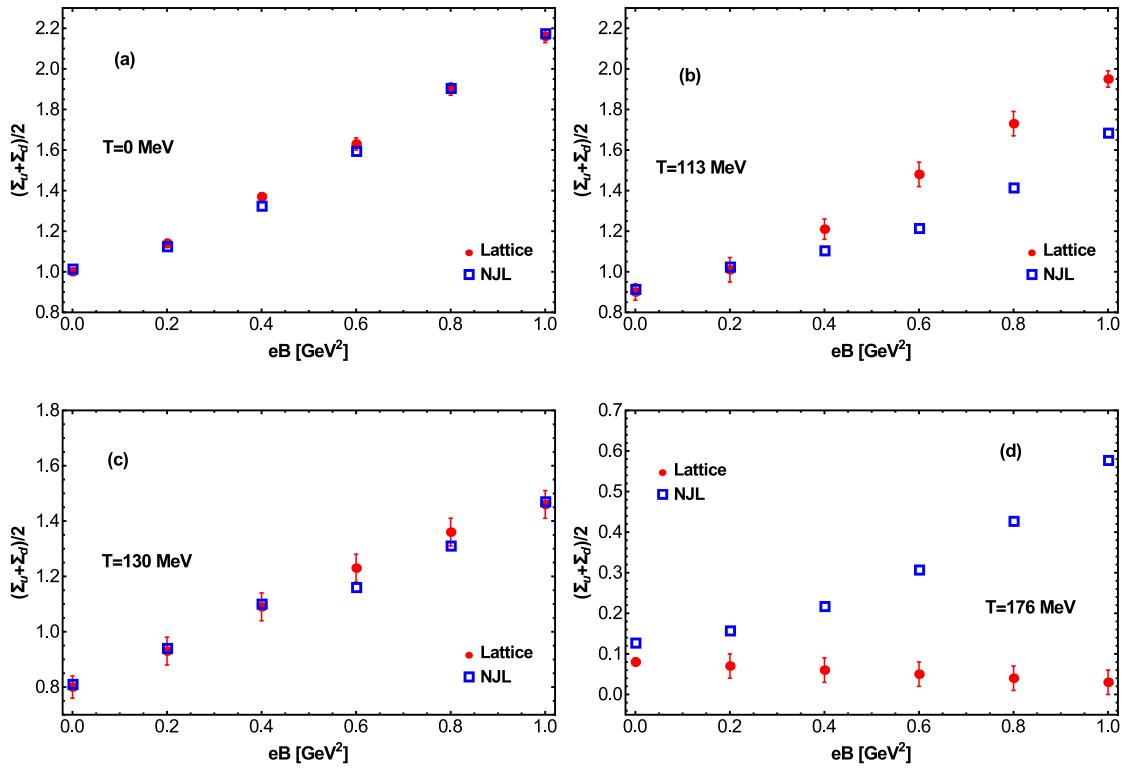

Figure 6.12: Comparison between the lattice QCD results from Ref. [79] for the average quark condensate and the model calculation, as a function of the magnetic field. Curves (a), (b), (c) and (d) correspond to $T = 0,\ 113,\ 130$ and $176\,\text{MeV}$, respectively. The model describes better the lattice results for lower temperatures.

We now proceed to use eqs. (6.54) and (6.55) to find the thermo-magnetic behaviour of the dynamically generated mass M and the coupling G and the consequences for the pressure. To establish how well the solutions for $M(B,T)$ describe the condensates as functions of eB and T one considers Figure 6.12. These figures show the LQCD average quark condensate $(\Sigma_u + \Sigma_d)/2$ compared to the equivalent quantity $\langle\bar{\psi}_f\psi_f\rangle_{B,T}/\langle\bar{\psi}_f\psi_f\rangle_0 + 1$ computed within

the model, using eq. (6.54) for $\langle\bar{\psi}_f\psi_f\rangle_{B,T}$ and one of the values in Table 6.1 for $\langle\bar{\psi}_f\psi_f\rangle_0$. Eq. (6.54) is a transcendental equation with none, one or multiple solutions for M, depending on the values of T and eB. The procedure we follow to find the reported values of M is to average the multiple solutions in the case that there is more than one or to define as solution the value of M that provides the closest distance between the lattice and the model values of condensates. From Figure 6.12 we notice that our description of the LQCD results is better for low temperatures. Figure 6.12 has been prepared using the first set of values in Table 6.1.

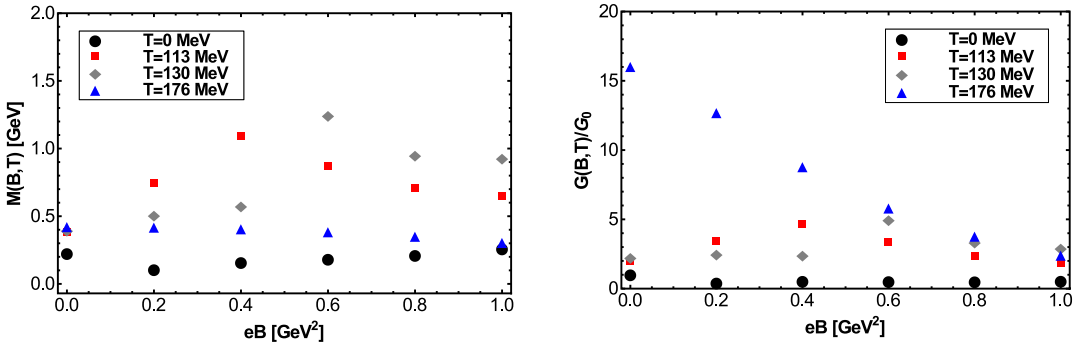

Figure 6.13: Left panel, Thermo-magnetic average quark mass $M(B,T)$ as a function of the field strength eB for the temperatures $T = 0,\ 113,\ 130$ and 176 MeV computed using the first set of values in Table 6.1. Right panel, thermo-magnetic average coupling $G(B,T)$ as a function of the field strength eB for the temperatures $T = 0,\ 113,\ 130$ and 176 MeV computed using the first set of values in Table 6.1.

The behaviour of the thermo-magnetic average mass $M(B,T)$ and coupling $G(B,T)$ as functions of the field strength are depicted in Figure 6.13. Notice that for $T = 0$, the mass increases monotonically with the magnetic field. However, there is a turn-over behaviour for intermediate values of T where, as functions of eB the masses start off increasing to then decrease as the field strength increases. For the largest temperature, which is above the transition temperature, the mass becomes a monotonically decreasing function of the field strength. A similar behaviour is observed for the coupling. Although $G(B,0)$ is practically constant, for the temperature above the transition temperature the coupling becomes a monotonically decreasing function of the field strength. For intermediate temperatures there is also a a turn-over behaviour where as functions of eB the couplings start off increasing and then decrease as the field strength increases.

To test the sensitivity of the results to a change in the vacuum parameters, Figure 6.14 shows the behaviour of the $M(B,T)$ and $G(B,T)$ as functions of the field strength for different temperatures, when using the second set of values in Table 6.1 for the calculation.

Notice that the results are qualitative and quantitatively similar to the ones obtained from the first set of values in Table 6.1.

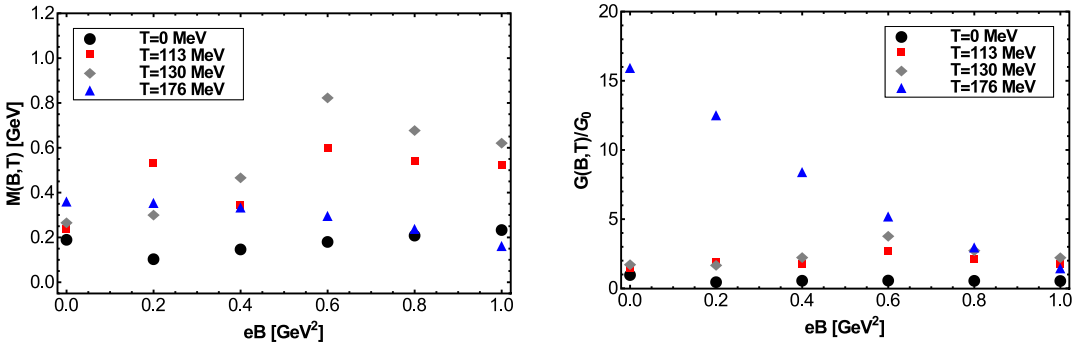

Figure 6.14: Thermo-magnetic average quark mass $M(B,T)$ as a function of the field strength eB for the temperatures $T = 0,\ 113,\ 130$ and 176 MeV computed using the second set of values in Table 6.1. Thermo-magnetic average coupling $G(B,T)$ as a function of the field strength eB for the temperatures $T = 0,\ 113,\ 130$ and 176 MeV computed using the second set of values in Table 6.1.

In order to study one of the consequences of the behaviour of the mass and coupling, we proceed to compute the thermo-magnetic contribution to the pressure. Notice that the magnetic field induces a difference between the pressure in the directions parallel and perpendicular to the field; a magnetization in the former direction is absent and it is included in the latter. We call the first kind of pressure *longitudinal*, that is, directed along the $\hat{z}$ axis, whereas we call the second kind of pressure *isotropic*, that is, directed along the $\hat{x}$, $\hat{y}$ directions. We consider only the renormalized contribution to the pressure in the so called "Φ-scheme" [78]. In the mean field approximation, the longitudinal contribution to the pressure can be written as

$$P_z = -V^{\text{eff}}, \tag{6.60}$$

where V^{eff}, is the effective potential. Therefore, using eqs. (6.38) and (6.39), P_z can be written as

$$P_z = -\frac{(M(B,T)-m)^2}{4G} - \frac{i}{2}\sum_f \text{Tr}\int \frac{d^4p}{(2\pi)^4}\ln(iS_f^{-1}), \tag{6.61}$$

whereas the magnetization $\vec{\mathcal{M}}$ is given by

$$\vec{\mathcal{M}} = -\frac{\partial V^{\text{eff}}}{\partial(eB)}\hat{z}, \tag{6.62}$$

from where the transverse pressure can be computed as [78]

$$P_{x,y} = P_z + e\vec{B} \cdot \vec{\mathcal{M}}. \tag{6.63}$$

To compute $\vec{\mathcal{M}}$, we observe that $M(B,T)$ has a mild dependence on eB. Therefore, we only consider the terms coming from the explicit dependence of eB of the effective potential and of $G(B,T)$, which are by far the dominant contributions.

Notice that for the computation of the pressure we use $M(B,T)$ and $G(B,T)$, namely, the average mass and coupling, respectively. Therefore, the pressure and magnetization are correspondingly also computed as an average over the light flavors.

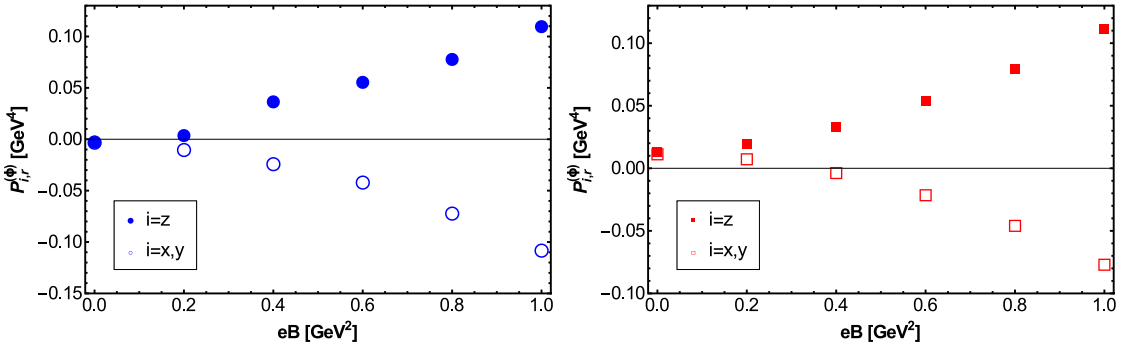

Figure 6.15: Left panel, longitudinal and transverse pressures as functions of the field strength eB for $T = 113$ MeV, computed using the first set of vacuum values in Table 6.1. The longitudinal (isotropic) pressure is a monotonically increasing (decreasing) function that for this temperature starts off from zero and grows (decreases) towards positive (negative) values as the field strength increases. Right panel, longitudinal and transverse pressures as functions of the field strength eB for $T = 176$ MeV, computed using the first set of vacuum values in Table 6.1. The longitudinal (isotropic) pressure is a monotonically increasing (decreasing) function that for this temperature starts off from positive values and grows (decreases) towards positive (negative) values as the field strength increases.

Figure 6.15 shows the longitudinal and transverse pressures as functions of the field strength, for $T = 113$ MeV and $T = 176$ MeV, respectively, computed using the first set of vacuum parameters in Table 6.1. Notice that for $T = 113$ MeV, that is, for a temperature below T_c, these pressures start off from zero and have opposite behaviors; the longitudinal pressure is a monotonically increasing function towards positive values whereas the isotropic pressure is a monotonically decreasing function towards negative values. For the case of $T = 176$ MeV, that is for a temperature above T_c, both pressures start off from positive values. However, there is an interval of field strengths where the isotropic pressure is positive to then change sign and become negative. This results are in agreement with the findings of Ref. [78].

One more time, with the intention to test the sensitivity of the results to the vacuum

parameters, Figure 6.16 shows the same pressures computed using the second set of parameters in Table 6.1, we get equivalent results.

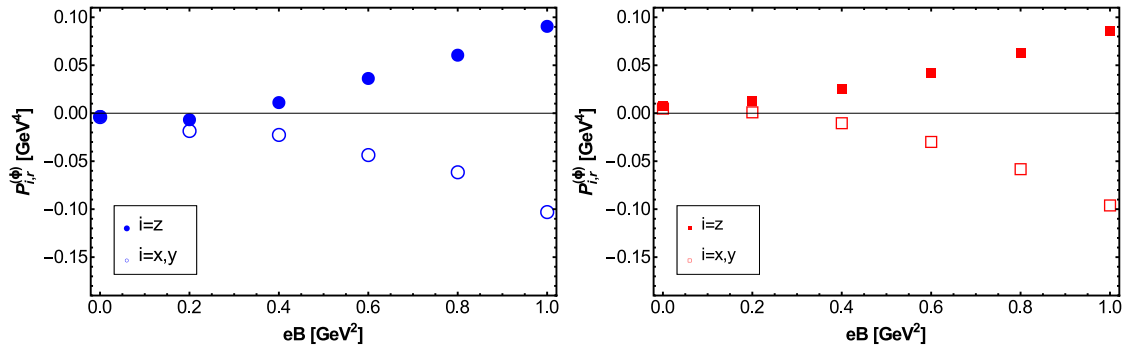

Figure 6.16: Left panel, longitudinal and transverse pressures as functions of the field strength eB for $T = 113\,\text{MeV}$, computed using the second set of vacuum values in Table 6.1. The results are equivalent to the ones obtained using the first set of vacuum values. Right panel, longitudinal and transverse pressures as functions of the field strength eB for $T = 176\,\text{MeV}$, computed using the second set of vacuum values in Table 6.1. The results are equivalent to the ones obtained using the first set of vacuum values.

It is important to notice that the calculation describing the longitudinal pressure in Figure 6.15 and Figure 6.16 agree with the LQCD findings [78], provided that

$$e\vec{B}\cdot\vec{\mathcal{M}} = -eB\mathcal{M}, \tag{6.64}$$

where $\mathcal{M}$ represents the magnitude of the magnetization vector. This means, that the magnetization is overal opposite to the magnetic field which in turn means that the system is well described in the model as possessing diamagnetic properties, both, below and above the critical temperature.

Finally, in order to study the pressure behavior referred to purely thermal effects, Figure 6.17 shows $\Delta P \equiv P_z(B,T) - P_z(0,T)$, computed for the first and second set of vacuum values in Table 6.1, respectively. In all cases ΔP is well described by a monotonically and positive definite increasing function of eB. This behavior is also in agreement with LQCD calculations [78]. We observe that the rate of change shows a turn over behavior as the temperature increases. For $T = 0$ the rate of increase is small, becoming faster for intermediate temperatures to then decrease for the higher temperatures.

After the analysis done within NJL model, our results show that for temperatures above the transition temperature, the couplings are monotonically decreasing functions of the field strength. This means that at these temperatures the melting of the quark condensates is accompanied by a corresponding decrease in the strength of the interaction that binds

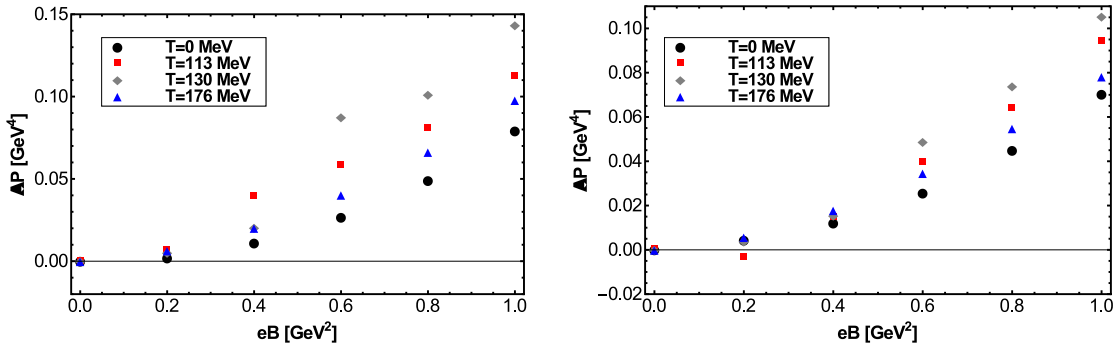

Figure 6.17: $\Delta P \equiv P_z(B,T) - P_z(0,T)$, computed for the first set of vacuum values in Table 6.1 (left panel) and computed for the second set of vacuum values in Table 6.1, both for $T = 0,\ 113,\ 130$ and 176 MeV.

these quarks.

For temperatures close to, but below the transition temperature, we find a turn over behavior of the couplings. As the field strength starts increasing, the couplings increase. However, for intermediate values of the field strength the couplings decrease. This signals that as the temperature decreases below, but close to the transition temperature, the strength of the coupling increases. This increase is accompanied by a corresponding increase in the value of the condensate, as shown by LQCD calculations. Nevertheless, this increase is not sustained, as for stronger fields the couplings decrease, as do the LQCD computed condensates.

The behavior of $G(B,T)$ strengthens the picture advocated in Refs. [119, 125] where the behavior of the condensate as a function of the magnetic field is directly linked to the properties of the strong coupling constant at high and low temperatures.

We also computed the thermo-magnetic contribution to the longitudinal and isotropic pressures. We found that below T_c, the isotropic pressure as a function of the magnetic field, decreases towards negative values starting off from zero. However, for temperatures above the transition temperature, although the isotropic pressure still decreases as a function of the field strength, it stars off from positive values. This turnover behavior of the isotropic pressure means that above T_c particles are pulled closer together. The fact that at the same time the coupling decreases can be viewed as signaling that the strength of the bound of the condensate is smaller, due to asymptotic freedom and this can be responsible for the decrease of the condensate as the magnetic field strength is turned on.

Overall, the results in this chapter suggest that IMC, as described by the thermo-magnetic behavior of the quark condensate, can be linked to the properties of the coupling constant

as a function of the magnetic field in a wide range of temperatures.

CHAPTER 7

PHOTON YIELD: ONE OBSERVABLE SHOWING MAGNETIC FIELDS EFFECTS IN HEAVY-ION COLLISIONS.

The second part of this thesis (chapter 4 - chapter 6) was related primarily with the understanding of chiral symmetry restoration in presence of magnetic fields, in other words we studied the phenomena *magnetic catalysis* and *inverse magnetic catalysis*, by analysing the behaviour of the light quark condensate and the pseudo critical temperature as function of magnetic field strength, the former plays the role of order parameter in the phase transition and the latter gives us the information when the chiral symmetry is restored for a many body system, namely hadronic matter becomes a matter described by free quarks and gluons. Hitherto magnetic field strength have been computed for different situations that we have already mentioned above, systems with high density and low temperature like cores of compact stars [137], systems with large temperature and low density like heavy-ion collisions [90], [138]- [139] or systems with zero density and large temperature like the early universe [140], however no one can measure directly the intensity of those magnetic field. Therefore, some observables in those systems must be used to show the magnetic effects and the size of that magnetic fields.

Following the idea above in this chapter we will focus on the analysis of one possible clear observable in heavy-ion collisions which could show the magnetic effects in it and if it is right then we will able to quantify the size of magnetic field in this kind of systems.

The results from heavy-ion experiments carried out at the BNL Relativistic Heavy-Ion Collider (RHIC), and at the CERN Large Hadron Collider (LHC), show that a state of matter is formed where quarks and gluons are not confined to individual nucleons [141] - [142]. Non-central collisions produce magnetic fields with an intensity that at the beginning of the reaction is estimated to be as high as several times the mass of the pion squared [90], [138]- [139]. The intensity of these fields fades out fast with time. However, the recent observation of charge separation along the magnetic field direction [143] opens the possibility to connect a measurable effect with the presence of these fields.

A magnetic field makes it possible to produce photons from processes otherwise not allowed. For instance, it has been shown that the QCD trace anomaly can turn the energy momentum of the soft gluon bulk into photons [144]- [145]. In addition, quarks can emit photons by synchrotron radiation [146]. Other approaches to study photon production in the presence of an intense magnetic field include the gauge/gravity correspondence in a strongly coupled $\mathcal{N} = 4$ plasma [147]. These novel calculations have recently been implemented to explain the experimentally measured excess [148] of thermal photons over models that describe well other low momentum observables. The enhanced production of photons in heavy-ion reactions has also been studied in the absence of magnetic field effects, *e.g.* by assuming the modification of the quark and gluon distributions to be a power-like tail at high energies [149], or by the delayed formation of the quark-gluon plasma [150].

A magnetic field naturally produces an asymmetry in the emission of electromagnetic radiation. Therefore, magnetic fields can also be a source of not only an excess in the photon yield, but also of the puzzling large strength of the coefficient v_2 in the Fourier expansion of the azimuthal distribution. The latter has been found to be as large as that of pions [151]. Although some recently improved hydrodynamic [152] - [153] and transport [154] calculations obtain a better agreement with ALICE and PHENIX measurements of low transverse momentum photons, this agreement is not yet complete [155]. Therefore, it remains important to quantify the fraction of the yield, and of the asymmetry arising from magnetic field effects, to better characterize the initial stages of heavy-ion reactions.

In non-central collisions, and at early times, the magnetic field reaches its highest intensity. It is also at early times that the largest temperatures are achieved and when the soft dynamics is dominated by gluons [145]. It is then natural to explore a mechanism where

collisions of these gluons induce the emission of photons. In this work we compute, and to our knowledge for the first time, the production of thermal photons from the perturbative fusion of gluons at these early collision times.

The amplitude for the process is depicted by the Feynman diagrams in Figure 7.1, which also defines the kinematical variables. The thick loop lines represent the quark propagator in the presence of the magnetic field. In the absence of this field, the diagrams cancel each other. It is the presence of the field which makes it possible that both diagrams contribute with the same relative sign.

The fermion propagator in coordinate space cannot longer be written as a simple Fourier transform of a momentum propagator but instead it is written as eq. (4.55), where

$$\Phi(x,x') = \exp\left\{ iq_f \int_{x'}^{x} d\xi^\mu \left[A_\mu + \frac{1}{2} F_{\mu\nu}(\xi - x')^\nu \right] \right\}, \tag{7.1}$$

is called the *Schwinger phase factor*, and q_f is the absolute value of the quark charge. We consider the contribution of two light flavours, thus $q_u = 2|e|/3$ and $q_d = |e|/3$. The propagator in momentum-space, $S(p)$, is given by

$$iS(p) = \int_0^\infty \frac{ds}{\cos(q_f Bs)} e^{is(p_\parallel^2 - p_\perp^2 \frac{\tan(q_f Bs)}{q_f Bs} - m_f^2 + i\epsilon)} \left[(\cos(q_f Bs) + \gamma_1\gamma_2 \sin(q_f Bs))(m_f + \not{p}_\parallel) - \frac{\not{p}_\perp}{\cos(q_f Bs)} \right], \tag{7.2}$$

where m_f is the quark mass. We have chosen the homogeneous magnetic field to point in the $\hat{z}$ direction, namely $\boldsymbol{B} = B\hat{z}$. This configuration can be obtained from an external vector potential which we choose in the so called *symmetric gauge*, $A^\mu = \frac{B}{2}(0, -y, x, 0)$. We also use the notation in eq. (5.13).

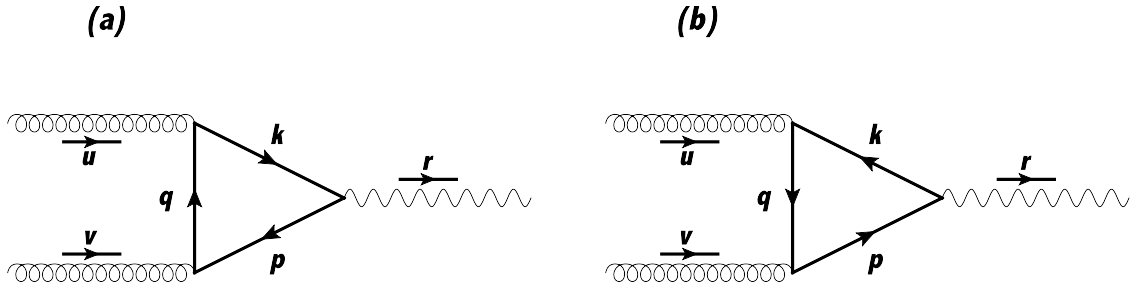

Figure 7.1: Feynman diagrams for the amplitude for photon production from gluon fusion. The thick lines in the loop represent the quark propagators in the presence of the magnetic field.

Since the two Feynman diagrams of Figure 7.1 give the same contribution, we concentrate on the computation of the amplitude depicted in Figure 7.1(a) which becomes

$$\begin{aligned}\mathcal{M}^{(a)} = &-\int d^4x \int d^4y \int d^4z \int \frac{d^4p}{(2\pi)^4} \int \frac{d^4q}{(2\pi)^4} \int \frac{d^4k}{(2\pi)^4} \\ &\times e^{-ip\cdot(y-x)} e^{-iq\cdot(z-y)} e^{-ik\cdot(x-z)} e^{-iu\cdot z} e^{-iv\cdot y} e^{ir\cdot x} \\ &\times \mathrm{Tr}\left[iq_f\gamma_\mu iS(k) ig\gamma_\alpha t^c iS(q) ig\gamma_\nu t^d iS(p)\right] \\ &\times \epsilon^{*\mu}(\lambda_r)\Phi(x,y)\Phi(y,z)\Phi(z,x)\epsilon^{\alpha}(\lambda_u)\epsilon^{\nu}(\lambda_v). \end{aligned} \tag{7.3}$$

The product of phase factors can be written as

$$\Phi(x,y)\Phi(y,z)\Phi(z,x) = e^{i\frac{q_f B}{2}\epsilon_{ij}(z-x)_i(x-y)_j}, \tag{7.4}$$

where we used the explicit form of A^μ which gives

$$F_{12} = -F_{21} = -B, \tag{7.5}$$

with the rest of the components of $F_{\mu\nu}$ vanishing [75], and ϵ_{ij} being the Levi-Civita symbol. The integrations in eq. (7.3) are carried out more easily by making the change of variables $\omega = z - x$ and $l = x - y$, after which the integration over the spatial coordinates becomes

$$(2\pi)^4\delta^4(r-v-u)\int d^4\omega \int d^4l\; e^{-i\omega\cdot(q-k+u)} e^{-il\cdot(q-p-v)} e^{i\frac{q_f B}{2}\epsilon_{ij}\omega_i l_j}, \tag{7.6}$$

which exhibits the overall energy-momentum conservation in the process. Furthermore, we split the integrals over ω and l in transverse and longitudinal parts

$$\begin{aligned}&\int d^4\omega \int d^4l\; e^{-i\omega\cdot(q-k+u)} e^{-il\cdot(q-p-v)} e^{i\frac{q_f B}{2}\epsilon_{ij}\omega_i l_j} \\ =&(2\pi)^4\delta^2\left[(q-k+u)_\parallel\right]\delta^2\left[(q-p-v)_\parallel\right]\prod_{i,j=1,2}\int d\omega_i \int dl_j e^{i\omega_i(q-k+u)_i} e^{il_j(q-p-v)_j} e^{i\frac{q_f B}{2}\epsilon_{ij}\omega_i l_j} \\ =&(2\pi)^4\delta^2\left[(q-k+u)_\parallel\right]\delta^2\left[(q-p-v)_\parallel\right]\left(\frac{4\pi}{q_f B}\right)^2 \prod_{i,j=1,2} e^{i\frac{2}{q_f B}\epsilon_{ij}(q-k+u)_i(q-p-v)_j}. \end{aligned} \tag{7.7}$$

This shows that the longitudinal momentum is explicitly conserved at the vertices, whereas the transverse momentum is not but instead its components are mixed up by the magnetic field.

We now use the fact that when the magnetic field is very intense, as compared to the any other energy (squared) scales involved, the quark dynamics is dominated by the lowest Landau level (LLL). For the case of quarks that have not yet thermalized, this means that

the magnetic field is taken to satisfy $eB \gg m_f^2$. For the LLL, the propagator in eq. (7.2) can explicitly be written as eq. (4.81).

The operator $\mathcal{O}_\parallel = [1 - i\gamma_1\gamma_2]/2$ projects onto the longitudinal space. Therefore the matrix element can be factorized into a product of transverse and longitudinal pieces, namely

$$\mathcal{M}^{(a)} = (2\pi)^4\delta^4(r-v-u)\mathcal{M}_\perp^{(a)}\mathcal{M}_\parallel^{(a)} \tag{7.8}$$

$$\begin{aligned}\mathcal{M}_\perp^{(a)} &= \left(\frac{4\pi}{q_f B}\right)^2 \int \frac{d^2p_\perp}{(2\pi)^2}\int \frac{d^2q_\perp}{(2\pi)^2}\int \frac{d^2k_\perp}{(2\pi)^2} \\ &\quad \times e^{-\frac{k_\perp^2}{q_f B}} e^{-\frac{q_\perp^2}{q_f B}} e^{-\frac{p_\perp^2}{q_f B}} \prod_{i,j=1,2} e^{i\frac{2}{q_f B}\epsilon_{ij}(q-k+u)_i(q-p-v)_j} \\ &= \left(\frac{q_f B}{12\pi}\right) e^{-\frac{(u+v)_\perp^2}{3q_f B}},\end{aligned} \tag{7.9}$$

$$\begin{aligned}\mathcal{M}_\parallel^{(a)} &= -8\left(\frac{q_f g^2\delta^{cd}}{2}\right)\int \frac{d^2p_\parallel}{(2\pi)^2}\int \frac{d^2q_\parallel}{(2\pi)^2}\int \frac{d^2k_\parallel}{(2\pi)^2} \\ &\quad \times (2\pi)^4\delta^2\left[(q-k+u)_\parallel\right]\delta^2\left[(q-p-v)_\parallel\right] \\ &\quad \times \epsilon^{*\mu}(\lambda_r)\frac{\mathrm{Tr}\left[\gamma_\mu \not{k}_\parallel \mathcal{O}_\parallel \gamma_\alpha \not{q}_\parallel \mathcal{O}_\parallel \gamma_\nu \not{p}_\parallel \mathcal{O}_\parallel\right]}{k_\parallel^2 q_\parallel^2 p_\parallel^2}\epsilon^\alpha(\lambda_u)\epsilon^\nu(\lambda_v).\end{aligned} \tag{7.10}$$

Since at the early stages of the collision gluons are far more abundant than quarks, we compute eq. (7.10) under the assumption that quarks do not yet thermalize. Accordingly, we set $m_f = 0$ since in the absence of thermal corrections, the light-quark vacuum masses are negligible. The trace in eq. (7.10) contains the product of up to twelve gamma matrices. The resulting expression is long and involved. It is however easy to show (see Appendix G)that upon squaring and summing over polarizations, only a small piece survives so that the trace can be expressed as

$$\begin{aligned}&\mathrm{Tr}\left[\gamma_\mu \not{k}_\parallel \mathcal{O}_\parallel \gamma_\alpha \not{q}_\parallel \mathcal{O}_\parallel \gamma_\nu \not{p}_\parallel \mathcal{O}_\parallel\right] \longrightarrow k_{\parallel\nu}(p_{\parallel\mu}q_{\parallel\alpha} - p_{\parallel\alpha}q_{\parallel\mu}) \\ &+ k_{\parallel\mu}(p_{\parallel\nu}q_{\parallel\alpha} + p_{\parallel\alpha}q_{\parallel\nu}) + k_{\parallel\alpha}(p_{\parallel\nu}q_{\parallel\mu} - p_{\parallel\mu}q_{\parallel\nu}),\end{aligned} \tag{7.11}$$

where the arrow indicates this to be the only contributing portion. Two of the integrations in eq. (7.10) become straightforward using the delta-function restrictions. We choose those two as the integrals over $k_\parallel$ and $q_\parallel$. The remaining integral contains the product of momenta in the denominator that we write in its Feynman parametrization form

$$\frac{1}{p_\parallel^2(p+v)_\parallel^2(p+v+u)_\parallel^2} = 2\int_0^1\int_0^{x_1}\frac{dx_1dx_2}{\left[[p_\parallel + (x_1v_\parallel + x_2u_\parallel)]^2 - \Delta\right]^3}, \tag{7.12}$$

where

$$\Delta = x_1(x_1-1)v_\parallel^2 + x_2(x_2-1)u_\parallel^2 + 2x_2(x_1-1)(u\cdot v)_\parallel. \tag{7.13}$$

In order to make tractable the calculation of the longitudinal piece of the photon emission rate, eq. (7.10), here we proceed to make some simplifying assumptions. For photons emitted at mid-rapidity the momentum components along the beam axis are small. Since the reaction plane is perpendicular to the magnetic field and we are treating the perpendicular (to the magnetic field) momentum components as equivalent, we take the momentum components along the reaction plane as small. Therefore we have

$$r_\perp = (u+v)_\perp \simeq 0. \tag{7.14}$$

The remaining component of the photon momentum is the one directed along the plane containing the magnetic field for which we have

$$r_3 = (v_3 + u_3). \tag{7.15}$$

Notice that when treating the gluons as thermal, their momentum can be considered as small when compared to the collision energy. Thus we take

$$r_3 = (v_3 + u_3) \simeq 0. \tag{7.16}$$

Also, because we focus on describing the emission of real photons we have

$$r^2 = (u+v)^2 \simeq (u+v)_\parallel^2 = 0 \simeq v_0^2 + u_0^2 + 2(v\cdot u)_0 \simeq v_0^2 + u_0^2 + 2(v\cdot u)_\parallel. \tag{7.17}$$

Since the main thermal effect on low momentum gluons is their developing a thermal mass m_g, we can write

$$v_0^2 = u_0^2 \simeq m_g^2 \tag{7.18}$$

to find

$$u_\parallel^2 \simeq v_\parallel^2 \simeq m_g^2, (v\cdot u)_\parallel \simeq -m_g^2, \Delta \simeq m_g^2(x_1-x_2)(x_1-x_2-1). \tag{7.19}$$

We emphasize that since the photon spectrum inherits the thermal features of the gluon spectrum, the kinematical regime here studied is expected to capture the main characteristics of the photon momentum distribution.
We make the shift

$$p_\parallel \longrightarrow l_\parallel = p_\parallel + (x_1 v_\parallel + x_2 u_\parallel) \tag{7.20}$$

and get rid of odd powers of $l_{\parallel\mu}$ in the numerator of the momentum integrand. The remaining terms can be computed using the well known relations

$$\begin{aligned}
\int \frac{d^d l}{(2\pi)^d} \frac{1}{[l^2-\Delta]^n} &= \frac{(-1)^n i}{(4\pi)^{d/2}} \frac{\Gamma(m)}{\Gamma(n)} \left(\frac{1}{\Delta}\right)^m \\
\int \frac{d^d l}{(2\pi)^d} \frac{l_\mu l_\nu}{[l^2-\Delta]^n} &= \frac{(-1)^{n-1} i}{(4\pi)^{d/2}} \frac{g_{\mu\nu}}{2} \frac{\Gamma(m')}{\Gamma(n)} \left(\frac{1}{\Delta}\right)^{m'},
\end{aligned} \tag{7.21}$$

with $m = n - d/2$, $m' = n - d/2 - 1$, $d = 2$, $n = 3$.

To compute the integrals over the Feynman parameters x_1 and x_2 we use the principal value prescription. This results into a polynomial containing linear and cubic terms in the components α, μ, ν of $u_\parallel$ and $v_\parallel$. The final expression for the matrix element (eqs. (7.8), (7.9) and (7.10)) squared, after adding the contribution from the Feynman diagram in Figure 7.1(b), summed over polarizations, becomes

$$\sum_{\text{pol},f} |\mathcal{M}|^2 = \left(\frac{6256}{2187}\right) \left(\frac{\mathcal{VT}}{m_g^2}\right) \delta^4(r-v-u) \sum_f \left(q_f g^2\right)^2 (q_f B)^2 \, e^{-2\frac{r_\perp^2}{3q_f B}}, \tag{7.22}$$

where $\mathcal{VT}$ represents the space-time volume of the reaction coming from squaring $(2\pi)^4\delta(r-v-u)$ and we have included the sum over the two light flavours $f = u, d$. The odd-looking factor $6256/2187 \sim 2.86$ is obtained from the longitudinal piece of the matrix element squared after collecting the coefficients of the contraction of the polynomial in the components of $u_\parallel$ and $v_\parallel$. Notice that after the approximations made to compute eq. (7.10), the dependence on $r_\perp$ of eq. (7.22) comes exclusively from the transverse piece of the matrix element, eq. (7.9).

This remarkably simple result exhibits several interesting features. First, since the gluon thermal mass is $m_g = \sqrt{N_f/3}\, gT$, the photon emission probability is proportional to g^2 instead of g^4, *i.e.* it is not as suppressed as could be naively expected. Second, the emission probability is proportional to B^2 and contains a space volume factor $\mathcal{V} = \mathcal{A} \times \mathcal{L}$, where $\mathcal{A}$ and $\mathcal{L}$ represent the transverse (with respect to the magnetic field) area and longitudinal length of the reaction zone, respectively. A factor $\mathcal{T}$ represents the time duration of the reaction. It has been shown that in a heavy-ion collision the product $B\mathcal{T}$ is approximately constant with energy [90]. Therefore, the dependence of the photon emission probability on the centrality of the reaction and on the beam energy, is captured in this calculation by the dependence on the flux factor $B\mathcal{A}$. This means that when going from RHIC to LHC

energies, the photon emission probability can be expected to increase approximately at a linear, instead of quadratic rate with B.

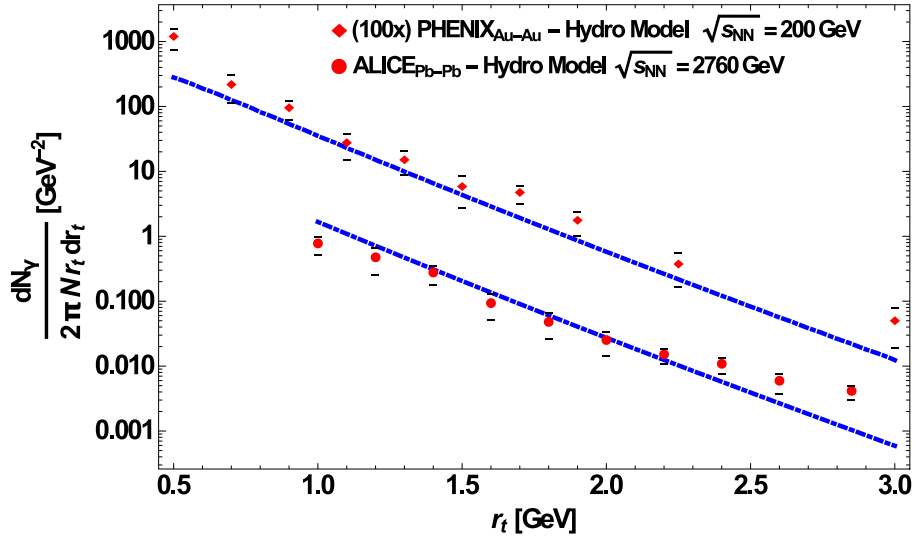

Figure 7.2: Experimental excess photon yield with respect to the hydro calculation compared to our calculation for the centrality class $0-20\%$. The upper set corresponds to PHENIX data (multiplied by 100) and the lower set to ALICE data. Red dots (diamonds) are obtained by substracting the theoretical photon yield computed in [152] from the experimental direct photon spectra of [148]. The error bars are the experimentally reported statistical errors.

The invariant photon yield is obtained by integrating over the corresponding phase space weighed with the thermal distribution, namely

$$\frac{r_0 dN}{d^3r} = \frac{1}{2(2\pi)^3}\int \frac{d^3u}{2u_0(2\pi)^3}\int \frac{d^3v}{2v_0(2\pi)^3}\sum_{\text{pol},f}|\mathcal{M}|^2\, n(u_0)n(v_0), \tag{7.23}$$

where

$$n(E) = \frac{1}{e^{\sqrt{\frac{E^2+m_g^2}{T}}}-1} \tag{7.24}$$

is the Bose-Einstein distribution and T is the temperature. The total number of photons N is obtained by integrating the above yield over the photon momentum. Notice that the photons in the final state are not weighed by a thermal distribution since they basically escape from the interaction region once they are produced. Notice also that the assumption of gluon thermalization at very early times may be difficult to meet. Nevertheless, at early times, gluons, albeit not necessarily thermal, densely populate the phase space. Hereafter we assume for simplicity that the gluon occupation number is approximately described by

a thermal distribution, though other choices for their occupation number can certainly be explored.

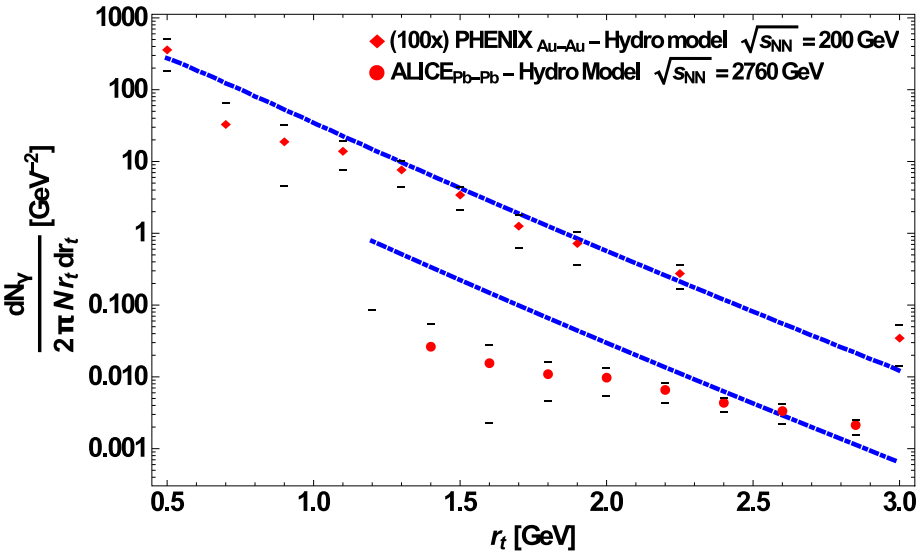

Figure 7.3: Experimental excess photon yield with respect to the hydro calculation compared to our calculation for the centrality class $20-40\%$. The upper set corresponds to PHENIX data (multiplied by 100) and the lower set to ALICE data. Red dots (diamonds) are obtained by substracting the theoretical photon yield computed in [152] from the experimental direct photon spectra of [148]. The error bars are the experimentally reported statistical errors.

We write

$$\frac{d^3r}{r_0} = r_t dr_t dy d\phi \tag{7.25}$$

where r_t is the magnitude of the photon momentum in the plane transverse to the beam axis, y the rapidity and ϕ the azimuthal angle. Notice that since $r_\perp = r_t \sinh(y)$, for $y \simeq 0$, $r_\perp \simeq y r_t$, $r_0 = r_t \cosh(y) \simeq r_t$. Therefore, the number of photons per unit momentum transverse to the beam axis, integrated over the full azimuthal angle, and around mid-rapidity, is explicitly given by

$$\frac{dN}{dr_t} = \mathcal{C}\left[\left(\frac{1}{3}\right)^4 e^{-2\frac{y_0^2 r_t^2}{eB}} + \left(\frac{2}{3}\right)^4 e^{-\frac{y_0^2 r_t^2}{eB}}\right] I\left(\frac{r_t}{T}; \sqrt{\frac{2}{3}g}\right), \tag{7.26}$$

where we have evaluated the distribution at $y = y_0 = 0.5$, given that the rapidity interval $\Delta y \sim 1$ is centered around mid-rapidity. Notice that we could have equally well have chosen to evaluate eq. (7.26) at $y = 0$ since, given the magnetic field dependence of the exponential factors, one or the other choice makes no numerical difference. The choice in

eq. (7.26) is just made to emphasize that for rapidities other than central, the distribution does have a rapidity dependence. We have also defined

$$\mathcal{C} = \frac{g^4 T e^4 B^2}{8(2\pi)^7}\left(\frac{6256}{2187}\right)\left(\frac{\mathcal{V}\mathcal{T}}{m_g^2}\right), \tag{7.27}$$

and

$$I(z;\lambda) \equiv \int_0^z \frac{dx x^2 n\left(\sqrt{(z+x)^2-(2x)^2}\right) n(x)}{\left(\sqrt{x^2+\lambda^2}\right)\left(\sqrt{(z+x)^2-(2x)^2+\lambda^2}\right)}. \tag{7.28}$$

We have also used that in QCD with two flavours, $m_g^2 = (2/3)g^2T^2$. The yield given by eq. (7.26) can be properly called *thermal* because its computation assumes that the gluons are thermally distributed in phase space. However, notice that this yield *is not* proportional to T^4, as could be naively expected. Rather, it is inversely proportional to T, after accounting for the gluon mass squared in the denominator. This behaviour is due to the fact that at the early stages of the collision it is the magnetic field which provides the largest of all energy scales. In fact, since we are working with the energy scale hierarchy

$$(eB)^{1/2} > m_g \tag{7.29}$$

it is of no surprise that the yield is proportional to the fourth power of the largest energy involved, namely $(eB)^{1/2}$. The normalized yield is finally given by

$$\frac{1}{2\pi N r_t dr_t}\frac{dN}{} = \frac{\left[\left(\frac{1}{3}\right)^4 e^{-2\frac{y_0^2 r_t^2}{eB}} + \left(\frac{2}{3}\right)^4 e^{-\frac{y_0^2 r_t^2}{eB}}\right]\frac{I(r_t/T)}{2\pi}}{\sqrt{3\pi eB/2}\left[\left(\frac{2}{3}\right)^{9/2}+\left(\frac{1}{3}\right)^{9/2}\right]\int_0^\infty dr_t I(r_t/T)}, \tag{7.30}$$

where the factor $\sqrt{3\pi eB/2}$ in the denominator comes from the integration over rapidity. Notice that, despite having approximated $r_\perp \simeq 0$ for the calculation of the longitudinal matrix element, the normalization N is computed extending the integration range over r_t up to $+\infty$. This is a valid approximation, given that the main behaviour of the rate is dictated by the exponential fall off in this variable coming from the transverse part of the matrix element squared.

The normalized distribution is independent of the space-time region of the reaction. The impact parameter dependence is due to the dependence on the field intensity. The photon transverse yield given by eq. (7.30) is an *excess yield* that should be added to calculations that do not consider magnetic field effects for photon emission.

In order to compare with experimental data we first proceed to use appropriate values for the temperature, the coupling g, and the magnetic field strength. Rather than pursuing

an exhaustive search in the parameter space, we only consider here reasonable values for the above mentioned parameters. Here we use $T = 300$ MeV for RHIC and $T = 350$ MeV for LHC. Also, since the analysis is valid for a gluon thermal mass smaller than T, we take $g = 1$ (the results turn out to be only marginally sensitive to the value of g). The variation of the field intensity with time and impact parameter for RHIC and LHC energies is taken from [156]. We chose one of the earliest times, $\tau \sim 0.05$ fm, hence one of the largest values of eB which for RHIC, $\sqrt{s_{NN}} = 200$ GeV, correspond to $0.5 \times 10^4 < eB/(\text{MeV})^2 < 10^5$ and for LHC, $\sqrt{s_{NN}} = 2.76$ TeV, $eB/(\text{MeV})^2 \simeq 10^4$, with small variations coming from a slight dependence on the impact parameter. To relate the centrality class of the collision with the impact parameter we follow the geometrical model of [157]. Figure 7.2 and Figure 7.3 show our results compared to the experimental excess photon yield with respect to one recent hydrodynamical calculation [152]. The latter has been shown to approach the description of the experimental data within the lowest part of the uncertainties. Figure 7.2 (Figure 7.3) shows a comparison with the centrality class case $0-20\%$ ($20-40\%$). In each graph the upper set corresponds to PHENIX (multiplied by 100) and the lower to ALICE data. Notice that even with the ballpark choices of the parameters involved, our calculation provides a very good description of the excess photons. For the case of ALICE $20-40\%$ our calculation overshoots the data. This can be due to the fact that the hydrodynamic calculation [152] which we use as the reference to compute the excess also overshoots the data, for this centrality class at low p_t.

CHAPTER 8

SUMMARY.

We have analysed and showed results from two important topics, on the one hand the first part of this work is related to finite energy QCD sum rules, within this framework we started in the second chapter to talk about quark-hadron duality violation; we probed potential quark-hadron duality violation by using vector and axial-vector ALEPH hadronic spectral functions. We showed the very good agreement of finite energy QCD sum rules results and data when these include a pinched integration kernel, but without DV model and beyond the kinematical τ-decay end-point. We concluded that error from the duality violation is contained within other bigger sources of errors involved in the computation. We confirm our results when they are confronted with those from a specific model, in both cases sum rules are well satisfied, this shows that inclusion of DV models is not necessary in these applications. However this kind of procedure should be essential for classifying applications where it is important to include DV models and where it is not necessary.

In chapter three, we use QCD sum rules including pinched integration kernels together with the latest update ALEPH data on hadronic decays of the τ-lepton. We determine vacuum condensates of dimension two and four and chiral condensates of dimension six and eight, verify the validity of the Weinberg sum rules and compute the chiral perturbation theory values $\bar{L}_{10}$ and C_{87}. All the results are consistent within the errors with other works, many of them that include DV models, therefore one more time we can see there are many application where DV models can be omitted. In the same third chapter, we determined the gluon condensate from e^+e^- annihilation data in the charm-quark region. The determination was done with finite energy QCD sum rules, weighted by a suitable

integration kernel. The novel procedure consists of introducing the gluon condensate through the low energy QCD expansion of the vector current correlator due to the Cauchy residue at the pole. The relevance of this determination is based on confirming or not if the gluon condensate is an invariant itself. At the same time the method used shows a new and independent way to compute the gluon condensate within the sum rule framework.

The second topic involves (1) the consequences of including magnetic fields in the chiral symmetry restoration and (2) the possible clear signal observed in the photon yield to show the existence of strong magnetic fields in heavy-ion collisions. It is well known that systems where it is possible analyse the restoration of chiral symmetry produce at the same time strong magnetic fields. Therefore if magnetic field strength is comparable to the energy scales during the symmetry restoration, then their implications in this phenomenon must be taken into account; fortunately it is the case. By remaining within the framework of QCD sum rules, in chapter five we show the behaviour of the gluon condensate and the phenomenological parameter s_0 as function of magnetic field strength. Both have a monotonic increasing behaviour. It allows to say that magnetic fields encourage the confinement because s_0 is understood as the threshold from which perturbative QCD starts to be valid. Being the gluon condensate one of the terms in the operator product expansion which contains the information about confinement, it strengthens the statement that magnetic fields catalyse confinement. It should be noticed that results are model independent.

In chapter six, we explore the effective QCD phase diagram. We used the linear sigma model coupled to quarks. This model allows to explore the restoration of the chiral symmetry. The way to get the phase diagram in the temperature versus quark chemical potential is through computing the effective potential, including corrections beyond mean field approximation. These corrections are the proper screening effects and the thermo-magnetic corrections to the coupling constants. They are essential corrections of these coupling constants in order to obtain the inverse magnetic catalysis. One relevant issue in the phase diagram is the modification of the critical end point. It moves toward lower values of the critical quark chemical potential and larger values of the critical temperature. This behaviour shows that magnetic fields also can modify the nature of the transition. Looking at the thermo-magnetic corrections to the coupling constants it plays a crucial role. Then we computed the magnetic correction to the QCD vertex and together with the result of the same analysis but at finite temperature, we found that in the perturbative region the behaviour of the light quark condensate and the effective QCD couplings are the same. This result is quite strong because it suggests a source of the magnetic catalysis

and the inverse magnetic catalysis, improving the knowledge on this phenomena. Keeping this result in mind, we then analyse the behaviour of the coupling constant within the Nambu Jona-Lasinio model. In the mean field approximation it is possible to compute the dependence of the coupling by using the gap equation. Hence this coupling acquires thermo-magnetic dependence. One more time we found that the light quark-condensate and the coupling constant in NJL model, both have qualitative the same behaviour. It strengthens even more the crucial role of the coupling strength in the magnetic catalysis and inverse magnetic catalysis. Added to this we compute the pressure as function of strength field for different temperatures which cover values below and above the physical critical temperature. The results are in very good agreement with lattice QCD analyses. At the end, in chapter seven we compute the production of photons due to the fusion of gluons in the presence of strong magnetic fields. It is done as a possible answer to the unknown phenomenon in the photon yield measurement referred to as photon excess. This way to take into account new sources of photon production is particularly clean. I mean, without magnetic fields this kind of process is not allowed. The contribution of this process cannot be compared with the photon yield, actually this new process needs to be added to the hydrodynamic result in order to compare with the experimental data. We found our result is in agreement with the relative excess of photons found between RHIC and LHC with hydrodynamic computations, for different centrality classes. Then, based on the fact that this process cannot be related with another one in the absence of magnetic fields, and including the other processes (computed by other people) allowed by the presence of strong magnetic fields, then we can thing that the photon excess is an ideal candidate to show roundly the existence and impact of strong magnetic fields in heavy-ion collisions.

APPENDIX A

FIRST ORDER MAGNETIC CORRECTION TO THE PQCD CONTRIBUTION TO THE AXIAL-VECTOR CURRENT CORRELATOR.

The contribution to the pQCD axial-vector current correlator of order (eB) is given by

$$\Pi^{B}_{\mu\nu}(q^2) = \Pi^{(10)}_{\mu\nu}(q^2) + \Pi^{(01)}_{\mu\nu}(q^2) \tag{A.1}$$

where

$$\begin{aligned}
\Pi^{(10)}_{\mu\nu}(q^2) &= N_c(q_u B)\int \frac{d^4k}{(2\pi)^4}\frac{\mathrm{Tr}\left[\gamma_1\gamma_2[\gamma\cdot(k-q)_{\parallel}]\gamma_\mu \not{k}\gamma_\nu\right]}{k^2(k-q)^4} \\
\Pi^{(01)}_{\mu\nu}(q^2) &= N_c(q_d B)\int \frac{d^4k}{(2\pi)^4}\frac{\mathrm{Tr}\left[(\not{k}-\not{q})\gamma_\mu\gamma_1\gamma_2[\gamma\cdot q]_{\parallel}\gamma_\nu\right]}{(k-q)^2k^4}
\end{aligned} \tag{A.2}$$

Note that the traces in eqs. (A.2) are equal, due to the ordering of elements inside the trace. Therefore, we evaluate one of the traces,

$$
\begin{aligned}
&\mathrm{Tr}\left[\gamma_1\gamma_2[\gamma\cdot(k-q)_\parallel]\gamma_\mu \not{k}\gamma_\nu\right] \\
&= -i\mathrm{Tr}\left[\gamma_\mu \not{k}\gamma_\nu \left\{\not{b}[(k-q)\cdot u] - \not{u}[(k-q)\cdot b]\right\}\gamma_5\right] \\
&= -ik^\alpha \mathrm{Tr}\left[\gamma_\mu\gamma_\alpha\gamma_\nu\gamma_\beta\gamma_5\right]\left\{b^\beta[(k-q)\cdot u] - u^\beta[(k-q)\cdot b]\right\}
\end{aligned} \tag{A.3}
$$

where u^β and b^β are four-vectors describing the particle's rest frame and the direction of the magnetic field, respectively. In the rest frame, there are given by

$$
\begin{aligned}
u &= (1,0,0,0), \\
b &= (0,0,0,1).
\end{aligned} \tag{A.4}
$$

Looking at the trace structure in eq. (A.3), we have

$$
\mathrm{Tr}\left[\gamma_\mu\gamma_\alpha\gamma_\nu\gamma_\rho\gamma_5\right] = -4i\epsilon_{\mu\alpha\nu\rho}, \tag{A.5}
$$

Hence, when we substitute eq. (A.5) into eq. (A.3) and add all the terms, we get a null contribution.

APPENDIX B

EULER-MACLAURIN METHOD.

Euler-MacLaurin approximation is a technique which provides a powerful connection between integrals and sums. Given a real or complex function $f(x)$, with x real in the interval $[n, m]$, it relates a sum

$$S = f(m+1) + \cdots + f(n-1) + f(n), \tag{B.1}$$

with m, n integers, with an integral

$$I = \int_m^n f(x)dx. \tag{B.2}$$

The general relation can be written as follows

$$\sum_{k=m+1}^{n-1} f_k = \int_m^n f(k)dk - \frac{1}{2}[f(n) - f(m)] + \sum_{k=1}^{\infty} \frac{B_{2k}}{(2k)!}[f^{(2k-1)}(n) - f^{(2k-1)}(m)] + R, \tag{B.3}$$

where B_2k is the 2kth Bernoulli number and

$$R = \int_m^n f^{(2k+1)}(x) P_{2k+1}(x)dx, \tag{B.4}$$

the error term. From eq. (B.3) we find that Euler-MacLaurin method provides the expression for the difference between the sum and the integral in terms of higher derivatives $f^{(k)}(x)$, evaluated at the end points of the interval, *i.e.*, $x = m$ and $x = n$. Now, by the mean value theorem

$$\int_m^n f^{(2k+1)}(x)P_{(2k+1)}(x)dx = (n-m)f^{(2k+1)}(\alpha)P_{(2k+1)}(\alpha), \tag{B.5}$$

for some $\alpha\epsilon[m,n]$. Hence

$$\int_m^n f(x)dx = \sum_{s=m}^{n-1}\frac{1}{2}[f(s)+f(s+1)] - \sum_{i=1}^{k}\frac{B_{2i}}{(2i)!}[f^{(2i-1)}(n) - f^{(2i-1)}(m)] - (n-m)f^{(2k+1)}(\alpha)P_{2k+1}(\alpha). \tag{B.6}$$

Eq. (B.6) exhibits the connection of the Euler-MacLaurin formula with the well-known trapezoid rule, which states that

$$\int_a^{a+h} f(x)dx \simeq \frac{h}{2}[f(a)+f(a+h)]. \tag{B.7}$$

From the geometric point of view, iy shows the area underneath the curve of a function on the interval $[a, a+h]$ is approximately the area of a trapezoid with sides $(a, f(a))$ and $(a+h, f(a+h))$.

The Euler-MacLaurin method related with the mean value theorem is used in chapter 6 to compute the sum over Landau levels that appear in the one-loop contribution to the effective potential, it is done as follows.

For the bosonic case, we start with eq. (6.12). Note that we can write the sum over Landau levels as

$$S_b \equiv \sum_{l=0}^{\infty}(2eB)g_l, \tag{B.8}$$

where

$$g_l = \frac{1}{8\pi}\int\frac{dk_3}{2\pi}\left[\omega_l + 2T\log\left(1-e^{-\omega_l/T}\right)\right]. \tag{B.9}$$

From $\omega_l = \sqrt{k_3^2+m_b^2+(2l+1)eB}$, we note that the increment in the summation index is $h = 2eB$ and the sum is evaluated at the mid point between consecutive values of l. We can thus use the Euler-MacLaurin approximation for the sum, written as

$$S_b \equiv \left\{\int dy g(y) - \frac{1}{2}\frac{B_2 h^2}{2!}[g'(y=\infty) - g'(y=0)]\right\}, \tag{B.10}$$

where $B_2 = 1/6$ is the second Bernoulli number, $y = (2l+1)eB$, $g'(y) = \partial_y g(y)$ and we have kept the expression explicitly only up to $\mathcal{O}(h^2)$.

For the fermionic case, let us now look eq. (6.14). We can write the sum over Landau levels and the spin index as

$$S_f \equiv -\sum_{l=0}^{\infty}\sum_{r=\pm 1}(2q_fB)g_{l,r}, \tag{B.11}$$

where

$$g_{l,r} = \frac{1}{4\pi}\int\frac{dk_3}{2\pi}\left[\omega_{l,r} + T\log\left(1-e^{-(\omega_{l,r}-\mu)/T}\right) + T\log\left(1-e^{-(\omega_{l,r}+\mu)/T}\right)\right]. \tag{B.12}$$

From $\omega_{l,r} = \sqrt{k_3^2+m_f^2+(2l+1+r)q_fB}$, the increment in the summation index is still $h = 2eB$, but this time the sum is evaluated at the end points of consecutive values of l. We can thus use Euler-MacLaurin approximation for the sum, now written as

$$S_f = \left\{\int dy\widetilde{g}(y) + \frac{B_2h^2}{2!}[\widetilde{g}'(y=\infty) - \widetilde{g}'(y=0)]\right\}, \tag{B.13}$$

where $\widetilde{g}(y) = 2g(y)$, now $y = 2lq_fB$, $\widetilde{g}'(y) = \partial_y\widetilde{g}(y)$, and we have kept the expression explicitly only up to $\mathcal{O}(h^2)$.

APPENDIX C

THERMO-MAGNETIC CORRECTIONS TO THE BOSON COUPLING.

The thermo-magnetic correction to λ involves the diagrams shown in Figure 6.1, column (a). It is only necessary to consider the case where the loop is made of charged pions (the bottom diagram in column (a) of Figure 6.1, since the other contributions can be obtained from this one after letting $qB \to 0$. The calculation is carried out in the static limit, *i.e.* where $P_i = (\Pi, \mathbf{p} = 0)$. The explicit expression is given by

$$J(P_i; m_i^2) = T \sum_n \int \frac{d^3k}{(2\pi)^3} D_B(P_i - K) D_B(K) = J_{n=0}(P_i; m_i^2) + J_{n\neq 0}(P_i; m_i^2). \quad \text{(C.1)}$$

First we consider the contribution from the zero mode

$$\begin{aligned} J_{n=0}(P_i; m_i^2) =& T \int \frac{d^3k}{(2\pi)^3} \int_0^\infty ds \frac{e^{-s(\omega_n^2 + (p_3 - k_3)^2 + (p_\perp - k_\perp)^2 \frac{\tanh(qBs)}{qBs} + m^2)}}{\cosh(qBs)} \\ & \times \int_0^\infty d\tau \frac{e^{-\tau(k_3^2 + k_\perp^2 \frac{\tanh(qB\tau)}{qB\tau} + m^2)}}{\cosh(qB\tau)}. \end{aligned} \quad \text{(C.2)}$$

In the Hard Thermal Loop Approximation (HTL), P_3 y $P_\perp$ are small quantities with respect to T, and the same occurs with the mass. In this way we find

$$J_{n=0} = T \int \frac{d^3k}{(2\pi)^3} \int_0^\infty ds \frac{e^{-s(\omega_n^2 + k_3^2 + k_\perp^2 \frac{\tanh(qBs)}{qBs})}}{\cosh(qBs)} \int_0^\infty d\tau \frac{e^{-\tau(k_3^2 + k_\perp^2 \frac{\tanh(qB\tau)}{qB\tau})}}{\cosh(qB\tau)}. \quad \text{(C.3)}$$

Carrying out the integrals, we obtain

$$J_{n=0}(\omega=\Pi)=\frac{T}{16\pi}\frac{1}{(2qB)^{1/2}}\zeta\left(\frac{3}{2},\frac{1}{2}+\frac{\Pi(T,\mu)}{2qB}\right). \tag{C.4}$$

For the non-zero modes ($\omega_n\neq 0$) we find

$$\begin{aligned}J_{n\neq0}(P_i;m_i^2)=T\sum_{n\neq0}\int\frac{d^3k}{(2\pi)^3}\Bigg[\Bigg(&\frac{1}{\omega_n^2+k^2+m^2}-\frac{(eB)^2}{(\omega_n^2+k^2+m^2)^3}+\frac{2(eB)^2k_\perp^2}{(\omega_n^2+k^2+m^2)^4}\Bigg)\\&\Bigg(\frac{1}{(\omega-\omega_n)^2+(p-k)^2+m^2}-\frac{(eB)^2}{((\omega-\omega_n)^2+(p-k)^2+m^2)^3}\\&+\frac{2(eB)^2k_\perp^2}{((\omega-\omega_n)^2+(p-k)^2+m^2)^4}\Bigg)\Bigg].\end{aligned} \tag{C.5}$$

Still in the HTL approximation we find

$$\begin{aligned}J_{n\neq0}(P_i;m_i^2)=&T\sum_{n\neq0}\int\frac{d^3k}{(2\pi)^3}\Bigg[\Bigg(\frac{1}{\omega_n^2+k^2}-\frac{(eB)^2}{2(\omega_n^2+k^2)^3}\Bigg)\\&\Bigg(\frac{1}{(\omega-\omega_n)^2+k^2}-\frac{(eB)^2}{((\omega-\omega_n)^2+k^2)^3}\Bigg)\Bigg].\end{aligned} \tag{C.6}$$

Since we only consider terms up to order $\mathcal{O}\ (qB)^2$, we have

$$J_{n\neq0}(P_i;m_i^2)=T\sum_{n\neq0}\int\frac{d^3k}{(2\pi)^3}\left[\frac{1}{(\omega_n^2+k^2+\omega^2)^2}-\frac{(eB)^2}{(\omega_n^2+k^2+\omega^2)^4}\right]. \tag{C.7}$$

In order to calculate the above integrals we make use of dimensional regularization, and of the Mellin summation technique [158], to find

$$\begin{aligned}J_{n\neq0}(\omega^2=\Pi)=&-\frac{1}{16\pi^2}\left[\ln\left(\frac{(4\pi T)^2}{2a^2}\right)+1-2\gamma_E+\zeta(3)\left(\frac{\sqrt{\Pi}}{2\pi T}\right)^2\right]\\&-\frac{(qB)^2}{1024\pi^6T^4}\zeta(5).\end{aligned} \tag{C.8}$$

Joining both contributions we find

$$\begin{aligned}J(\omega=\Pi)=&\frac{T}{16\pi}\frac{1}{(2qB)^{1/2}}\zeta\left(\frac{3}{2},\frac{1}{2}+\frac{\Pi}{2qB}\right)-\frac{1}{16\pi^2}\left[\ln\left(\frac{(4\pi T)^2}{2a^2}\right)\right.\\&\left.+1-2\gamma_E+\zeta(3)\left(\frac{\sqrt{\Pi}}{2\pi T}\right)^2\right]-\frac{(qB)^2}{1024\pi^6T^4}\zeta(5).\end{aligned} \tag{C.9}$$

In the case of the diagrams involving neutral bosons we have

$$I(P_i;m_i^2)=T\sum_n\int\frac{d^3k}{(2\pi)^3}D(P_i-K)D(K)=I_{n=0}(P_i;m_i^2)+I_{n\neq0}(P_i;m_i^2). \tag{C.10}$$

In order to calculate $I(P_i; m_i^2)$, we take limit $(qB) \to 0$ in eq. (C.9). The limit of the Hurwitz Zeta function is not trivial and we use the following asymptotic expansion [159]

$$\zeta(s, y) = \frac{1}{2} y^{-s} + \frac{y^{1-2}}{s-1} + \sum_{k=1}^{\infty} \frac{B_{2k}}{(2k)!} \frac{\Gamma(2k+s-1)}{\Gamma(s) y^{2k+s-1}}, \tag{C.11}$$

where B_{2k} are Bernoulli numbers. This expansion is valid for large values of y, which is equivalent to having a small value for qB. In our case $s = 3/2$ and $y = \frac{1}{2} + \frac{\Pi}{2qB}$ and we find

$$\zeta\left(\frac{3}{2}, \frac{1}{2} + \frac{\Pi}{2qB}\right) \approx \frac{2(2qB)^{1/2}}{\sqrt{\Pi}} - \frac{1}{16} \frac{(2qB)^{5/2}}{\Pi^{5/2}} + \cdots . \tag{C.12}$$

Using the above expansion in eq. (C.9) we finally obtain

$$I(\omega = \Pi) = \frac{T}{8\pi} \frac{1}{\sqrt{\Pi}} - \frac{1}{16\pi^2} \Big[\ln\left(\frac{(4\pi T)^2}{2a^2}\right) + 1 - 2\gamma_E + \zeta(3) \left(\frac{\sqrt{\Pi}}{2\pi T}\right)^2 \Big]. \tag{C.13}$$

APPENDIX D

THERMO-MAGNETIC CORRECTIONS TO THE FERMION-BOSON COUPLING.

The determination of the thermo-magnetic correction to the coupling g involves the diagram shown in Figure 6.2 (a). We call the one-loop effective vertex Γ. The calculation is done up to order $\mathcal{O}\,(qB)$

$$\begin{aligned}\Gamma &= -g + g^3 T \sum_n \int \frac{d^3k}{(2\pi)^3} \gamma_5 S(P_1 - K) S(P_2 - K) \gamma_5 D(K) \\ &\equiv -g(1 + \delta\Gamma),\end{aligned} \tag{D.1}$$

where

$$\gamma_5 = \gamma_4 \gamma_1 \gamma_2 \gamma_3. \tag{D.2}$$

Concentrating on $\delta\Gamma$

$$\begin{aligned}\delta\Gamma =& - g^2 T \sum_n \int \frac{d^3k}{(2\pi)^3} \gamma_5 S(P_1 - K) S(P_2 - K) \gamma_5 D(K) \\ =& - g^2 T \sum_n \int \frac{d^3k}{(2\pi)^3} \left[\frac{-(\not{P}_1 - \not{K})}{(P_1 - K)^2 + m^2} + \frac{iqB\gamma_1\gamma_2(\gamma \cdot (P_2 - K)_{||})}{[(P_2 - K)^2 + m^2]^2} \right] \\ & \times \left[\frac{-(\not{P}_2 - \not{K})}{(P_2 - K)^2 + m^2} + \frac{iqB\gamma_1\gamma_2(\gamma \cdot (P_2 - K)_{||})}{[(P_2 - K)^2 + m^2]^2} \right] \frac{1}{K^2 + m_\pi^2}.\end{aligned} \tag{D.3}$$

In the HTL approximation, we get

$$\begin{aligned}\delta\Gamma =& -g^2T\sum_n\int\frac{d^3k}{(2\pi)^3}\Big[(\not{K})^2\tilde{\Delta}(P_1-K)\tilde{\Delta}(P_2-K)\Delta(K)\\ &-iqB\not{K}\gamma_1\gamma_2(\gamma\cdot K)_{||}\tilde{\Delta}(P_1-K)\tilde{\Delta}^2(P_2-K)\Delta(K)\\ &-iqB\gamma_1\gamma_2(\gamma\cdot K)_{||}\not{K}\tilde{\Delta}(P_1-K)\tilde{\Delta}^2(P_2-K)\Delta(K)\Big]\\ =&\delta\Gamma_{TV}+\delta\Gamma_{TB},\end{aligned}\tag{D.4}$$

where

$$\delta\Gamma_{TV}=-g^2T\sum_n\int\frac{d^3k}{(2\pi)^3}\not{K}\not{K}\tilde{\Delta}(P_1-K)\tilde{\Delta}(P_2-K)\Delta(K),\tag{D.5}$$

is the vacuum+thermal contribution, and where

$$\begin{aligned}\delta\Gamma_{TB} =& -g^2T\sum_n\int\frac{d^3k}{(2\pi)^3}\Big[-iqB\not{K}\gamma_1\gamma_2(\gamma\cdot K)_{||}\tilde{\Delta}(P_1-K)\tilde{\Delta}^2(P_2-K)\Delta(K)\\ &-iqB\gamma_1\gamma_2(\gamma\cdot K)_{||}\not{K}\tilde{\Delta}(P_1-K)\tilde{\Delta}^2(P_2-K)\Delta(K)\Big],\end{aligned}\tag{D.6}$$

is the thermo-magnetic contribution. We now consider $\delta\Gamma_{TV}$ in the HTL approximation

$$\begin{aligned}\delta\Gamma_{TV} &= -g^2T\sum_n\int\frac{d^3k}{(2\pi)^3}\not{K}\not{K}\tilde{\Delta}(P_1-K)\tilde{\Delta}(P_2-K)\Delta(K)\\ &= g^2T\sum_n\int\frac{d^3k}{(2\pi)^3}\tilde{\Delta}(P_1-K)\tilde{\Delta}(P_2-K)\\ &= \frac{1}{8\pi^2}\left(\ln\left(\frac{a}{T\pi}\right)+\frac{\gamma_E}{2}-\frac{1}{2}-\ln(2\pi)\right).\end{aligned}\tag{D.7}$$

Next, we concentrate on the last two terms of eq. (D.4), which make up the thermo-magnetic contribution $\delta\Gamma_{TB}$. First, we recall that γ_5 anti-commutes with the other gamma matrices. We introduce the decomposition

$$\gamma_1\gamma_2\not{K}_{\parallel}=\gamma_5\left[(K\cdot b)\not{u}-(K\cdot u)\not{b}\right],\tag{D.8}$$

where we have introduced the four-vectors

$$\begin{aligned}u_\mu &= (1,0,0,0)\\ b_\mu &= (0,0,0,1).\end{aligned}\tag{D.9}$$

We stress that in the HTL approximation, P_1 y P_2 are small quantities that can be considered of the same order. In this way the thermo-magnetic contribution can be written

as

$$\delta\Gamma_{TB} = -g^2 T \sum_n \int \frac{d^3k}{(2\pi)^3} \tilde{\Delta}(P_1 - K)\tilde{\Delta}^2(P_2 - K)\Delta(K) \times [-2iqB\gamma_5(\not{\psi}(K\cdot b)) - \not{b}(K\cdot u)]\not{K}. \tag{D.10}$$

We define

$$\tilde{G}(P_1, P_2) = T \sum_n \int \frac{d^3k}{(2\pi)^3} \tilde{\Delta}(P_1 - K)\tilde{\Delta}^2(P_2 - K)\Delta(K) \times [(\not{\psi}(K\cdot b)) - \not{b}(K\cdot u)]\not{K}, \tag{D.11}$$

to obtain

$$\delta\Gamma_{TB} = 2ig^2(qB)\gamma_5 \tilde{G}(P_1, P_2), \tag{D.12}$$

where $\tilde{G}(P_1, P_2)$ can be expressed in terms of the tensor $\mathcal{J}_{\alpha i}$ ($\alpha = 1, \ldots 4,\ i = 3, 4$) given by

$$\mathcal{J}_{\alpha i} = T \sum_n \int \frac{d^3k}{(2\pi)^3} K_\alpha K_i \widetilde{\Delta}^2(K)\Delta(P_1 - K)\Delta(P_2 - K). \tag{D.13}$$

In order to calculate the sum over Matsubara frequencies we use

$$\begin{aligned}
\widetilde{Y}_0 &= T \sum_n \widetilde{\Delta}^2(K)\Delta(P_1 - K)\Delta(P_2 - K) \\
&= \left(-\frac{\partial}{\partial m^2}\right) T \sum_n \widetilde{\Delta}(K)\Delta(P_1 - K)\Delta(P_2 - K) \\
&\equiv \left(-\frac{\partial}{\partial m^2}\right) \widetilde{X}_0 \\
\widetilde{Y}_1 &= T \sum_n \omega_n \widetilde{\Delta}^2(K)\Delta(P_1 - K)\Delta(P_2 - K) \\
&= \left(-\frac{\partial}{\partial m^2}\right) T \sum_n \omega_n \widetilde{\Delta}(K)\Delta(P_1 - K)\Delta(P_2 - K) \\
&\equiv \left(-\frac{\partial}{\partial m^2}\right) \widetilde{X}_1 \\
\widetilde{Y}_2 &= T \sum_n \omega_n^2 \widetilde{\Delta}^2(K)\Delta(P_1 - K)\Delta(P_2 - K) \\
&= \left(-\frac{\partial}{\partial m^2}\right) T \sum_n \omega_n^2 \widetilde{\Delta}(K)\Delta(P_1 - K)\Delta(P_2 - K) \\
&\equiv \left(-\frac{\partial}{\partial m^2}\right) \widetilde{X}_2,
\end{aligned} \tag{D.14}$$

where $\widetilde{X}_0$, $\widetilde{X}_1$, $\widetilde{X}_2$ are given by

$$\begin{aligned}
\widetilde{X}_0 &= -\sum_{s,s_1,s_2} \frac{s s_1 s_2}{8EE_1E_2} \frac{1}{i(\omega_1-\omega_2)-s_1E_1+s_2E_2} \\
&\quad\times\left[\frac{1-\widetilde{f}(sE)+f(s_1E_1)}{i\omega_1-sE-s_1E_1}-\frac{1-\widetilde{f}(sE)+f(s_2E_2)}{i\omega_2-sE-s_2E_2}\right] \\
\widetilde{X}_1 &= i\sum_{s,s_1,s_2} \frac{s_1 s_2 E}{8EE_1E_2} \frac{1}{i(\omega_1-\omega_2)-s_1E_1+s_2E_2} \\
&\quad\times\left[\frac{1-\widetilde{f}(sE)+f(s_1E_1)}{i\omega_1-sE-s_1E_1}-\frac{1-\widetilde{f}(sE)+f(s_2E_2)}{i\omega_2-sE-s_2E_2}\right] \\
\widetilde{X}_2 &= \sum_{s,s_1,s_2} \frac{s s_1 s_2 E^2}{8EE_1E_2} \frac{1}{i(\omega_1-\omega_2)-s_1E_1+s_2E_2} \\
&\quad\times\left[\frac{1-\widetilde{f}(sE)+f(s_1E_1)}{i\omega_1-sE-s_1E_1}-\frac{1-\widetilde{f}(sE)+f(s_2E_2)}{i\omega_2-sE-s_2E_2}\right].
\end{aligned} \tag{D.15}$$

The leading temperature behaviour is obtained from the terms with $s=-s_1=-s_2$. We consider in detail the calculation of $\widetilde{X}_0$ for those terms and make the approximation where $f(E_1)\simeq f(E_2)\simeq f(E)$, namely, that the Bose-Einstein distribution depends on $E=\sqrt{k^2+m^2}$ and thus on the quark mass. This approximation allows to find the leading temperature behaviour for $m\to 0$, since it amounts to keep the quark mass as an infrared regulator. Also, using that $E_i\simeq k-\vec{p}_i\cdot\hat{k}$, $i=1,2$, we find

$$\widetilde{X}_0 \simeq -\frac{1}{8k^2}\frac{\left[\widetilde{f}(E)+f(E)\right]}{E}\left\{\frac{1}{(i\omega_1+\vec{p}_1\cdot\hat{k})(i\omega_2+\vec{p}_2\cdot\hat{k})}+\frac{1}{(i\omega_1-\vec{p}_1\cdot\hat{k})(i\omega_2-\vec{p}_2\cdot\hat{k})}\right\}, \tag{D.16}$$

where we have set $E_1=E_2=k$ in the denominator of the first fraction. Similarly

$$\begin{aligned}
\widetilde{X}_1 &\simeq -\frac{i}{8k}\frac{\left[\widetilde{f}(E)+f(E)\right]}{E}\left\{\frac{1}{(i\omega_1+\vec{p}_1\cdot\hat{k})(i\omega_2+\vec{p}_2\cdot\hat{k})}-\frac{1}{(i\omega_1-\vec{p}_1\cdot\hat{k})(i\omega_2-\vec{p}_2\cdot\hat{k})}\right\} \\
\widetilde{X}_2 &\simeq \frac{1}{8}\frac{\left[\widetilde{f}(E)+f(E)\right]}{E}\left\{\frac{1}{(i\omega_1+\vec{p}_1\cdot\hat{k})(i\omega_2+\vec{p}_2\cdot\hat{k})}+\frac{1}{(i\omega_1-\vec{p}_1\cdot\hat{k})(i\omega_2-\vec{p}_2\cdot\hat{k})}\right\}.
\end{aligned} \tag{D.17}$$

Using eqs. (D.16) and (D.17) in eqs. (D.14) and (D.13), we find

$$\begin{aligned}
\mathcal{J}_{\alpha i} = &-\frac{1}{8\pi^2}\left(-\frac{\partial}{\partial y^2}\right)\int_0^\infty \frac{dx\ x^2}{\sqrt{x^2+y^2}}\left[\widetilde{f}(\sqrt{x^2+y^2})+f(\sqrt{x^2+y^2})\right] \\
&\int\frac{d\Omega}{4\pi}\frac{\hat{K}_\alpha\hat{K}_i}{(P_1\cdot\hat{K})(P_2\cdot\hat{K})},
\end{aligned} \tag{D.18}$$

where we have defined $x = k/T$, $y = m/T$, $\hat{K} = (-i, \hat{k})$, $P_1 = (-\omega_1, \vec{p}_1)$ and $P_2 = (-\omega_2, \vec{p}_2)$. The integrals over x can be expressed in terms of the well known functions [160]

$$\begin{aligned} h_n(y) &= \frac{1}{\Gamma(n)} \int_0^\infty \frac{dx\ x^{n-1}}{\sqrt{x^2+y^2}} \frac{1}{e^{\sqrt{x^2+y^2}} - 1} \\ f_n(y) &= \frac{1}{\Gamma(n)} \int_0^\infty \frac{dx\ x^{n-1}}{\sqrt{x^2+y^2}} \frac{1}{e^{\sqrt{x^2+y^2}} + 1}, \end{aligned} \tag{D.19}$$

which satisfy the differential equations

$$\begin{aligned} \frac{\partial h_{n+1}}{\partial y^2} &= -\frac{h_{n-1}}{2n} \\ \frac{\partial f_{n+1}}{\partial y^2} &= -\frac{f_{n-1}}{2n}, \end{aligned} \tag{D.20}$$

therefore

$$\mathcal{J}_{\alpha i} = -\frac{1}{16\pi^2} \left[h_1(y) + f_1(y)\right] \int \frac{d\Omega}{4\pi} \frac{\hat{K}_\alpha \hat{K}_i}{(P_1 \cdot \hat{K})(P_2 \cdot \hat{K})}. \tag{D.21}$$

Using the high temperature expansions for $h_1(y)$ and $f_1(y)$ [117]

$$\begin{aligned} h_1(y) &= \frac{\pi}{2y} + \frac{1}{2} \ln\left(\frac{y}{4\pi}\right) + \frac{1}{2}\gamma_E + \dots \\ f_1(y) &= -\frac{1}{2} \ln\left(\frac{y}{\pi}\right) - \frac{1}{2}\gamma_E + \dots, \end{aligned} \tag{D.22}$$

and keeping the leading terms, we obtain

$$\mathcal{J}_{\alpha i} = \frac{1}{16\pi^2} \left[\ln(2) - \frac{\pi}{2} \frac{T}{\sqrt{\Pi}}\right] \int \frac{d\Omega}{4\pi} \frac{\hat{K}_\alpha \hat{K}_i}{(P_1 \cdot \hat{K})(P_2 \cdot \hat{K})}. \tag{D.23}$$

Hence

$$\delta\Gamma_{TB} = -\frac{2ig^2(qB)\gamma_5}{16\pi^2} \left[\ln(2) - \frac{\pi}{2} \frac{T}{\sqrt{\Pi}}\right] \int \frac{d\Omega}{4\pi} \frac{[(\not{y}(\hat{K} \cdot b)) - \not{b}(\hat{K} \cdot u)]\not{\hat{K}}}{(P_1 \cdot \hat{K})(P_2 \cdot \hat{K})}. \tag{D.24}$$

In order to consider the thermo-magnetic dependence of the fermion-boson coupling we consider explicitly the quantities appearing on the *r.h.s.* of eq. (D.24)

$$J_{\alpha i}(P_1, P_2) \equiv \int \frac{d\Omega}{4\pi} \frac{\hat{K}_\alpha \hat{K}_i}{(P_1 \cdot \hat{K})(P_2 \cdot \hat{K})}, \tag{D.25}$$

For simplicity we choose a configuration where the momenta $\vec{p}_1$ and $\vec{p}_2$ form a relative angle $\theta_{12} = \pi$. This configuration corresponds, for instance, to a thermal gluon decaying into a quark-antiquark pair in the center of mass system, and is therefore general enough. Consider first $J_{44}(P_1, P_2)$

$$\begin{aligned} J_{44}(P_1, P_2) &= -\frac{1}{2} \frac{1}{i\omega_1 p_2 + i\omega_2 p_1} \int_{-1}^{1} dx \left\{ \frac{p_1}{i\omega_1 + p_1 x} + \frac{p_2}{i\omega_2 - p_2 x} \right\} \\ &= -\frac{1}{2} \frac{1}{i\omega_1 p_2 + i\omega_2 p_1} \left\{ \ln\left(\frac{i\omega_1 + p_1}{i\omega_1 - p_1}\right) + \ln\left(\frac{i\omega_2 + p_2}{i\omega_2 - p_2}\right) \right\}. \end{aligned} \tag{D.26}$$

We now perform the analytic continuation to Minkowski space $i\omega_{1,2} \to p_{01,02}$ [$\hat{K} \to (-1, \hat{k})$], and consider the scenario where $p_{01} = p_{02} \equiv p_0$ and $p_1 = p_2 \equiv p$, leading to

$$J_{44} \to J_{00} = \frac{1}{2p_0 p} \ln\left(\frac{p_0 + p}{p_0 - p}\right). \tag{D.27}$$

Furthermore, we consider the *static limit* where the quarks are almost at rest, namely $p \to 0$, to find

$$J_{00} \xrightarrow{p\to 0} \frac{1}{p_0^2}. \tag{D.28}$$

Now we consider $J_{33}(P_1, P_2)$ in the same momenta configuration

$$\begin{aligned} J_{33}(P_1, P_2) =& \frac{1}{2} \frac{1}{i\omega_1 p_2 + i\omega_2 p_1} \int_{-1}^{1} dx\ x^2 \left\{ \frac{p_1}{i\omega_1 + p_1 x} + \frac{p_2}{i\omega_2 - p_2 x} \right\} \\ =& -\frac{1}{i\omega_1 p_2 + i\omega_2 p_1} \left\{ \frac{i\omega_1}{p_1} \left[1 - \frac{i\omega_1}{2p_1} \ln\left(\frac{i\omega_1 + p_1}{i\omega_1 - p_1}\right) \right] \right. \\ &\left. + \frac{i\omega_2}{p_2} \left[1 - \frac{i\omega_2}{2p_2} \ln\left(\frac{i\omega_2 + p_2}{i\omega_2 - p_2}\right) \right] \right\}. \end{aligned} \tag{D.29}$$

After analytical continuation to Minkowski space and in the same scenario where $p_{01} = p_{02} \equiv p_0$ and $p_1 = p_2 \equiv p$, we obtain

$$J_{33} = -\frac{1}{p^2} \left[1 - \frac{p_0}{2p} \ln\left(\frac{p_0 + p}{p_0 - p}\right) \right]. \tag{D.30}$$

In the limit where $p \to 0$ this gives

$$J_{33} \xrightarrow{p\to 0} \frac{1}{3p_0^2}. \tag{D.31}$$

In this same limit, $p \to 0$, we find

$$\begin{aligned} \delta\Gamma_{TB} &= 2g^2 (J_{33} + J_{44}) q\vec{\Sigma} \cdot \vec{B} \frac{\left[\ln(2) - \frac{\pi}{2} \frac{T}{\sqrt{\Pi}} \right]}{16\pi^2} \\ &= 2g^2 \left(\frac{4}{3p_0^2} \right) \frac{\left[\ln(2) - \frac{\pi}{2} \frac{T}{\sqrt{\Pi}} \right]}{16\pi^2} q\vec{\Sigma} \cdot \vec{B}, \end{aligned} \tag{D.32}$$

where

$$\vec{\Sigma} \cdot \vec{B} = i\gamma_1 \gamma_2 B. \tag{D.33}$$

By taking both contributions into account, $\delta\Gamma_{TV} + \delta\Gamma_{TB}$, we can find Γ. Considering the contributions of the *up*- and *down*-quarks explicitly, and taking $p_0^2 \to m_f^2$ we finally obtain the correction to the coupling g.

$$g_{\text{eff}} = g(1 + g^2(g_{\text{TB}} + g_{\text{TV}})), \tag{D.34}$$

where

$$g_{\mathrm{TB}} = \frac{(q_u + q_d)B}{8\pi^2}\left(\frac{4}{3m_f^2}\right)\left(\ln(2) - \frac{\pi T}{2\sqrt{\Pi}}\right)$$
$$g_{\mathrm{TV}} = \frac{1}{8\pi^2}\left(\ln\left(\frac{a}{T\pi}\right) + \frac{\gamma_E}{2} - \frac{1}{2} - \ln(2\pi)\right). \tag{D.35}$$

APPENDIX E

FERMION THERMAL AND DENSITY DEPENDENT MASS.

This calculation involves the three diagrams shown in Figure E.1. We only consider the first one, since the computation of the other two diagrams is completely equivalent. We call this diagram Σ_σ

$$\Sigma_\sigma = -g^2 \int \frac{d^4K}{(2\pi)^4} S(P-K)\Delta(K). \tag{E.1}$$

In the HTL approximation this gives

$$\Sigma_\sigma = -g^2 \int \frac{d^4K}{(2\pi)^4} \not{K} \Delta(K)\tilde{\Delta}(P-K), \tag{E.2}$$

where

$$\begin{aligned} \Delta(Q) &= \frac{1}{\omega_n + k^2} \\ \tilde{\Delta}(Q) &= \frac{1}{\tilde{\omega}_n + k^2}. \end{aligned} \tag{E.3}$$

The determination of Σ_σ involves two kinds of Matsubara sums

$$\begin{aligned} \Sigma_{\sigma_{i=1,2,3}} &= T\sum_n \Delta(K)\tilde{\Delta}(P-K) \\ \Sigma_{\sigma_{i=4}} &= T\sum_n \omega_n \Delta(K)\tilde{\Delta}(P-K). \end{aligned} \tag{E.4}$$

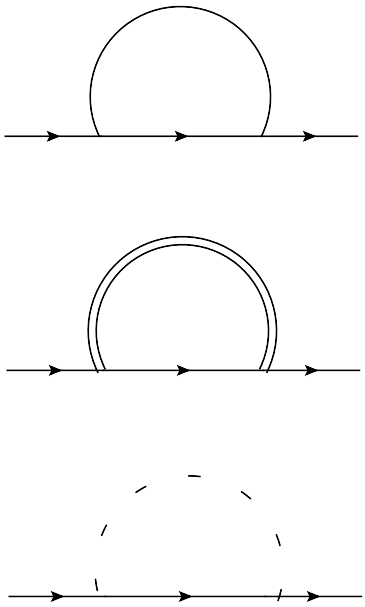

Figure E.1: Diagrams contributing to the calculation of the fermion thermal mass.

The first case refers to $i = 1, 2, 3$ and the second case to $i = 4$. The first kind of contribution is

$$\begin{aligned}\Sigma_{\sigma_{i=1,2,3}} =& T\sum_n \int \frac{d^3K}{(2\pi)^3} K_i \Delta(K)\tilde{\Delta}(P-K) \\ =& -\frac{1}{2\pi^2}\int \frac{d\Omega}{4\pi}\hat{K}_i \int dk K\left[\frac{f(k)+\tilde{f}(k-\mu)}{i\omega+\hat{k}\cdot\vec{p}}\right. \\ & \left. -\frac{f(k)+\tilde{f}(k+\mu)}{i\omega-\hat{k}\cdot\vec{p}}\right]. \end{aligned} \tag{E.5}$$

We have to deal with both the radial as well as the angular part. For the radial contribution we find

$$\int dK\ K[f(k)+\tilde{f}(k\pm\mu)] = \frac{\pi^2T^2}{6} - T^2 Li_2(-e^{\mp\mu/T}). \tag{E.6}$$

For the angular part we notice that the integral is symmetric under the transformation

$$\begin{aligned}\hat{k} &\to -\hat{k} \\ d\Omega &\to d\Omega, \end{aligned} \tag{E.7}$$

implying

$$\int \frac{d\Omega}{4\pi}\frac{1}{i\tilde{\omega}-\hat{k}\cdot\vec{p}} \to -\int \frac{d\Omega}{4\pi}\frac{1}{i\tilde{\omega}+\hat{k}\cdot\vec{p}}. \tag{E.8}$$

Therefore, we finally find

$$\Sigma_{\sigma_{i=1,2,3}} = -\frac{1}{8\pi^2}\left[2\left(\frac{\pi^2T^2}{6}\right) - T^2Li_2(-e^{\mu/T}) - T^2Li_2(-e^{-\mu/T})\right]\int \frac{d\Omega}{4\pi}\frac{1}{i\tilde{\omega}+\hat{k}\cdot\vec{p}}. \tag{E.9}$$

The second contribution $\Sigma_{\sigma_{i=4}}$ is

$$\begin{aligned}\Sigma_{\sigma_{i=4}} &= T\sum_n \int \frac{d^3K}{(2\pi)^3}\omega_n \Delta(K)\tilde{\Delta}(P-K) \\ &= -\frac{i}{8\pi^2}\int \frac{d\Omega}{4\pi}\int dkK\left[\frac{f(k)+\tilde{f}(k-\mu)}{i\omega+\hat{k}\cdot\vec{p}}+\frac{f(k)+\tilde{f}(k+\mu)}{i\omega-\hat{k}\cdot\vec{p}}\right]. \end{aligned} \tag{E.10}$$

Carrying out the radial and the angular integrals, in a completely analogous way as before, we have

$$\begin{aligned}\Sigma_{\sigma_{i=4}} &= T\sum_n \int \frac{d^3K}{(2\pi)^3}\omega_n \Delta(K)\tilde{\Delta}(P-K) \\ &= -\frac{1}{8\pi^2}\left[2\left(\frac{\pi^2T^2}{6}\right)-T^2Li_2(-e^{\mu/T})-T^2Li_2(-e^{-\mu/T})\right]\int\frac{d\Omega}{4\pi}\frac{1}{i\tilde{\omega}+\hat{k}\cdot\vec{p}}. \end{aligned} \tag{E.11}$$

The sum of the contribution of the different diagrams finally yields the thermal and density dependent correction to the fermion mass

$$(m_f^{\text{them}})^2 = g^2T^2\left(\frac{1}{3}-\frac{Li_2(-e^{\mu/T})}{\pi^2}-\frac{Li_2(-e^{-\mu/T})}{\pi^2}\right). \tag{E.12}$$

APPENDIX F

MAGNETIC DEPENDENCE OF THE QUARK-GLUON VERTEX.

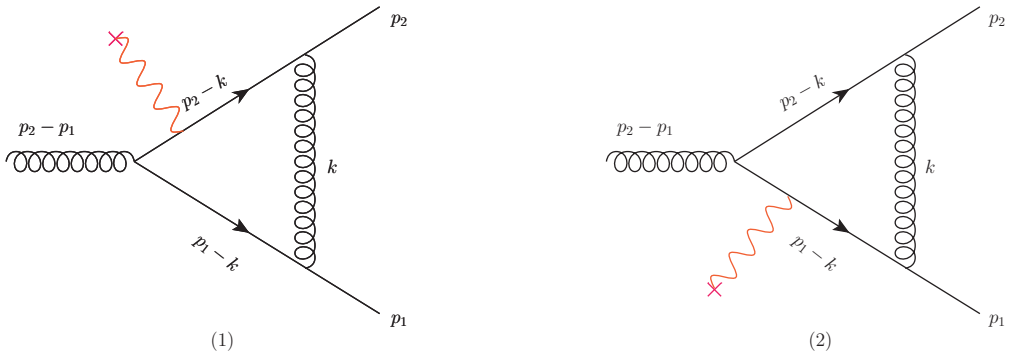

Figure F.1: QED-like diagram with magnetic correction, in the weak field approximation up to $\mathcal{O}(eB)$ order. The wavy red line ending in a cross represents the external magnetic field. For this contribution there are two contributions, one for each quark field in the loop.

First, we write the magnetic contribution from the QED-like diagram Figure F.1, for this diagram we have two contributions. Following Feynman rules and working in the weak field approximation, the vertex correction to this diagram is given by

$$\Gamma^{\mu\alpha}_{(a)} = I_{(1)} + I_{(2)}, \tag{F.1}$$

where

$$I_{(1)} = \int \frac{d^4k}{(2\pi)^4} \frac{-ig_{\nu\rho}}{k^2} \delta^{\alpha\beta} t^\beta ig\gamma^\rho \frac{i}{\not p_1 - \not k - m} t^\alpha ig\gamma^\mu i \Bigg[\frac{p_2 - k + m}{(\not p_2 - \not k)^2 - m^2} + i\gamma_1\gamma_2 \frac{(\not p_2 - \not k)_\parallel + m}{[(p_2 - k)^2 - m^2]^2} qB \Bigg] t^\alpha ig\gamma^\nu, \tag{F.2}$$

and

$$I_{(2)} = \int \frac{d^4k}{(2\pi)^4} \frac{-ig_{\nu\rho}}{k^2} \delta^{\alpha\beta} t^\beta ig\gamma^\rho i \Bigg[\frac{p_1 - k + m}{(\not p_1 - \not k)^2 - m^2} + i\gamma_1\gamma_2 \frac{(\not p_1 - \not k)_\parallel + m}{[(p_1 - k)^2 - m^2]^2} qB \Bigg] t^\alpha ig\gamma^\mu \frac{i}{\not p_2 - \not k - m} t^\alpha ig\gamma^\nu. \tag{F.3}$$

From eqs. (F.2) and (F.3), we take only the magnetic correction, then we have

$$\begin{aligned} \delta\Gamma^{\mu\alpha}_{(a)} = {} & qB \int \frac{d^4k}{(2\pi)^4} \frac{-ig_{\nu\rho}}{k^2} \delta^{\alpha\beta} t^\beta ig\gamma^\rho \frac{i}{\not p_1 - \not k - m} t^\alpha ig\gamma^\mu i\gamma_1\gamma_2 i \frac{(\not p_2 - \not k)_\parallel + m}{[(p_2 - k)^2 - m^2]^2} t^\alpha ig\gamma^\nu \\ & + qB \int \frac{d^4k}{(2\pi)^4} \frac{-ig_{\nu\rho}}{k^2} \delta^{\alpha\beta} t^\beta ig\gamma^\rho i\gamma_1\gamma_2 i \frac{(\not p_1 - \not k)_\parallel + m}{[(p_1 - k)^2 - m^2]^2} t^\alpha ig\gamma^\mu \frac{i}{\not p_2 - \not k - m} t^\alpha ig\gamma^\nu. \end{aligned} \tag{F.4}$$

Simplifying eq. (F.4), we get

$$\begin{aligned} \delta\Gamma^{\mu\alpha}_{(a)} = {} & ig^3 \delta^{\alpha\beta} t^\alpha t^\beta t^\alpha (qB) \int \frac{d^4k}{(2\pi)^4} \frac{1}{k^2} \Bigg\{ \frac{\gamma_\nu (\not p_1 - \not k + m)\gamma^\mu \gamma_1\gamma_2 ((\not p_2 - \not k)_\parallel + m)\gamma^\nu}{[(p_1 - k)^2 - m^2][(p_2 - k)^2 - m^2]^2} \\ & + \frac{\gamma_\nu \gamma_1\gamma_2 ((\not p_1 - \not k)_\parallel + m)\gamma^\mu ((\not p_2 - \not k) + m)\gamma^\nu}{[(p_1 - k)^2 - m^2]^2 [(p_2 - k)^2 - m^2]} \Bigg\}, \end{aligned} \tag{F.5}$$

with the colour factor $\delta^{\alpha\beta} t^\alpha t^\beta = C_F - \frac{C_A}{2}$, notice eq. (F.5) is the same as eq. (6.28). Working in the limit where $m \to 0$ and writing eq. (F.5) in terms of vectors eq. (A.4) and γ_5, then we get

$$\begin{aligned} \delta\Gamma^{\mu\alpha}_{(a)} = {} & ig^3 \left(C_F - \frac{C_A}{2} \right) t^\alpha (qB) \int \frac{d^4k}{(2\pi)^4} \frac{1}{k^2} \Bigg\{ \frac{\gamma_\nu (\not p_1 - \not k)\gamma^\mu i\gamma_5 [\not b [(p_2 - k)\cdot u] - \not u [(p_2 - k)\cdot b]]\gamma^\nu}{[p_1 - k]^2 [p_2 - k]^4} \\ & + \frac{\gamma_\nu i\gamma_5 [\not b [(p_1 - k)\cdot u] - \not u [(p_1 - k)\cdot b]]\gamma^\mu (\not p_2 - \not k)\gamma^\nu}{[p_1 - k]^4 [p_2 - k]^2} \Bigg\}. \end{aligned} \tag{F.6}$$

We move now to the left γ_5 and remember that $\gamma_\lambda \not a \not b \not c \gamma^\lambda$ or $\gamma_\lambda \gamma^\mu \gamma^\nu \gamma^\sigma \gamma^\lambda$ are equal to $-2\not a \not b \not c$ or $-2\gamma^\mu\gamma^\nu\gamma^\sigma$, respectively. Then

$$\delta\Gamma^{\mu\alpha}_{(a)} = -2ig^3\left(C_F - \frac{C_A}{2}\right)t^\alpha(qB)\int\frac{d^4k}{(2\pi)^4}\frac{i\gamma_5}{k^2}\left\{\frac{(\not p_1 - \not k)\gamma^\mu[\not b[(p_2-k)\cdot u] - \not u[(p_2-k)\cdot b]]}{[p_1-k]^2[p_2-k]^4}\right.$$
$$\left. + \frac{[\not b[(p_1-k)\cdot u] - \not u[(p_1-k)\cdot b]]\gamma^\mu(\not p_2 - \not k)}{[p_1-k]^4[p_2-k]^2}\right\}. \tag{F.7}$$

Now it is time to manage the denominator of eq. (F.7), we use Feynman parametrization

$$\frac{1}{A_1^{a_1}\cdots A_n^{a_n}} = \frac{\Gamma(a_1+a_2+\cdots+a_n)}{\Gamma(a_1)\Gamma(a_2)\cdots\Gamma(a_n)}\int_0^1 dx_1\cdots\int_0^1 dx_n\ \delta(1-(x_1+\cdots+x_n))$$
$$\times\frac{x_1^{a_1-1}\cdots x_n^{a_n-1}}{[x_1A_1+\cdots+x_nA_n]^{a_1+\cdots+a_n}} \tag{F.8}$$

In our case the structures of both denominators are quite similar, we need permute only p_1 by p_2, then we work with only one of them $I_{(1)}$, therefore we have

$$\frac{1}{k^2[p_2-k]^2[p_1-k]^4} = \frac{\Gamma(2+1+1)}{\Gamma(2)\Gamma(1)\Gamma(1)}\int_0^1 dx_1\int_0^1 dx_2\int_0^1 dx_3\frac{\delta(1-x_1-x_2-x_3)x_1}{[x_1(p_1-k)^2+x_2(p_2-k)^2+x_3k^2]^4}$$
$$= 3!\int_0^1 dx_1\int_0^{1-x_1} dx_2\frac{x_1}{[(k-(x_1p_1+x_2p_2))^2 - x_1p_1^2(x_1-1) - x_2p_2^2(x_2-1) - 2x_1x_2p_1\cdot p_2]^4}, \tag{F.9}$$

we do a change of variables, being $l = k-(x_1p_1+x_2p_2)$ and $\Delta = x_1p_1^2(x_1-1)+x_2p_2^2(x_2-1)+2x_1x_2p_1$, and eq. (F.9) becomes

$$\frac{1}{k^2[p_2-k]^2[p_1-k]^4} = 3!\int_0^1 dx_1\int_0^{1-x_1} dx_2\frac{x_1}{[l^2-\Delta]^4}. \tag{F.10}$$

We need to rewrite eq. (F.7) in terms of the new variables, it is

$$\delta\Gamma^{\mu\alpha}_{(a)} = -2ig^3\left(C_F - \frac{C_A}{2}\right)t^\alpha(qB)\int\frac{d^4l}{(2\pi)^4}3!\int_0^1 dx_1\int_0^{1-x_1}dx_2$$
$$\times i\gamma_5\Big\{(\not l + (x_1-1)\not p_1 + x_2\not p_2)\gamma^\mu$$
$$\times[\not b[(l+x_1p_1+(x_2-1)p_2)\cdot u] - \not u[(l+x_1p_1+(x_2-1)p_2)\cdot b]]$$
$$+[\not b[(l+(x_1-1)p_2+x_2p_1)\cdot u] - \not u[(l+(x_1-1)p_2+x_2p_1)\cdot b]]$$
$$\times\gamma^\mu(\not l + x_1\not p_2 + (x_2-1)\not p_1)\Big\}\frac{x_1}{[l^2-\Delta]^4}. \tag{F.11}$$

Looking at the numerator structure in eq. (F.11), terms proportional to $\not l$ do not contribute and only we have two kind of momentum integrals, they are in general the following

$$\int \frac{d^dl}{(2\pi)^d}\frac{1}{[l^2-\Delta]^n} = \frac{(-1)^n i}{(4\pi)^{d/2}}\frac{\Gamma(n-d/2)}{\Gamma(n)}\left(\frac{1}{\Delta}\right)^{n-d/2},$$
$$\int \frac{d^dl}{(2\pi)^d}\frac{l^\mu l^\nu}{[l^2-\Delta]^n} = \frac{(-1)^{n-1} i}{(4\pi)^{d/2}}\frac{g^{\mu\nu}}{2}\frac{\Gamma(n-1-d/2)}{\Gamma(n)}\left(\frac{1}{\Delta}\right)^{n-1-d/2}, \tag{F.12}$$

using eq. (F.12) into eq. (F.11), we obtain

$$\begin{aligned}
\delta\Gamma^{\mu\alpha}_{(a)} =& -2ig^3\left(C_F-\frac{C_A}{2}\right)t^\alpha(qB)3!\int_0^1 dx_1\; x_1\int_0^{1-x_1}dx_2 i\gamma_5\\
&\times\Bigg\{[u_\sigma \not{b}\gamma^\mu\gamma_\beta - b_\sigma \not{u}\gamma^\mu\gamma_\beta]\frac{g^{\sigma\beta}}{2}\frac{(-i)}{(4\pi)^2}\frac{\Gamma(1)}{\Gamma(4)}\left(\frac{1}{\Delta}\right)\\
&+[((x_1-1)p_1+x_2p_2)\cdot u\not{b}\gamma^\mu((x_2-1)\not{p}_2+x_1\not{p}_1)\\
&-((x_1-1)p_1+x_2p_2)\cdot b\not{u}\gamma^\mu((x_2-1)\not{p}_2+x_1\not{p}_1)]\frac{i}{(4\pi)^2}\frac{\Gamma(2)}{\Gamma(4)}\left(\frac{1}{\Delta}\right)^2\\
&+[u_\sigma\gamma_\beta\gamma^\mu\not{b}-b_\sigma\gamma_\beta\gamma^\mu\not{u}]\frac{g^{\sigma\beta}}{2}\frac{(-i)}{(4\pi)^2}\frac{\Gamma(1)}{\Gamma(4)}\left(\frac{1}{\Delta'}\right)\\
&+[((x_1-1)p_2+x_2p_1)\cdot u((x_2-1)\not{p}_1+x_1\not{p}_2)\gamma^\mu\not{b}\\
&-((x_1-1)p_2+x_2p_1)\cdot b((x_2-1)\not{p}_1+x_1\not{p}_2)\gamma^\mu\not{u}]\frac{i}{(4\pi)^2}\frac{\Gamma(2)}{\Gamma(4)}\left(\frac{1}{\Delta'}\right)^2\Bigg\},
\end{aligned} \tag{F.13}$$

where $\Delta' = \Delta(p_1 \leftrightarrow p_2)$. Now, let us do another change of variables, *i.e.*, $Q = p_1 - p_2$ and $P = \frac{p_1+p_2}{2}$, besides we choose to work in the symmetric three-momentum configuration, where $p_1 = (E,\vec{p})$ and $-p_2 = (E,-\vec{p})$, hence $Q = (2E,0)$ and $P = (0,\vec{p})$. Finally if we work in the static limit $P^2 = 0$, then $\Delta = \Delta'$ and we can compute the integrals on x_1 and x_2, leading to

$$\begin{aligned}
\delta\Gamma^{\mu\alpha}_{(a)} =& ig^3\left(C_F-\frac{C_A}{2}\right)t^\alpha(qB)(-2i\gamma_5)\frac{(-i)}{(4\pi)^2}\left(\frac{8}{3}\right)\\
&\times(1+\log(4))\frac{(Q\cdot u)^2}{Q^4}[b^\mu\not{u}+u^\mu\not{b}].
\end{aligned} \tag{F.14}$$

Finally, we manipulate a little bit the tensor structures as follow

$$\begin{aligned}
\gamma_5\not{b}u^\mu &= i\gamma_1\gamma_2\not{u}u^\mu,\\
\gamma_5\not{u}b^\mu &= i\gamma_1\gamma_2\not{b}b^\mu.
\end{aligned} \tag{F.15}$$

and we have

$$\delta\Gamma^{\mu\alpha}_{(a)} = -ig^3\left(C_F - \frac{C_A}{2}\right)t^\alpha \frac{[1+\log(4)]}{3\pi^2}\frac{(Q\cdot u)^2}{Q^4}[i\gamma_1\gamma_2 qB][\not{u}u^\mu + \not{b}b^\mu]$$
$$= -ig^3\left(C_F - \frac{C_A}{2}\right)t^\alpha \frac{[1+\log(4)]}{3\pi^2}\frac{q\vec{\Sigma}\cdot\vec{B}}{Q^2}(\not{u}u^\mu + \not{b}b^\mu). \tag{F.16}$$

Notice eq. (F.16) is actually eq. (6.30).

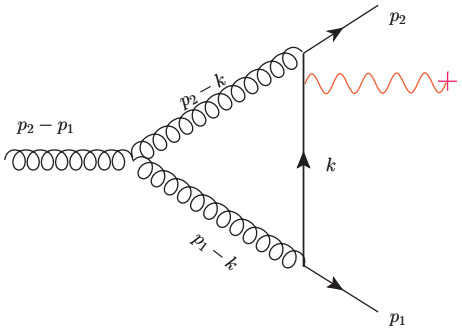

Figure F.2: Pure QCD diagram with magnetic correction, in the weak field approximation up to $\mathcal{O}(eB)$ order. The wavy red line ending in a cross represents the external magnetic field.

Now we proceed to the pure QCD diagram shown in Figure F.2. For this contribution we have

$$\Gamma^{\mu\alpha}_{(b)} = 2\int \frac{d^4k}{(2\pi)^4} i\left[\frac{\not{k}+m}{k^2-m^2} + i\gamma_1\gamma_2\frac{(\not{k}_\parallel + m)}{[k^2-m^2]^2}eB\right]$$
$$\times t^\kappa ig\gamma^{\nu'}\frac{-ig_{\nu'\nu}}{(p-k_1)^2}\delta^{\kappa\beta}gf^{\alpha\beta\eta}[g^{\mu\nu}(p_2-p_1-p_1+k)^\rho$$
$$+ g^{\nu\rho}(p_1-k-k+p_2)^\mu + g^{\rho\mu}(k-p_2-p_2+p_1)^\nu]\frac{-ig_{\rho\rho'}}{(p_2-k)^2}\delta^{\eta\theta}ig\gamma^\rho t^\theta, \tag{F.17}$$

where the explicit factor 2 takes into account both charge's fluxes of fermionic line. We pick up only the magnetic contribution, and we factorize constants and contract terms in the tensor structure from eq. (F.17), then we obtain

$$\delta\Gamma^{\mu\alpha}_{(b)} = -2g^3 f^{\alpha\beta\eta}t^\beta t^\eta (qB)\int \frac{d^4k}{(2\pi)^4}\left[\gamma_1\gamma_2\frac{\not{k}_\parallel + m}{(k^2-m^2)^2}\right]\gamma_\nu[g^{\mu\nu}(p_2-p_1-p_1+k)^\rho$$
$$+ g^{\nu\rho}(p_1-k-k+p_2)^\mu + g^{\rho\mu}(k-p_2-p_2+p_1)^\nu]\gamma_\rho\frac{1}{(k-p_1)^2(k-p_2)^2}, \tag{F.18}$$

with the colour factor $if^{\alpha\beta\eta}t^{\beta}t^{\eta} = \frac{C_A t^{\alpha}}{2}$. Besides we work in the case $m \to 0$, and remember $\gamma_1\gamma_2 = -i\not{u}\gamma_5\not{b}$ and $(\gamma\cdot k)_{\parallel} = \not{u}(k\cdot u) - \not{b}(k\cdot b)$; four-vectors u and b are defined in eq. (A.4), after we consider these last changes, we get

$$\begin{aligned}\delta\Gamma^{\mu\alpha}_{(b)} =& 2g^3\frac{C_A t^{\alpha}}{2}(qB)\int\frac{d^4k}{(2\pi)^4}\frac{1}{k^4(k-p_1)^2(k-p_2)^2}\\ &\times[(\not{u}\gamma_5\not{b})[\not{u}(k\cdot u)-\not{b}(k\cdot b)]]\gamma_\nu[g^{\mu\nu}(p_2-p_1-p_1+k)^\rho\\ &+g^{\nu\rho}(p_1-k-k+p_2)^\mu+g^{\rho\mu}(k-p_2-p_2+p_1)^\nu]\gamma_\rho. \end{aligned}\tag{F.19}$$

We now change variables $Q = p_1 - p_2$ and $P = \frac{p_1+p_2}{2}$ (at the moment only in the numerator) and work in the static limit, then we write eq. (F.19) as follows

$$\begin{aligned}\delta\Gamma^{\mu\alpha}_{(b)} =& -2ig^3\frac{C_A t^{\alpha}}{2}(qB)\int\frac{d^4k}{(2\pi)^4}\frac{1}{k^4(k-p_1)^2(k-p_2)^2}[i\gamma_5[-\not{b}(k\cdot u)+\not{u}(k\cdot b)]]\\ &\gamma_\nu\left[g^{\mu\nu}(-\frac{3}{2}Q+k)^\rho+g^{\nu\rho}(-2k)^\mu+g^{\rho\mu}(k+\frac{3}{2}Q)^\nu\right]\gamma_\rho, \end{aligned}\tag{F.20}$$

we manipulate a little bit eq. (F.20), then after distribute the numerator products, we find that

$$\begin{aligned}\delta\Gamma^{\mu\alpha}_{(b)} =& -2ig^3\frac{C_A t^{\alpha}}{2}(qB)(i\gamma_5)\int\frac{d^4k}{(2\pi)^4}\frac{1}{k^4(k-p_1)^2(k-p_2)^2}\\ &\times\Big\{2[\not{b}(k\cdot u)-\not{u}(k\cdot b)]k^\mu+2[b^\mu(k\cdot u)-u^\mu(k\cdot b)]\not{k}\\ &+3[b^\mu(k\cdot u)-u^\mu(k\cdot b)]\not{Q}-3[\not{b}(k\cdot u)-\not{u}(k\cdot b)]Q^\mu\\ &+3[\not{b}(k\cdot u)-\not{u}(k\cdot b)]\not{Q}\gamma^\mu-3[(k\cdot u)(Q\cdot b)-(k\cdot b)(Q\cdot u)]\gamma^\mu\Big\}. \end{aligned}\tag{F.21}$$

The denominator in eq. (F.21), after use Feynman parametrization eq. (F.8), becomes

$$3!\int_0^1 dx_1\int_0^{1-x_1}dx_2\frac{(1-x_1-x_2)}{l^2-\Delta},\tag{F.22}$$

with $\Delta = \frac{Q^2}{4}[(x_1-x_2)^2-(x_1+x_2)]$ and $l = k - \frac{Q}{2}(x_1-x_2)$. Hence, we need to rewrite the numerator in eq. (F.21) in terms of the new variable l and we remember that lineal terms of l do not contribute, then we have

$$\delta\Gamma^{\mu\alpha}_{(b)} = -2ig^3\frac{C_A t^\alpha}{2}(qB)(i\gamma_5)\int\frac{d^4l}{(2\pi)^4}3!\int_0^1 dx_1\int_0^{1-x_1}dx_2\frac{(1-x_1-x_2)}{l^2-\Delta}$$
$$\times\left\{\frac{5}{2}(x_1-x_2)[(Q\cdot u)b^\mu-(Q\cdot b)u^\mu]+\frac{1}{2}[(x_1-x_2)^2-3(x_1-x_2)]\right.$$
$$\times[(Q\cdot u)\not{b}-(Q\cdot b)\not{u}]Q^\mu+\frac{3}{2}(x_1-x_2)[(Q\cdot u)\not{b}-(Q\cdot b)\not{u}]\not{Q}\gamma^\mu$$
$$\left.+2[(l\cdot u)\not{b}-(l\cdot b)\not{u}]l^\mu\right\}. \tag{F.23}$$

The first and third terms within curly brackets in eq. (F.23) have a general structure for l as follows

$$\int\frac{d^dl}{(2\pi)^d}\frac{1}{[l^2-\Delta]^n}=i\frac{(-1)^n}{(4\pi)^{d/2}}\frac{\Gamma(n-d/2)}{\Gamma(n)}\left(\frac{1}{\Delta}\right)^{n-d/2}, \tag{F.24}$$

then after we integrate respect l these terms, we have the following general structure for them

$$3!\int_0^1 dx_1\int_0^{1-x_1}dx_2\frac{(1-x_1-x_2)(x_1-x_2)}{\Delta^2}=0, \tag{F.25}$$

therefore they do not contribute. The second term in eq. (F.23) after we integrate respect l has the following general structure

$$3!\int_0^1 dx_1\int_0^{1-x_1}dx_2\frac{(1-x_1-x_2)[(x_1-x_2)^2-3(x_1-x_2)]}{\Delta^2}=\frac{3!\left(\frac{-2}{15}\right)(-1+\log(4))}{Q^4}. \tag{F.26}$$

The last term to analyse $2[(l\cdot u)\not{b}-(l\cdot b)\not{u}]l^\mu = 2l^2[u^\mu\not{b}-b^\mu\not{u}]$, has the general integral structure respect l

$$\int\frac{d^dl}{(2\pi)^d}\frac{l^2}{[l^2-\Delta]^n}=i\frac{(-1)^{n-1}}{(4\pi)^{d/2}}\frac{d}{2}\frac{\Gamma(n-1-d/2)}{\Gamma(n)}\left(\frac{1}{\Delta}\right)^{n-1-d/2}, \tag{F.27}$$

hence after we integrate respect l the integrals respect x_1 and x_2 for this term become

$$3!\int_0^1 dx_1\int_0^{1-x_1}dx_2\frac{(1-x_1-x_2)}{\Delta}=3!\frac{\left(\frac{4}{3}\right)(1-4\log(2))}{Q^2}. \tag{F.28}$$

We now put all together, *i.e.*, substituting the results from eqs. (F.24)- (F.28) into eq. (F.23), we obtain

$$\delta\Gamma^{\mu\alpha}_{(b)} = ig^3 C_A t^\alpha (qB)(-i\gamma_5)\frac{i}{(4\pi)^2}\left(\frac{16}{15}\right)(-1+\log(4))\frac{(Q\cdot u)^2}{Q^4}[\not{b}u^\mu + \not{u}b^\mu]. \tag{F.29}$$

We use that

$$\begin{aligned}\gamma_5\not{b}u^\mu &= i\gamma_1\gamma_2\not{u}u^\mu,\\ \gamma_5\not{u}b^\mu &= i\gamma_1\gamma_2\not{b}b^\mu.\end{aligned} \tag{F.30}$$

After we substitute eq. (F.30) into eq. (F.29), we finally get

$$\begin{aligned}\delta\Gamma^{\mu\alpha}_{(b)} &= -ig^3 C_A t^\alpha \frac{1}{(4\pi)^2}\left(\frac{16}{15}\right)(-1+\log(4))\frac{(Q\cdot u)^2}{Q^4}[i\gamma_1\gamma_2 qB][\not{b}b^\mu + \not{u}u^\mu]\\ &= -ig^3 C_A t^\alpha \frac{1}{(4\pi)^2}\left(\frac{16}{15}\right)(-1+\log(4))\frac{q\vec{\Sigma}\cdot\vec{B}}{Q^2}[\not{b}b^\mu + \not{u}u^\mu].\end{aligned} \tag{F.31}$$

Notice eq. (F.31) is the same as eq. (6.31).

APPENDIX G

TRACE OF PARALLEL MATRIX ELEMENT.

We start writting the trace of eq. (7.10), it is

$$\mathrm{Tr}[\gamma_\parallel \not{k}_\parallel \mathcal{O}_\parallel \gamma_\alpha \not{q}_\parallel \mathcal{O}_\parallel \gamma_\nu \not{p}_\parallel \mathcal{O}\ \parallel] = \mathrm{Tr}[\gamma_\parallel \not{k}_\parallel \frac{[1-i\gamma_1\gamma_2]}{2}\gamma_\alpha \not{q}_\parallel \frac{[1-i\gamma_1\gamma_2]}{2}\gamma_\nu \not{p}_\parallel \frac{[1-i\gamma_1\gamma_2]}{2}], \quad \text{(G.1)}$$

we can notice that $\gamma_\nu = \gamma_\nu^\perp + \gamma_\nu^\parallel$, therefore we have the following relations

$$\begin{aligned}[1-i\gamma_1\gamma_2]\gamma_\nu &= [1-i\gamma_1\gamma_2](\gamma_\nu^\perp + \gamma_\nu^\parallel) \\ &= \gamma_\nu^\perp[1+i\gamma_1\gamma_2] + \gamma_\nu^\parallel[1-i\gamma_1\gamma_2], \end{aligned} \quad \text{(G.2)}$$

$$[1 \pm i\gamma_1\gamma_2]\not{p}_\parallel = \not{p}_\parallel[1 \pm i\gamma_1\gamma_2], \quad \text{(G.3)}$$

then collecting terms, we have

$$[1-i\gamma_1\gamma_2]\gamma_\nu \not{p}_\parallel = \gamma_\nu^\perp \not{p}_\parallel[1+i\gamma_1\gamma_2] + \gamma_\nu^\parallel \not{p}_\parallel[1-i\gamma_1\gamma_2] \quad \text{(G.4)}$$

and

$$\begin{aligned}[1-i\gamma_1\gamma_2]\gamma_\nu \not{p}_\parallel[1-i\gamma_1\gamma_2] &= \gamma_\nu^\perp \not{p}_\parallel[1+i\gamma_1\gamma_2][1-i\gamma_1\gamma_2] + \gamma_\nu^\parallel \not{p}_\parallel[1-i\gamma_1\gamma_2][1-i\gamma_1\gamma_2] \\ &= \gamma_\nu^\parallel \not{p}_\parallel[1-i\gamma_1\gamma_2]. \end{aligned} \quad \text{(G.5)}$$

We use the result in eq. (G.5) and then eq. (G.1) becomes

$$\begin{aligned}\mathrm{Tr}[\gamma_\parallel \not{k}_\parallel \mathcal{O}_\parallel \gamma_\alpha \not{q}_\parallel \mathcal{O}_\parallel \gamma_\nu \not{p}_\parallel \mathcal{O}\ \|] &= \frac{1}{8}\mathrm{Tr}[(\gamma_\mu^\parallel + \gamma_\mu^\perp)\not{k}_\parallel \gamma_\alpha^\parallel \not{q}_\parallel \gamma_\nu^\parallel \not{p}_\parallel (1 - i\gamma_1\gamma_2)] \\ &= \frac{1}{8}\big\{\mathrm{Tr}[\gamma_\mu^\parallel \not{k}_\parallel \gamma_\alpha^\parallel \not{q}_\parallel \gamma_\nu^\parallel \not{p}_\parallel] + \mathrm{Tr}[\gamma_\mu^\perp \not{k}_\parallel \gamma_\alpha^\parallel \not{q}_\parallel \gamma_\nu^\parallel \not{p}_\parallel] \\ &- i\mathrm{Tr}[\gamma_\mu^\parallel \not{k}_\parallel \gamma_\alpha^\parallel \not{q}_\parallel \gamma_\nu^\parallel \not{p}_\parallel \gamma_1\gamma_2] - i\mathrm{Tr}[\gamma_\mu^\perp \not{k}_\parallel \gamma_\alpha^\parallel \not{q}_\parallel \gamma_\nu^\parallel \not{p}_\parallel \gamma_1\gamma_2]\big\}. \quad \text{(G.6)}\end{aligned}$$

In eq. (G.6), we get four terms at the end, and only the first one of them is finite, the other three terms are zero due to the combination between parallel and perpendicular components inside the traces. Thus

$$\begin{aligned}\mathrm{Tr}[\gamma_\parallel \not{k}_\parallel \mathcal{O}_\parallel \gamma_\alpha \not{q}_\parallel \mathcal{O}_\parallel \gamma_\nu \not{p}_\parallel \mathcal{O}\ \|] &= \frac{1}{8}\mathrm{Tr}[\gamma_\mu^\parallel \not{k}_\parallel \gamma_\alpha^\parallel \not{q}_\parallel \gamma_\nu^\parallel \not{p}_\parallel] \\ &= \frac{1}{4}\big\{(-g_{\mu\nu}k_\alpha - g_{\alpha\nu}k_\mu + g_{\alpha\mu}k_\nu)^\parallel (p\cdot q)_\parallel \\ &+ (g_{\mu\nu}p_\alpha - g_{\alpha\nu}p_\mu - g_{\alpha\mu}p_\nu)^\parallel (k\cdot q)_\parallel \\ &+ (-g_{\mu\nu}q_\alpha + g_{\alpha\nu}q_\mu - g_{\alpha\mu}q_\nu)^\parallel (p\cdot k)_\parallel \\ &+ k_\nu^\parallel (p_\mu q_\alpha - p_\alpha q_\mu)_\parallel \\ &+ k_\mu^\parallel (p_\nu q_\alpha + p_\alpha q_\nu)_\parallel \\ &+ k_\alpha^\parallel (p_\nu q_\mu + p_\mu q_\nu)_\parallel\big\}. \quad \text{(G.7)}\end{aligned}$$

We now think to multiply by the complex conjugate amplitude, it involves to multiply by the complex conjugate polarization vector. Adding up over polarizations, we get

$$\begin{aligned}\sum_{\lambda_u} \varepsilon^\alpha(\lambda_u, u)\varepsilon^{*\alpha'}(\lambda_u, u) &= -g^{\alpha\alpha'} \\ \sum_{\lambda_v} \varepsilon^\nu(\lambda_v, v)\varepsilon^{*\nu'}(\lambda_v, v) &= -g^{\nu\nu'} \\ \sum_{\lambda_r} \varepsilon^\mu(\lambda_r, r)\varepsilon^{*\mu'}(\lambda_r, r) &= -g^{\mu\mu'}. \quad \text{(G.8)}\end{aligned}$$

When we make the product between the amplitude and its complex conjugate, then we get finite contributions from the next terms

$$\begin{aligned}&- (-g_{\mu\nu}k_\alpha - g_{\alpha\nu}k_\mu + g_{\alpha\mu}k_\nu)_\parallel (g^{\alpha\alpha'}g^{\nu\nu'}g^{\mu\mu'}) \\ &\times (-g_{\mu'\nu'}k'_{\alpha'} - g_{\alpha'\nu'}k'_{\mu'} + g_{\alpha'\mu'}k_{\nu'})_\parallel (p\cdot q)_\parallel (p'\cdot q')_\parallel \\ &= -4(k\cdot k')_\parallel (p\cdot q)_\parallel (p'\cdot q')_\parallel. \quad \text{(G.9)}\end{aligned}$$

$$
\begin{aligned}
&-(-g_{\mu\nu}k_\alpha - g_{\alpha\nu}k_\mu + g_{\alpha\mu}k_\nu)_\parallel (p\cdot q)_\parallel (g^{\alpha\alpha'}g^{\nu\nu'}g^{\mu\mu'})\\
&\times [k'_{\nu'}(p'_{\mu'}q'_{\alpha'} - p'_{\alpha'}q'_{\mu'}) + k'_{\mu'}(p'_{\nu'}q'_{\alpha'} + p'_{\alpha'}q'_{\nu'})\\
&+ k'_{\alpha'}(p'_{\mu'}q'_{\nu'} + p'_{\nu'}q'_{\mu'})]_\parallel = 4(k\cdot k')_\parallel (p'\cdot q')_\parallel (p\cdot q)_\parallel .
\end{aligned}
\tag{G.10}
$$

$$
\begin{aligned}
&-(g_{\mu\nu}p_\alpha - g_{\alpha\nu}p_\mu - g_{\alpha\mu}p_\nu)_\parallel (k\cdot q)_\parallel (g^{\alpha\alpha'}g^{\nu\nu'}g^{\mu\mu'})\\
&\times [k'_{\nu'}(p'_{\mu'}q'_{\alpha'} - p'_{\alpha'}q'_{\mu'}) + k'_{\mu'}(p'_{\nu'}q'_{\alpha'} + p'_{\alpha'}q'_{\nu'})\\
&+ k'_{\alpha'}(p'_{\nu'}q'_{\mu'} + p'_{\mu'}q'_{\nu'})]_\parallel = 4(p\cdot p')_\parallel (k'\cdot q')_\parallel (k\cdot q)_\parallel .
\end{aligned}
\tag{G.11}
$$

$$
\begin{aligned}
&-(-g_{\mu\nu}q_\alpha + g_{\alpha\nu}q_\mu - g_{\alpha\mu}q_\nu)_\parallel (p\cdot k)_\parallel (g^{\alpha\alpha'}g^{\nu\nu'}g^{\mu\mu'})\\
&\times (-g_{\mu'\nu'}q'_{\alpha'} + g_{\alpha'\nu'}q'_{\mu'} - g_{\alpha'\mu'}q'_{\nu'})_\parallel (p'\cdot k')_\parallel = -4(q\cdot q')_\parallel (p\cdot k)_\parallel (p'\cdot k')_\parallel .
\end{aligned}
\tag{G.12}
$$

$$
\begin{aligned}
&-(-g_{\mu\nu}q_\alpha + g_{\alpha\nu}q_\mu - g_{\alpha\mu}q_\nu)_\parallel (p\cdot k)_\parallel (g^{\alpha\alpha'}g^{\nu\nu'}g^{\mu\mu'})\\
&\times [k'_{\nu'}(p'_{\mu'}q'_{\alpha'} - p'_{\alpha'}q'_{\mu'}) + k'_{\mu'}(p'_{\nu'}q'_{\alpha'} + p'_{\alpha'}q'_{\nu'})\\
&+ k'_{\alpha'}(p'_{\nu'}q'_{\mu'} + p'_{\mu'}q'_{\nu'})]_\parallel = 4(q\cdot q')_\parallel (k'\cdot p')_\parallel (k\cdot p)_\parallel .
\end{aligned}
\tag{G.13}
$$

$$
\begin{aligned}
&-[k_\nu(p_\mu q_\alpha - p_\alpha q_\mu) + k_\mu(p_\nu q_\alpha + p_\alpha q_\nu) + k_\alpha(p_\nu q_\mu + p_\mu q_\nu)]_\parallel (g^{\alpha\alpha'}g^{\nu\nu'}g^{\mu\mu'})\\
&\times [k'_{\nu'}(p'_{\mu'}q'_{\alpha'} - p'_{\alpha'}q'_{\mu'}) + k'_{\mu'}(p'_{\nu'}q'_{\alpha'} + p'_{\alpha'}q'_{\nu'}) + k'_{\alpha'}(p'_{\nu'}q'_{\mu'} + p'_{\mu'}q'_{\nu'})]_\parallel\\
&= -2[(k\cdot k')_\parallel (p\cdot q')_\parallel (q\cdot p')_\parallel + (k\cdot p')_\parallel (p\cdot k')_\parallel (q\cdot q')_\parallel + (k\cdot q')_\parallel (p\cdot k')_\parallel (q\cdot p')_\parallel\\
&+ (k\cdot p')_\parallel (p\cdot q')_\parallel (q\cdot k')_\parallel + (k\cdot q')_\parallel (p\cdot p')_\parallel (q\cdot k')_\parallel + 3(k\cdot k')_\parallel (p\cdot p')_\parallel (q\cdot q')_\parallel].
\end{aligned}
\tag{G.14}
$$

We add from eq. (G.9) to eq. (G.14) and the result only comes from the contribution of eq. (G.14), therefore the trace in eq. (G.1) can be written as

$$
\begin{aligned}
&\mathrm{Tr}\left[\gamma_\mu \not{k}_\parallel \mathcal{O}_\parallel \gamma_\alpha \not{q}_\parallel \mathcal{O}_\parallel \gamma_\nu \not{p}_\parallel \mathcal{O}_\parallel\right] \longrightarrow k_{\parallel\nu}(p_\mu q_\alpha - p_\alpha q_\mu)_\parallel\\
&+ k_{\parallel\mu}(p_\nu q_\alpha + p_\alpha q_\nu)_\parallel + k_{\parallel\alpha}(p_\nu q_\mu - p_\mu q_\nu)_\parallel .
\end{aligned}
\tag{G.15}
$$

Notice eq. (G.15) is the same as eq. (7.11).

BIBLIOGRAPHY

[1] H. Fritzsch and M. Gell-Mann, *in* Proc. *XVI* Int. Conf. on High Energy Physics, Batavia 1972, Vol. 2, p. 135.

[2] D. J. Gross and F. Wilczek, Phys. Rev. Lett. **30**, (1973) 1343; H. D. Politzer, Phys. Rev. Lett. **30**, (1973) 1346.

[3] M. A. Shifman, A. I. Vainshtein and V. I. Zakharov, Nucl. Phys. B **147**, (1979) 385, 448.

[4] K. Wilson, Phys. Rev. **179** (1969) 1499; K. Wilson and J. Kogut, Phys. Reports **12** (1974) 75.

[5] P. Colangelo and A. Khodjamirian, in: *At the frontier of Particle Physics/ Handbook of QCD*, M. A. Shifman, ed. (World Scientific, Singapore 2001), Vol. 3, 1495; E. de Rafael, Lectures at Les Houches Summer School, Session 68, Les Houches, France (1997), hep-ph/9802448; M. Shifman, Prog. Theor. Phys. Suppl. **131**, 1 (1998).

[6] R. Shankar, Phys. Rev. D **15**, (1977) 755.

[7] E. C. Poggio, H. R. Quinn and S. Weinberg, Phys. Rev. D **13**, (1976) 1958.

[8] F. Le Diberder and A. Pich, Phys. Lett. B **289** (1992) 165; K. Maltman, Phys. Lett. B **440**, (1998) 367; C. A. Dominguez and K. Schilcher, Phys. Lett. B **448**, (1999) 93.

[9] M. Gonzalez-Alonso, A. Pich, and J. Prades, Phys. Rev. D **81** (2010) 074007.

[10] O. Cata, M. Golterman, and S. Peris, J. High Energy Phys. **08** (2005) 076; Phys. Rev. D **79** (2009) 053002;

[11] D. Boito, M. Golterman, M. Jamin, K. Maltman, and S. Peris, Phys. Rev. D **87** (2013) 094008.

[12] R. Barate *et al.* (ALEPH Collaboration), Eur. Phys. J. C **4** (1998), 409; S. Schael *et al.* (ALEPH Collaboration), Phys. Rept. **421** (2005) 191.

[13] K. Ackerstaff *et al.* (OPAL Collaboration), Eur. Phys. J. C **7** (1999) 571.

[14] M. Davier, A. Höcker, B. Malaescu, C. Z. Yuan and Z. Zhang, Eur. Phys. J. C **74** (2014) 2803.

[15] A. Rodríguez-Sánchez, M. González-Alonso and A. Pich, Phys. Rev. D **94**, no. 1, 014017 (2016).

[16] C. A. Dominguez, L. A. Hernandez, K. Schilcher, and H. Spiesberger, J. High Energy Phys. **03** (2015) 053.

[17] C. A. Dominguez and K. Schilcher, Phys. Lett. B **581** (2004) 193.

[18] J. Bordes, C. A. Dominguez, J. Penarrocha, and K. Schilcher, J. High Energy Phys. **02** (2006) 037.

[19] M. Gonzalez-Alonso, A. Pich, and J. Prades, Phys. Rev. D **82** (2010) 014019.

[20] A. Pich, Progr. Part. Nucl. Phys. **75** (2014) 41.

[21] C. A. Dominguez, N. F. Nasrallah, and, K. Schilcher, Phys. Rev. D **80** (2009) 054014.

[22] D. Boito, M. Golterman, K. Maltman, J. Osborne, and S. Peris, Phys. Rev. D **91** (2015) 034003.

[23] K. A. Olive *et al.* (Particle Data Group), Chin. Phys. C **38** (2014) 090001.

[24] For a compilation see V. V. Ezhela, S. B. Lugovsky, and O. V. Zenin, arXiv:hep-ph/0312114.

[25] J. P. Miller, E. de Rafael, and B. Lee Roberts, Rep. Prog. Phys. **70**, 795 (2007); F. Jegerlehner, and A. Nyffeler, Phys. Rep. **477**, 1 (2009), and references therein.

[26] D. R. Boito *et al.*, Nucl. Phys. B (Proc. Suppl.) **218** (2011) 104.

[27] K. G. Chetyrkin, A. L. Kataev and F. V. Tkachov, Phys. Lett. **B 85** (1979) 277; M. Dine and J. Sapirstein, Phys. Rev. Lett. **43** (1979) 668; W. Celmaster and R. Gonsalves, Phys. Rev. Lett. **44** (1980) 560; S. G. Gorishny, A. L. Kataev, and S. A.

Larin, Phys. Lett. **B 259** (1991) 144; L. R. Surguladze and M. Samuel, Phys. Rev. Lett. **66** (1991) 560.

[28] M. Davier, A. Höcker and Z. Zhang, Rev. Mod. Phys. **78** (2006) 1043.

[29] C. A. Dominguez and K. Schilcher, J. High Energy Phys. **01** (2007) 093.

[30] P. A. Baikov, K. G. Chetyrkin and J. H. Kühn, Phys. Rev. Lett. **101** (2008) 012002.

[31] W. Marciano, A. Sirlin, Phys. Rev. Lett. **61** (1988) 1815.

[32] S. Weinberg, Phys. Rev. Lett. **18**, 507 (1967).

[33] T. Das, V. S. Mathur, and S. Okubo, Phys. Rev. Lett. **19** (1967) 859.

[34] S. R. Amendolia *et al.*, Nucl. Phys. B **277** (1986) 168.

[35] J. Gasser and H. Leutwyler, Nucl. Phys. B **250** (1985) 465; G. Ecker, J. Gasser, A. Pich, and E. de Rafael, Nucl. Phys. B **321** (1989) 311.

[36] E. Shintani *et al.*, Phys. Rev. Lett. **101** (2008) 242001; P. A. Boyle *et al.*, Phys. Rev. D **81** (2010) 014504.

[37] L. V. Lanin, V. P. Spidorov and K. G. Chetyrkin, Sov. J. Nucl. Phys. **44** (1986) 892.

[38] V. I. Zakharov, Int. J. Mod. Phys. A **14** (1999) 4865.

[39] G. S. Bali, C. Bauer and A. Pineda, Phys. Rev. Lett. **113** (2014) 092001.

[40] B. Chakraborty *et al.*, Phys. Rev. D **91**, no. 5, 054508 (2015).

[41] R. Horsley *et al.*, Phys. Rev. D **86**, 054502 (2012).

[42] S. Eidelman, L. M. Kurdadze and A. I. Vanshtein, Phys. Lett. B **82** (1979) 278.

[43] C. A. Dominguez and J. Sola, Z. Phys. C **40** (1988) 63.

[44] B. Guberina, R. Meckbach, R. D. Peccei and R. Rückl, Nucl. Phys. B **184** (1981) 476.

[45] L. J. Reinders, H. Rubinstein, and S. Yazaki, Phys. Rep. **127** (1985) 1.

[46] V. Gimenez, J. A. Peñarrocha, and J. Bordes, Phys. Lett. B **214** (1988) 247.

[47] E. Di Salvo, and M. Pallavicini, Nucl. Phys. B **427** (1994) 22.

[48] K. Schilcher, and M. D. Tran, Phys. Rev. D **29** (1984) 570.

[49] G. Launer, Z. Phys. C **32** (1986) 557.

[50] A. A. Almasy, K. Schilcher and H. Spiesberger, Phys. Lett. B **650** (2007) 179.

[51] A. A. Almasy, K. Schilcher and H. Spiesberger, Eur. Phys. J. C **55** (2008) 237.

[52] J. H. Kühn, M. Steinhauser and C. Sturm, Nucl. Phys. B **778** (2007) 192.

[53] K. G. Chetyrkin, R. Harlander, J. H. Kühn, and M. Steinhauser, Nucl. Phys. B **503** (1997) 339.

[54] P. A. Baikov, K. G. Chetyrkin, and J. H. Kühn, Nucl. Phys. B (Proc. Suppl.) **189** (2009) 49.

[55] K. G. Chetyrkin, R. Harlander, J. H. Kühn, Nucl. Phys. B **586** (2000) 56.

[56] P. A. Baikov, K. G. Chetyrkin, and J. H. Kühn, Nucl. Phys. B (Proc. Suppl.) **135** (2004) 243.

[57] R. Boughezal, M. Czakon, and T. Schutzmeier, Phys. Rev. D **74** (2006) 074006.

[58] R. Boughezal, M. Czakon, and T. Schutzmeier, Nucl. Phys. B (Proc. Suppl.) **160** (2006) 164.

[59] A. Maier, P. Maierhöfer, and P. Marquard, Nucl. Phys. B **797** (2008) 218.

[60] A. Maier, P. Maierhöfer, and P. Marquard, Phys. Lett. B **669** (2008) 88.

[61] K. G. Chetyrkin, J. H. Kühn, and C. Sturm, Eur. Phys. J. C **48** (2006) 107.

[62] A. Maier, P. Maierhöfer, P. Marquard, and A. V. Smirnov, Nucl. Phys. B **824** (2010) 1.

[63] D. Cronin-Hennessy *et al.* (CLEO 2009), Phys. Rev. D **80** (2009) 072001.

[64] J. Z. Bai *et al.* (BES 2002), Phys. Rev. Lett. **88** (2002) 101802.

[65] J. Z. Bai *et al.* (BES 2006), Phys. Rev. Lett. **97**, (2006) 262001.

[66] D. J. Broadhurst *et al.*, Phys. Lett. B **329** (1994) 103.

[67] C. McNeile *et al.*, PQCD Collaboration, Phys. Rev. D **82** (2010) 034512.

[68] S. Bodenstein, J. Bordes, C. A. Dominguez, J. Peñarrocha and K. Schilcher, Phys. Rev. D **83** (2011) 074014.

[69] K. Chetyrkin *et al.*, Theor. Math. Phys. **170** (2012) 217.

[70] K. G. Chetyrkin *et al.*, Phys. Rev. D **80** (2009) 074010.

[71] A. Hoang, and M. Jamin, Phys. Lett. B **594** (2004) 127.

[72] S. Eidelman, F. Jegerlehner, A. L. Kataev, and O. Veretin, Phys. Lett. B **454** (1999) 369.

[73] B. V. Geshkenbein, Phys. Rev. D **70** (2004) 074027.

[74] J. S. Schwinger, Phys. Rev. **82**, (1951) 664.

[75] T.-K. Chyi, *et al.*, Phys. Rev. D **62**, (2000) 105014.

[76] V. P. Gusynin *et al.*, Nucl. Phys. B **462**, (1996) 249-290.

[77] G. S. Bali, F. Bruckmann, G. Endrődi, Z. Fodor, S. D. Katz, S. Krieg, A. Schäfer and K. K. Szabo, J. High Energy Phys. **02**, 044 (2012).

[78] G. S. Bali, F. Bruckmann, G. Endrődi, S. D. Katz and A. Schäfer, J. High Energy Phys. **08**, 177 (2014).

[79] G. S. Bali, F. Bruckmann, G. Endrődi, Z. Fodor, S. D. Katz, and A. Schäfer, Phys. Rev. D **86**, 071502 (2012).

[80] J. P. Carlomagno, D. Gomez Dumm, N. N. Scoccola, Phys. Rev. D **88**, 074034 (2014).

[81] A. J. Mizher, M. N. Chernodub and E. S. Fraga, Phys. Rev. D **82**, 105016 (2010).

[82] L. D. McLerran and B. Svetitsky, Phys. Lett. B **98**, 195 (1981).

[83] K. Fukushima, Phys. Lett. B **591**, 277 (2004).

[84] QCD sum rules at finite temperature were first proposed in A. I. Bochkarev and M. E. Shaposnikov, Nucl. Phys. B **268**, 220 (1986); for a review see e.g. C. A. Dominguez, AIP Conf. Proc. **342**, 383 (1995).

[85] C. A. Dominguez and M. Loewe, Phys. Lett. B **233**, 201 (1989). A. Barducci, R. Casalbuoni, S. De Curtis, R. Gatto and G. Pettini, Phys. Lett. B **244**, 311 (1990).

[86] A. Ayala, A. Bashir, C. A. Dominguez, E. Gutierrez, M. Loewe, A. Raya, Phys. Rev. D **84**, 056004 (2011).

[87] A. Ayala, C. A. Dominguez and M. Loewe, arXiv:1604.06623 [hep-ph].

[88] A. Ayala, C. A. Dominguez, L. A. Hernandez, M. Loewe and A. J. Mizher, Phys. Rev. D **88**, 114028 (2013).

[89] N. O. Agasian and I. A. Shushpanov, J. High Energy Phys. **10**, 006 (2001).

[90] V. Skokov, A. Y. Illarionov and V. Toneev, Int. J. Mod. Phys. A **24** (2009) 5925.

[91] E. S. Fraga, J. Noronha and L. F. Palhares, Phys. Rev. D **87**, 114014 (2013).

[92] F. Bruckmann, G. Endrődi and T. G. Kovacs, J. High Energy Phys. **1304**, 112 (2013).

[93] M. Ferreira, P. Costa, D. P. Menezes, C. Providencia and N. N. Scoccola, Phys. Rev. D**89**, 016002 (2014).

[94] K. Fukushima and Y. Hidaka, Phys. Rev. Lett. **110**, 031601 (2013).

[95] N. Mueller and J. M. Pawlowski, Phys. Rev. D **91**, 11, 116010 (2015).

[96] J. O. Andersen and A. Tranberg, J. High Energy Phys. **1208**, 002 (2012); J. O. Andersen, W. R. Naylor, and A. Tranberg, J. High Energy Phys. **1404**, 187 (2014).

[97] J. Braun, W. A. Mian, S. Rechenberger, arXiv:1412.6025 [hep-ph].

[98] G. S. Bali, F. Bruckmann, G. Endrődi, F. Gruber, A. Schäfer, J. High Energy Phys. **1304**, 130 (2013).

[99] E. J. Ferrer, V. de la Incera, X. J. Wen, Phys. Rev. D **91**, 054006 (2015).

[100] Sh. Fayazbakhsh and N. Sadooghi, Phys. Rev. D **90**, 105030 (2014).

[101] R. L. S. Farias, K. P. Gomes, G. Krein and M. B. Pinto, Phys. Rev. C **90**, 025203 (2014).

[102] M. Ferreira, P. Costa, O. Lourenço, T. Frederico, C. Providência, Phys. Rev. D **89**, 116011 (2014).

[103] J. O. Andersen, W. R. Naylor, A. Tranberg, J. High Energy Phys. **1502**, 042 (2015).

[104] E. S. Fraga and A. J. Mizher, Phys. Rev. D **78**, 025016 (2008).

[105] M. Loewe, C. Villavicencio, R. Zamora, Phys. Rev. D **89**, 016004 (2014).

[106] N. O. Agasian and S. M. Fedorov, Phys. Lett. B **663**, 445 (2008).

[107] E. S. Fraga, B. W. Mintz, J. Schaffner-Bielich, Phys. Lett. B **731**, 154 (2014).

[108] A. Ayala, L. A. Hernandez, A. J. Mizher, J. C. Rojas, C. Villavicencio, Phys. Rev. D **89**, 116017 (2014).

[109] A. Ayala, M. Loewe, A. J. Mizher, R. Zamora, Phys. Rev. D **90**, 036001 (2014).

[110] A. Ayala, M. Loewe and R. Zamora, Phys. Rev. D **91**, 016002 (2015).

[111] A. Ayala, J.J. Cobos-Martinez, M. Loewe, M. E. Tejeda-Yeomans, and R. Zamora, Phys. Rev. D **91**, 016007 (2015).

[112] S. Sharma, Adv. High Energy Phys. **2013**, 452978 (2013).

[113] S.-x. Qin, L. Chang, H. Chen, Y.-x. Liu and C. D. Roberts, Phys. Rev. Lett. **106**, 172301 (2011).

[114] G. Endrödi, J. High Energy Phys. **1507**, 173 (2015).

[115] P. Costa, M. Ferreira, D. P. Menezes, J. Moreira and C. Providncia, Phys. Rev. D **92**, no. 3, 036012 (2015); M. Ferreira, P. Costa and C. Providncia, arXiv:1509.01181 [hep].

[116] J. Goldstone, Nuovo Cim. **19**, 154 (1961); Y. Nambu and G. Jona-Lasinio, Phys. Rev. **124**, 246 (1961); Y. Nambu and G. Jona-Lasinio, Phys. Rev. **122** (1961) 345.

[117] J. I. Kapusta and C. Gale, *Finite-Temperature Field Theory: Principles and applications*, Cambridge University Press (1994). M. Le Bellac, *Thermal Field Theory*, Cambridge University Press (1996); A. Das, *Finite Temperature Field Theory*, World Scientific (1997).

[118] Y. Maezawa, S. Aoki, S. Ejiri, T. Hatsuda, N. Ishii, K. Kanaya, N. Ukita, J. Phys. G **34**, S651 (2007).

[119] A. Ayala, J.J. Cobos-Martinez, M. Loewe, M. E. Tejeda-Yeomans, and R. Zamora, Phys. Rev. D **91**, 016007 (2015).

[120] I. A. Shuspanov and A. V. Smilga, Phys. Lett. B **402**, 351 (1997); N. O. Agasian and I. A. Shushpanov, Phys. Lett. B **472**, 143 (2000); T. D. Cohen, D. A. McGady,

and E. S. Werbos, Phys. Rev. C **76**, 055201 (2007); E. S. Werbos, Phys. Rev. C **77**, 065202 (2008).

[121] E. J. Ferrer, V. de la Incera, I. Portillo and M. Quiroz, Phys. Rev. D **89**, 8, 085034 (2014); E. J. Ferrer, V. de la Incera, Phys. Rev. Lett. **102**, 050402 (2009); Nucl. Phys. B **824**, 217-238 (2010).

[122] V. A. Miransky, I. A. Shovkovy, Phys. Rev. D **66**, 045006 (2002).

[123] T. Kojo, N. Su, Phys. Lett. B **720**, 192-197 (2013); N. Mueller, J. A. Bonnet, C. S. Fischer, Phys. Rev. D **89**, 094023 (2014).

[124] J. O. Andersen, W. R. Naylor and A. Tranberg, Rev. Mod. Phys. **88** (2016) 025001

[125] A. Ayala, C. A. Dominguez, L. A. Hernandez, M. Loewe and R. Zamora, Phys. Lett. B**759**, 99-103 (2016).

[126] A. Ayala, C. A. Dominguez, L. A. Hernandez, M. Loewe, J. C. Rojas, C. Villavicencio, Phys. Rev. D **92**, 016006 (2015).

[127] R. Rougemont, R. Critelli, J. Noronha, arXiv:1505.07894 [hep-th].

[128] J. Chao, P. Chu, M. Huang, Phys.Rev. D **88**, 054009 (2013);

[129] A. Ayala, C. A. Dominguez, L. A. Hernandez, M. Loewe, R. Zamora, Phys. Rev. D **92**, 096011 (2015);

[130] A. Ahmad and A. Raya, J. Phys. G **43**, no. 6, 065002 (2016).

[131] J. K. Boomsma and D. Boer, Phys. Rev. D **81**, 074005 (2010).

[132] J. O. Andersen and R. Khan, Phys. Rev. D **85**, 065026 (2012).

[133] D. Blaschke, S. Fredriksson, H. Grigorian, A. M. Oztas, and F. Sandin, Phys. Rev. D **72**, 065020 (2005).

[134] I. General, D. Gomez-Dumm, and N. Scoccola, Phys. Lett. **B506**, 267 (2001).

[135] M. Buballa, Phys. Rept. **407**, 2015 (2005).

[136] S. Klevansky, Rev. Mod. Phys. **64**, 649 (1992).

[137] A. K. Harding and D. Lai, Rept. Prog. Phys. **69**, 2631 (2006).

[138] D. E. Kharzeev, L. D. McLerran and H. J. Warringa, Nucl. Phys. A **803**, 227 (2008).

[139] V. Voronyuk, V. D. Toneev, W. Cassing, E. L. Bratkovskaya, V. P. Konchakovski, S. A. Voloshin, Phys. Rev. C **83**, 054911 (2011).

[140] D. Grasso and H. R. Rubinstein, Phys. Rept. **348**, 163 (2001).

[141] I. Arsene *et al.* (BRAHMS Collaboration), Nucl. Phys. A757, 1 (2005); B. B. Back *et al.*, Nucl. Phys. A **757**, 28 (2005); J. Adams *et al.* (STAR Collaboration), Nucl. Phys. **A757**, 102 (2005); K. Adcox *et al.* (PHENIX Collaboration), Nucl. Phys. **A757**, 184 (2005); P. Jacobs and X. N. Wang, Prog. Part. Nucl. Phys. **54**, 443 (2005).

[142] F. Becattini, J. Phys. Conf. Ser. **527**, 012012 (2014) and references therein.

[143] L. Adamczyk *et al.* (STAR Collaboration), Phys. Rev. Lett. **113**, 052302.

[144] G. Basar, D. E. Kharzeev, V. Skokov, Phys. Rev. Lett. **109**, 202303 (2012).

[145] G. Basar, D. E. Kharzeev, E. V. Shuryak, Phys. Rev. C **90**, 014905 (2014).

[146] K. Tuchin, Phys. Rev. C **91**, 014902 (2015).

[147] G. Arciniega, P. Ortega, L. Patiño, J. High Energy Phys. **1404**, 192 (2014); S. Y. Wu and D. L. Yang, J. High Energy Phys. **1308**, 032 (2013) K. A. Mamo, J. High Energy Phys. **1308**, 083 (2013).

[148] A. Adare *et al.* [PHENIX Collaboration], Phys. Rev. C **91**, 064904 (2015); J. Adam *et al.* [ALICE Collaboration], Phys. Lett. B **754**, 235 (2016).

[149] L. McLerran and B. Schenke, Nucl. Phys. A **946**, 158 (2016).

[150] F. M. Liu, S. X. Liu and K. Werner, arXiv:1512.08833 [nucl-th].

[151] A. Adare *et al.* [PHENIX Collaboration], e-Print: arXiv:1509.07758 [nucl-ex]; D. Lohner [ALICE Collaboration], J. Phys. Conf. Ser. **446**, 012028 (2013).

[152] J. F. Paquet, C. Shen, G. S. Denicol, M. Luzum, B. Schenke, S. Jeon and C. Gale, Phys. Rev. C **93**, no. 4, 044906 (2016).

[153] H. van Hees, M. He, R. Rapp, Nucl. Phys. A **933**, 256-271 (2015).

[154] O. Linnyk, V. Konchakovski, T. Steinert, W. Cassing, E. L. Bratkovskaya, Phys. Rev. C **92**, 054914 (2015).

[155] For a recent review see C. Shen, e-Print: arXiv:1601.02563 [nucl-th].

[156] Y. Zhong, C.-B. Yang, X. Cai, S.-Q. Feng, Adv. High Energry Phys. **2014**, 193039 (2014).

[157] W. Broniowski, W. Florkowski, Phys. Rev. **C** 65, 024905 (2002).

[158] D. Bedingham, arXiv:hep-ph/0011012 (2000).

[159] B. R. Paris, Proc. R. Soc. A **461**, 297 (2004).

[160] L. Dolan and R. Jackiw, Phys. Rev. D **9**, 3320 (1974).